Department of Civil Engineering

The University of Michigan

REINFORCED CONCRETE STRUCTURAL WALLS WITH STAGGERED OPENING CONFIGURATIONS UNDER REVERSED CYCLIC LOADING

by

Aejaz Ali
and
James K. Wight

April 1990 Report No. UMCE 90-05

A Report on Research Sponsored by
National Science Foundation
Grant No. ECE-8603624

Ann Arbor, Michigan

engn
UMR 0357

ABSTRACT

REINFORCED CONCRETE STRUCTURAL WALLS WITH STAGGERED OPENING CONFIGURATIONS UNDER REVERSED CYCLIC LOADING

Results of an experimental study on the behavior of reinforced concrete structural walls with staggered door openings under reversed cyclic loadings are presented. The program was part of a larger project involving a detailed study of a few selected Chilean buildings that experienced the earthquake of March 3, 1985, and was inspired by the remarkably good performance of the wall-dominated reinforced concrete buildings in that region. The following two characteristics were found typical of Chilean buildings: (i) a generous use of structural walls in all buildings, and (ii) a staggered door opening configuration.

To study the effect of staggered openings on wall behavior, four scaled reinforced concrete wall specimens were constructed and tested under this program. The lightly reinforced specimens, which were constructed on about one-fifth scale, were five stories high and barbell shaped in cross-section. Reinforcement ratios were in the range of light to moderate. While specimen W-1 had no openings, specimens W-2, W-3, and W-4 had a horizontal stagger between door openings of approximately 30, 15, and 10 percent of the total wall length, respectively. Wall specimens were tested in a vertical position under a constant axial stress. Reversed cyclic loads were applied at the top.

In general, all the test specimens exhibited ductile behavior. Energy was mainly dissipated through flexural action. There was significant flexural yielding and the development of an intersecting pattern of flexural-shear cracks at drift ratios of 1.0 percent, but no sign of impending failure. At an average drift ratio of 1.5 percent, the three specimens with door openings failed by shear-compression in the compressed portion of the wall outside the opening in the first story level.

In the analytical part of this study the force-displacement response envelope curve for the wall specimens was predicted using three techniques, namely, (i) basic principles of mechanics, (ii) equivalent column analogy, and (iii) finite element method. Predicted response was generally good and within acceptable limits.

Results of dynamic analysis of the 23-story Almendral Building subjected to three different ground motion histories are presented. The equivalent column analogy was used to model the structural walls of the building. An almost elastic response to the earthquake motion, which was recorded in the close vicinity of the building, compared favorably with the reported light damage to the building during the earthquake.

ACKNOWLEDGMENTS

This report was submitted by Aejaz Ali in partial fulfillment of the requirements for the degree of Doctor of Philosophy (Civil Engineering) in the Horace H. Rackham School of Graduate Studies at the University of Michigan. Dr. Ali wishes to express his sincere appreciation to Professor James K. Wight, chairman of the doctoral committee, for his guidance, encouragement, and continuous support throughout this research. The authors would like to thank Professors William J. Anderson, Robert D. Hanson and Ralf Peek (members of the doctoral committee) for reviewing this report and offering helpful suggestions.

Co-operation of Professor R. D. Woods in conducting vibration tests on wall specimens is gratefully acknowledged. The experimental phase of this research could not have been completed without the help of Jim Schiffer, who was involved with the project from the casting of first specimen to the testing of last one. Efforts of several others who gave a hand when needed most is also gratefully acknowledged.

Finally, acknowledgement is due to the National Science Foundation for funding the project through Grant No. ECE-8603624 and to the University of Michigan for the use of its lab facilities. The conclusions and opinions expressed in this report are solely those of the authors and do not necessarily represent the views of the sponsors.

TABLE OF CONTENTS

LIST OF FIGURES

LIST OF TABLES

CHAPTER I

INTRODUCTION

1.1 GENERAL

Reinforced concrete structural walls are frequently used as major lateral load carrying elements in modern day medium to high-rise buildings. Also referred to as shear walls, they are normally designed to resist a major portion of lateral loading due to wind or earthquake. Because of their stiffness, they are used to keep lateral drift within reasonable limits so as to avoid damage to non-structural components during more frequent ground shaking of less intensity. For severe earthquakes, however, it is generally not practical to design structural walls to remain elastic. Therefore, structural walls must be designed to sustain inelastic excursions without significant loss of strength and be able to absorb and dissipate energy. Current research trends in this area, which are almost entirely focussed on the inelastic behavior of structural walls, have shown that their performance when subjected to earthquake loading is dependent upon their stiffness, strength and deformation capacity. The view, which has long been held, that walls are inherently brittle components is gradually being reversed due to the continued publication of reports on the good performance of well-detailed walls subjected to earthquake loadings. From the pace of the current research on structural walls, it can be anticipated that the day when building codes stop penalizing the wall structures by specifying significantly increased design forces is not far away.

The location of structural walls in a building plan is generally dictated by functional requirements. When designing for wind loading, the location of the walls within the building plan does not play an important role in determining the building response to wind loads, and almost any kind of wall arrangement can be accommodated without changing the response significantly. In the case of seismic loading, however, wall locations are a critical factor in determining response. This difference in behavior due to the two loadings arises from the fact that under wind loading a fully elastic response is expected, while during strong earthquakes significant inelastic deformations are anticipated. A wall configuration which has very little eccentricity between the center of building mass and stiffness and results in a reasonably uniform distribution of inelastic deformations under seismic loading should be the goal of the structural engineer.

A review of test reports will reveal that most of the specimens tested up to this date have been either isolated members or sub-assemblages. Although these tests of isolated members do not accurately represent their behavior as part of a structural system, they do provide the designers with an upper limit on their strength and deformation capacities. In an actual structure the redistribution of forces should favorably influence their strength and deformation requirements. However, due to practical and economic reasons, it is not usually possible to test a full-scale structure or even a scaled model of a complete structure. The data obtained from the tests of isolated members or sub-assemblages are particularly valuable in providing building codes, which are basically member-oriented rather than structure-oriented, with guidelines for future improvements.

1.2 Types of Walls

Structural walls can be classified into following two main types based on their height-to-horizontal length ratio, also referred to as the overall aspect ratio of the wall: (i) low-rise or squat walls, which have an aspect ratio less than about 0.5, as shown in Fig.

1.1(a), and, (ii) long or slender walls, which have an aspect ratio greater than 2.0, as shown in Fig. 1.1(b). This classification also distinguishes between two distinct types of behaviors and modes of failure. Behavior of squat walls is primarily governed by shear stiffness and strength, and they are more likely to fail in shear. There have been attempts to predict the behavior of squat walls from tests on deep beams because of their geometrical similarities. Slender walls behave like cantilever beams whose failure is normally controlled by flexural strength. Walls having aspect ratios between 0.5 and 2.0 exhibit intermediate behavior. Their behavior is generally dependent on factors such as amount of reinforcement, axial load, etc.

Structural walls are usually connected to other walls or frames by means of either coupling beams or slabs. In cases where the walls also serve as partitions, they need to be pierced for window, door or other openings. Figure 1.2 shows three general types of wall systems, namely, coupled walls, wall-frame, and pierced wall. Although coupled wall systems and pierced wall systems have openings aligned along one vertical axis, there is a marked difference in their behavior. In the coupled wall system the openings are big enough to separate the walls and energy is mainly dissipated through the coupling beams. A pierced wall system, on the other hand, behaves as a single isolated wall in which the effect of openings are often neglected, depending on the opening-to-wall area ratio. It is the shear span-to-depth ratio of the coupling beams which classifies the systems as either coupled or pierced. A considerable amount of research on the above-mentioned types of wall systems has been conducted to date and is discussed in detail in the next chapter.

Most of the research on walls with openings has primarily been devoted to the designing and detailing of the coupling beams. Because of the special reinforcement details and potential hinging zones in the coupling beams of coupled wall systems, other configurations of openings in walls are worthy of attention. A staggered configuration of door or window openings changes the wall system from a coupled to a pierced system. Due to the limited use of pierced wall systems in the United States, no literature exists on

their behavior. An experimental and analytical program was, therefore, carried out to study the effects of different staggered configurations on the behavior of structural walls subjected to reversed cyclic loadings. A comparison of their behavior with that of solid walls and coupled walls will provide the designers with an alternative in selecting an optimum configuration of openings.

1.3 RESEARCH PROGRAM

A strong earthquake of magnitude $M_S = 7.8$ was recorded off the coast of Chile on March 3, 1985, causing serious damage and casualties in the central portion of Chile. A post-earthquake examination of building structures in major cities revealed that the majority of the multi-story reinforced concrete buildings performed quite satisfactorily [54]. A more detailed examination of structural drawings and analysis of a few selected buildings which suffered light to no damage during the above-mentioned earthquake revealed the following characteristics typical of Chilean buildings and non-existent in building structures of the United States:

(i) a generous use of shear walls in all buildings, and, in some cases, walls being the only vertical load-carrying elements,

(ii) a staggered door opening configuration,

(iii) a high percentage of vertical reinforcement in the built-in boundary elements of walls, sometimes reaching as high as 12 percent,

(iv) very light to no confinement of the built-in boundary elements along the height of the walls.

It is of interest to note that almost all the buildings under study were in the medium-height range and were of residential apartment nature. The structural walls also served as partition walls between the apartments and door openings in these served as means of access to the apartments. Figures 1.3 and 1.4 show a typical plan view and wall

elevations of two of the buildings under study. In contrast to the Chilean buildings, most of the medium to high-rise buildings in the United States, particularly office buildings, consist typically of walls coupled with frames.

In view of the satisfactory performance under severe earthquake loading of the Chilean buildings, a program of experimental and analytical study on scaled models of isolated walls simulating typical walls in Chilean buildings was carried out to gain further insight into their behavior. A detailed description of the program is discussed in chapters that follow.

1.4 OBJECTIVES AND SCOPE

Objectives of the reported research were:

1. To determine the effects of different staggered configurations of door openings on strength, stiffness, and deformation capacity of structural walls under reversed cyclic loadings simulating earthquake loading.
2. To compare the behavior of walls with staggered opening configurations to that of a solid wall and to draw appropriate conclusions regarding changes in stiffness and deformation capacities.
3. To compare the data obtained from these tests with that of walls tested under similar conditions and to draw necessary conclusions regarding the effects of boundary element confinement on the overall behavior of structural walls.
4. To develop an analytical model representing the observed behavior of the walls using existing techniques, with possible modifications to accommodate behavioral changes due to the presence of openings.

CHAPTER II

BACKGROUND INFORMATION

This chapter summarizes the experimental and analytical research conducted to date on isolated structural walls and structural wall systems. For clarity, the discussion that follows has been categorized on the basis of wall types because of the vastness of the topic. References for any significant research not discussed in this chapter is listed in the bibliography. Because of their wide use in tall buildings, slender walls and slender wall structural systems have been the subject of most of the recent research. A relatively limited amount of research has been reported on squat shear walls, and is briefly included in this chapter for completeness.

2.1 SQUAT SHEAR WALLS

The ultimate strength of these walls is generally governed by shear because of the low overall aspect ratio. Shear is a brittle and undesirable mode of failure; therefore, research efforts in the field of squat walls have been focussed on trying to find ways to inhibit shear failure so that flexural strength will govern.

Because of their geometric similarities, results of tests on deep beams were directly used to predict the behavior of squat walls in 1960's. Since then, however, a number of experimental investigations on squat walls have been made [8,9,10,11,15,50].

Barda et al. [8,9] in his experimental program studied the effect of various parameters on the shear strength of squat walls. The wall aspect ratio was varied from 1 to 0.25. Shear dominance of behavior was not affected by the amount of flexural

reinforcement as long as reinforcement was properly anchored to the foundation. Horizontal web reinforcement was not as effective as the vertical reinforcement in increasing the shear strength of the walls, but its effectiveness reduced as the aspect ratio increased. Both reinforcements were, however, equally effective in uniformly distributing the orthogonal crack patterns formed by reverse cyclic loading. The uniform crack distribution marginally increased the wall shear capacity.

Cardenas et al. [15] tested seven rectangular wall specimens without boundary elements which had an aspect ratio of 1.0. Shear stresses on the order of $10\sqrt{f'_c}$ psi were obtained in walls without axial load.

Paulay [50] concluded that with properly detailed web reinforcement it is possible to ensure inelastic flexural response, even though energy dissipation will be diminished by the effects of shear. For squat walls, it is advisable to design them for larger lateral load resistance in order to reduce ductility demands [45].

2.2 Isolated Slender Structural Walls

Due to their increased use as major lateral load carrying elements in medium to high-rise buildings, there has been a significant increase in the amount of experimental and analytical research on slender structural walls during the past two decades. The most comprehensive and extensive study was undertaken at the Construction Technology Labs of Portland Cement Association. The research, which initiated in 1974, concluded in 1983 and has been reported in detail in Refs. [37,39,43]. Important conclusions on specific topics based on the test results of this work have been reported in Refs.[4,20,38,40,41,42].

The primary purpose of the investigation carried out at PCA [20,41,42] was to determine the ductility, energy dissipation capacity, and strength of structural walls and to develop design criteria for walls in earthquake resistant buildings. In order to attain these

objectives, twenty-two isolated wall specimens of 1/3 scale were subjected to monotonic and reversed cyclic loadings. Controlled variables included shape of the wall cross-section, amount of main flexural reinforcement at the wall boundaries, amount of transverse reinforcement around the main flexural reinforcement, amount of horizontal shear reinforcement, axial compression, concrete strength, load history, use of diagonal reinforcement, and lap splices. Specimens were designed following the requirements of 1977 ACI Building Code. The results of the tests indicated that almost all the specimens within the range of selected parameters possessed good inelastic deformation capacity. All the test specimens sustained loading through yield of the flexural reinforcement, allowing a reinforced concrete plastic hinge to form at the base of the wall. Inelastic deformation capacity was, however, limited primarily by the following two failure modes: (i) crushing of web concrete, and (ii) combined crushing and shearing failure of compression zone concrete. In all, six different modes of failure were observed and were associated with the cross-sectional shapes of the wall specimens and the level of applied shear stress: (i) bar fracture, (ii) inelastic bar buckling, (iii) instability of compression zone, (iv) web crushing, (v) sliding shear, and (vi) boundary element crushing.

Based on the results of the PCA experimental study, recommendations on reinforcement detailing for earthquake resistant walls have been made [41]. The importance of providing sufficient confinement reinforcement in the boundary elements was emphasized. It served four primary functions: (i) increased the limiting strain capacity of concrete, (ii) supported vertical reinforcement against inelastic buckling, (iii) contained concrete after cracking, and (iv) improved shear capacity and stiffness. Test results [41] also suggested that special confinement reinforcement was needed only within the hinging region of the walls which normally extends over a height approximately equal to the horizontal length of the wall. Details on proper anchorage of horizontal wall reinforcement into the boundary elements were also recommended for improved performance of structural walls.

The experimental work at PCA was followed by development of an analytical model to predict the in-plane inelastic strength of structural walls subjected to reversed cyclic loadings [43]. Simplified analytical procedures were developed to determine the strength, inelastic deformation capacity, and failure modes for the hinging region of the shear walls. Effects of stress-strain relationships for concrete and steel, aggregate interlock, dowel action, and interaction of compressive stress and shear stress in the compressive zone were included and the analysis procedure was computerized to accurately reproduce the inelastic behavior of shear walls. A parametric study of various parameters using the developed computer program indicated that current building code requirements were overly conservative for certain combination of design parameters and unconservative for others. Improved design criteria based on the results of analytical study were proposed.

Additional analytical studies were reported to calculate the natural frequencies of isolated walls [4,38]. A mathematical model which took into account flexural and shear deformations, rotary moment of inertia, and axial loads was developed to calculate the initial natural frequencies of walls. Close agreement between calculated and measured "uncracked" fundamental frequencies from snap and hammer tests was reported. Frequencies of walls with large boundary elements were found to be particularly affected by shear deformations.

Another active center of shear wall research has been the University of California, Berkeley. A number of experimental research projects have been reported to date on hysteretic response of structural walls [24,63,65].

Hysteretic behavior of structural walls was studied and reported by testing four three-story scaled wall specimens under reversed cyclic loading [63]. Effects of shape of confinement reinforcement (spiral or hoop), shape of wall cross-section, moment-to-shear ratios, loading type, and repairing procedures on stiffness, strength, ductility, contribution of different mechanisms to the overall deformations, energy dissipation capacity, and

modes of failure were studied. Experimental work was followed by an analytical investigation in which a finite element technique was used to model the flexural deformations and a multi-linear model for shearing deformations was used to predict the wall behavior under high shear stresses.

In a related study [24], effects of amount and arrangement of wall panel reinforcement on the hysteretic behavior of structural walls were investigated. A diagonal arrangement of wall panel reinforcement resulted in an improved behavior of specimens compared to walls with the conventional horizontal and vertical bar arrangement. Results of repair and strengthening techniques were also reported. Tests on isolated boundary elements of shear wall to assess their mechanical behavior were carried out by Wagner and Bertero [65]. Results indicated that high compressive forces lead to high shear resistance accompanied by large shear stiffness.

2.3 COUPLED WALLS

Many shear walls contain one or more rows of openings, a typical example being the elevator shaft core of a tall building which provides access through door openings. In coupled walls, the main components of energy absorption and dissipation are the coupling beams. Researchers involved in the investigation of coupled wall systems have, therefore, concentrated their efforts towards improving the energy-dissipation capacity of coupling beams in order to achieve a better response of the whole system.

Significant contributions in this area have come from Paulay [47,48,49]. He tested two 1/4 scale seven-story coupled shear walls at the University of Canterbury, New Zealand. One specimen had conventionally reinforced coupling beams, while the other had beams with diagonal reinforcement. Both specimens were designed for the same ultimate load capacity. Specimens were subjected to a reversed cyclic deformation which simulated triangular loading along their heights. A sliding shear failure of all coupling

beams occurred in the specimen with conventionally reinforced beams before the coupled wall system reached its theoretical ultimate load. The specimen which had diagonally reinforced beams sustained much less damage and showed a far more ductile behavior than the former specimen, eventually failing because of lateral instability of compression wall. Tests on isolated beams with different reinforcement arrangements verified the previously obtained results [47].

The effect of weak and strong coupling beams on the overall behavior of coupled wall system was studied at the Construction Technology Labs of Portland Cement Association [57,59]. Two 1/3 scale models of coupled walls were tested under reversed cyclic loading. Under repeated inelastic load cycles the lightly coupled walls with weak beams suffered serious damage in the coupling beams before yielding occurred in the wall elements, causing the coupled walls to behave as two isolated walls in parallel. The heavily coupled system, however, behaved as a single structural element. An analytical investigation followed to simulate experimental results.

2.4 PIERCED WALLS

Wall systems pierced with openings small enough so as to not significantly affect their behavior as a single structural unit have been the subject of limited research work. Benjamin [11] found that stress concentration around corners of openings were significant. High levels of stress around corners was found to reduce wall capacity if not properly considered in design.

More recently, two 1/3 scale wall specimens, one with and the other without openings, were tested at the Construction Technology Labs of Portland Cement Association [17,58]. Openings, which were located centrally within a story level, represented windows or ducts. The openings consisted of 8.33% of the total wall area. It was concluded after comparison of responses for the two specimens that openings did not

significantly affect the behavior of a pierced wall. Both specimens exhibited large deformation and energy dissipation capacity. The results of this study could not be generalized to other opening shapes or configurations.

2.5 WALL-FRAME SYSTEM

Wall-frame systems are the most commonly used structural system for tall buildings in the United States. When walls in a structure are coupled with frames, response of each structural system is modified because of their interaction. Interaction of walls and frames has introduced another area of research involving structural walls.

A large scale seven-story frame-wall building was tested in Japan under the U.S. Japan Co-operative Research Program [44,66,69]. The building was designed in accordance with the provisions of 1979 Uniform Building Code and Japanese codes. It was concluded that if the wall-frame system is designed to keep the wall shear stresses low, reinforced concrete structural walls can offer sufficient dissipation of energy (ductile and stable hysteretic behavior) to resist the effects of extreme ground shaking through flexural yielding [1,66,69]. Following the tests on the full-scale structure, tests were carried out on scaled models of the actual structure to correlate the results of full-scale and small-scale testing [66,69]. It was concluded that overall load-deformation response of large scale components and structures can be reproduced adequately in tests of carefully designed and detailed small scale models. However, certain parameters like crack width, shear and bond effects are influenced by scale effects.

Four small-scale irregular frame-wall specimens were constructed and tested on the shaking table at the University of Illinois under a modified time history of the 1940 El Centro earthquake [34,35]. Effects of discontinuing the shear wall at different heights were studied. Continuation of the structural wall along the full height of the structure resulted in a more uniform distribution of story drifts and story shears.

CHAPTER III

EXPERIMENTAL PROGRAM

To attain the objectives outlined in Chapter 1, an experimental program consisting of testing four scaled models of reinforced concrete structural walls was formulated and carried out. This chapter discusses the experimental program in detail. Observations and discussion of results are presented in the chapters that follow.

3.1 GENERAL

The experimental program was designed to investigate the assumption that response of pierced structural walls is affected by, among other factors, the location of openings with respect to each other in two adjacent stories. Accordingly, the wall specimens involved only one variable, namely, the stagger between openings. Four structural wall specimens, namely, W-1, W-2, W-3 and W-4 were constructed and tested under reversed cyclic loading.

All four specimens had a scale factor of approximately one-fifth and represented a five-story wall. Differences and similarities between test specimens and structural walls in Almendral Building, which served as a rough prototype, are highlighted in Table 3.1. To provide an equivalent basis of comparison, specimen W-1 did not have any openings. The other three specimens were identical to W-1, but were pierced with three different configurations of staggered door openings. Figures 3.1(a) through 3.1(d) show the overall dimensions of the four specimens.

Table 3.1 : Comparison between Almendral Building And Test Specimens.

	Almendral Building	Specimen
X-Sectional Shape	U Shaped	Barbell Shaped
Height	60.2 m	140 in.
Wall Length	10.0 m	48 in.
Wall Aspect Ratio	6.0	2.9
Story Height	2.55 m	28 in.
Story Aspect Ratio	0.25	0.58
Web Reinf. Ratio (Hor)	0.004 to 0.005	0.003
Web Reinf. Ratio (Ver)	0.002 to 0.003	0.003
Boundary Element Reinf. Ratio (Longit)	0.08 to 0.12	0.03
Boundary Element Reinf. Ratio (Trans)	0.0	0.004
(Opening/Wall) Area	7.55%	13.4%
Lintel Beam Depth	0.45 m	8 in.
Angle Between Corners	32 deg.	32 deg., 45 deg., 62 deg.

Section 1.3 stated some characteristics typical of Chilean buildings. A special effort was made to faithfully represent as many of these characteristics and other typical Chilean construction practices as possible in coming up with a final design of test specimens. Common Chilean construction practices have been discussed in the following section whenever they have been adopted for the test specimens. Most requirements of the 1988 Uniform Building Code [25] were satisfied by the final design of the specimens; however, a few were deemed to be inappropriate for scaled models and were not met. The following section discusses the design of specimens in greater detail.

3.2 Design of Specimens

The design procedure for a scaled model which is not based on a specific prototype is entirely different from that for any other structure, model or prototype. Unlike the usual case when a prototype structure is designed and scaled down to a size which represents its overall behavior, design of a scaled model not representing a particular prototype is governed by several factors. A final choice from amongst several cases satisfying the limitations of testing facilities must be made in order to achieve the sought objectives.

For the test series reported herein, the following two factors played the most important role in selecting the specimens' overall dimensions: (a) available testing facilities, and (b) faithful representation of walls in Chilean buildings. Testing facilities in the Structural Lab at the University of Michigan include a structural floor and reaction walls. The structural floor comprises of a square pattern of bolt pads spaced at 4 feet on centers. Each pad is used to fix test specimens to the structural floor through four $1\frac{1}{4}$ inch diameter steel bolts spaced at 8 inches on centers. A similar pattern of bolt pads exists on the reaction walls.

As all the Chilean buildings under investigation were in medium to high-rise range, a high value of overall aspect ratio (height to width ratio) of their component walls

classified them as slender walls dominated by flexural behavior. Hence, maximization of overall aspect ratio of the specimens was the main factor in selecting their width, after the height had been chosen. The specimen overall aspect ratio of about 3.0 was much smaller than that of the Chilean buildings' walls, but was large enough to ensure a flexurally dominated behavior. Selection of the final cross-sectional shape and reinforcement ratio was basically governed by the maximum capacity of 50 kips of the available hydraulic actuator. A nominal flexural strength of about 30 kips was sought from a section in order to ensure that complete failure may be achieved. A concrete strength of 5000 psi, reinforcement yield strength of 60 ksi without strain hardening and a linear strain distribution across the section were used to get the axial load vs. moment relationships for several sections. The moment capacity of these sections was checked as one criterion for selection for an axial compressive stress between 300 to 400 psi, a value typical in Chilean walls.

The cross-section of the specimens finally selected for the series of tests is shown in Fig. 3.2. The axial load vs. moment interaction diagram for the same section is given in Fig. 3.3. The final reinforcement ratio, both for boundary elements and the web, was lower than that in the Chilean walls. This lower reinforcement ratio, which was dictated by the lower wall aspect ratio, was selected to ensure good inelastic flexural behavior and to avoid a premature shear failure.

3.2.1 Code Requirements

Building Codes are basically formulated for full-scale structures. Hence, many code requirements which specify absolute quantities rather than proportions become inappropriate and impractical when applied to scaled models. In such circumstances it is common practice to scale the absolute requirements down to a level compatible with the model's scale before applying it.

The specimens tested in this test series had a scale factor of approximately one-fifth. It was, therefore, not possible to satisfy a few of the 1988 UBC [25] requirements. Section numbers used to check the design requirements for the specimen in the following paragraphs refer to the 1988 Uniform Building Code [25].

The boundary element longitudinal reinforcement ratio of 3.1 percent satisfies the code requirement of Sec 2625(f)3 for seismic design. However, the transverse reinforcement requirement of A_{sh}= 0.025 sq. in./leg/in. calculated in accordance with Sec 2625(e)4 for seismic design was not met. The transverse reinforcement of $\frac{3}{16}$ in. diameter hoops at 2.5 in. on centers constituted an A_{sh} of 0.011 sq. in./leg/in. As less serious damage was anticipated above the second story level, transverse reinforcement spacing was increased to 5 in. on centers above that level, which violates the code specified maximum spacing of 4 inches.

The minimum web reinforcement ratio requirement of Section 2625(f)2 of 0.0025 was satisfied by providing No. 2 bars at 6 in. on centers horizontally and vertically for a reinforcement ratio of 0.0027. Because of the non-availability of deformed bars in size No. 2, plain bars were used; thus, violating the requirements of Sec. 2603(f)2. Requirement of Sec 2625(f)2B for providing at least two curtains of web reinforcement was also violated. Figures 3.4(a) and 3.4(b) show photos depicting arrangement of reinforcement in walls W-1 and W-3, respectively.

To prevent the occurrence of premature cracking due to load transfer at the top, the fifth story level was strengthened by providing extra reinforcement. Web reinforcement spacing was reduced to 2 in. on centers in both directions, longitudinal boundary column reinforcement was doubled and the spacing of transverse reinforcement was reduced to 2 in. on centers. A detailed description of load transfer setup is given in Section 3.4. Pictures showing the extra reinforcement in the fifth stories of W-1 and W-3 are shown in Figs. 3.5(a) and 3.5(b), respectively.

3.2.2 Special Reinforcement Details

Unlike wall W-1, which had no openings, the other three walls required special reinforcement details, especially around openings. Locations of horizontal and vertical bars were readjusted in the unpierced portions of the walls to provide a fairly uniform mesh distribution. Reinforcement interrupted by openings was distributed equally on each side of the opening following standard Chilean practice. Pieces of 18 inch long $\frac{3}{16}$ in. diameter bars were tied at an inclination of 45 degrees around the corners of openings, also following common practice in Chile. The effect of a lintel beam and/or slab was reproduced by increasing horizontal reinforcement between floor levels. Typical wall reinforcement details in elevation and cross-section are shown in Figs. 3.6(a) - 3.6(d).

3.3 Construction Procedure

Construction of specimens was completed in two phases. First phase involved construction of base blocks and the second consisted of erection of walls. The two phases are discussed in detail in this section.

3.3.1 Construction of Base Blocks

The purpose of base blocks was to provide a stiff foundation for the specimens. The base blocks were, therefore, heavily overdesigned to provide this stiffness. The blocks were 18 in. wide and 24 in. deep in cross-section as shown in Fig. 3.7.

Two sets of $\frac{3}{4}$ in. thick plywood forms were used to cast the blocks. Because all of the vertical wall reinforcement was to be embedded into the base blocks, strain gages were applied to the bars before erecting them for casting. Thin plywood templates having

proper size cut outs were used at the top and bottom of the forms to hold the vertical bars firmly in their proper locations.

It was intended to simulate a "fixed end" condition at the base of the wall by bolting the blocks to the floor. Two bolt pads were to be used for this purpose. Pieces of $\frac{1}{8}$ in. thick PVC pipes with an inner diameter of $1\frac{1}{8}$ in. were used to make the holes for the bolts. These pipes were also held upright by thin plywood templates at top and bottom which prevented any movement during casting operation.

The base block was also utilized to anchor one end of the prestressing strands which were to be used to apply axial load to the specimen during the test. Resistance to strand pullout was provided by attaching strand chucks and 2"x 2" x 1/2" steel plates on the anchored ends of the strands. Strands were placed approximately 6 in. from the outermost longitudinal reinforcement bar for the boundary element. Figure 3.8 shows a photograph of base blocks ready to be cast.

Concrete for the base blocks was ordered from a commercial plant. Blocks for specimens W-1 and W-2 were cast in January, 1988 and those for W-3 and W-4 in June, 1988. Average concrete strength for both batches was 6500 psi. A construction joint was made by roughening up the top surface of the blocks at the intended wall location. Forms were removed after five days.

3.3.2 Design Mix for Walls

Several mixes were tried before finalizing the mix to be used. The objective was to achieve the desired strength of 5000 psi, while maximizing the workability. Good workability was considered essential when casting the deep thin wall sections in order to allow good compaction and reduce the formation of voids and honeycombs. A water-to-cement ratio (by weight) of 0.55 was selected. Crushed limestone with a maximum aggregate size of $\frac{3}{8}$ in. was used in the proportion of 0.8:1.0 with common sand.

Table 3.2 : Quantities for Design Mix

Volume of Mix	Water, lbs.	Cement, lbs.	Coarse Aggregate, lbs.	Sand, lbs.	Water/Cement Ratio	C.A./Sand Ratio
1 Cu. Yd.	385	702	1242	1571	0.55	0.79
5 Cu. Ft.	71.3	130.0	230.0	291.0	0.55	0.79

Table 3.2 shows the amount of materials for a cubic yard of mix. During the numerous castings the measured slump varied from 6.5 in. to 9 in. with an average value of 8.5 in.

3.3.3 Construction of Walls

Each wall was cast vertically in five lifts, each lift representing one story. Although only one story was cast per batch, two sets of forms were used to speed up construction. The forms were made 12 in. longer than the 28 in. story height of the wall. After the first story had been cast, this extra length was attached to the story below before casting the next story. As each set of forms was to be used ten times, it was expected that wall cross-section would be affected by the gradual deterioration of the forms as the plywood grows older. To control this problem three rows of equally spaced holes were drilled in the web portion of the forms. These holes were then connected across the wall by six inch long pieces of $\frac{1}{4}$ in. diameter threaded rods (form ties). A constant web thickness of three inches was maintained by adjusting the nuts on either ends of the form ties. These ties were left to be cast in concrete. The top row of these ties for each story was also used to support the forms when casting the next story. Plumb lines and carpenter's levels were used to ensure the vertical erection of walls. Three inch thick styrofoam pieces cut to the size of openings were used to block out the openings.

Wall construction was started on June 17, 1988 and the last pour was made on Sept. 2, 1988. Approximately five cubic feet of concrete was mixed for each batch using an electrically powered six cu. ft. capacity mixer. Forms were stripped after three days. Figures 3.9 and 3.10 show different stages of construction.

3.4 TEST SETUP

All specimens were bolted to the floor using two bolt pads and tested vertically. Figure 3.11 shows a schematic diagram of the general test setup. Special features of test setup are presented in detail in the following sections.

3.4.1 Load History

A one point lateral load was applied at the top through a 50-kip capacity hydraulic actuator. Loading was displacement controlled throughout the tests. Each displacement cycle was repeated once before increasing the drift level to the next higher value. An increment of 0.25 percent of total height was used until 1.0 percent was reached; thereafter, the increment was increased to 0.5 percent. Figure 3.12 shows the loading history used for all the tests.

3.4.2 Lateral Load Transfer Assembly

Lateral load was transferred from a steel beam to the specimen at four locations. The same load transfer beam was used for all four specimens. It consisted of two six ft. long pieces of 12 in. deep steel channels welded together in a back-to-back position with a 0.75 in. gap, using tie plates at the top and bottom (Fig. 3.13). A 1.5 in. thick vertical plate welded to one end of the assembly was used to provide a connection to the actuator.

Connection between the beam assembly and the specimen was provided through two vertical and two horizontal rods. Vertical threaded rods of $1\frac{1}{8}$ in. diameter were embedded 18 in. into the boundary elements of each specimen. Portions of the webs of the beam assembly were cut out to accommodate the vertical rods. Also, two pairs of

vertical saddle plates with a $1\frac{1}{8}$ in. diameter hole in the center were welded to the load transfer beam (Fig. 3.13). These holes aligned with holes of same size that were cast in specimens' webs and 1.0 in. diameter horizontal rods were fit through. These rods were threaded at both ends and nuts were used to secure them in place. Figure 3.14 shows the beam assembly attached to the specimen.

3.4.3 Axial Load System

An axial load of approximately 60 kips, which corresponded to a compressive stress of 365 psi, was kept constant throughout the test. The load was applied through a pair of half-inch diameter 7 wire prestressing strands which were anchored in the base block, as previously explained in Sec. 3.3.1. As shown in Fig. 3.15, the steel load transfer beam at the top supported the hydraulic jack and strand chuck assemblies which were used to stress the strands. The pressure in the hydraulic lines was maintained at the desired level by manually adjusting the pump valves. A dial gage indicated the pressure in each hydraulic line. A more accurate measurement of axial force was, however, taken at selected points throughout the tests using a pair of load cells. A more detailed description of load cells is given in Section 3.5.3.

3.4.4 Lateral Support

An increased cross-section of boundary elements was meant to provide lateral stability against out-of -plane buckling. However, slenderness of the wall specimens and anticipated softening at the base during large displacement cycles called for provision of a system that would ensure an in-plane application of load at all times. A stiff steel frame adjacent to the test setup was used to seek the required lateral support. A linear bearing assembly which constrained movement in one (horizontal) direction parallel to the

specimen was attached to the steel frame. Connection between the linear bearing assembly and the load transfer beam was provided by bolting two 6 inch deep steel I-beams at two points along the same height. The connection points, two feet apart horizontally, were located 6 in. from the top of the load transfer beam, thus aligning them with the point of load application. This alignment ensured the in-plane application of load throughout the test. The connections were designed not to restrain any vertical movement which might result due to flexural rotation during large displacement cycles. Figure 3.16 shows the lateral support assembly.

3.5 INSTRUMENTATION

The first story of each specimen was instrumented more extensively because major inelastic action was expected to occur in that region. Internal instrumentation consisted of strain gages while displacement transducers and load cells comprised external instrumentation.

3.5.1 Strain Gages

Strains in reinforcing bars were measured by strain gages. These gages were installed on the bars at locations shown in Figs. 3.6(a) - 3.6(d). Standard procedures for application of gages was followed.

3.5.2 Displacement Transducers

A total of seven displacement transducers (potentiometers) were used to measure the displacements at different points. Two displacement transducers, each with a maximum travel length of 9 inches, measured the axial displacement of boundary elements

in the first story level. These were attached to the wall at a point 28 in. from the base, thus providing a gage length equal to the story height.

The displacement profile of the wall was measured with five displacement transducers, one at each floor level. A wooden frame with five platforms at proper locations was erected to mount these displacement transducers.

Half-inch thick aluminum target plates with a threaded hole in their center were epoxied to the specimen W-1 and provided a positive connection between the displacement transducers and the specimen. During the first test some targets were pulled off the wall as the displacement transducer rods got flexed and stressed as a result of bending action in the wall. Springs were attached to the rods of the affected displacement transducers and their readings were adjusted for the remainder of the test. This problem was, however, resolved for the remaining three tests by replacing the positive connection between the specimen and displacement transducers with a sliding connection. This was done by attaching springs to the rods of displacement transducers, enabling them to rebound after being compressed, and by replacing the aluminum targets with smooth plexiglass, thus facilitating free movement.

3.5.3 Load Cells

Two load cells were used to measure the axial force applied by the hydraulic jacks. Each cell consisted of a solid 2 in. steel cube with 5"x 5"x 1/2" steel plates welded onto opposite sides to provide a larger contact area. A hole drilled through the center of the assembly provided room for passage of a strand. Two full-bridged strain gages installed on the cube measured the resulting strain due to applied axial load. Cells were calibrated for the desired range of axial load.

3.5.4 Data Acquisition System

All the instrumentation described in the previous three sections was connected to a low-speed HP 3497A data acquisition system. Readings for each data point from each channel were stored on a tape cartridge and later transferred to floppy disks. In addition, readings from selected channels were printed instantaneously to monitor the progress of tests. A continuous plot of actuator load vs. displacement was also recorded for each specimen. In order to reproduce the response realistically, at least twelve data points were recorded during each full cycle of displacement reversal.

A complete photographic record of all tests was maintained using color slides, color prints and black and white prints. In addition, video recordings of selected portions of tests were also done.

3.5.5 Vibration Tests

Four vibration tests to measure the frequency and damping characteristics were conducted on each wall specimen. Each test consisted of measuring these characteristics in the two principal directions. Two of the tests were conducted on the specimen in its undamaged state, while the remaining two were performed after the test had been completed. Of the two vibration tests performed in each state, one was conducted without the axial stress and the other was performed with the axial load.

All the vibration tests were forced vibration tests. The specimen was excited with a blow using an 8-lb. hammer. Induced vibrations, sensed by a transducer placed at the top of specimen, were recorded graphically by Soltec Lumigraph 5F15 Oscillographic Recorder. Steel beam assembly was bolted to the top of the wall before the start of each

test. Lateral supports and actuator were disconnected from the specimen before running the test so that the specimen could vibrate freely after excitation.

3.6 MECHANICAL PROPERTIES OF MATERIALS

Mechanical properties of concrete and reinforcing steel are presented in this section.

3.6.1 Concrete

As mentioned in Section 3.3, a total of 20 batches of concrete were made. A mixed volume of five cubic feet for each batch provided enough concrete to cast one story level, six 12"x 6" cylinders and two 6"x 6"x 20" beams for flexure tests.

All cylinders and flexure beams were cured in accordance with ASTM specifications. Of the six cylinders that were cast, two were tested for compressive strength at 28 days, two were tested for split cylinder strength at 28 days and the remaining two were tested for compressive strength on the specimen test dates. Flexure beams were tested under two-point loading for Modulus of Rupture at 28 days.

For each property, an average of two values for each story level of each specimen was taken and the mean value for the specimen represents an average of these five values. Table 3.3 gives these values for each specimen. Figure 3.17(a) - (d) shows the variation of compressive strengths for specimens W-1 through W-4 respectively. Split cylinder strength and Modulus of Rupture values are graphically presented in Figs. 3.18 and 3.19 respectively. Representative stress-strain relationships were obtained by graphically recording the test results for compressive strength of selected cylinders. This relationship

Table 3.3 : Concrete Material Properties

		f'_c psi.			Split Cylinder Strength, psi.	Modulus of Rupture, psi.
		28 days	Age at Test (days)	On Test Date		
W-1	Story # 1	4650	172	4670	389	887
	Story # 2	5380	160	4440	418	815
	Story # 3	4150	146	4370	440	739
	Story # 4	5330	124	5320	442	939
	Story # 5	5210	104	5980	391	857
	Specimen	4940	141	4960	416	847
W-2	Story # 1	5090	181	4440	382	830
	Story # 2	4110	167	5250	495	781
	Story # 3	4530	154	4620	433	816
	Story # 4	4540	132	5520	431	775
	Story # 5	5210	113	4320	382	878
	Specimen	4690	149	4830	425	816
W-3	Story # 1	4700	189	5020	447	771
	Story # 2	5200	181	5640	416	827
	Story # 3	5080	174	5360	462	749
	Story # 4	5000	167	5090	331	884
	Story # 5	3960	145	4690	314	841
	Specimen	4790	171	5160	394	814
W-4	Story # 1	4490	205	5080	453	841
	Story # 2	5240	194	5180	380	857
	Story # 3	5130	188	5900	365	842
	Story # 4	5190	180	5450	380	824
	Story # 5	4730	152	4690	469	897
	Specimen	4960	184	5260	409	852

is reproduced in Fig. 3.20.

3.6.2 Reinforcing Steel

Reinforcing bars of three different sizes were used. Deformed No. 4 bars were used as longitudinal reinforcement in the boundary elements. Plain No. 2 bars were used for the horizontal and vertical web reinforcement. Knurled $\frac{3}{16}$ in. diameter bars were used as transverse reinforcement in boundary elements.

Four 20 in. long pieces of each bar size were tested for tensile strength. Results shown in Figs. 3.21-3.23 represent plots of stress vs. normalized head displacement. Because of slippage between the bar and the grip holding it during the tensile test, head displacement readings recorded from the testing machine did not represent the actual extension of bar. Applied load, however, was displayed accurately. The plots in Figs. 3.21 to 3.23 are, therefore, presented only to show the general behavior of reinforcing steel under tension.

The values of yield strain tabulated in Table 3.4 were calculated by using the measured yield stress and an assumed modulus of elasticity value of 29000 ksi.

Although the specified yield strength for all bars was 60 ksi, results of tensile tests show a higher value for all of them. Only the No. 4 bar, however, showed a clear yield plateau and exhibited strain hardening.

Table 3.4 : Material Properties for Reinforcing Steel

	Yield Stress, f_y ksi	Young's Modulus ksi	Yield Strain, ε_y in./in.
#4 Bar	78.4	29000	0.0027
#2 Bar	81.5	29000	0.0028
3/16" Bar	90.0	29000	0.0031

CHAPTER IV

EXPERIMENTAL RESULTS AND DISCUSSION

This chapter presents in detail experimental observations, results and discussion of tests of the concrete wall specimens. For clarity, the chapter has been divided into two main parts. Observed behavior during the series of tests has been presented in the first part. Presentation of results and discussion comprises the second part of the chapter. It may be emphasized here that important events as they occurred during the tests are merely stated in a 'general' sense in the section on observed behavior and their detailed explanation has been left to the sections that follow.

4.1 OBSERVED BEHAVIOR

As mentioned earlier in Chapter 3, each specimen was loaded axially and then subjected to reversed cyclic loading according to the loading history shown in Fig. 3.12. Two cycles at each new displacement level were applied. In the discussion henceforth, odd numbered cycles represent a new displacement level and even numbered ones represent the repeat cycle.

The following convention correlates the displacements shown in photographs to those in the figures and text of this document:

- Displacement in the east direction is taken as positive displacement.
- Lateral force causing positive displacement (i.e. in the east direction) is taken as positive.

Peak drift levels, load values and induced shear stresses for each cycle are tabulated in Tables 4.1 to 4.4 for specimens W-1 to W-4 respectively. Shear stresses for Specimen W-1 in Table 4.1 are calculated based on the gross cross-sectional area of 164 sq. in. of the wall. A net cross-sectional area of 137 sq. in has been used for the remaining three specimens in Tables 4.2 to 4.4.

4.1.1 Specimen W-1

The complete top lateral load vs. top lateral displacement relationship for specimen W-1, reproduced from the recorded data points at discrete displacement intervals, is shown in Fig. 4.1.

During cycles 1 and 2, a number of almost equally spaced flexural cracks originated in the boundary columns of lower two stories during the first cycle and as the peak displacement was reached, these cracks had penetrated into the web portion inclining as they grew at an angle of approximately 20 degrees with the horizontal. Repeat cycle 2 at the same drift level resulted in formation of similar cracks in the third story level but these were confined to the boundary columns only. No major extensions to the cracks in the lower stories were, however, observed for the repeat cycle.

Cycles 3 and 4 represented a top level drift of 0.5 percent. Flexural cracks initiated in the previous cycles became steeper as they grew, transforming into flexural shear cracks. A flexural crack, which had initiated in cycle 1 and had grown in the repeat cycle along the construction joint between first and second stories, traversed across the width of the wall in cycle 3. It opened further in cycle 4 and some sliding was observed along the joint. Cycle 4 also saw the cracking zone extend to story level 4. Most previously formed cracks widened in cycle 4. Lateral displacement transducers at levels 1 and 3 malfunctioned as the target aluminum discs epoxied to the specimen pulled off. Springs were attached to the transducer shafts and necessary adjustments were made to record the

Table 4.1: Loads, Top Displacements and Induced Shear Stresses in Specimen W-1

Cycle No.	Top Displacement		Initial Cycle				Repeat Cycle			
	inches	% of height	East		West		East		West	
			Load (kips)	Shear Stress $\sqrt{f'_c}$ (psi)	Load (kips)	Shear Stress $\sqrt{f'_c}$ (psi)	Load (kips)	Shear Stress $\sqrt{f'_c}$ (psi)	Load (kips)	Shear Stress $\sqrt{f'_c}$ (psi)
1 and 2	0.36	0.25	18.8	1.62	16.5	1.43	18.8	1.63	15.9	1.37
3 and 4	0.72	0.50	25.2	2.18	22.7	1.97	24.2	2.09	22.6	1.95
5 and 6	1.08	0.75	31.5	2.73	29.3	2.54	30.6	2.65	27.9	2.41
7 and 8	1.44	1.00	33.9	2.94	31.3	2.71	33.6	2.91	30.1	2.61
9 and 10	2.16	1.50	34.9	3.03	31.7	2.74	35.3	3.05	32.8	2.84
11 and 12	2.88	2.00	35.0	3.03	33.3	2.89	34.5	2.99	32.9	2.85
13 and 14	3.60	2.50	36.1	3.13	35.2	3.05	34.9	3.02	32.4	2.80
15	4.32	3.00	35.0	3.03	32.4	2.80	-	-	-	-

f'_c = 4.94 ksi.

Shear Stress based on gross cross-sectional area (164 sq. in.)

remaining data points. Figure 4.2 shows crack patterns at a displacement of 0.72" west (cycle 3).

During cycles 5 and 6 almost all cracks had transformed into flexural shear cracks inclined at an angle of 45 degrees with the horizontal. Cracks in the upper stories grew steadily with each new displacement level while the ones in the lower stories opened up more with each additional cycle. The widest diagonal crack in the first story was measured to be 0.025 inch wide in cycle 5 and opened up to 0.040 inch in the repeat cycle 6. Sliding at the joint between the first and second stories was measured to be 0.030 inch in cycle 5.

An average load of 32.2 kips representing a shear stress of $2.8\sqrt{f'_c}$ was sustained by the specimen in cycles 7 and 8. Cracks at the base of the wall were observed for the first time during cycle 7. Two major diagonal cracks could clearly be observed to be opening up more than the other cracks. Sliding at the construction joint at level 1 had also increased and was measured to be 0.05 inch during cycle 8. During the same cycle the widest diagonal crack was measured to be 0.06 inch in width. Figure 4.3 shows the specimen during cycle 8 at top displacement of 1.44" west. A comparison with Fig. 4.2 does not indicate any significant deterioration in terms of formation of additional cracks, even though the displacement has been doubled. What the camera could not capture was the widening of major cracks, and, hence, is not noticeable in Fig. 4.3.

The next peak displacement level represented an increase of 0.5 percent. Some major events were expected as the drift level of 1.5 percent was approached. Formation of diagonal struts carrying compressive forces could be clearly noticed in the upper stories of the wall. Parallel diagonal cracks shown in Fig. 4.4 for each loading direction outlined these struts. Some cracks were disrupted at construction joints between story levels, and after traversing along the joints horizontally, were redirected in a direction parallel to the crack above the disruption. No additional sliding along the construction joint between first and second stories was observed. Minor crushing of the east boundary column initiated at

a displacement level of 1.80 in. during cycle 9 and cover concrete started spalling during the subsequent repeat cycle (Figs. 4.5 and 4.6). No discernable crushing was, however, noticed in the west boundary column.

The specimen was next cycled at a peak displacement of 2.88 in. An average load of 33.8 kips, which was almost identical to that of previous two cycles, was required to achieve this displacement level. A number of diagonal cracks widened during cycles 11 and 12. The width of the widest diagonal crack was measured to be 0.12 in. at this stage. West boundary column showed signs of crushing in cycle 12. It had become quite clear that the energy input into the specimen was mainly being absorbed by widening of cracks and by the plastic deformation of the reinforcing bars (induced greatly by the opening of cracks). The lateral displacement transducer at level 4 malfunctioned and was reinstalled after being repaired.

An almost identical average maximum load of 33.9 kips was sustained by the specimen during cycles 13 and 14. Shear deformations continued to increase, but plastic flexural deformations were still predominant. No dramatic events occurred during these cycles. The main diagonal crack in the first story level had opened to a width of 0.2 in. This crack is clearly visible in the photograph taken at a 3.60 inch displacement (in the west direction) shown in Fig. 4.7.

The specimen was finally subjected to one complete cycle at 3.0 percent drift level before the test was completed. The actuator had reached its maximum travel limit. Fig. 4.8 shows the general view of the specimen during the fifteenth cycle Open cracks are quite visible in the photograph. No additional damage was observed during this last cycle.

An axial load of approximately 60 kips was maintained throughout the test. As pumps were monitored manually, the load was not exactly 60 kips at all times, and an effort was made to keep the deviation within reasonable limits. The variation of axial load is plotted in Fig. 4.9. The large displacement levels which were achieved during this test resulted in more loading and unloading of axial load cables than in the other three tests.

Overall, a satisfactory flexurally dominated response was obtained from specimen W-1. Damage was moderate (i.e. crushing and spalling of concrete), and the specimen was able to sustain the peak load till the end of the test.

4.1.2 Specimen W-2

The complete top lateral load vs. top lateral displacement relationship for specimen W-2, reproduced from the recorded data points at discrete displacement intervals, is shown in Fig. 4.10.

Specimen W-2 was the first of the three specimens with openings to be tested in this experimental program. The horizontal stagger of 15 in. was the largest among the three pierced walls. Because the openings were close to the wall edges, a lower maximum top drift level, as compared to W-1, was expected for specimen W-2.

First cycle resulted mainly in the formation of horizontal flexural cracks in the boundary columns. Two steep diagonal cracks originated from the lower corner of the openings in the third and fifth levels during the second half of the first cycle. By the end of the cycle, flexural cracks had penetrated into the web and had re-oriented along a 30 degree angle with the horizontal. A horizontal crack had traversed over the specimen length along the construction joint at level 1.

Several new cracks were formed during cycles 3 and 4. Diagonal cracks originating from the corners of the openings for loading in each direction were more noticeable at this stage of the test. Fig. 4.11 shows the lower portion of the specimen during cycle 4. Unlike specimen W-1 at this stage of loading, cracks were not limited to the lower two stories. Diagonal cracking had extended up to the fourth story level for W-2 as shown in Fig. 4.12. Cracks formed during the previous displacement level became more inclined as they progressed during cycles 3 and 4. No appreciable widening of cracks was, however, observed.

Table 4.2: Loads, Top Displacements and Induced Shear Stresses in Specimen W-2

Cycle No.	Top Displacement		Initial Cycle				Repeat Cycle			
	inches	% of height	East		West		East		West	
			Load (kips)	Shear Stress $\frac{}{\sqrt{f'_c}}$ (psi)	Load (kips)	Shear Stress $\frac{}{\sqrt{f'_c}}$ (psi)	Load (kips)	Shear Stress $\frac{}{\sqrt{f'_c}}$ (psi)	Load (kips)	Shear Stress $\frac{}{\sqrt{f'_c}}$ (psi)
1 and 2	0.36	0.25	13.4	1.40	17.4	1.83	13.4	1.41	17.4	1.83
3 and 4	0.72	0.50	20.6	2.16	24.0	2.52	20.6	2.16	24.2	2.54
5 and 6	1.08	0.75	27.2	2.86	30.8	3.23	25.9	2.72	29.8	3.13
7 and 8	1.44	1.00	31.3	3.29	34.1	3.58	30.0	3.15	34.1	3.58
9 and 10	2.16	1.50	34.3	3.61	37.8	3.97	24.2	2.54	37.1	3.89
11	2.88	2.00	19.2	2.02	37.4	3.93	-	-	-	-

f_c' = 4.83 ksi.

Shear Stress based on net cross-sectional area (137 sq. in.)

No new major cracks were observed in cycles 5 and 6. Existing cracks extended further and almost all diagonal cracks had traversed across the portion of the web between the two rows of openings. The main cracks in the first story level started to open up during cycle 5 and the width of the widest diagonal crack was measured to be 0.030 in. The crack along the construction joint at level 1 opened to 0.025 in. in width. No significant sliding, however, was observed.

In cycles 7 and 8, average load in the east direction reached a value of 30.6 kips. In the other direction, the average value was 34.1 kips. Diagonal cracks in the upper stories grew longer, although at a much slower rate than in the initial stages. The main diagonal crack in the first story level had opened up more and was measured to be 0.050 in. wide in cycle 7. By the end of cycle 7, diagonal cracks, especially in the lower two stories, had stretched across the web. Some of these cracks traversed uninterrupted between the gap that existed between the two rows of openings. Compression struts, thus formed, are more detectable in Fig. 4.13 than in the upper levels (Fig. 4.14). Some cracks forming the struts were interrupted by the construction joint, but others continued across the joint.

The next two cycles (cycles 9 and 10) represented a top drift level of 1.5 percent. Till the end of cycle 8 no crushing had been observed. During the first half of cycle 9 some major damage to the east portion of the wall occurred and is described in detail here. The specimen had carried a maximum load of 33.9 kips in the east direction at a drift level of approximately 1.35 percent when an inclined crack, which seemed to originate from the top east corner of the opening in the first story, opened up and penetrated into the boundary column (Fig. 4.15). This was accompanied by crushing of the east boundary column and spalling of the cover as shown in Fig. 4.16. The peak load dropped by 25 percent to 25.7 kips. The east boundary column and part of the web which were isolated and left unconfined by the location of opening, finally crushed under increasing displacement. Loading in the west direction did not cause any additional damage to the

specimen and a maximum load of 37.8 kips, corresponding to a shear stress of $4.0\sqrt{f'_c}$, was recorded. Repeat cycle 10 caused additional spalling of concrete in the east boundary column. A load of 24.2 kips was resisted by the specimen in the east direction for this cycle. An identical load of 37.8 kips was recorded in the west direction for cycle 10. No crushing in the west boundary column was evident.

The east boundary column of W-2 had essentially failed during cycle 10, so the next top displacement increment to 2.0 percent drift was anticipated to be the final one. Maximum load in the east direction dropped to 19.2 kips for cycle 11. Crushing was observed on the west edge of the opening and is shown in Fig. 4.17. Further crushing of the web along the east boundary column and spalling of concrete had made the damaged region increasingly unstable. The boundary column longitudinal reinforcement and the vertical web reinforcement bars around the opening which were exposed and started to buckle as the peak drift level was approached (Fig. 4.18). At this point the axial load in the east cable also started to drop as the boundary column was unable to sustain the applied load. The load was reversed to complete the remaining half of 11th cycle. The wall sustained a load of 37.4 kips and still showed no signs of crushing in the west portion. The behavior was very stable for this half of the 11th cycle. In view of the unstable condition of the east boundary column, it was decided not to continue the test any further.

The axial load during this test was kept within reasonable deviation from the target value of 60 kips. The variation plotted in Fig. 4.19 shows the scatter from the target value of 30 kips for each cable. The major deviations occurred during the last three cycles when the east boundary column started deteriorating and relieving the east axial load cable.

A satisfactory response up to a drift level of 1.0 percent was achieved from specimen W-2. The large horizontal stagger between the openings led to a reduction of available compression area near the east boundary column. Furthermore, the opening also

eliminated the confinement provided to the available compression zone, thus permitting a shear compression failure.

4.1.3 Specimen W-3

The complete top lateral load vs. top lateral displacement relationship for specimen W-3, reproduced from the recorded data points at discrete displacement intervals, is shown in Fig. 4.20.

Specimen W-3 had openings staggered 8 in. apart horizontally. Since the vertical spacing between the openings (which was kept constant for all pierced specimens) was also 8 in., the resulting angle of 45 degrees between inner corners of openings at adjacent levels was identical to the expected angle of inclination of shear cracks.

Unlike specimen W-2, load resisted by this specimen in east direction was on average, more than that in the other direction. As expected, diagonal cracks traversing between corners of openings were observed during cycle 1 in the first three stories. Some horizontal cracks which initiated during the first cycle, penetrated into the web region during repeat cycle 2. Figure 4.21 shows these cracks during the second half of cycle 2.

Flexural cracking zone extended into the third story level as several new flexural cracks initiated during the third cycle. These turned to flexural shear cracks as they progressed at an inclination of 45 degrees within the web. No further extensions to these cracks were observed during repeat cycle 4. The width of the widest diagonal crack in the first story at this stage of the test was 0.016 in.

A few diagonal cracks extended further and traversed across the web in cycle 5. Other diagonal cracks closer to the base started to open up during cycle 6. The width of the widest open crack was measured to be 0.040 in. Some small cracks had formed in the earlier cycles along the construction joint at levels 1 and 2, but no further cracking along joints was observed. As compared to the conditions of joints at the same stage of test for

Table 4.3: Loads, Top Displacements and Induced Shear Stresses in Specimen W-3

Cycle No.	Top Displacement		Initial Cycle				Repeat Cycle			
	inches	% of height	East		West		East		West	
			Load (kips)	Shear Stress $\frac{}{\sqrt{f'_c}}$ (psi)	Load (kips)	Shear Stress $\frac{}{\sqrt{f'_c}}$ (psi)	Load (kips)	Shear Stress $\frac{}{\sqrt{f'_c}}$ (psi)	Load (kips)	Shear Stress $\frac{}{\sqrt{f'_c}}$ (psi)
1 and 2	0.36	0.25	18.0	1.83	16.0	1.63	18.0	1.83	14.8	1.50
3 and 4	0.72	0.50	24.6	2.50	22.0	2.23	24.6	2.50	21.8	2.21
5 and 6	1.08	0.75	30.8	3.13	28.8	2.93	29.9	3.04	27.4	2.99
7 and 8	1.44	1.00	34.4	3.49	30.5	3.10	33.4	3.40	31.1	3.16
9 and 10	2.16	1.50	36.1	3.66	33.4	3.40	21.5	2.18	32.4	3.29
11	2.88	2.00	8.7 *	0.88	31.8 *	3.23	-	-	-	-

f'_c = 5.16 ksi.

Shear Stress based on net cross-sectional area (137 sq. in.

* For maximum top displacement of 2.25 in.

the first two specimens, construction joints in W-3 were in much better shape. The general crack pattern during the first half of cycle 6 in the lower half of the specimen is shown in Fig. 4.22.

Cycles 7 and 8 represented a top drift level of 1.0 percent. No new major cracks were observed. Cracks near the base opened up more during this cycle, while those in the second story level extended slightly. Signs of concrete crushing at the base of the east boundary column were first observed in cycle 8 (Fig. 4.23). A crisscross pattern of flexural shear cracks can be observed in the upper stories of W-3 in Fig. 4.24, as was seen in W-2 at this stage. The only difference was the interruption of those cracks caused by the new location of openings in W-3. This configuration of openings interrupted the formation of some compression struts.

An identical series of events to those of the previous test occurred in cycle 9 of this test. During the first half of cycle 9, the specimen carried a maximum load of 36.0 kips. But, as the maximum drift was approached, a shear compression crack which was similar in nature to that in W-2 opened up in the web and penetrated into the east boundary column at an approximate drift level of 1.4 percent. This was accompanied by a 23 percent drop in the load carrying capacity of the specimen. As can be seen in Fig. 4.25, this crack can be traced back to the second story level where it originated as a flexural crack. With increasing lateral displacement, it grew into a flexural shear crack and finally penetrated into the east boundary column, causing a shear compression failure as the displacement increased. In addition to spalling of cover concrete in the boundary column, crushing of concrete in the web along a horizontal crack approximately 14 in. from the base can also be observed in Fig. 4.25. In the remaining half of cycle 9, the specimen carried a maximum load of 33.4 kips in the west direction. Minor crushing of concrete at the base of west boundary column was noticed during this excursion.

The repeat cycle 10 further deteriorated the east boundary column. More crushing was observed along the horizontal crack during the repeat cycle. Cover had almost totally

spalled off the base of east boundary column. By the time the maximum drift was reached the main longitudinal reinforcement had started buckling out of plane. Out of plane movement of east boundary column is shown in Fig. 4.26. A load of 21.4 kips was carried by the specimen in this direction. However, the specimen was still able to resist 32.4 kips in the west direction. Cycle 10 was completed without any additional damage to the west boundary column.

Although the specimen W-3 was in a more precarious condition after 10 cycle than W-2, it was decided to continue the test through one more cycle. A top displacement of 2.25 in. was reached when excessive buckling, unstable behavior and loss of load carrying capacity made any further displacement in the east direction unsafe and the cycle was reversed. The additional crushing of the web concrete at this stage is illustrated in Fig. 4.27. Weakened thus by web crushing, the specimen failed suddenly in shear when the displacement in the west direction had reached 2.26 in. A load of 31.8 kips was being applied to the specimen when the shear failure occurred. The load dropped to zero and the wall was virtually torn from the base block, except for the reinforcing bars. Figure 4.28 shows the specimen after the test was over.

Axial load variation for this test is shown in Fig. 4.29 and the same reasons for deviation as were given for specimen W-2 are valid here.

Again, for this specimen, a stable behavior was successfully achieved up to a top drift level of 1.0 percent. Not until a drift ratio of approximately 1.5 percent did considerable deterioration occur.

4.1.4 Specimen W-4

The complete top lateral load vs. top lateral displacement relationship for specimen W-4, reproduced from the recorded data points at discrete displacement intervals, is shown in Fig. 4.30.

Table 4.4: Loads, Top Displacements and Induced Shear Stresses in Specimen W-4

Cycle No.	Top Displacement		Initial Cycle				Repeat Cycle			
	inches	% of height	East		West		East		West	
			Load (kips)	Shear Stress $\frac{}{\sqrt{f'_c}}$ (psi)	Load (kips)	Shear Stress $\frac{}{\sqrt{f'_c}}$ (psi)	Load (kips)	Shear Stress $\frac{}{\sqrt{f'_c}}$ (psi)	Load (kips)	Shear Stress $\frac{}{\sqrt{f'_c}}$ (psi)
1 and 2	0.36	0.25	18.6	1.87	13.7	1.38	20.0	2.02	13.3	1.34
3 and 4	0.72	0.50	27.1	2.73	20.6	2.07	26.7	2.69	20.4	2.06
5 and 6	1.08	0.75	32.7	3.29	26.2	2.63	32.2	3.24	26.6	2.68
7 and 8	1.44	1.00	36.5	3.67	29.5	2.96	35.8	3.60	28.0	2.81
9 and 10	2.16	1.50	36.7	3.69	29.9	3.00	17.6	1.77	29.3	2.95
11	2.88	2.00	12.9*	1.30	29.6	2.98	-	-	-	-

f'_c = 5.26 ksi.

Shear Stress based on net cross-sectional area (137 sq. in.)

* For maximum top displacement of 2.25 in.

The last of the four specimens tested in this experimental program had the two rows of openings spaced at 5 in. apart. Moving the location of the openings away from the boundary columns seemed to be a better alternative after witnessing the shear compression failures in the previous two specimens. How much effect, if any, this change was to have on the general behavior of this specimen remained to be seen. A vastly improved behavior in terms of ultimate failure mode was not expected because the reduction in horizontal stagger as compared to W-3 was only 3 in.

As was the case for W-3, the average load applied in the east direction at each drift level was greater than that in the west direction, although the difference between the two values was larger. Diagonal cracks traversing between corners of openings, identical in nature to those in W-3, were the first to appear in the first cycle along with sparsely spaced flexural cracks. Figure 4.31 also shows the almost horizontal crack which traversed across the web at 10 in. above the base in the first cycle. Repeat cycle 2 was eventless.

In cycles 3 and 4, the applied load had increased to 26.9 kips in the east direction and 20.5 kips in the west direction. Flexural cracking extended into the fourth story level and flexural shear cracking pattern shown in Fig. 4.32 was not much different than what was observed for the previous two specimens. The widest crack was measured to be 0.013 in. wide in cycle 3 and had opened up to 0.016 in. in cycle 4.

Cycles 5 and 6 at a top drift level of 0.75 percent resulted in further extension of flexural shear cracks in the upper stories. Major cracks in the lower part of the specimen started to open up in cycle 6. Figure 4.33 shows the general crack pattern during cycle 6. Again, formation of compression struts is quite noticeable in the upper stories.

First signs of crushing at the base of the east boundary column appeared during cycle 7. Besides some minor cracking, no significant damage was obvious along any of the construction joints. The widest crack near the base was now measured to be 0.060 in. in width. Figure 4.34 shows the diagonal compression struts which now seem to be complete. During the first half of cycle 8, one of the wires in the west axial load cable (a

seven-wire strand) snapped. As a safety precaution the axial load was reduced to 25 kips for each cable for the remainder of the test.

At a drift of approximately 1.45 percent, the load in the east direction peaked to 37.0 kips corresponding to $3.7\sqrt{f'_c}$ in cycle 9 before the shear compression crack, similar in nature to those in W-2 and W-3, penetrated through the east boundary column (Fig. 4.35). The load carrying capacity was reduced by 35 percent to 24.4 kips. The crack causing shear compression failure could be traced back to mid-height of the second story where it originated as a flexural crack. Compared to W-2 and W-3 at the same stage of loading, the damage to the east boundary column appeared to be less. Figure 4.35 also shows the wide crack at mid-height of the first story. More details of damage to the east boundary column are shown in Fig. 4.36. A load of 29.8 kips was sustained during the excursion in the west direction of cycle 9.

Peak load during the repeat cycle 10 could only reach a value of 17.6 kips in the east direction. Like specimen W-3, out of plane buckling of the east boundary column was observed as the peak top displacement of 2.16 in. was reached. Additional spalling and crushing of concrete along the web crack in the first story was also observed (Fig. 4.37). A load almost identical to that of the previous cycle in the west direction was recorded, although first signs of crushing at the base of west boundary column were visible as the peak load was approached.

A load of only 12.9 kips was sustained by the specimen in the east direction during cycle 11. Due to increasing instability of the east boundary column, the peak displacement was reduced to 2.26 in. in the east direction. Reduction of the axial load was also noticed as the reinforcement bars buckled out of plane. The cycle was completed by enforcing a full 2.0 percent peak drift in the west direction. Although additional crushing at the base of west boundary column was observed, no reduction in the sustained load of 29.6 kips was recorded. The test was over after completion of cycle 11. Figure 4.38 shows the specimen during the last cycle of loading.

More scatter in the axial load data in Fig. 4.39 occurred as the load in both cables had to be reduced to 25 kips each after one wire in the west strand snapped during cycle 8.

No significant change in overall behavior from the previous specimen was observed for this specimen. Physical damage appeared to be less after the shear compression failure, but the load carrying capacity was equally reduced.

4.2 COMMENTS ON GENERAL BEHAVIOR

An overall satisfactory behavior was achieved from all four specimens. Solid wall specimen, W-1, which was tested to provide a basis for comparison with the other three specimens, sustained its peak load with little loss of stiffness up to a drift level of 3 percent. The other three specimens also exhibited ductile flexural behavior. Drifts in excess of 1.0 percent were successfully achieved without any serious damage in all three specimens. The loss of in-plane confinement of the compression zone in the first story level, which was caused by the location of door openings, resulted in the sudden shear compression failure of the three pierced walls. Considering the stiff nature of structural walls, a drift level of 1.0 percent is seldom expected from wall dominated structures subjected to severe ground motion [36].

The largest horizontal stagger present in wall W-2 had forced the location of openings too close to the boundary elements. A shear compression failure was, therefore, not a surprise. However, for walls W-3 and W-4, which had a decreasing amount of stagger between openings, a different behavior was anticipated. The decrease in the horizontal stagger between openings was thought to create a zone potentially weak in shear between the two rows of openings. However, there was no significant shear distress between the openings for specimens W-3 and W-4. The decrease in horizontal stagger for W-3 and W-4 did improve the in-plane confinement of the compression zone, but not sufficiently enough to suppress the eventual shear-compression failure of the specimens.

As mentioned in the previous section, initial diagonal cracks traversing between the corners of openings in W-3 and W-4 did develop, but it was the splitting of the compression zone which governed the strength. The overall physical condition of specimen W-4 at the end of the test appeared to be better than that of W-2 or W-3, but since the load carrying capacity was equally reduced, its physical appearance had little meaning. The overall better physical condition in which this specimen ended up being at completion of the test can partly be accredited to the reduced axial load. Had the load not been reduced (as a safety precaution when one wire in the axial load cable snapped), its physical condition might have been similar to W-2 or W-3 at the end of the test. It was observed in all three tests of walls with openings that the east boundary column's capacity to carry compressive loads rapidly declined after the shear compression failure.

An important point to note is that despite the apparent weakness caused by the presence of door openings, the pierced walls were able to reach approximately the same peak load as the solid wall. However, they were not able to sustain it to large drift levels. If the shear compression failure had been suppressed, a more comparable behavior to that of solid walls would have been achieved. Models having larger wall width-to-story height ratios should be able to provide sufficient in-plane confinement to the compression zone and thus, may inhibit shear compression failure.

Reduced transverse reinforcement in boundary columns, which was approximately half the amount required by the code [25], had no adverse effect on the response of specimens. The core was effectively held intact after spalling of cover concrete. The core was damaged only in the final cycles for W-2, W-3 and W-4 specimens when the crushed east portion of the walls was subject to tensile forces in the second half of the penultimate cycle. For wall W-1, however, the boundary column core stayed intact till the end.

4.3 PRESENTATION AND DISCUSSION OF RESULTS

Results for all four test specimens are presented and discussed quantitatively in this section. For ease of presentation, sub-sections discussing a particular aspect of the results have been introduced.

4.3.1 Force-Displacement Relationship

Force-displacement relationships, reconstructed from the recorded data points, for specimens W-1, W-2, W-3 and W-4 are shown in Figs. 4.1, 4.10, 4.20 and 4.30 respectively.

4.3.1.1 Specimen W-1

As expected, force-displacement relationship curves for the solid wall W-1 (Fig. 4.1) are symmetric for each loading direction and indicate stable behavior. First cracking was observed during the first cycle as the peak load exceeded the calculated cracking load value of 10.3 kips. First yielding of main boundary column reinforcement initiated during the late stages of the 0.5 percent drift excursion cycle and continued into the next displacement increment cycle (cycle 5). Yielding of all bars in the boundary column was complete midway through cycle 5. These observations agree quite well with the calculated yield load value of approximately 27 kips. Post yield behavior was dominated by flexural action as energy was mainly absorbed by widening of previously formed cracks. A gradual widening of hysteresis loops in Fig. 4.1 illustrates this point. Repeat cycles, even at high drift levels during the last stages of test, caused little or no additional stiffness degradation. Loading and unloading branches of the repeat cycles in the hysteresis curve

of Fig. 4.1 almost traced those for the initial cycle, providing a clear indication of specimen's stability.

Recorded values of load at the maximum displacement for each initial cycle were divided by the corresponding displacement values to provide a measure of effective secant stiffness at different levels of peak displacement. It may be noted that these values are considerably lower than the actual stiffness at the beginning of each cycle, but are presented because they provide a basis of comparison with other specimens. These values, henceforth referred to as secant stiffnesses, are plotted for each initial cycle for wall W-1 in Fig. 4.40. Symmetry of the specimen is verified by the approximately equal values in each direction. A decrease of approximately 30 percent in secant stiffness probably signals the onset of first yielding at the completion of cycle 3. The reduction became more gradual after the yielding of the boundary column reinforcement was complete.

4.3.1.2 Specimen W-2

The force-displacement relationship for wall W-2, shown in Fig. 4.10, depicts a behavior which is similar to that of wall W-1 for the first few cycles. Differences, however, do exist as are discussed later in this section. Cracking occurred at about the same stage as it did in wall W-1. Yielding, however, appeared to be more gradual in the east direction than in the west direction. First bars in the west direction loading appeared to have yielded at about the same stage as for W-1, but for the east direction loading the onset of yielding didn't start until the 5th cycle. Again, as for the previous wall, the behavior after yield was dominated by flexural action, although limited by the weakness created by the door opening. Loading cycle 10 in the east direction, subsequent to the shear compression failure, reached the reduced peak load of cycle 9 and unloaded along the same path as was traced by the previous cycle. Excessive yielding and buckling of

boundary column reinforcement severely limited the stability of the specimen after the shear compression failure. In the west direction, however, the hysteresis loops look stable and comparable to those of wall W-1.

One significant difference, which is not obvious in comparison of hysteresis loops for wall W-1 with W-2, can be observed by comparing Figs. 4.40 and 4.41. Figure 4.41 shows the comparison of secant stiffnesses in the east and west directions for wall W-2. Secant stiffness in the east direction is about 20 percent lower than that in the west direction for cycle 1 in W-2. The difference between the two secant stiffnesses gradually decreases until the shear compression failure in cycle 9.

The difference between the two secant stiffnesses may be explained by studying the variation of strain distribution across the solid wall section at cracking and yielding, which was calculated from the moment-curvature analysis of wall W-1 using actual material properties from Chapter 3 (The analysis is presented in detail in the following chapter). Assumption of linear a variation of strain may not be strictly true for discontinuous sections like W-2, W-3 and W-4, but it is believed that the error introduced by such an assumption for pre-yield region is within acceptable limits. Figure 4.42(a) represents the strain distributions in specimen W-1 for loading in the east direction. For the other three specimens, the neutral axis locations differ very slightly (within 1 inch). Therefore, strain distributions for specimen W-1 have been used to represent typical strain profiles in all walls. The neutral axis is located at 33.4 in. from the extreme compression fiber at cracking load and moves to 12.4 in. from the same location at yield load. As a result of the loss of concrete area in compression due to the location of opening, the stiffness in the east direction for walls with openings was reduced, thus reducing the secant stiffness in the early stages of the test. The difference between the walls with openings and W-1 was reduced as the neutral axis shifted gradually across the opening (in the east direction) for loads beyond the yield load value.

For loading in the west direction, the strain distribution for wall W-1 is shown in Fig. 4.42(b). At the cracking point, neutral axis location falls within the openings of W-2, W-3 and W-4, but moves in the west direction with increasing loads. No loss in capacity was observed at the cracking load. Once the neutral axis was across the opening, the section behaved in a similar fashion to the solid wall for loading in the west direction. While the loss of concrete in tension does not affect the capacity as its contribution is neglected in post-cracked region, loss of bars acting in tension which were cut off to allow for the opening is compensated for by their replacement on either side of the opening.

4.3.1.3 Specimen W-3

The overall pattern of load-displacement curve for wall W-3, shown in Fig. 4.19, looks identical to that of wall W-2. Again, some differences in behavior do exist and are discussed later in this section. The average load per unit displacement (secant stiffness) in the east direction was greater than that in west direction, unlike that of W-2. General yielding of bars was complete in the 0.75 percent drift excursion.

Comparison of secant stiffness values plotted in Fig. 4.43 with those for W-1 and W-2 shows: (i) Values in the east direction are greater than those in the west on average by 12 percent unlike those for W-2, (ii) the difference gradually gets smaller with higher displacement cycles, and (iii) comparison with corresponding values for W-1 indicates that a decrease in the values for the west direction is mainly responsible for the difference of secant stiffnesses in the east and west directions. The situation is reversed in the 9th cycle, when the stiffness in the east direction is lost due to shear compression failure.

This change of trend in the variation of secant stiffness in the east and west direction from that observed in the case of wall W-2 was unexpected. As mentioned above and observed in Figs. 4.40, 4.41, 4.43, and 4.44, the difference arises from a loss of secant stiffness in the west direction rather than from an increase in the other direction.

A partial explanation of this reduction of secant stiffness in the west direction may be given by considering Fig. 4.42(b). The neutral axis location at cracking point falls well within the opening and more compression area, as compared to W-2 is lost, resulting in a net loss of capacity. However, this net loss in the secant stiffness is believed to be a small proportion of the observed reduction. Other factors responsible for this drop in secant stiffness values are not very clear and a flaw in the load or displacement measurement system cannot be ruled out.

4.3.1.4 Specimen W-4

As mentioned in Section 4.1.4, the difference in horizontal stagger between W-3 and W-4 was small and thus, little change in the overall response was expected. The expectation did materialize except for the dramatic failure in the 11th cycle, which did not occur in W-4. The force-displacement relationships for walls W-3 and W-4 in Figs. 4.19 and 4.29 respectively compare reasonably well. Almost identical series of events occurred during the test of W-4 as did in the previous test. There was a slight decrease, however, in the secant stiffness in the west direction as compared to W-3 (Fig. 4.44).

The secant stiffness variation for wall W-4, shown in Fig. 4.44, depicts a similar trend as was observed for W-3 in Fig. 4.43; however, the difference between the values in the east and west direction for cycle 1 is about 20 percent as opposed to 12 percent in the case of W-3. The additional 8 percent difference is solely due to a decrease of secant stiffness in the west direction. Again, only a fraction of this additional decrease in secant stiffness may be accredited to the new location of the opening which results in more compression area being lost as compared to the previous case of specimen W-3. The explanation for the rest of the additional drop in secant stiffness values that was presented for W-3 may be given in this case also.

4.3.2 Moment-Rotation Relationship

Figures 4.45 to 4.48 represent the base moment vs. first story rotation relationships for specimens W-1 thru W-4 respectively. Base moment was calculated as the product of applied lateral load (which was recorded at discrete intervals) and the moment arm from point of application of load to the base of the wall (equal to 146 in.). Rotation measured over the first story height is defined here as the difference of the vertical movement of the two sides of the wall at the same elevation divided by the distance between them. Recorded readings from the displacement transducers mounted vertically with a gage length equal to one story height were used to calculate the rotation.

Moment-rotation relationships provide a measure of contribution of flexural behavior to the overall response of the specimen. The relationship shown in Figs. 4.45 thru 4.48 closely resemble the general shapes of the corresponding force-displacement relationships discussed in the previous sections. The resemblance implies a predominance of flexural action in the overall response of all four specimens. The location of the door openings did not seem to have affected the walls' flexural behavior in an adverse way.

Another measure to assess the contribution of first story's flexural rotations to the overall response of the specimens would be to compare the measured top displacements with those calculated on the basis of first story flexural rotations. The top displacement can be calculated using the following equation:

$$\delta_{tc} = (H - h_1)\theta_1 + \delta_1 \qquad (4.1)$$

where δ_{tc} is the calculated horizontal displacement at top, H is the total height of the wall, h_1 is the height of the first story, θ_1 is the first story rotation, and δ_1 is the measured horizontal displacement at first story level. The model above assumes that all the flexural

rotation is concentrated in the first story level and that above the first story level the specimen displaces in a rigid body mode. The calculated displacement, δ_{tc}, is not purely due to flexural action in the first story level because the measured first story displacement term, δ_1, also includes the effects of non-flexural deformation components which typically consist of shear deformation and slippage at construction joints.

The results are plotted in Figs. 4.49 thru 4.52 for walls W-1 thru W-4 respectively. The measured top displacement envelope values are plotted against themselves and represent a 45 degree reference line from which the vertical and horizontal axes are the same. The other line represents the calculated top displacement using Eq. 4.1. Figures 4.49 - 4.52 show that the contribution of first story rotation to top displacement changed with increasing lateral displacement. In all four cases, first story flexural rotation accounted for up to 50 to 60 percent of the total displacement until a top drift level of 0.75 percent was reached. Thereafter, this contribution increased to about 75 to 80 percent of the total value. It may be recalled from Sec. 4.3.1 that complete flexural yielding of boundary column reinforcement was also achieved during the 0.75 percent excursion cycle. This result confirms the observation that the walls' inelastic response was dominated by flexural action. Part of the remaining portion of top displacement would have come from flexural rotations in the second story level, as yielding of boundary column reinforcement was recorded at the first story level during late stages in all four tests (Sec. 4.3.4). Shear displacement components in the first story level, as calculated in the following section, are expected to reduce the high percentage of top displacement calculated above, but the inelastic response will still be dominated by the flexural action.

4.3.3 Displacement Profiles

Displacement profiles along the height of the four wall specimens are presented in this section. These displacements were measured by displacement transducers at each

story level. Later in this section, an estimate of flexural and shear components ot lateral displacements is made.

Figure 4.53 shows the measured lateral displacement response of wall W-1. As the displacement profile in the repeat cycle traced the path of the initial cycle, only the data from the initial cycles is presented for clarity. The observed displacement profile can be approximated by a straight line for all drift levels. A few kinks in the earlier cycles at levels 1 and 3 are believed to be due to transducer malfunction as reported earlier in Sec. 4.1. Profiles like this are typical of tests of isolated structural components.

A similar pattern of displacement profiles along the heights of walls W-2, W-3 and W-4 can also be observed in Figs. 4.54, 4.55 and 4.56, respectively.

Total lateral displacement consisted mainly of three components, namely, flexural, shear and bar slip. Studies [37,39,63] indicate that as compared to the other two components, the contribution of bar slip, sometimes also referred to as fixed end rotation, is rather small for this type of specimen. Proper anchorage of vertical reinforcement bars reduces the percentage of fixed end rotation. In the present series of tests, these requirements were amply satisfied and it is anticipated that no significant fixed end rotation due to bar slip occurred during the tests. However, no attempt was made to measure these deformations.

In the analysis which follows, total deformations at the first story level of the four wall specimens have been decomposed into flexural and non-flexural components. An approximate estimate of the flexural component has been made by utilizing the measured rotations at the first story level and making assumptions on the curvature and rotation distributions along the story height. The remaining portion of the first story total displacement would constitute the non-flexural component, the major part of which was assumed to be shear deformation. This non-flexural component will be referred to as shear deformation, henceforth. It may be noted here that the formulation adopted here for

the calculation of flexural component of displacement implicitly includes any fixed end displacements due to bar slip at the base as part of the flexural displacements.

Total displacements at level 1 were measured for all specimens and flexural rotations over the first story height were calculated from measured vertical displacements of the boundary columns. It may be recalled here that a gage length of one story height was used to measure the vertical displacement in boundary columns. Calculation of flexural displacements from rotations involves an implicit assumption of curvature distribution, if one has not already been made explicitly.

According to Hiraishi [22], the bending deformation component in a flexural type shear wall can be estimated with sufficient accuracy by

$$u_B = \alpha\theta h \tag{4.2}$$

where θ is the rotation at a height h, and α is a factor defined by

$$\alpha = \frac{\int_0^1 \theta_\eta \, d\eta}{\theta} \tag{4.3}$$

where $\eta = y/h$ and θ_η is the rotation at height η in Fig. 4.57(a). In effect, α represents the ratio of the shaded area to that surrounded by lines ABCD in Fig. 4.57(a) (shown for the case of top displacement). Its value ranges between 0.5 and 1.0 when the point of contraflexure is located above the story under consideration [22].

A factor of 0.5 used to calculate flexural deformations implies a linear variation of rotation and a constant curvature along the story height. The actual rotation distribution for a cantilever with a concentrated load acting at its tip is quadratic in the elastic range. Assumption of a linear rotation distribution, i.e. $\alpha = 0.5$, would always underestimate the

actual rotation (and flexural displacement) at any height (Fig. 4.57(b)). A higher value of α is warranted for a better estimation of existing flexural displacement. Therefore, a factor of 0.67 has been used for the walls under study. The results are plotted in Figs. 4.58 to 4.61 for walls W-1 to W-4 respectively. In all four plots, shear deformation constitutes more than 50 percent of the total value of first story displacement and increases for higher top displacement cycles. An estimate of the percentage of flexural deformation component in the elastic region may be made by using elastic theory to calculate total deformation (including shear) at a distance of *0.2L* from the support of a cantilever of length *L*, loaded at its tip with a load *P*.

The total elastic deformation including shear effects is given by

$$\Delta_t = \frac{PL^3\,(1 + j)\{0.22(4 + j) - 0.64\}}{13.33\,EI} \tag{4.4}$$

where P is the applied load, L is the length of cantilever, E is the Young's Modulus of elasticity, I is the moment of inertia and j is the factor accounting for shear deformations given by

$$j = \frac{12\,EI}{L^2\,G\,a_r} \tag{4.5}$$

in which G is the shear modulus defined as

$$G = \frac{E}{2(1 + \mu)} \tag{4.6}$$

μ is the Poisson's ratio, and a_r is the effective shear area

$$a_r = \frac{A}{k} \tag{4.7}$$

in which A is the cross-sectional area and k is the shape factor. If the factor j is taken to be zero, Eq. 4.4 gives the flexural deformation Δ_f, and reduces to

$$\Delta_f = \frac{0.112\ PL^3}{6\ EI} \tag{4.8}$$

Using the dimensions of wall specimens, the factor j was calculated to be 0.40. A calculation using Eqs. 4.4 and 4.8 showed that the flexural deformations, Δ_f, accounted for about 52 percent of the total Δ_t.

Comparison between the flexural deformation component calculated for the first few cycles with the elastic percentage of the flexural component calculated above indicates that a higher value of α may be justified. High values of shear deformations are expected in regions close to the support, but their contribution to total displacement rapidly decreases as one moves away from the support. The contribution of flexural deformation at the top of the wall is over 90 percent in the elastic region, as calculated from elastic theory.

4.3.4 Strain Gage Data

As mentioned in the previous chapter, all four wall specimens were gaged internally at locations shown in Figs. 3.6(a) - 3.6(d). Readings from these strain gages were recorded at discrete intervals along with readings from external displacement transducers and load cells. Data from strain gages has been presented in this section under two categories, namely, (i) strain profiles, and (ii) strain histories. Strain distribution along the wall section is presented in the first section, while strain histories of selected gages are discussed in the following section.

4.3.4.1 Strain Profiles

To study the variation of strains along the width of the walls, every other vertical reinforcement bar was strain gaged at the base of the wall and at a height of 28 in. from the base i.e. first story level (henceforth referred to as level 1). Readings from these gages should reasonably represent the actual strain distribution along the wall section. It may be noted that these measurements are rather sensitive to localized effects such as cracking of concrete within the vicinity of strain gages. A general trend of strain profile can, however, be obtained by plotting the point-wise variation of strains recorded from strain gages. An alternate way to achieve the same objective would be to replace the gages by external displacement transducers. Readings from the displacement transducers when divided by the gage length provide a measure of average strain at the particular location. Average strains in the boundary columns in the first story of each specimen were calculated using this procedure.

Strain profiles across the walls' cross sections are presented for the first five cycles. Most gages were damaged after cycle five and their readings became unreliable. The average strains calculated from the boundary column displacement transducer readings are plotted along with the strain profiles at the base.

Figure 4.62 shows the strain distribution along the base of wall W-1. Generally, there is a good agreement between the average and measured local strain values. The average values of strain calculated from the vertical displacements are slightly higher in the initial cycles, but with increasing top displacement, the two quantities approach each other. Differences can be partly attributed to the formation of cracks within the interval where the displacements were measured, but cracks may have been away from the strain gage location so as not to affect the recorded bar strain. As the test progressed, the opening and

closing of cracks resulted in deterioration of bond between steel and concrete and caused local strain increases in the reinforcing bars.

It is evident in the diagram shown in Fig. 4.62 that most of the wall is under tension. The low web reinforcement ratio shifted the neutral axis position towards the boundary column under compression. The non-linearity of the strain distribution and the lower strain in the boundary column under tension is worth noting. It is partly due to the relatively larger amount of reinforcement present in the boundary column as compared to the adjacent web. A similar observation was made by Oesterle [37,39] and Sattary [55] in their tests involving shear walls. Figure 4.63 shows the strain profile along the width of W-1 at first story level. Because of the lower moment-to-shear ratio, lesser wall area is in tension as compared to section at the base. Local effects of sliding along the construction joint at the first story level, which was observed during the first few cycles, are noticeable in measurement from gages applied to the vertical bars in the west boundary column (west directional loading in Fig. 4.63).

The strain profiles shown in Figs. 4.62 and 4.63 clearly depict a non-linear trend. This effect becomes more pronounced with reversing of cycles and higher displacement magnitude. Therefore, any section analysis which assumes plane sections remaining plane after bending, and does not incorporate the effects of load reversals will not represent the observed behavior accurately.

Diagrams showing strain profiles of the three pierced specimens are presented differently than Figs. 4.62 and 4.63. The measured strains indicated that it was not appropriate to connect the points representing strain measurements on either side of the door openings. The strain profile on either side of the opening did not follow a continuous pattern in most cases.

Two strain gages at the base were damaged during construction of wall W-2. The strain profile at the base of W-2, as shown in Fig. 4.64, therefore has fewer data points to interpret the strain distribution. There appears to be little discontinuity in the strain profile

for loading in the east direction and the general trend resembles to that observed in the case of wall W-1. However, for loading in the west direction a clear discontinuity in strain profile is noticeable. This discontinuity may be attributed to either of the two factors: (i) the two portions on either side of the door opening were bending independently, or (ii) an excess amount of vertical reinforcement in the portion on the east side of the opening. It was unlikely that independent bending of the two portions had a major contribution to the observed profile because (a) no signs of distress were observed in the area between the two rows of openings during the cycles under consideration which would have led to partially independent bending, and (b) for loading in the east direction, this effect was totally absent. It is believed that providing more vertical web reinforcement in the east portion of the wall led to this drop in the strain value across the opening. Referring to Fig. 3.6(b), the interrupted vertical bar was replaced by one on each side of the opening. The provision of this extra bar in the 2.5 in. long east portion of the web raised its reinforcement ratio as compared to the much longer west portion. As a result, when this portion of the wall was subjected to tensile forces, the comparatively larger vertical reinforcement ratio reduced the tensile strains in the reinforcement. A similar drop occurred in the boundary columns of wall W-1 as discussed before. This effect is diminished, but can still be noticed at level 1 (Fig. 4.65).

Strain distribution profiles for wall W-3 at the base and level 1 are shown in Figs. 4.66 and 4.67 respectively. For wall W-4 these profiles are shown in Fig. 4.68 and 4.69. The general trend of the profiles for W-3 and W-4 is very similar. A clear discontinuity across the opening, much more prominent than that observed for W-2, for loading in both directions is very obvious in Figs. 4.66 and 4.68. Again, in this case, the two factors mentioned previously may be held partly responsible for this action. The influence of second factor has been reduced by moving the opening inwards and providing more area on the east portion of the web. The effect of an extra reinforcing bar does not raise the vertical reinforcement ratio in the east portion of the web as much as it did in wall W-2.

There is not much evidence, however, from the observations to support the assumption that the two portions of the wall might have acted independently. First cracks did initiate in the region between the two rows of openings in earlier cycles, but any major damage which would render the portions on either side of the opening independent of each other was not observed. Neither did the measurement readings from strain gages installed in the area between the two rows of openings indicate any unusual behavior. Walls W-3 and W-4 were geometrically closest to a coupled wall system, but a behavior similar to that of a coupled wall was not expected.

4.3.4.2 Strain Histories

Strain histories for selected strain gages are presented in this section. They give an indication of local strains experienced in the vicinities of the respective gages. For the strain history diagrams presented in this section, load in the east direction and tensile strain are taken as positive quantities.

Gages 1 through 4 in all four wall specimens were installed in the boundary columns' vertical reinforcement at the base level. Gages 5 through 8 were installed on the same bars at the first story level. As strains are usually highest at the extreme fiber, these gages were generally damaged before any of the others did. Figures 4.70 - 4.73 show the strain histories for gages in walls W-1 through W-4 respectively. Reference is made to Figs. 3.6(a) - 3.6(d) to correspond a gage number to its location.

In wall W-1, gages installed on horizontal web reinforcement (gage nos. 15 - 19) did not experience any compressive strains. This indicates the presence of truss action where compression is carried by diagonal compression struts formed by cracked concrete and tension by the steel reinforcement. Although it is difficult to judge just by looking at the strain histories whether or not the bars did yield because some gages malfunctioned

before yielding occurred, it is reasonable to assume that all horizontal reinforcement in the lower stories must have yielded when the cracks opened as wide as they did (Sec 4.1.1).

For the three pierced walls, it is interesting to look at the strain histories of gages installed in the region between the two rows of openings. For W-2, these were gage nos. 13, 14 and 15. Yielding in gages 13 and 14 was recorded in the final three cycles, apparently after the shear compression failure had occurred. Observations not too different from this can also be made in the case of walls W-3 and W-4 where gages 14 and 15 installed at the same location behaved in a similar manner. Strains larger than yield were also recorded in the horizontal bars at the top of second story opening.

4.3.5 Energy Dissipation

Another method for assessing the inelastic response of structures or structural components under reversed loading is their energy dissipation capacity. Dissipated energy for a complete cycle is defined as the area enclosed within the load-displacement curve described for that cycle. As structures dissipating more energy are less susceptible to collapse under severe ground shaking, load-deflection characteristics having more open and full loops, signifying greater energy dissipation capacity, are more desirable. It is interesting to compare the energy dissipated before and after the yielding of main reinforcement in the wall boundary columns has occurred. Energy calculations for all four specimens have been made for cycles 3 through 10. The energy values were calculated as the area enclosed within a loop using a linear variation between the recorded data points at discrete intervals. It may be recalled that yielding had initiated during the 0.5 percent average drift excursions (cycles 3 and 4). The last complete cycle common to all specimens was the repeat cycle 10 at a top drift ratio of 1.5 percent.

This information is presented in Figs. 4.74 and 4.75 for initial and repeat cycles, respectively. For both sketches, energy absorbed in cycle i has been normalized to the

energy absorbed in cycle 3 for each specimen. The normalizing values for specimens W-1 through W-4 were 8.63, 7.17, 6.51, and 6.13 k-in, respectively. An almost similar trend can be observed in both plots. The rate of increase in energy dissipation increases with increasing top drift ratios as more cracks open up and more steel reinforcement bars yield. At the maximum top drift ratio of 1.5 percent (cycles 9 and 10), the large increase in energy for wall specimens W-2, W-3 and W-4 includes energy released due to shear-compression failure during cycle 9. While comparing the normalized values between different specimens, even at the same drift level, it may be noticed that the normalizing factor for each specimen is not the same value, i.e. in cycle 3, walls W-2, W-3 and W-4 dissipate about 83 percent, 76 percent and 71 percent of the energy dissipated by wall W-1, respectively. An absolute comparison of these values for each specimen indicates that there is little variation in the general trend stated above, and generally wall W-1 dissipated more energy in "absolute terms" than the other three walls at the same drift ratio up to a drift level of 1.5 percent was reached.

4.3.6 Dynamic Characteristics

Results from the vibration tests on the wall specimens are presented in this section. A total of four tests were carried out on each of the four specimens in their undamaged state. These four tests were repeated on all specimens, except W-3, after the completion of testing. Due to the precarious condition of specimen W-3 at the completion of test, it was not found safe to conduct the vibration test on it. The four vibration tests represented the following four cases: (i) inplane with no axial load, (ii) inplane with an axial load of 60 kips, (iii) transverse with no axial load, and (iv) transverse with an axial load of 60 kips.

Table 4.5 lists the measured frequencies and damping ratios of the test specimens. Specimens were excited with hammer blows inflicted at the top. The resulting vibrations

were recorded through vibration transducers. Damping ratios for the specimens were determined from the record using Logarithmic Decrement Method.

Analytical value of the fundamental frequency for solid wall W-1 was calculated from the relationship for a cantilever beam of length L, with a uniform mass per unit length of m, and a lumped mass of M, at its tip:

$$f_1 = \frac{3.516}{2\pi}\sqrt{\frac{EI}{L^3(mL + 4M)}} \tag{4.9}$$

EI represents the flexural stiffness of the cantilever beam. This model was chosen for calculation of the fundamental frequency because it represented the actual test conditions more closely, where the vibration tests were carried out with the load transfer beam attached to the specimen. Mass of the wall specimen was taken as distributed mass m along the height and the mass of the load transfer beam was accounted for as the lumped mass M. Stiffness EI was based on gross section properties. Using a length of 146 in. to the center of the loading beam, a fundamental frequency value of 37.1 hz. was calculated. The difference between the calculated and measured value of 32.8 hz. could be due to two reasons: (i) assumption of fixed-end support condition in the analytically calculated value (a perfect fixed-end support is difficult to simulate in actual test conditions), and (ii) it was difficult to inflict sharp and clear blows in the inplane direction because of space limitations.

A comparison of measured frequencies of virgin specimens indicates that presence of openings as well as their location has an effect on the fundamental frequency, and, hence, on their stiffness in the inplane direction. The reduction in frequency (and stiffness) was large for the specimens with widely spaced openings. This observation is consistent with calculated values for the moment of inertia across the net section of the

walls with openings. Frequencies in the transverse direction do not seem to be affected by the openings.

Comparing the values of fundamental frequencies before and after the test reveals a 60 to 75 percent reduction of frequency in the inplane direction. This implies a 84 to 94 percent reduction in the corresponding flexural stiffness *EI*. Frequencies in the transverse direction were measured to be approximately half the corresponding value in their undamaged state. Damping coefficients for all virgin specimens were calculated to be less than 1.5 percent of the critical value. As expected, the damping coefficients increased following the damage to the specimens during testing. The highest value of damping coefficient calculated was less than 5 percent of the critical value.

Table 4.5: Dynamic Characteristics of Wall Specimens.

State	Direction	Axial Load	Specimen							
			W-1		W-2		W-3		W-4	
			Funda-mental Frequency Hz.	Damping Factor ζ	Funda-mental Frequency Hz.	Damping Factor ζ	Funda-mental Frequency Hz.	Damping Factor ζ	Funda-mental Frequency Hz.	Damping Factor ζ
Virgin	Inplane	None	32.8	-	26.8	.0078	29.0	.0093	30.8	.0079
		60 kips	33.2	-	27.1	.010	29.4	.013	31.5	.0083
	Transverse	None	2.3	-	2.3	.0054	2.3	.0059	2.5	.0073
		60 kips	2.4	-	2.4	.0093	2.3	.0053	2.4	.0068
Tested	Inplane	None	9.1	.034	9.5	.048	-	-	11.1	.031
		60 kips	10.8	-	14.3	.015	-	-	11.8	-
	Transverse	None	1.0	.0073	1.1	.016	-	-	1.0	.023
		60 kips	1.1	-	1.4	.017	-	-	1.5	.018

CHAPTER V

ANALYTICAL MODELING AND COMPARISON WITH EXPERIMENTAL RESULTS

This chapter presents the results of analyses carried out on the wall specimens to predict their overall response. Development of a new and rigorous analytical model was not among the main objectives of this study; hence, the analytical study presented in this chapter relies on the use of basic principles and existing modeling techniques.

The material included in this chapter has been divided into three sections, each section discussing a separate analysis technique. In Sec. 5.1, basic principles are used to predict the overall response of specimens. Results from an equivalent column model of wall specimen W-1 are presented in Sec. 5.2. Finally, in Sec. 5.3, a finite element analysis of the four wall specimens is presented.

5.1 SECTION ANALYSIS

Estimates of monotonic moment-curvature and force-displacement envelopes for each of the four wall specimens are presented in this section. Also, a comparison between the calculated shear strength and the maximum measured shear applied to the walls is presented.

5.1.1 Moment-Curvature Analysis

In general, moment-curvature analysis of a reinforced concrete section involves two basic assumptions: (i) a linear strain distribution across the section, and (ii) inability of cracked concrete to carry any tensile forces. Material stress-strain relationships for steel and concrete are assumed and the section analysis is carried out for specific values of extreme fiber strains. The analysis is based on strain compatibility and the equilibrium of internal and externally applied forces, including axial load.

For the wall specimens, the measured stress-strain relationship for steel reinforcing bars including strain hardening was used in the calculations. The following material model by Hognestad [23] was used for concrete:

$$f_c = f'_c\left[2\left(\frac{\varepsilon_c}{\varepsilon_o}\right) - \left(\frac{\varepsilon_c}{\varepsilon_o}\right)^2\right] \qquad \text{for } 0 \le \varepsilon_c \le \varepsilon_o \tag{5.1a}$$

and

$$f_c = f'_c\left[1 - 150(\varepsilon_c - \varepsilon_o)\right] \qquad \text{for } \varepsilon_c > \varepsilon_o \tag{5.1b}$$

where $\varepsilon_o = 0.002$ is the assumed strain at maximum concrete stress f'_c. The following six points on the moment-curvature diagram were calculated: (i) cracking point (i.e. maximum extreme fiber tensile strain equal to concrete cracking strain), (ii) yield point (i.e. maximum tensile strain in extreme steel layer equal to yield strain), and maximum extreme fiber compressive strains of (iii) 0.003, (iv) 0.004, (v) 0.005, and (vi) 0.006. For walls with openings, section analyses were carried out across the net section ignoring the contribution of missing concrete at the opening location when it was under compression. Two analyses were made for the walls with openings, one for each direction of loading.

Comparisons of the calculated moment-curvature relationships of walls W-2, W-3, and W-4 to that of wall W-1 are shown in Figs. 5.1 to 5.3, respectively. The relationship up to the yield point is almost identical for all four specimens. Beyond the yield point, walls W-2, W-3, and W-4 have a slightly higher moment carrying capacity than wall W-1. This slightly higher capacity in the three walls with openings is due to slightly higher reinforcement ratio. It may be recalled from Chapter 3 that each vertical No. 2 bar interrupted due to an opening was replaced by one bar of the same size on either side of the opening, resulting in one extra bar at any cross-section taken across the net section.

The maximum average calculated flexural strengths of the four walls (i.e. moment capacities at maximum extreme fiber compressive strain of 0.006) are compared to the experimentally obtained values of maximum average base moment in Fig. 5.4. Moment arm for the calculation of base moment was taken to be 146 in. Considering the fact that strain distributions along the section were not linear (Sec. 4.3.4), a reasonably good agreement between the calculated and experimental maximum flexural capacities was obtained.

5.1.2 Load-Top Displacement Envelope

The moment-curvature relationships calculated in Sec. 5.1.1 were used to extract the load vs. top displacement envelope for the four wall specimens. The first moment of the area under the curvature diagram was taken about the tip of the wall to obtain the top displacement. Figures 5.5(a) and 5.5(b) show the effective area under the curvature diagram considered for the displacement calculation at the six calculated values of curvatures for a typical wall specimen.

In reinforced concrete flexural members, inelastic curvature spreads over a certain length of the wall commonly referred to as plastic hinge length, l_p. Therefore, the theoretical curvature distribution beyond the yield point corresponding to the actual

moment distribution becomes inaccurate. An effective curvature distribution must be determined. Rotation and displacements at a specific level can then be calculated using the effective curvature distribution. Several expressions to determine the hinge length, l_p, effective moment within the hinge length, and effective curvature distribution exist in literature [7,32,46].

In this study, the hinge length, l_p, is assumed to be equal to the length of the wall from the base to the point of location of yield curvature (i.e. wall length experiencing curvatures in excess of or equal to yield value). In the calculation of displacements from curvature diagram, the effective curvature distribution is assumed to be constant within the hinge length and equal to the maximum value of curvature (at the base). Figure 5.5(a) and (b) show the gradual increase in hinge length as the applied load/moment is increased. At the maximum extreme fiber compressive strain of 0.006, Fig. 5.5(b) indicates that the hinging zone had spread to a height just above the first story. This fact was verified by the larger than yield strains recorded by the strain gages installed at the first story levels.

The calculated lateral load vs. top displacement envelopes are superimposed on the recorded hysteresis response of walls W-1 through W-4 in Figs. 5.6 through 5.9, respectively. The calculated envelope curve for W-1 is quite accurate except that the post-cracking stiffness is slightly higher than the observed experimental stiffness. This was assumed to be partially due to the softening of the test specimen caused by load reversals. Judging from the similarities of the moment-curvature relationships of the four wall specimens, it would be reasonable to expect similar load-displacement relationships. A comparison of the calculated and measured curves in Figs. 5.6 - 5.9 demonstrates this. However, it appears that presence of openings caused a reduction of the initial tangent stiffnesses of walls W-2, W-3 and W-4. This reduction of initial tangent stiffness diminishes gradually from W-2 to W-4 as the openings were moved inwards. The simple analytical model is unable to simulate this effect and seems to be more in error for wall W-

2 than for walls W-3 or W-4. As mentioned before, peak loads for all the four walls are predicted quite accurately.

5.1.3 Shear Capacity

ACI Building Code Chapter 21 [3] gives the following expression for calculation of nominal shear strength, V_n, of a structural wall:

$$V_n = A_{cv} (2\sqrt{f'_c} + \rho_n f_y) \tag{5.2}$$

$$\text{where } \rho_n = \frac{A_v}{hs_2} \qquad \text{and} \qquad A_{cv} = hl_w \tag{5.2a}$$

where h is the wall thickness, A_v is the area of horizontal reinforcement per spacing s_2, l_w is the length of the wall, f'_c is the concrete compressive strength and f_y is the yield strength of reinforcing steel. Measured yield strength of steel with corresponding measured values of concrete strength for each specimen was used to calculate their nominal shear capacities. The calculated nominal shear capacities are compared with the maximum base shear for each specimen in Fig. 5.10. The figure shows that the maximum measured shears in the four wall specimens were on average 25 to 35 percent below their calculated nominal capacities.

5.2 Equivalent Column Model

Analytical models for predicting the nonlinear response of reinforced concrete structural walls can be classified into two broad groups: (i) models based on a microscopic approach, and (ii) models based on a macroscopic approach.

Models based on a microscopic approach are detailed models derived using mechanics of solids. They are more desirable when a detailed interpretation of local behavior is required. Implementation of the microscopic approach based models involves many difficulties due both to the lack of completely reliable material models and the complexities involved in a detailed solution. As computation using this approach generally becomes very time consuming and requires large computer memory, use of this approach is limited to less complex structures.

On the other hand, models based on a macroscopic approach are simplified models used to predict a specific overall behavior. Use of simplified idealizations result in less computational effort. One of the main disadvantages of models based on a macroscopic approach is that analytical results are valid only for the conditions on which the derivation of the model is based.

The use of an equivalent column model for simulating wall behavior falls into the category of models based on a macroscopic approach. The modeling technique, generally used for frame-wall systems, replaces the generic structural wall member by a line element at its centroidal axis. This line element is connected to rigid links which extend to the edge of the wall. The fixed-end rotation at any connection interface with a frame beam can be taken into account by introducing a non-linear rotational spring whose mechanical properties can be defined on the basis of bar slippage due to bond deterioration [64].

The main limitation of modeling reinforced concrete structural walls by adopting an equivalent column model lies in the implicit assumption that rotations occur around the centroidal axis of the wall. With this assumption, important features of the behavior of reinforced concrete frame-wall structural systems (i.e., migration of the neutral axis over the wall cross-section, rocking of the wall, etc.) and their consequent effects (i.e., outriggering interaction with the frame surrounding the wall, etc.) are not accounted for adequately [64].

5.2.1 Modeling of Wall Specimen W-1

The purpose of presenting the modeling and analysis of wall specimen W-1 is to demonstrate the ability of the equivalent column model to adequately represent the general behavior of isolated reinforced concrete walls. For this reason, comparison of results for only one wall specimen, W-1, is presented. Structural walls in the analysis of Almendral Building, which is presented in the next chapter, are also modeled using the equivalent column technique.

Each of the five stories of specimen W-1 was modeled as one equivalent column element, located at the centroid of the wall cross-section. As opposed to the case of a frame-wall structure, the width of the wall need not be modeled by rigid links for analyzing an isolated wall specimen. The analysis is thus reduced to that of a cantilever beam composed of five equivalent column elements with section properties of specimen W-1.

Properties for the wall specimen were calculated assuming a cracked section. Cracked flexural stiffness for the wall W-1 was calculated from the moment-curvature relationship shown in Fig. 5.1 by calculating the slope of the line joining the origin and yield point. This value of flexural stiffness was roughly 35 percent of the calculated stiffness based on gross section properties. Nominal values of moment and axial load (i.e., values at maximum compressive fiber strain of 0.003) were used to define the axial load-moment interaction surface. The effect of shear deformations was not included.

Analysis was performed using the computer program DRAIN-2DM [62] for a step-by-step incremental monotonic loading. An axial load of 60 kips was kept constant throughout the analysis.

A brief description of the DRAIN-2DM program and the "beam-column" element used to model the wall is presented in the following two sections. Parts of the description

have been adopted from [27,53,62] and a more interested reader is referred to these references for a more detailed description. Comparison of analytical and experimental results is presented in Sec. 5.2.4.

5.2.2 DRAIN-2DM Computer Program [62]

DRAIN-2DM [62], a general purpose computer program for inelastic dynamic and static analysis of two-dimensional structures, is an extended version of DRAIN-2D [27,53] originally developed at the University of California, Berkeley. Ever since its initial development in 1973, DRAIN-2D has been the subject of additions and modifications. The modified version which has been used in this study, DRAIN-2DM, was developed at the University of Michigan.

DRAIN-2DM is organized in two levels: structure level and element level. The subroutines at the structure level process the structural data such as joint coordinates, degrees of freedom, loads, etc. The subroutines at the element level are primarily responsible for calculating element properties, describing element force-deformation relationships and determining element stiffnesses at each time step, etc. The subroutines for different types of elements are put together to form an element library which can be conveniently used to model complex structures.

The program uses the direct assembly method to form element and structural stiffness matrices and employs Newmark's constant acceleration method to solve dynamic differential equations. It uses the central core system for data management and a space saving technique for stiffness matrix formation, storage and an efficient Gauss elimination routine to solve the coupled equations. Because of its efficiency and economical advantages, the program DRAIN-2D has been widely used in both research and practice in earthquake engineering.

5.2.2 Beam-Column Element E2 [27,53]

Beam-column elements may be arbitrarily oriented in the x-y plane. The elements possess flexural and axial stiffness, and elements of variable cross-section can be considered by specifying appropriate flexural stiffness coefficients. Flexural shear deformations and the effects of eccentric end connections can be taken into account.

Yielding may take place only in concentrated plastic hinges at the element ends. Strain hardening is approximated by assuming that the element consists of elastic and elasto-plastic components in parallel. The hinges in the elasto-plastic component yield under constant moment, but the moment in the elastic component may continue to increase.

The yield moments may be specified to be different at the two element ends, and for positive and negative bending. The interaction between axial force and moment in producing yield may be taken into account approximately. The general interaction surface used for reinforced concrete sections is shown in Fig. 5.11.

Static loads applied along any element length may be taken into account by specifying fixed-end values. The results of separate static load analyses can be incorporated by specifying initial force values.

Large displacement effects may be approximated in the dynamic analysis by including simple geometric stiffnesses based on the element axial forces under static load.

5.2.4 Comparison of Results

The response envelope curve obtained from the equivalent column model for W-1 is superimposed on the experimentally recorded hysteretic response in Fig. 5.12. General agreement between the two curves is good. However, the following may be noted from

the figure: (i) initial stiffness of the envelope curve appears to be less than that recorded experimentally, (ii) stiffness in the post-cracked region of the envelope curve is higher than the recorded value, and (iii) the load level for the envelope curve is steadily on the rise, even at high displacement levels.

Explanations for the three points mentioned above can be provided by comparing the moment-rotation/curvature relationships of a typical reinforced concrete flexural member with that modeled for the beam-column element, E2. For a typical reinforced concrete flexural member, moment-rotation/curvature relationship can be idealized using a tri-linear curve with the three portions of the curve representing, (i) uncracked, (ii) cracked elastic, and (iii) post-yield regions. A bi-linear moment-rotation/curvature relationship representing elastic and plastic regions, typically observed for steel members, has been used for the beam-column element, E2. The element is, therefore, more suited for modeling of steel members.

A secant stiffness value at yield used in the analysis of wall W-1 was smaller than the uncracked stiffness based on gross concrete section, but greater than the cracked elastic stiffness. A predicted response confirming to these observations was, therefore, obtained from analysis. Crushing, yielding, slippage due to bond deterioration and other effects typical of reinforced concrete limit its load carrying capacity at large displacements. For steel, however, homogeneity of material eliminates these effects and load carrying capacity keeps increasing gradually (depending on strain hardening slope) at larger displacements until it reaches its ultimate strength.

The differences in the moment-rotation/curvature relationships for steel and concrete outlined above become more prominent in cases of small scale tests where loading is gradually increased in a systematic fashion. Specimen response can be traced as it gradually transforms from uncracked to the post-yield state. For large scale structures subjected to random earthquake loading, a general response is usually sought. In such a

case, a bi-linear relationship suffices to describe the overall response of the structure, and differences in moment-rotation/curvature relationships become less significant.

5.3 FINITE ELEMENT MODEL

The Finite Element Method has become one of the more popular methods of analysis with the advancement of high-speed digital computers. Several commercially available codes exist which are based on this solution technique. However, choice of a code to solve a particular problem is dictated by the ability of the models (nonlinear, material, etc.) incorporated into the code to adequately represent the actual behavior.

A finite element code, SNAC program, for the analysis of shear wall dominant buildings subjected to lateral loadings was developed by Bolander [13] at the University of Michigan. The SNAC program has been used in this study to reproduce the analytical response of the four wall specimens. The next section briefly describes the SNAC program. Parts of the description presented in the next section have been adopted from [13] and interested reader is referred to this reference for a detailed description.

5.3.1 The SNAC Program [13]

The SNAC (Simple Nonlinear Analysis of reinforced Concrete structures) finite element program was developed for use as a tool to investigate the inelastic response of shear wall dominant buildings subjected to quasi-static loading histories. The program is based on the finite element displacement formulation. Loading in the form of controlled nodal forces and/or displacements is applied incrementally with iterations within each increment to reestablish equilibrium. The program formulation allows for realistic representation of the material nonlinearities which are essential in an ultimate analysis of reinforced concrete structures. Nonlinearity is limited to material response where the

models have been taken from existing literature. SNAC program development was based on a macro-model approach to nonlinear reinforced concrete analysis. Within this type of approach the global structural response is of primary importance and the details of highly localized phenomena are generally neglected.

The current version of SNAC is limited to material-only nonlinearity in the structural response. The assumption that kinematic (geometric) nonlinear effects need not be accounted for is reasonable for many types of reinforced concrete analyses, especially the case of shear wall dominant structures where displacements prove to be limited in magnitude. The nonlinearity in the stiffness formulation during loading comes from the material behavior as expressed by the constitutive relations. Causes of reinforced concrete nonlinear behavior include: (1) nonlinear behavior of concrete under multi-axial stress states, (2) tensile cracking of concrete, (3) nonlinear behavior of reinforcing steel, (4) bond slippage at the reinforcing steel-concrete interface, (5) doweling action of the reinforcing steel across cracks, and (6) stress transfer across cracks due to aggregate interlock. With the exception of Item (4), all the above items have been modeled either directly or indirectly within the continuum element modeling of shear walls.

The current version of SNAC supports three element types, namely: (1) QUADC - Two dimensional continuum element, (2) TRUSS - Two node truss element, and (3) BEAM - Two node beam-column element. Each of these element types is based on standard finite element formulations and possess nonlinear material capabilities. One of the most notable features of the SNAC program is the two dimensional continuum element (QUADC) modeling of shear walls in a state of plane stress. This is seen as a necessary improvement over the traditional beam-column approach to modeling of shear wall type structures.

Element stiffness matrices for the QUADC element are based on standard isoparametric finite element formulations (i.e. both the element coordinates and the element displacements are represented using the same shape functions which are defined in a

structural coordinate system). The QUADC element may be used in triangular (three-node) or quadrilateral (four-node) form. Consistent with smeared modeling approach which treats cracked concrete as a continuum material, as if the local discontinuities due to cracking were distributed evenly over a certain tributary area of the finite element, material nonlinearity in QUADC element is simulated by adjusting the element material response matrix coefficients at the appropriate integration points. Each QUADC element is identified with one of three material types as specified on its "material card" during program input. The first material type allows for linear elastic isotropic material behavior as defined by Young's modulus and Poisson's ratio. The second and third material type models are called "Non-orthogonal cracking model with tensile softening" and "Plasticity based model with abrupt tension cutoff." Explanation of these material type models is more involved and will not be presented here (refer to [13]).

There is also an option (independent of material type) which allows for the smeared representation of a steel reinforcing mesh within the concrete material. The user is able to specify the reinforcing ratios of the steel mesh in the two orthogonal directions aligned with the global coordinate axes. Reinforcing mesh material nonlinearity is limited to elastic-perfectly plastic behavior in each of the two orthogonal directions. The reinforcing mesh is assumed to be incapable of resisting shearing stress.

The TRUSS element is included as a means of representing the reinforcing bars in a discrete manner, as opposed to smearing the effects of the reinforcing steel over the entire volume. Both the discrete and the smeared representations could be formulated to provide similar results in a global sense. Material stress-strain (or element force-deformation) relations are idealized as bi-linear elastic strain-hardening plastic type.

The BEAM element is a discrete line element which may be used to represent structural members (e.g. beams, beam-columns, slender walls) which are arbitrarily oriented in two dimensions. The BEAM element possesses both translational and rotational degrees of freedom identified at each of its end nodes. Inelastic behavior is

approximated by assuming the element consists of a linear elastic beam element with a nonlinear zero-length hinge at each end. The elastic portion of the beam is defined by an axial stiffness, a flexural stiffness, and an effective shear rigidity. Hinge nonlinearity is assumed to be dependent on the bending moment acting at the corresponding end node.

5.3.2 Modeling of the Wall Specimens

Two types of elements were used to model the wall specimens. Wall W-1 was discretized into 350 four-node quadrilateral QUADC elements, and the remaining three walls were discretized into 370 four-node quadrilateral QUADC elements. While the web reinforcement mesh was modeled using the smeared representation option, each layer of longitudinal reinforcement in the boundary elements was modeled by a separate TRUSS element. Hence, a total of 140 TRUSS elements represented the boundary element longitudinal reinforcement in each of the four specimens. The smeared representation option was also used to model the transverse reinforcement in the boundary elements. Figures 5.17(a) - 5.20(a) show the undeformed finite element mesh for wall specimens W-1 through W-4, respectively.

The SNAC plasticity model for the continuum QUADC element, which is incapable of modeling non-orthogonal secondary cracking, but can represent the compressive softening of concrete, was used to model the concrete behavior within a reinforced concrete shear wall specimen subjected to lateral loading. To avoid any localized effects of enforced displacement, a linear elastic isotropic material behavior was assumed for the top row of QUADC elements.

Measured material properties were used in the analysis. Horizontal and vertical web reinforcement and transverse boundary column reinforcement, which were modeled using the smeared representation approach, were assumed to behave in an elastic-perfectly plastic manner, slightly contradicting their observed stress-strain relationships. Strain-

hardening was, however, included for the longitudinal boundary element reinforcement, which was modeled as a TRUSS element. For concrete, an assumed strain value of 0.002 at maximum stress was used along with the quadratic stress-strain relationship expressed in Eq. (5.1a) to define the pre-peak curve. The constant which defines the slope of the post-peak linear branch was taken to be 50 as opposed to 150 used in Eq. (5.1b). This was done to increase the solution life of the model because a high value of post-peak slope results in a faster rate of softening/crushing and thus, an early divergence of the solution process. A lower value of post-peak slope is justified for well-confined concrete.

5.3.3 Results and Discussion

Each specimen was assumed to be fixed at the base and an incremental lateral load in the form of enforced displacement was applied at the top. An increment of 0.1 inch was used for all specimens. An axial compressive load of 60 kips was also maintained in all the analyses.

Results from numerical model are superimposed on the experimentally recorded force vs. displacement hysteretic response in Figs. 5.13 - 5.16 for specimens W-1 through W-4, respectively. Generally, the predicted response from the numeric model is stiffer than the experimentally recorded response. The general trend of the numeric response indicates a better agreement between the experimental and analytical values as the door openings are moved closer together. A comparison of the analytical responses for the three specimens with openings shows little variation of their load-displacement curves. The better agreement between numeric and experimental values for wall W-4 as compared to wall W-2 is because of the recorded higher initial stiffness in the case of wall W-4, especially for loading in the east direction.

An exact agreement between the cyclic loading envelope and the monotonic curve was not expected. If the only nonlinearities were due to concrete cracking, steel yielding

and concrete softening, then maybe they would agree well. However, bond degradation, crack tangential sliding and the associated loss of aggregate interlock strength, etc. take on completely different characteristics when comparing monotonic and cyclic situations. The assumption of a perfectly rigid base could also partly contribute to a stiffer numeric response. A flexible base model for wall W-1 gave about 2 percent less stiff response in the early stages [52]. The model allowed no horizontal movement, but allowed some flexibility in the vertical direction.

The graphics post-processing program for plotting the nonlinear trends from the SNAC output data was used to plot the wall specimens' deformations at selected load levels. These plots are shown for walls W-1 through W-4 in Figs. 5.17 - 5.20, respectively. Flexural cracking initiated along the tensile perimeter of all the specimens within the first step of the numeric solution (for a top lateral displacement of 0.1 inch). The model was unable to predict either the observed diagonal flexural shear cracks or the shear compression failure in the three walls with openings. Instead, the flexural cracking initiated during the first step keeps growing until crushing at the base of the boundary column caused the solution process to diverge. For walls with openings, significant distress in the numerical model is also observed between the openings at the first story level. This discrepancy between the observed and analytical cracking patterns is partly due to inability of the numerical procedure to model simultaneous non-orthogonal secondary cracking.

The need to include more general material models which are able to account for both non-orthogonal secondary cracking and compressive softening phenomena was recognized in [13]. At the time of writing of this report, these material models are in the process of being implemented. With these improvements forthcoming, it is anticipated that a better correlation between the observed and analytical responses, as well as closer prediction of cracking patterns and failure modes can be achieved.

CHAPTER VI

CHILEAN BUILDING ANALYSIS

6.1 INTRODUCTION

A strong motion earthquake of magnitude, $M_s = 7.8$, was recorded off the coast of central Chile on March 3, 1985. A network of accelerographs was in place to record the event and thirty-one strong motion records representing many soil conditions were obtained during the earthquake. Recorded acceleration histories indicated that strong ground shaking was experienced throughout the epicentral region with several stations reporting durations of strong motion (> 0.1g) lasting over 60 seconds. Peak horizontal acceleration greater than or equal to 0.6g were recorded at four stations [70].

As reported in earlier studies [54,70], considerable damage and casualties occurred in the central region of Chile from the earthquake. Most of the damage was limited to the failure of low rise adobe and unreinforced masonry dwellings. Most of the modern engineered structures, however, performed reasonably well and only a few of these structures suffered any serious damage. Of the 415 buildings surveyed in the city of Vina del Mar after the earthquake, which ranged in height from 5 to 23 stories, only six were identified as having suffered substantial structural damage. In view of the satisfactory performance of the Chilean buildings under severe earthquake loading, a joint effort between the University of California at Berkeley, University of Illinois at Urbana-Champaign and the University of Michigan was initiated to investigate the performance of

these buildings. The study presented in this report is part of the efforts undertaken at the University of Michigan and funded by the National Science Foundation.

The following general information about the Chilean buildings in the coastal cities of Vina del Mar and Valparaiso has been adopted from [13,54,70]:

- All buildings in Vina del Mar with five or more stories were constructed of reinforced concrete. Shear walls were predominantly the most common structural system for carrying gravity and lateral loads. In most cases, these walls tend to follow the architectural layout of the floor rather than being strictly limited to locations along the building perimeter or central core region.
- Very few buildings suffered major damage. In most of the cases where significant structural or nonstructural damage was incurred, problems linked to either local soil-site amplification or unrepaired damage from prior earthquakes were cited as possible causes. Most buildings had only minor or superficial damage.
- Ninety percent of the total 415 buildings considered in the survey were in the 5 to 10 story range. Less than three percent of these buildings were greater than 20 stories.
- The ratio of wall to plan area for these buildings was much greater than that of customary designs in the United States. The wall to plan area index for the Chilean buildings ranged from 3 to 8 percent with an average value near 6 percent.
- The Chilean philosophy with respect to acceptable damage and safety is the same as that commonly used in the United States: minor damage is acceptable in moderate earthquakes and structural failures should be avoided in severe earthquakes. However, the scales of earthquake intensity are not the same in the U.S. and Chile. Although bounds are not established explicitly, earthquakes with magnitudes between 6.5 and 7.0 are considered to be minor in Chile, and structural damage is not expected during such events. A magnitude on the order of 7.5 corresponds to a moderate earthquake.

- The Chilean code for reinforced concrete does not contain provisions for seismic design, and in particular no special detailing requirements to insure ductile behavior as is customary for buildings in seismic regions of United States. The Chilean engineers do look at the ACI Code (Chapter 21) for detailing frame type structures, but seldom use it for walls. No limits are placed on the amount of flexural reinforcement along the wall boundaries and no specifications exist regarding proper confinement of these boundary elements.
- For the most part, no clear trends were established when trying to link observed building damage to such variables as date of construction, structural type, building height, wall area to plan area index, etc. It was concluded that more detailed studies would be required to make a better assessment of the performance of these buildings.

Analysis of one building included in the above survey, the Almendral Building which is located in Valparaiso, is presented in this chapter.

6.2 BUILDING DESCRIPTION

The 22-story Almendral Building rises to a height of 60.2 meters above ground. Almendral Building was the only structure in the survey which was located in the city of Valparaiso. The date of construction of the building was not determined. However, the structural drawings are dated January, 1972.

The building's plan is almost square (Fig. 6.1(a)) and is made up of nine panels. The structural system is composed of two back-to-back channel shaped shear walls that are coupled with two three-bay frames through girders and the floor slabs. The channel shaped walls extend from the foundation level to the 21st story (Fig. 6.1(b)). The web portions of the walls continue to the 23rd floor, where they are joined together forming a sloping roof above the 23rd floor (Fig. 6.1(b)). The web portion varies in thickness from

45 cm at the first story level to 30 cm above the seventh and has staggered door openings along its elevation.

The building rests on a 1 meter thick mat foundation with its base located at 6.18 meters below grade. The typical story height is 2.55 m with the first story being 3.87 m. The two subterranean levels also consist of nine panels of similar dimensions as those for the stories above. However, these panels are surrounded by shear walls on all four sides and their plan resembles that of a multi-cellular square box. The plan view of the floors above the third level is fairly typical, although openings in the central panel of the 18 cm. thick slab are staggered. Column cross-sections remain rectangular and uniform along the height.

As mentioned in [70], a notable geological feature of Valparaiso is the large portion of the city which is founded on artificial fill. The depth of this fill is 10 m at the coast and tapers to zero approximately 2 km inland. Specific information about the soil conditions near the Almendral Building site were not available, but its location well inside the city would probably have rested its foundation under the artificial fill.

Available structural drawings for the building specified the following material properties:

Concrete : 28-day cylinder strength of 255 kgf/sq. cm (3.60 ksi)

Steel : Specified yield strength of 4200 kgf/sq. cm (60 ksi)

Almendral Building was one of the many reinforced concrete structures included in the post-earthquake survey which suffered minimal structural damage. The DRAIN-2DM [62] computer program was used to calculate the dynamic response of the building for selected ground motion records. Modeling of the structure and analysis results are discussed in detail in the sections that follow.

6.3 STRUCTURAL MODELING

The inelastic dynamic response analysis of the Almendral Building was conducted for three ground acceleration histories. Equivalent column approach to modeling of structural walls in the building necessitated the use of the beam-column element EL2 [27,53], documented in the previous chapter, to model all the structural components. It may be emphasized here that interest was focussed on the global response of the building and precise details of localized events which contribute to the overall response were generally neglected. This point is reflected in the structural modeling of the building where some engineering judgement was used to ignore details which were not expected to significantly affect the overall response.

For the analysis presented here, loading in the form of ground motion will be applied along one of the principal axes of the building, labelled as direction 1 in Fig. 6.1(a). Stronger of the two ground motion component records recorded in the city of Valparaiso on March 3, 1985 and labelled as Almendral N50E in [70] will be used. This history was recorded by an instrument located at a Church which was founded on approximately 5 m of artificial fill. For the purposes of comparison, another Chilean record stronger than the Almendral N50E component and recorded at Vina del Mar will be used as a second record. It is referred to as Vina del Mar component S20W in [70]. The 1940 El Centro earthquake acceleration history will be used as a third record.

The task of modeling the Almendral Building was greatly simplified by its structural regularity and no drastic modeling assumptions had to be made. The plan view shown in Fig. 6.1(a) is typical from stories 3 through 21. Stories 1 and 2 differ slightly from the typical. These differences have been accounted for in the model. Story 22 is an open story with floor slab primarily covering the three central panels along direction 1.

These effects have been partially accounted for. Story 23 is a penthouse over the central panel only and has been ignored in the structural model.

The structural model for the building is shown in Fig. 6.2. Half of the structure has been modeled because of symmetry. Frame A refers to the interior three-bay frame consisting of shear wall and two exterior columns. The effect of exterior columns along column line B, bending about their strong axes, for the loading direction considered, is taken into account by linking the two columns to Frame A model by rigid links. Individual modeling aspects are discussed in the following sections.

6.3.1 Structural Walls

As mentioned previously, structural walls were modeled as equivalent columns at their centroidal axes with rigid links extending out on each side of the column at each floor level to simulate the wall length (Fig. 6.2).

A two-dimensional model of a three-dimensional structure always involves some approximation and at times realistic representation of the structure has to be sacrificed in order to analyze it within the two-dimensional framework. Building structures composed of intersecting shear walls fall into the category of structures for which the use of two-dimensional models involves subjective judgements by the analyst. In cases like these one has to anticipate the three-dimensional behavior and use this information to construct an acceptable model for a two-dimensional case.

In general, orthogonal walls act as flanges which may greatly increase the strength and stiffness of the walls in the direction been analyzed. Expressions for effective flange width(s) for walls are not provided in code provisions, but code provisions [3] for the effective width of compression flanges of T and L beams may be considered to be relevant, with the span of the equivalent beam being taken as twice the height of the cantilever wall [51]. For flanges acting in compression, the effective flange width is

determined by assuming the compression field created in the flange due to actions in the wall spreads out at a 1:1 slope away from the wall. The size of the effective flange increases in this manner until the limits set by the ACI Code are reached [51]:

$$b_e = \min \begin{cases} b_w + 6h_f \\ (b_w + s)/2 \\ b_w + l/2 \end{cases} \quad \text{for slab on one side of the member} \tag{6.1}$$

$$b_e = \min \begin{cases} b_w + 16h_f \\ s \\ l/4 \end{cases} \quad \text{for slab on two sides of the member} \tag{6.2}$$

where b_e is the effective width of the member, b_w is the length of the web, h_f is the thickness of the flange, s is the spacing between webs, and l is the span length.

For flanges acting in tension, the effective flange width is used to estimate the amount of tension reinforcement which is mobilized near ultimate conditions. The amount of flange reinforcing steel which is mobilized near ultimate conditions can be approximated by assuming the tension field created in the flange due to actions of the wall spreads out at a 2:1 slope away from the wall near ultimate [51].

In this study, the size of the tensile and compressive flanges defined by their respective slopes is limited by the flange length itself. As a result, except for the top few stories, full flange length contributes to the strength and stiffness of the wall section. However, to simplify calculations full flange lengths were used as effective flange widths for strength and stiffness calculations for all stories. Because inelastic actions are generally confined to the lower few story levels, this assumption was not expected to significantly affect the overall behavior of the structure.

Specified material properties were used in all strength calculations. The effect of boundary column reinforcement bars being cutoff at virtually every story level was

incorporated by calculating the strength for the resulting new cross-section at each story level. A maximum concrete compressive strain value of 0.003 was used for all strength calculations. The specified steel yield strength was used without any strain hardening.

6.3.2 Beams and Columns

Beams and columns in Almendral Building were also represented by element EL2 in the structural model. Strength calculations for columns included the effect of axial load carried by the column at each story level. Longitudinal reinforcement bars in columns were cutoff at less frequent intervals than those in shear walls. Effect of variation in reinforcement was included for all strength calculations.

Effect of slab was included in the strength calculations for beams. Effective width of slab was calculated from Eqs. 6.1 and 6.2 for the respective cases. Slab reinforcement within this effective flange width was included in strength calculations, when bending caused top fibers to be in tension. All calculations for input parameters of beams assumed no axial load. This assumption is consistent with the assumption that floor slab acted as rigid diaphragm. Centerline distances were taken as beam lengths and the option of providing rigid lengths at member ends was used to simulate the portion of the beam from centerline of columns to the column face.

6.3.3 Rigid Diaphragm Assumption

Floor slabs of the building were assumed to act as rigid diaphragms with respect to lateral translation, but provide no resistance with respect to vertical translation and rotation. The effect was achieved by constraining all the nodes at a story level to translate equally in the same direction, essentially providing only one horizontal degree of freedom per story. This assumption precludes any axial loading in the beams.

Accuracy of the rigid diaphragm assumption depends on the nature of structure which is being analyzed. In the case of Almendral Building, the general regularity of structural elements and similarity of floor plan layout all along the height of the building implies little change in the general resisting behavior of the building. The rigid floor diaphragm approximation should, therefore, be within acceptable limits of accuracy for the type of analysis being considered.

6.3.4 Fixed Base Assumption

The structure was assumed to be fully fixed to an infinitely rigid base at the ground level. The two subterranean levels were, therefore, not included in the analytical model. The assumption of a fully fixed base also ignores the effects of soil-structure interaction.

As mentioned in Sec. 6.2, the two subterranean levels resemble a multi-cellular box with the nine panels bounded by walls on all four sides. Presence of these structural walls in the subterranean level provides a high degree of strength and redundancy as compared to the rest of the structure above the ground level. With a system as stiff as this founded on a 1 meter thick continuous footing, which was resting on firm soil, it is not too unreasonable to assume a fully fixed base at the ground level.

6.3.5 Inertia and Damping

Inertial mass was calculated from the available information on loads (discussed in Sec. 6.4). Lumped masses were assigned to nodes at each story level.

Four percent of critical viscous damping was used in all analyses. Details on the available damping options and calculation of damping factors as used in the DRAIN-2DM program are given in [27].

6.4 Calculation of Loads

In a dynamic analysis, calculation of loads is generally limited to that of gravity loads. For the Almendral Building, calculations for gravity loads assigned to each floor level were based on a typical value of 1000 kgf/sq. m. of floor area. This value was representative of a typical building included in the Chilean survey. Actual calculations of dead weight for the Almendral Building verified the typical value and gravity loads of approximately 980 kgf/sq. m. for a typical floor level were calculated.

Gravity loads were assumed to act uniformly over each floor level. These were distributed amongst the supporting walls and beams on the basis of a certain tributary area assigned to the particular supporting component. Tributary areas were, in most cases, defined by boundaries bisecting the 90 degree angles at the slab span corners. Smaller floor areas at the first and top floor levels, resulted in lower gravity loads as compared to the rest of the floor levels, which were typical.

6.5 Analysis Results and Discussion

Different aspects of the results of dynamic analysis will be discussed in this section. Dynamic analysis of the Almendral Building using the previously discussed analytical model was carried out for three different acceleration time histories, namely, the Vina del Mar record (S20W), the Almendral record (N50E), and the first ten seconds of 1940 El Centro record. The available structural drawings of the building did not indicate its orientation with respect to the global axes. Hence, it cannot be stated with certainty if the building experienced the recorded ground motion along its principal directions. In any case, it is traditional to analyze the structure along its principal directions and draw appropriate conclusions about its general behavior.

6.5.1 Acceleration Records

The recorded acceleration histories for ground motion at Vina del Mar (component S20W) and Almendral (component N50E) are plotted in Figs. 6.3(a) and 6.4(a), respectively. Figure 6.5(a) shows the NS component of 1940 El Centro acceleration record for the first ten seconds. Peak horizontal ground accelerations of 0.36g recorded for the Vina del Mar S20W component was the highest value for the three records considered in this analysis. Peak horizontal ground accelerations for the N50E component of Almendral record was 0.29g. For the 1940 El Centro record, the peak ground acceleration was 0.32g, however, the duration of strong ground motion (ground acceleration in excess of 0.1g) did not last for more than ten seconds. Both Chilean records show that the duration of strong motion was of the order of 60 seconds. Frequency content of the two Chilean records considered in the analysis resembled closely to that of El Centro [70].

6.5.2 Fundamental Period

The value of fundamental period of a structure is often used to classify it into categories based on stiffness. A wall-dominant structure is expected to be stiffer than a regular frame structure of similar dimensions. Simplified expressions are often used to approximate a structure's fundamental period. For a typical U.S. frame building, a commonly used estimate of the fundamental period is N/10, where N is the number of stories. For a typical Chilean building, however, the fundamental period is better approximated by N/20 [36]. Using this expression, the approximate period for Almendral Building was determined to be 1.15 sec. The fundamental period of Almendral Building was measured to be 1.20 sec. during aftershocks.

The fundamental period of the structural model with cracked stiffness was analytically determined to be 1.19 sec. The close agreement between the measured and calculated values demonstrates that the analytical model, at least, represents the building's overall dynamic characteristics fairly well. It may also be noted that fundamental period of the building was measured after the main event and that it is appropriate to compare it with the analytical value based on cracked stiffness.

6.5.3 Roof Displacement

Time histories of roof displacements for Vina del Mar S20W and Almendral N50E components of Chilean record are plotted in Figs. 6.3(b) and 6.4(b), respectively. The results are based on cracked stiffness. The same entity is plotted in Fig. 6.5(b) for El Centro record. For comparison, Figs. 6.6(b), 6.7(b) and 6.8(b) show the top displacement time histories based on uncracked stiffness for Vina del Mar, Almendral and El Centro earthquake records.

The peak values of calculated top drifts expressed as a percentage of total building height for the components under consideration of the Vina del Mar and Almendral records were 0.40 percent and 0.35 percent, respectively, as compared to 0.26 percent for the El Centro record. The results of the analysis based on cracked stiffness also indicated that all the vertical load carrying members remained in the elastic range throughout the ground motion history for the El Centro record. Strong motion peaks between the 30 and 40 second marks of the Vina del Mar record were just enough to push the nodes at the base of the columns in Frame B of the model (Fig. 6.2) into the inelastic region, and plastic rotations were recorded at the lower story nodes. The plastic rotations recorded at these rotations were small in magnitude (on the order of 10^{-4} rad) and did not increase during subsequent excursions. Columns and walls in Frame A of the model did not experience any plastic rotations. Most beams in the analytical model experienced significantly larger

plastic rotations as compared to the columns of Frame B. The strongest peak, which occurred around the 40 second mark of the Vina del Mar record seemed to have caused most damage to the beams. The time history for the Almendral record was relatively less intense as compared to the Vina del Mar record. A similar, but less intense response than that for the Vina del Mar record, was consequently obtained. Strong ground shaking near the 30 second mark caused plastic rotations at the lower story nodes of Frame B. The plastic rotations at the base were extremely small in magnitude (on the order of 10^{-5} rad) and may be considered to represent only the "onset of yielding". Plastic rotations in the beams were also smaller in magnitude as compared to the previous case. Columns and walls in Frame A remained elastic throughout the Almendral ground motion also.

Results of a second set of analyses of the model using uncracked stiffness produced smaller top drifts, as expected. Top drift ratios ranged between 0.32 percent for Vina del Mar record and 0.21 percent for the Almendral record. Induced forces were also higher, as compared to the case of cracked stiffness. Unlike the previous case of cracked stiffness, plastic rotations of comparable magnitude were recorded at the base of the Frame B columns for all three records.

Elastic response spectra of absolute acceleration and relative displacement for the three records considered in this analysis were calculated and presented in [70]. It is also reported in [70] that the shapes of the elastic spectra for the Vina del Mar and Almendral records are notably similar and reveal a characteristic ground period of approximately 0.7 second. However, both the displacement and acceleration ordinates of the Chilean records exceed those of the El Centro record for that period range. In the period range above 0.6 sec, spectral accelerations for Vina del Mar record are higher than those for Almendral record. The results from the analyses of the analytical model were compared with the expected relative top displacement from the elastic displacement spectra, and the agreement between them was reasonably good.

According to Moehle [36], an estimate of local inelastic demands on the wall can be made for given wall displacements by using established procedures that account for elastic and inelastic deformations along the wall height. Assuming the absence of any torsion, wall displacement may be taken to be identical to the building displacement. The following expression is given in [36] for the displacement at the top of the wall:

$$\delta_u = \delta_y + \theta_p h_w = \frac{\phi_y h_w^2}{3} + (\phi_u - \phi_y)\frac{h_w l_w}{2} \tag{6.3}$$

where ϕ_y and ϕ_u are the curvatures at yield and ultimate, respectively, δ_y is the displacement at yield, and h_w and l_w are the height and length of the wall, respectively. Equation 6.3 relates the elastic and inelastic curvatures to the top displacement for a wall with a point load applied at its top. Its basic assumptions are the same as those for the model used in Sec. 5.1.2, i.e. elastic curvatures are distributed over the wall height. For inelastic response, the maximum elastic curvature is equal to the yield curvature, ϕ_y, and inelastic curvatures up to the maximum available curvature ϕ_u accumulate at the base of the wall along a height l_p. In Eq. 6.3 l_p is conservatively taken as equal to $0.5l_w$. Using the wall cross section at the base and specified material properties, the yield curvature for the section was calculated. Using this value of ϕ_y in the elastic (first) term of Eq. 6.3, the yield top displacement of the wall was estimated to be 0.6 percent of the wall height. This value represents the top displacement at first yield of boundary column reinforcement, and is a conservative estimate because of the material overstrengths which usually are not accounted for in such type of calculations, and existing interactions between the structural components. Whichever may be the case, neither the building nor the structural model did experience top drifts of 0.6 percent, and the calculated estimates of top drifts at yield are consistent with the observed damage.

In another related study on Chilean buildings, Sozen [61] developed a simplified model based on knowledge from elementary mechanics, ground motion response, and structural behavior to relate mean drift ratio (top displacement divided by building height) to variables such as H/D and p, where H and D are the wall height and length, respectively, and p is the ratio of wall area to tributary floor area. Based on an effective peak acceleration of 0.5g, the mean drift ratio MDR is given by:

$$MDR = \frac{1}{4}\frac{H}{D}\sqrt{\frac{wg}{Eph}} \tag{6.4}$$

where H, D, and p are as defined above, g is the acceleration due to gravity, h is the typical story height, E is the Young's modulus of elasticity for concrete and w is the unit weight of the building (in terms of unit floor area).

Using the typical values for the Almendral Building, it is estimated that the building can experience a top drift ratio of approximately 0.8 percent without undergoing serious structural damage.

Although the two models discussed above are based on plain approximations, the estimated results correlate quite well with the observed response, at least in the case of the Almendral Building.

6.5.4 Base Shear

Time histories for base shears based on the cracked stiffness model are plotted in Figs. 6.3(c), 6.4(c), and 6.5(c) for Vina del Mar, Almendral, and El Centro records, respectively. Maximum base shears of almost similar magnitude are induced by the three records on the structural model. Variation of maximum base shears ranges from approximately 28 percent of total weight of the building for the Almendral record to 25 percent of total weight for the Vina del Mar record.

For the model based on uncracked stiffness, the values are 5 to 6 percent higher and the variation ranges between approximately 34 percent of building weight in the case of the Almendral record to 30 percent of building weight for the other two records.

It is interesting to compare the induced maximum base shears for the Almendral Building from analysis with the design base shear using static force procedure of the Uniform Building Code 1988 edition [25]. The total design base shear, V, in a given direction is calculated from the following formula [25]:

$$V = \frac{Z\,I\,C}{R_w} W \tag{6.5}$$

where, Z is the Seismic Zone Factor = 0.4 (for Zone 4)

I is the Importance Factor = 1.25 (for Housing Structures)

$$C = \frac{1.25\,S}{T^{2/3}} \tag{6.6}$$

S is the Soil Coefficient = 1.5 (for Soil Type S_3)

T is the Building Period = 1.19 sec. (from earlier calculations)

R_w is the Coefficient based on Structure Type

Structural skeleton of Almendral Building may be classified as a dual system with shear walls and space frames. Using a conservative judgement for dual system type, a value of 9 for R_w specified by the code [25] for Intermediate Moment Resisting Space Frame was selected. An Intermediate Moment Resisting Space Frame is defined in the code [25] as concrete space frame designed in conformance with Sec. 2625(k) of [25]. Conformance with the stated section of the code was, however, not verified. Using the above values of coefficients in Eq. 6.5, a total design base shear of 9.3 percent of building weight is

calculated. A minimum design base shear of 10.4 percent of building weight is warranted if the building frame system is classified as a reinforced concrete shear wall system, ignoring the contribution of the space frames. Coefficient R_w for this case is taken equal to 8. It is important to note here that the design forces specified by the code are intended to keep the structure within the elastic range. The building was not designed according to UBC provisions, but the design forces for the building would probably have been less than what it did experience during the March 3, 1985 earthquake. The fact that the building was able to withstand forces much greater that its design strength indicates the amount of reserve strength.

6.5.5 Interstory Drifts

Interstory drift is the displacement of one level relative to the level above or below it. It gives a measure of the extent of damage within the story level. Maximum story drifts for the structural model of the Almendral Building based on cracked stiffness were 0.64 percent of story height for the Vina del Mar record, 0.57 percent for the Almendral record, and 0.41 percent for the El Centro record. These values were reduced to 0.49 percent, 0.32 percent, and 0.34 percent in the same respective order for the uncracked stiffness case. UBC 88 [25] restricts the story drifts to smaller of $0.03/R_w$ or 0.004 times the story height for buildings more than 65 ft in height. Using an R_w coefficient of 8, a drift limitation of 0.375 percent of story height is established for design base shear, V, as calculated from Eq. 6.5. The UBC 88, however, allows drifts greater than the specified limits when it is determined that greater limits can be tolerated by structural and non-structural elements.

6.5.6 Summary

A dynamic analysis of the Almendral Building, located in Valparaiso, subject to three earthquake records, namely, S20W component of the Vina Del Mar record, N50E component of the Almendral record, and NS component of the 1940 El Centro record, is presented. Although the building is most likely to have experienced ground shaking similar to the Almendral record because of its close proximity to the recording station, the Vina del Mar and the El Centro records have also been used as a basis of comparison of its response. Analysis was carried out along one of the building's principal directions.

It was reported in post-earthquake investigations that the building suffered little to no damage. It is expected that the building might have undergone a peak top drift ratio of 0.5 percent of its height during the earthquake. Reported damage was limited to minor cracking at the base of the building.

Results of the analysis of structural model of the building based on cracked stiffness predicted a peak top drift of 0.35 percent for the N50E component of the Almendral record. It is believed that the predicted top drift might have been slightly underestimated because of the following main reasons: (i) deficiencies in the model introduced by two-dimensional modeling assumptions, (ii) neglecting the effects of soil-structure interaction, and (iii) analysis of the building along its principal direction.

Results of the analysis also indicated some inelastic action at the base of the structural model, even though, as previously mentioned, the drift was slightly underestimated. Three factors could have contributed to the inelastic action: (i) the member strengths for the structural model components were based on specified material properties, which are usually lower than the actual values, (ii) inability of the hysteresis model for the element EL2 to accurately represent the behavior of reinforced concrete frame members and walls, (its contribution may not be very significant when considering

the general behavior), and (iii) the deficiencies introduced by two-dimensional modeling assumptions.

CHAPTER VII
SUMMARY AND CONCLUSIONS

7.1 SUMMARY

Results of an experimental study on the behavior of reinforced concrete structural walls with staggered door openings under reversed cyclic loads were presented in the first four chapters of this report. A comparison of the observed behavior was made with the analytically obtained results for the wall specimens in Chapter 5. In Chapter 6, results of a dynamic analysis of a 23-story building located in Valparaiso, Chile were presented for three different ground acceleration histories.

The experimental program, which was initiated as part of a larger project involving a detailed study into the behavior of a few selected Chilean buildings that experienced the earthquake of March 3, 1985, was inspired by a remarkably good performance of wall-dominated reinforced concrete buildings in that region. Apart from a high wall area to floor area ratio in a typical Chilean building, a staggered pattern of door openings in most structural walls was also revealed by the post-earthquake survey of more than 400 Chilean buildings. Because of the exceptional performance of walls with staggered door openings and relatively nonexistent experimental research on the topic, an experimental program to investigate the effect of amount of horizontal stagger on the behavior of walls under cyclic loads was initiated with a view to providing an alternate option for design engineers. The experimental study, though limited in its scope, did provide conclusive evidence on some aspects of the behavior of walls with staggered openings as presented in Sec. 7.2.

Research is, however, needed on some other aspects of response of these walls. Future areas of research on this topic are presented in Sec. 7.3.

Four isolated wall specimens, namely, W-1, W-2, W-3, and W-4 were constructed on approximately one-fifth scale. The specimens were barbell shaped and represented five-story walls. Specimen W-1 was a solid wall while specimens W-2, W-3, and W-4 had decreasing amount of horizontal stagger between openings. The specimens, which were lightly reinforced, were bolted to the structural floor and and tested in a vertical position. Reversed cyclic loads were applied at the top and an axial load of 60 kips was maintained throughout the tests.

In general, all the test specimens exhibited ductile behavior. General flexural yielding of the boundary column reinforcement in all the wall specimens occurred at an average drift ratio of approximately 0.75 percent. Specimen W-1 experienced average top drifts of as large as 3 percent of its height without loss of strength and relatively minor loss of stiffness. Significant flexural yielding and an evenly distributed pattern of intersecting flexural-shear cracks were obvious at a top drift ratio of 1 percent for all specimens, but no signs of impending failure. All three walls with door openings experienced a shear compression failure in the portion of the wall between the door opening and the compression edge of the wall in the first story level. The diagonal splitting of the failed region was accompanied by compression crushing of the boundary element. The failure was sudden and caused an approximately 20 percent drop in lateral load.

The observed shear compression failure was expected in the case of wall W-2 for which the openings were closest to the boundary column. The location of opening, in close proximity of the boundary element, removed the inplane confinement of the compression zone and a high concentration of shear and compression in the outer portion of the wall resulted in its failure. For walls W-3 and W-4, for which the openings were located closer together than wall W-2, some shear distress between the door openings was

expected because no special reinforcement was used in that region. This did not happen, and the governing failure mode was again shear compression in the outer portion of the wall.

Thus, the staggered opening concept worked well with much less reinforcement detail than required for coupled wall systems. It is anticipated, however, that the compression zone failure experienced by the test specimens would not be significant for longer walls, because the designer would be able to keep the openings away from the compression edge of the wall.

The response of the walls were modeled analytically using basic principles of mechanics and reinforced concrete theory. Predicted response, although not quite accurate in some cases, was within acceptable limits considering the simplicity of the model. An equivalent column analogy for representing shear walls and a finite element model were also used for this purpose. While the results from equivalent column analogy seemed to be overall in better agreement with the experimental results than those from the finite element model, the two techniques cannot be compared on an equivalent basis in that the former is based on a macro-model approach to modeling whereas the latter falls into the category of micro-modeling. The SNAC program, which is based on the finite element method, also failed to correctly predict the ultimate failure mode of the wall specimens. Its modeling approach would require modifications in its parameters in order to account for a change in wall response due to the presence of door openings. This step, however, is not warranted until enough experimental data is available to make generalizations on behavior of walls with staggered openings.

Dynamic response of the 23-story Almendral Building to three different earthquake records was determined by modeling the building using a two-dimensional framework. Walls were modeled as equivalent columns located at their centroidal axis. An almost elastic response to the stronger component of the earthquake record Almendral N50E, recorded at a station located close to the building and applied along the building's principal

direction, compared favorably with the reported light damage to the building during the earthquake. The structural model was able to successfully resist maximum base shears of approximately three times the design base shear stipulated by UBC 88 [25].

7.2 CONCLUSIONS

Based on the results of studies presented in this report, a few conclusions have been reached. Since the experimental study was not meant to be comprehensive in the area of interest, but was rather limited to the effect of one variable only, the results cannot be generalized indiscriminately. The conclusions related to the experimental study are based on the following assumptions: (1) the walls are slender with an aspect ratio (height/length) of at least 3, (2) axial stress on the wall is moderate i.e. less than 500 psi, (3) shear stress on the wall is also within the moderate range, i.e. between $3\sqrt{f'_c}$ and $4\sqrt{f'_c}$ psi, and (4) wall reinforcement, both boundary column and web, is light to moderate, i.e. less than 0.35 percent in the web and less than 4 percent in boundary columns.

(1) Average top story drifts of at least 1 percent may be achieved in walls satisfying the above conditions without significant damage. Higher drifts of 1.5 to 2 percent may be possible with moderately confined boundary elements. Wall W-2 represented the worst case in the four specimens tested with respect to the inplane confinement of compression zone, yet it was able to successfully withstand top drift levels in excess of 1 percent. A top drift as high as 1 percent is not normally expected in a wall-dominant building.

(2) The staggered opening concept is a viable alternative to the "in-line" door openings which create coupled walls. Significantly less detailing around and between the openings is required as compared to coupled walls.

(3) Wall specimens performed satisfactorily even without complying with the boundary column confinement requirements of the UBC 88 [25]. Crushing and

spalling of the boundary column core did not initiate or contribute in any way towards the ultimate failure mode of the wall specimens. Justification of lower transverse reinforcement in boundary columns and its further reduction along the height has also been given in earlier experimental and analytical studies [41,61].

(4) Dynamic analysis of the Almendral Building showed that the building had sufficient overstrength to withstand typical recorded strong ground motions. The results indicated that the building was able to successfully sustain a maximum base shear of approximately three times the UBC 88 [25] design value.

7.3 Recommendations for Future Research

The experimental program reported herein was limited to the study of changing one physical variable only, i.e. the horizontal stagger between openings. The effect of various other parameters, e.g. cross sectional shape, reinforcement ratio, axial load, opening size, wall aspect ratio, etc. needs to be investigated in order to gain further insight into the behavior of walls with staggered openings. It is only after comprehensive studies involving understanding of effects of different parameters should any general conclusions covering a broad spectrum of variables be made.

A couple of interesting features which were brought to light from the experimental results and may be worthy of immediate attention in future research were the ultimate failure mode of the walls and the absence of any damage in the area between the openings. It is anticipated that the shear compression failure mode observed in all three pierced wall specimens can be avoided or delayed by increasing the wall length. If this can be achieved successfully, will the walls with staggered door openings be able to stably withstand drift levels of 1.5 or 2 percent ? And if they can, what will be the ultimate mode of failure ? These are the questions which remain to be answered.

Walls with openings in the reported test program deteriorated rapidly after the shear compression failure, mainly because of loss of crushed concrete and buckling of longitudinal boundary column reinforcement bars. Wall cross sectional shapes with wide flanges, like I-shaped sections can be tested to investigate how much more stability, if any, would be provided by the flanges after the initiation of a shear compression failure.

In the analytical field, it is not feasible to create new concrete wall models or modify existing ones until a definite trend in behavior can be established from a series of experimental programs. When a definite trend in behavior is identified, reliable analytical concrete wall models can be developed which can supplement static and experimental test results.

BIBLIOGRAPHY

BIBLIOGRAPHY

1. Aktan, A. E., and Bertero, V. V., "States of the Art and Practice in the Optimum Seismic Design and Analytical Response Prediction of R/C Frame-Wall Structures", Report No. EERC 82-06, University of California, Berkeley.

2. Aktan, A. E., and Bertero, V. V., "RC Structural Walls: Seismic Design for Shear", Journal of Structural Engineering, ASCE, Vol. 111, No. 8, August 1985, pp. 1775-1791.

3. American Concrete Institute, "Building Code Requirements for Reinforced Concrete, ACI-318-89", 1989 Edition, Detroit, Michigan, 1989.

4. Aristizabal-Ochoa, J. D., "Cracking and Shear Effects on Structural Walls", Journal of Structural Engineering, ASCE, Vol. 109, No. 5, May 1983, pp. 1267-1277.

5. Arvidsson, K., "Shear Walls with Door Openings Near the Edge of the Wall", ACI Journal, Proceedings, v71, No. 7, July 1974, pp. 353-357.

6. Arvidsson, K., "Elastically Founded Shear Walls with Two Rows of Openings", ACI Journal, Proceedings, v73, No. 3, March 1976, pp. 151-154.

7. Bachmann, H., "Influence of Shear and Bond on Rotational Capacity of Reinforced Concrete Beams", Publications, International Association for Bridge and Structural Engineering, Vol. 30, Zurich, 1970, pp. 11-28.

8. Barda, F., Hanson, J. M., and Corley, W. G., "An Investigation of the Design and Repair of Low-Rise Shear Walls", Proceedings, Fifth World Conference on Earthquake Engineering, Rome, 1973.

9. Barda, F., Hanson, J. M., and Corley, W. G., "Shear Strength of Low-Rise Walls with Boundary Elements", Reinforced Concrete Structures in Seismic Zones, American Concrete Institute Special Publication 53, 1977, pp. 149-202.

10. Benjamin, J. R., and Williams, H., "The Behavior of One-Story Reinforced Concrete Shear Walls", Journal of the Structural Division, ASCE, Vol. 83, No. ST3, May 1957, pp. 1-49.

11. Benjamin, J. R., and Williams, H. A., "Behavior of One-Story Reinforced Concrete Shear Walls Containing Openings", Journal of ACI, Proceedings, v55, No. 5, November 1958, pp. 605-618.

12. Bertero, V. V., "Seismic Behavior of Reinforced Concrete Wall Structural Systems", State-of-the-Art in Earthquake Engineering 1981, Seventh World Conference on Earthquake Engineering, Proceedings, Istanbul, Turkey, 1981.

13. Bolander Jr., J. E., and Wight, J. K., "Towards Realistic FE Models for Reinforced Concrete Shear Wall Dominant Buildings Subjected to Lateral Loading", Report No. UMCE 89-2, Department of Civil Engineering, University of Michigan, January, 1989.

14. Cardenas, A. E., Hanson, J. M., Corley, W. G., and Hognestad, E., "Design Provisions for Shear Walls", ACI Journal, Proceedings, v70, No. 3, March 1973, pp. 221-230.

15. Cardenas, A. E., Russell, H. G., and Corley, W. G., "Strength of Low-Rise Structural Walls", Reinforced Concrete Structures Subjected to Wind and Earthquake Forces, American Concrete Institute Special Publication 63, 1980, pp. 221-242.

16. Choi, C., and Bang, M., "Plate Element with Cutout for Perforated Shear Wall", Journal of Structural Engineering, ASCE, Vol. 113, No. 2, February 1987, pp. 295-306.

17. Daniel, J. I., Shiu, K. N., and Corley, W. G., "Openings in Earthquake-Resistant Structural Walls", Journal of Structural Engineering, ASCE, Vol. 112, No. 7, July 1986, pp. 1660-1676.

18. Derecho, A. T., "Strength, Stiffness and Ductility Required in Reinforced Concrete Structural Walls for Earthquake Resistance", ACI Journal, Proceedings, v76, No. 8, August 1979, pp. 875-896.

19. Fintel, M., "Ductile Shear Walls in Earthquake Resistant Multistory Buildings", ACI Journal, Proceedings, v71, No. 6, June 1974, pp. 296-305.

20. Fiorato, A. E., Oesterle, R. G., and Corley, W. G., "Ductility of Structural Walls for Design of Earthquake-Resistant Buildings", Proceedings, Sixth World Conference on Earthquake Engineering, New Delhi, India, January 1977.

21. Green, N. B., "Factors in the Aseismic Design of Reinforced Concrete Shear Walls Without Openings", ACI Journal, Proceedings, v65, No. 8, August 1968, pp. 629-633.

22. Hiraishi, H., "Evaluation of Shear and Flexural Deformations of Flexural Type Shear Walls", Proceedings, 4th Joint Technical Coordinating Committee, U.S.-Japan Cooperative Earthquake Research Program, Building Research Institute, 1983.

23. Hognestad, E., "Confirmation of Inelastic Stress Distribution in Concrete", Journal, Structural Division, Proc. ASCE, Vol. 83, No. ST2, March, 1957.

24. Illiya, R., and Bertero, V. V., "Effect of Amount and Arrangement of Wall-Panel Reinforcement on Hysteretic Behavior of Reinforced Concrete Walls", Report No. EERC 80-04, University of California, Berkeley.

25. International Conference of Building Officials, "Uniform Building Code", 1988 Edition, Whittier, California, 1988.

26. Kabaila, A. P., and Edwards, R. J., "Hybrid Element Applied to Shear Wall Analysis", Journal of the Structural Division, ASCE, Vol. 105, No. ST12, December 1979, pp. 2753-2760.

27. Kanaan, A., and Powell, G. H., "General Purpose Computer Program for Inelastic Dynamic Response of Plane Structures", Report No. EERC 73/06, University of California, Berkeley.

28. Kumar, A., and Wight, J. K., "Nonlinear Analysis of Reinforced Concrete Frame-Shearwall Structures Subjected to Earthquake Motion (User's Guide to DRAIN-2D: EL7 for RC Shearwalls)", Report No. UMEE 83R4, University of Michigan, October 1983.

29. Macleod, I. A., "New Rectangular Finite Element for Shear Wall Analysis", Journal of the Structural Division, ASCE, Vol. 95, No. ST3, March 1969, pp. 399-409.

30. Macleod, I. A., "Connected Shear Walls of Unequal Width", ACI Journal, Proceedings, v67, No. 5, May 1970, pp. 408-412.

31. Mahin, S. A., and Bertero, V. V., "Nonlinear Seismic Response of a Coupled Wall System", Journal of the Structural Division, ASCE, Vol. 102, No. ST9, September 1976, pp. 1759-1780.

32. Mattock, A. H., Discussions of "Rotational Capacity of Reinforced Concrete Beams", by W. G. Corley, Proc. of ASCE, Journal of Structural Division, Vol. 93, ST2, April, 1967, pp. 519-522.

33. Mirza, M. S., "Study of the Behavior of Coupled Shear Wall Systems", Reinforced Concrete Structures Subjected to Wind and Earthquake Forces", American Concrete Institute Special Publication 63, 1980, pp. 301-328.

34. Moehle, J. P., "Seismic Response of Vertically Irregular Structures", Journal of Structural Engineering, ASCE, Vol. 110, No. 9, September 1984, pp. 2002-2014.

35. Moehle, J. P., "Seismic Analysis of R/C Frame-Wall Structures", Journal of Structural Engineering, ASCE, Vol. 110, No. 11, November 1984, pp. 2619-2634.

36. Moehle, J. P., and Wallace, J. W., "Ductility and Detailing Requirements of Shear Wall Buildings", Proceedings, 5th Chilean Conference on Earthquake Engineering, Santiago, Chile, August, 1989.

37. Oesterle, R. G., Fiorato, A. E., Johal, L. S., Carpenter, J. E., Russel, H. G., and Corley, W. G., "Earthquake-Resistant Structural Walls - Tests of Isolated Walls - Phase I", Report to National Science Foundation, Portland Cement Association, Nov. 1976.

38. Oesterle, R. G., and Fiorato, A. E., "Free Vibration Tests of Structural Concrete Walls", Report to National Science Foundation, Portland Cement Association, February 1980.

39. Oesterle, R. G., Fiorato, A. E., Johal, L. S., Carpenter, J. E., Russel, H. G., and Corley, W. G., "Earthquake-Resistant Structural Walls - Tests of Isolated Walls - Phase II", Report to National Science Foundation, Portland Cement Association, Nov. 1980.

40. Oesterle, R. G., Fiorato, A. E., Aristizabal-Ochoa, J. D., and Corley, W. G., "Hysteretic Response of Reinforced Concrete Structural Walls", Reinforced Concrete Structures Subjected to Wind and Earthquake Forces", American Concrete Institute Special Publication 63, 1980, pp. 243-274.

41. Oesterle, R. G., Fiorato, A. E., and Corley, W. G., "Reinforcement Details for Earthquake-Resistant Structural Walls", Concrete International, American Concrete Institute, Vol. 2, No. 12, Dec. 1980, pp. 55-66.

42. Oesterle, R. G., Aristizabal-Ochoa, J. D., Shiu, K. N., and Corley, W. G., "Web Crushing of Reinforced Concrete Structural Walls", ACI Journal, Proceedings, v81, No. 3, May-June 1984, pp. 231-241.

43. Oesterle, R. G., "Inelastic Analysis of Inplane Strength of Reinforced Concrete Shear Walls", Ph.D. Thesis, Northwestern University, Evanston, Illinois, June, 1986.

44. Okamoto, S., Wight, J. K., Nakata, S., Yoshimura, M., and Kaminosono, T., "Testing, Repair, Strengthening and Retesting of a Full-Scale Seven-Story R/C Building", Earthquake Effects on R/C Structures: U. S. - Japan Research, American Concrete Institute Special Publication 84, 1985.

45. Park, R., "Ductile Design Approach for Reinforced Concrete Frames", Earthquake Spectra, Earthquake Engineering Research Institute, Vol. 2, No. 3, May 1986, pp. 565-619.

46. Park, R., and Paulay, T., "Reinforced Concrete Structures", John Wiley and Sons, New York, 1975, 816 pp.

47. Paulay, T., and Binney, J. R., "Diagonally Reinforced Coupling Beams of Shear Walls", Shear in Reinforced Concrete, American Concrete Institute Special Publication 42, 1974, pp. 579-598.

48. Paulay, T., and Santhakumar, A. R., "Ductile Behavior of Coupled Shear Walls", Journal of the Structural Division, ASCE, Vol. 102, No. ST1, January 1976, pp. 93-108.

49. Paulay, T., "Earthquake Resisting Shear Walls - New Zealand Design Trends", ACI Journal, Proceedings, v77, No. 3, May-June 1980, pp. 144-152.

50. Paulay, T., Priestley, M. J. N., and Synge, A. J., "Ductility in Earthquake Resisting Squat Shear Walls", ACI Journal, Proceedings, v79, No. 4, July-August 1982, pp. 257-269.

51. Paulay, T., "The Design of Ductile Reinforced Concrete Structural Walls for Earthquake Resistance", Earthquake Spectra, Vol. 2, No. 4, Oct. 1986, pp. 783-823.

52. Personal Correspondence with J. E. Bolander Jr.

53. Powell, G. H., "DRAIN-2D User's Guide", Report No. EERC 73/22, University of California, Berkeley.

54. Riddell, R., Wood, S. L., and De La Llera, J. C., "The 1985 Chile Earthquake: Structural Characteristics and Damage Statistics for the Building Inventory in Vina del Mar", Civil Engineering Studies, Structural Research Series No. 534, University of Illinois, Urbana, April 1987.

55. Sattary, V., and Wight, J. K., "Analytical Studies of Reinforced Concrete Shear Walls", Report No. UMCE 88-6, Department of Civil Engineering, University of Michigan, May, 1988.

56. Schwaighofer, J., "Door Openings in Shear Walls", ACI Journal, Proceedings, v64, No. 11, November 1967, pp. 730-734.

57. Shiu, K. N., Aristizabal-Ochoa, J. D., Barney, G. B., Fiorato, A. E., and Corley, W. G., "Earthquake Resistant Structural Walls - Coupled Wall Tests", Report to National Science Foundation, Portland Cement Association, July 1981.

58. Shiu, K. N., Daniel, J. I., Aristizabal-Ochoa, J. D., Fiorato, A. E., and Corley, W. G., "Earthquake-Resistant Structural Walls - Tests of Walls With and Without Openings", Report to National Science Foundation, Portland Cement Association, July 1981.

59. Shiu, K. N., Takayanagi, T., and Corley, W. G., "Seismic Behavior of Coupled Wall Systems", Journal of Structural Engineering, ASCE, Vol. 110, No. 5, May 1984, pp. 1051-1066.

60. Sozen, M. A., "Review of Earthquake Response of R/C Buildings with a View to Drift Control", State-of-the-Art in Earthquake Engineering 1981, Seventh World Conference on Earthquake Engineering, Proceedings, Istanbul, Turkey, 1981.

61. Sozen, M. A., "Earthquake Response of Buildings with Robust Walls", Proceedings, 5th Chilean Conference on Earthquake Engineering, Santiago, Chile, August, 1989.

62. Tang, X., and Goel, S. C., "DRAIN-2DM - Technical Notes and User's Guide", Report No. UMCE 88-1, Department of Civil Engineering, University of Michigan, January, 1988.

63. Vallenas, J. M., Bertero, V. V., and Popov, E. P., "Hysteretic Behavior of Reinforced Concrete Structural Walls", Report No. EERC 79-20, University of California, Berkeley.

64. Vulcano, A., and Bertero, V. V., "Analytical Modelsfor Predicting the Lateral Response of RC Shear Walls: Evaluation of Their Reliability", Report No. UCB/EERC-87/19, University of California, Berkeley.

65. Wagner, M. T., and Bertero, V. V., "Mechanical Behavior of Shear Wall Vertical Boundary Members: An Experimental Investigation", Report No. EERC 82-18, University of California, Berkeley.

66. Wallace, B., and Krawinkler, H., "Small Scale Model Tests of Structural Components and Assemblies", Earthquake Effects on R/C Structures: U. S. - Japan Research, American Concrete Institute Special Publication 84, 1985.

67. Wang, T. Y., Bertero, V. V., and Popov, E. P., "Hysteretic Behavior of Reinforced Concrete Framed Walls", Report No. EERC 75-23, University of California, Berkeley.

68. Weaver Jr., W., Lee, D., and Derbalian, G., "Finite Element for Shear Walls in Multi-Story Frames", Journal of the Structural Division, ASCE, Vol. 107, No. ST7, July 1981, pp. 1365-1369.

69. Wolfgram, C., Rothe, D., Wilson, P., and Sozen, M. A., "Earthquake Simulation Tests of Three One-Tenth Scale Models", Earthquake Effects on R/C Structures: U. S. - Japan Research, American Concrete Institute Special Publication 84, 1985.

70. Wood, S. L., Wight, J. K., and Moehle, J. P., "The 1985 Chile Earthquake: Observations an Earthquake-Resistant Construction in Vina del Mar", Structural Research Studies, Structural Research Series No. 532, University of Illinois, Urbana, February, 1987.

71. Yamada, M., Kawamura, H., and Katagihara, K., "Reinforced Concrete Shear Walls Without Openings; Test and Analysis", Shear in Reinforced Concrete, American Concrete Institute Special Publication 42, 1974, pp. 539-558.

72. Yamada, M., Kawamura, H., and Katagihara, K., "Reinforced Concrete Shear Walls With Openings; Test and Analysis", Shear in Reinforced Concrete, American Concrete Institute Special Publication 42, 1974, pp. 559-578.

FIGURES

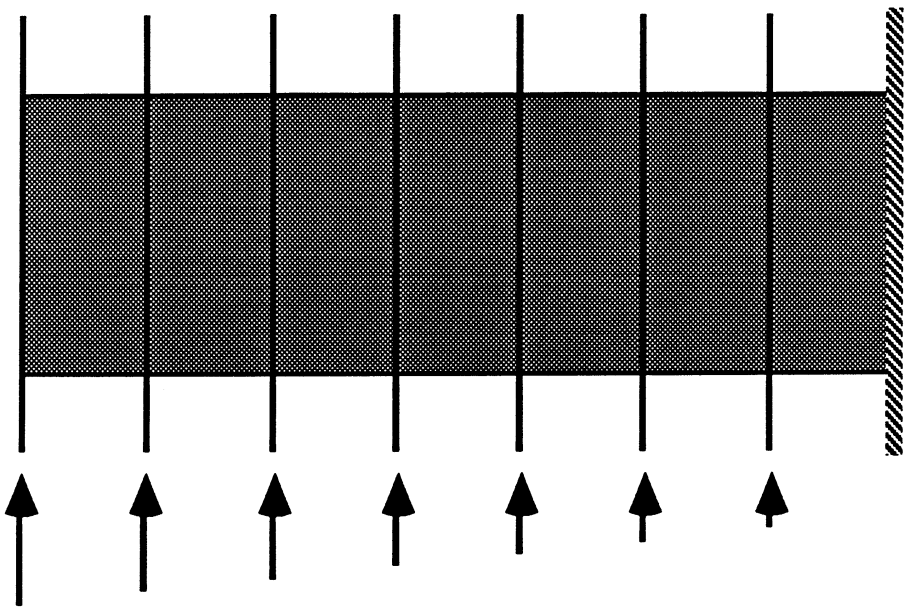

(b) Slender Wall

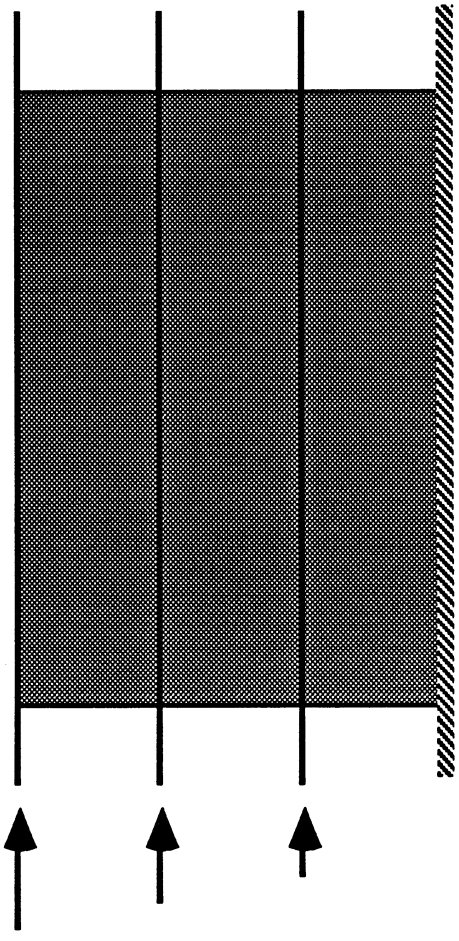

(a) Squat Wall

Fig. 1.1 : Cantilever Structural Walls.

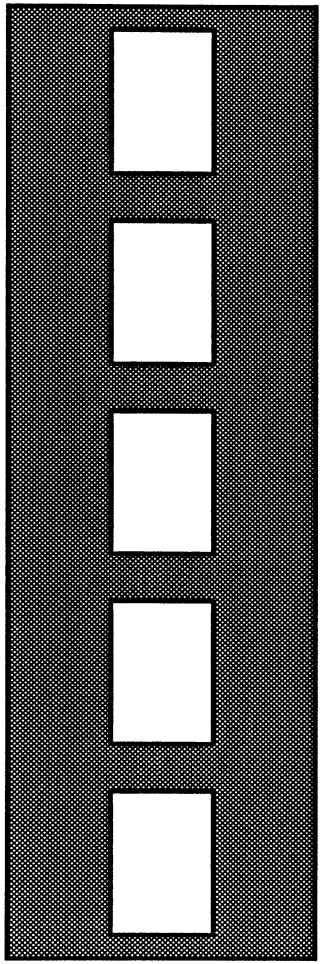

(a) Coupled Wall

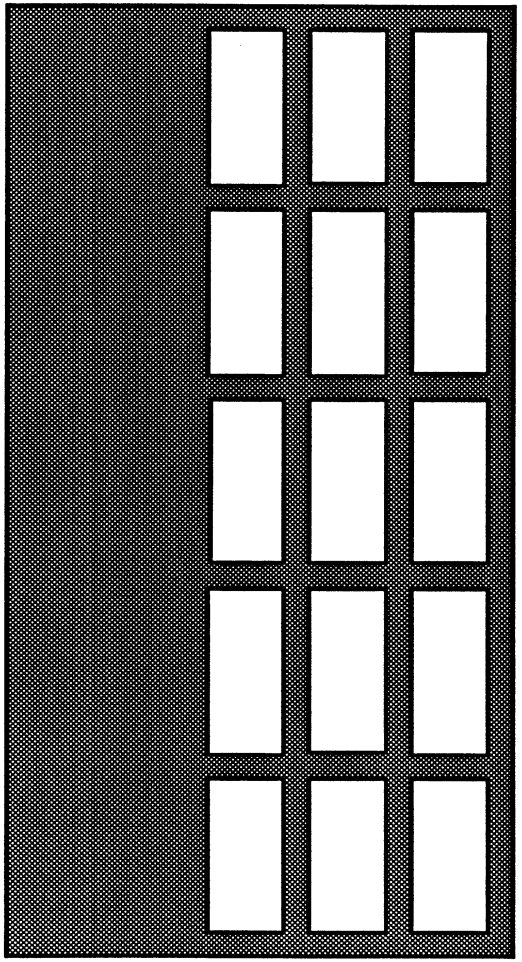

(b) Wall-Frame System

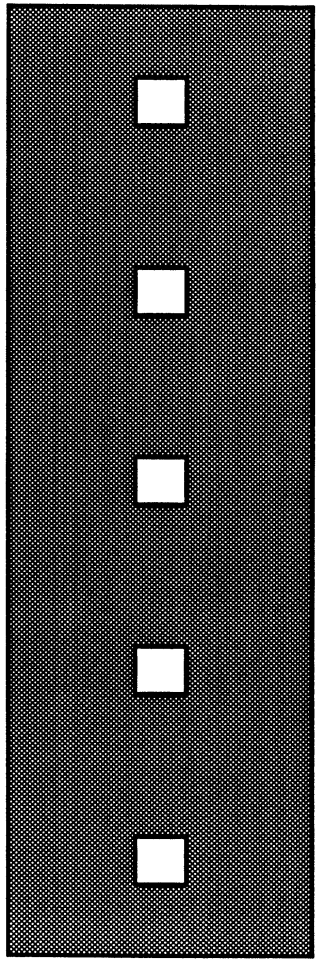

(c) Pierced Wall

Fig. 1.2 : Types of Wall Systems.

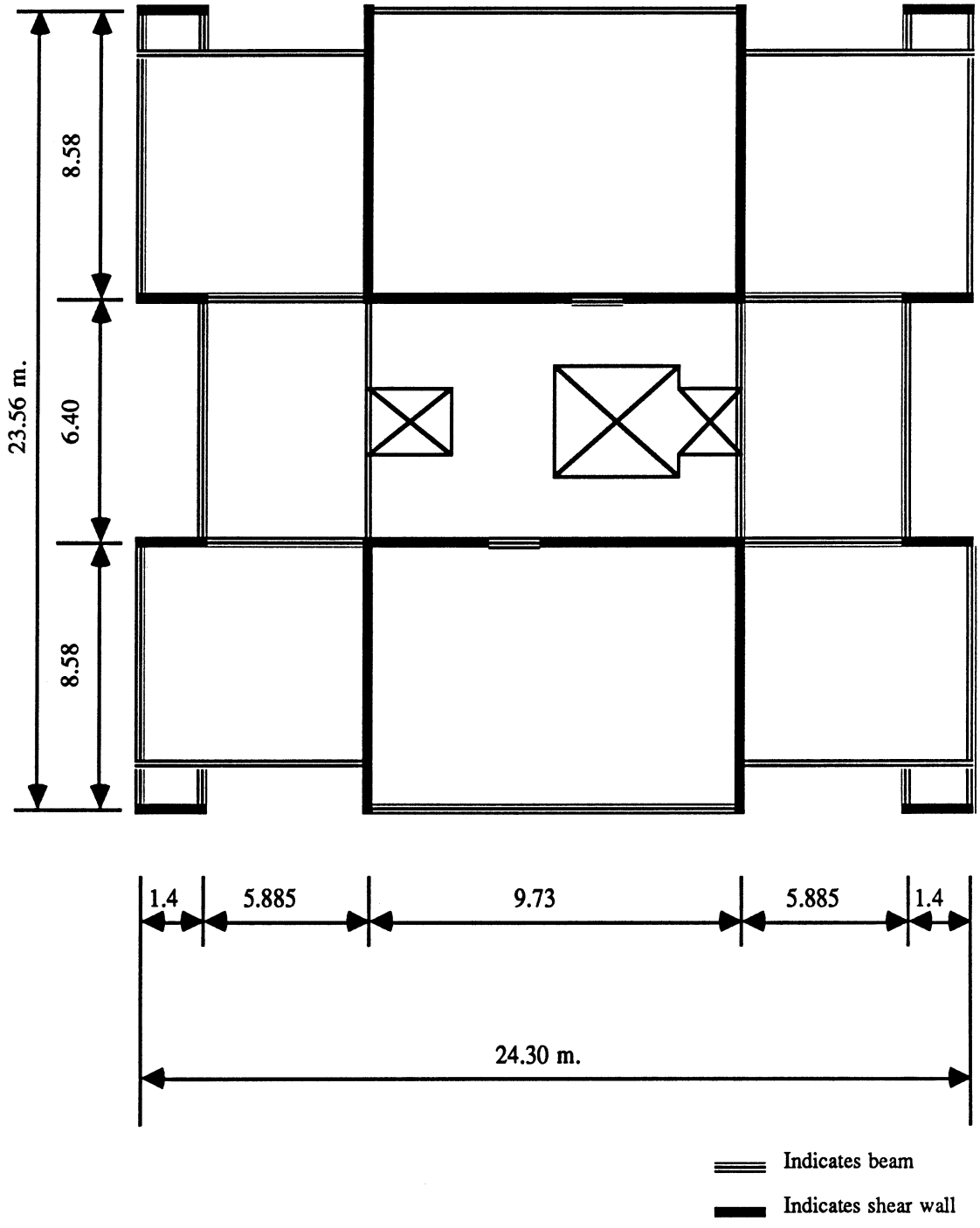

Fig 1.3(a) : Plan View of a Typical Story of Almendral Building.

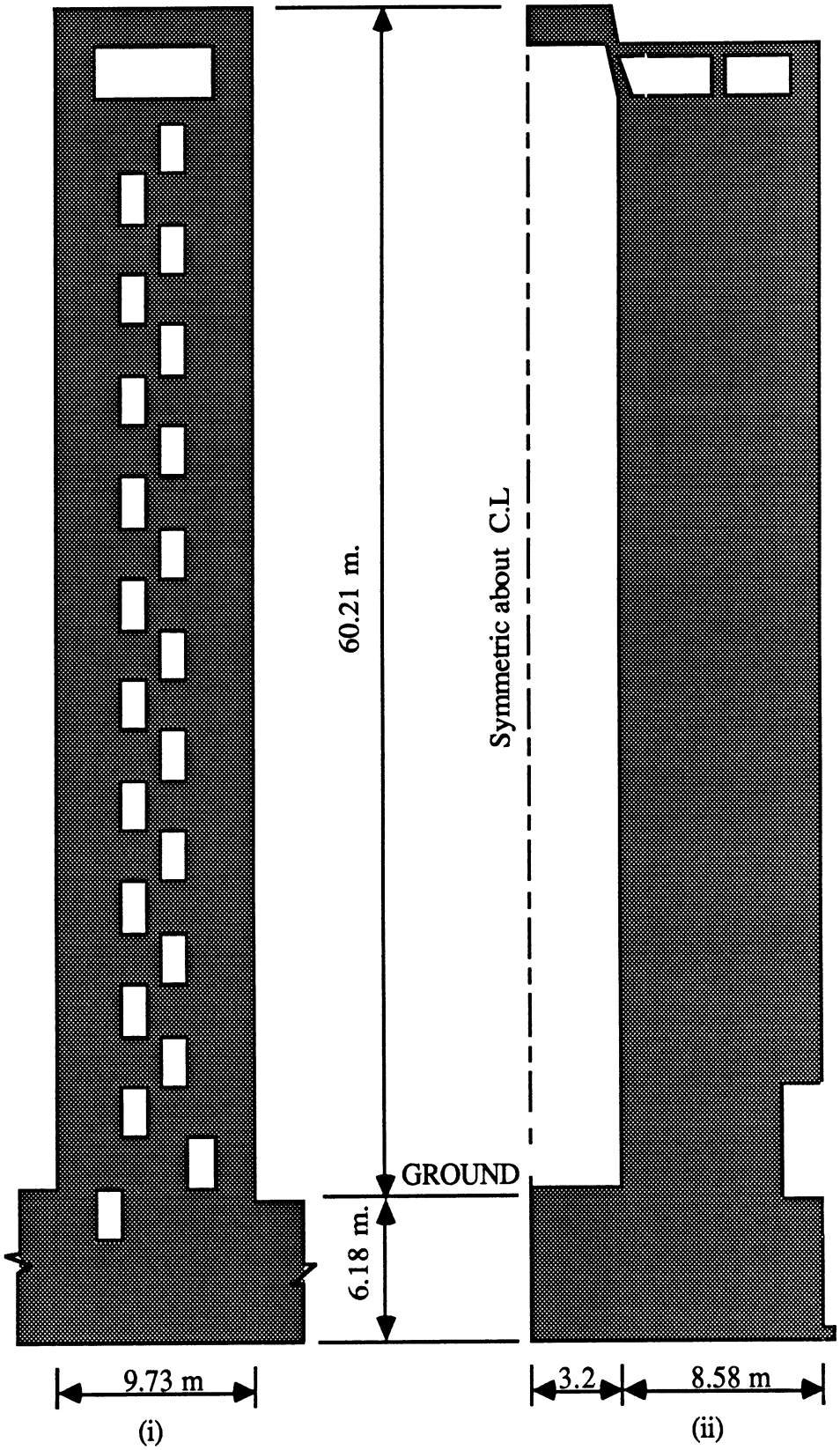

Fig. 1.3(b) : Elevations of Walls in Almendral Building along
(i) Web Portion (ii) Flange Portion.

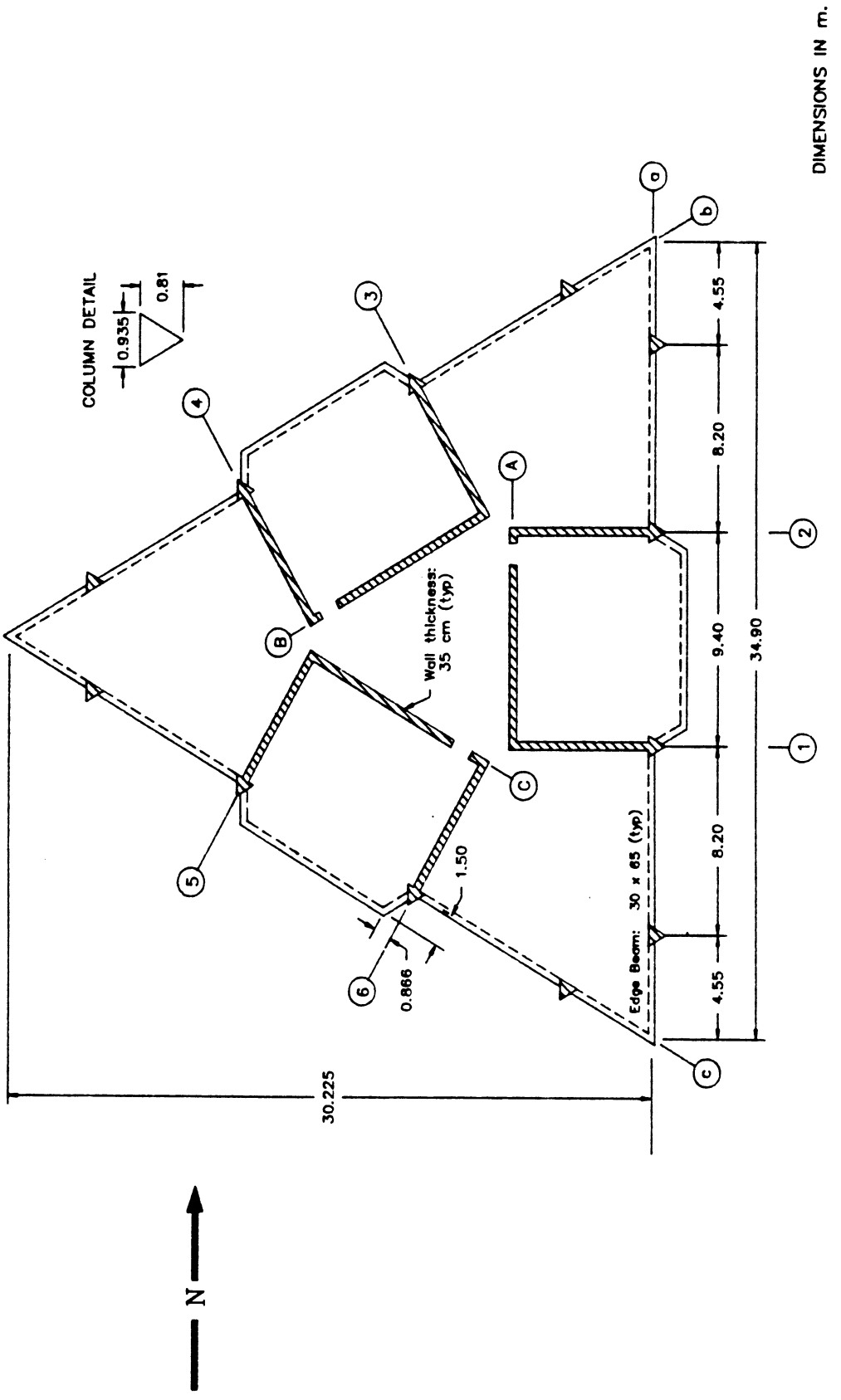

Fig. 1.4(a) : Plan View of a Typical Story of Miramar Building.

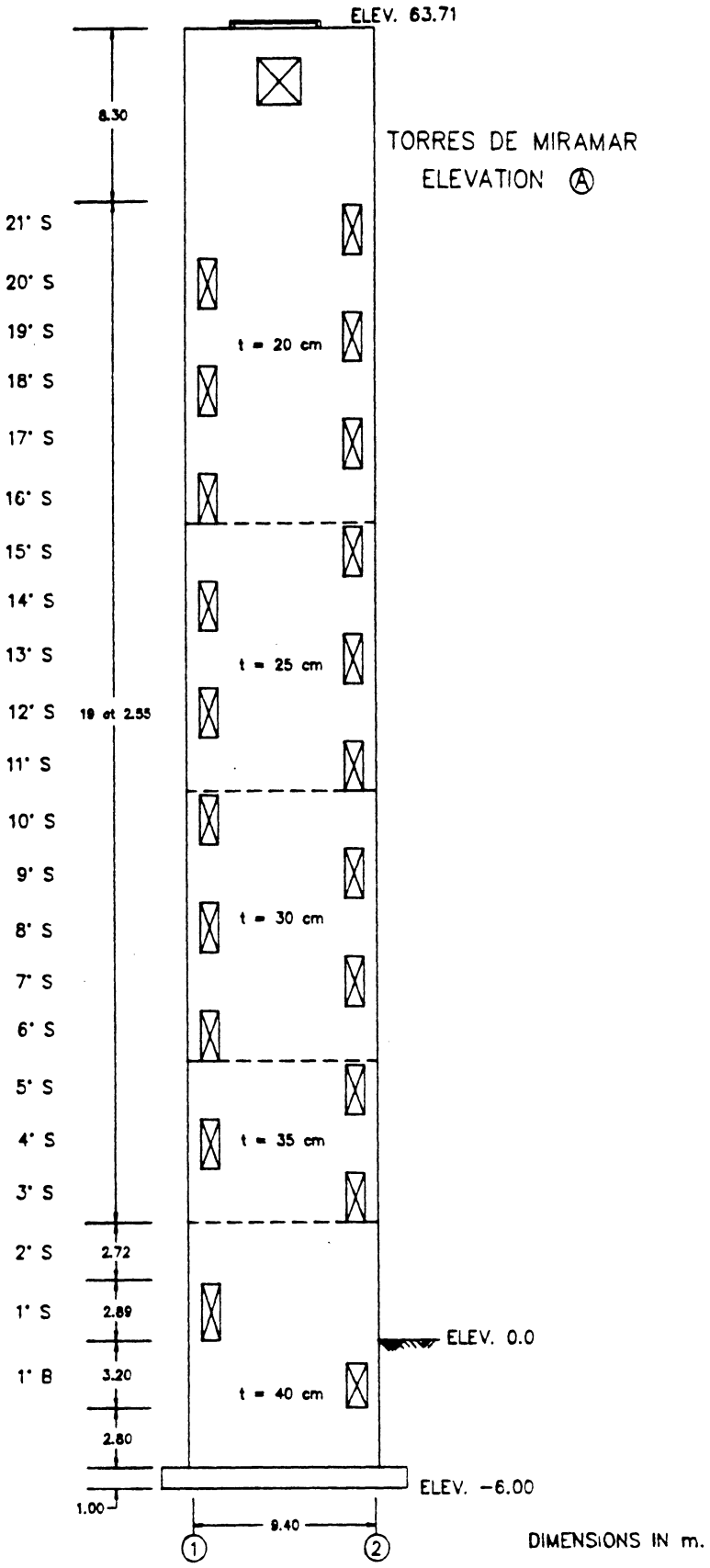

Fig. 1.4(b) : Elevation along Wall A of Miramar Building.

SPECIMEN W-1

Total height = 12' + 2' base block
Total width = 4'
Story Height = 2' - 4"
No. of Stories = 5
Wall Panel Thickness = 3"
Overall Aspect Ratio = 2.92
Story Aspect Ratio = 0.583

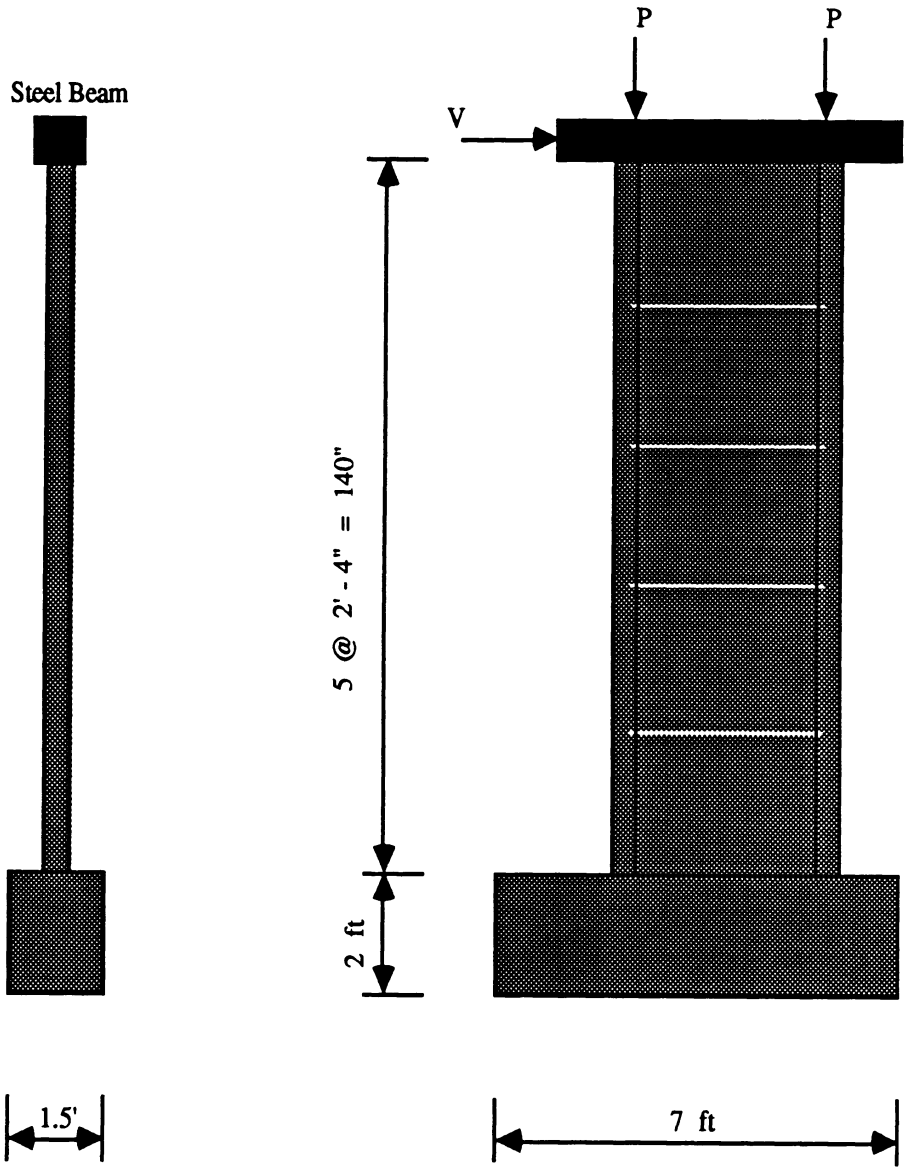

Fig. 3.1(a) : Specimen W-1.

SPECIMEN W-2

Total height = 12' + 2' base block
Total width = 4'
Story Height = 2' - 4"
No. of Stories = 5
Wall Panel Thickness = 3"
Overall Aspect Ratio = 2.92
Story Aspect Ratio = 0.583

Opening Size = 9" x 20"
Opening Area/Wall Area = 13.4 %
Lintel Beam Depth = 8"

Clear Vertical Distance between Openings = 8"
Clear Horizontal Distance between Openings = 15"
Angle between Corners = 28 deg.

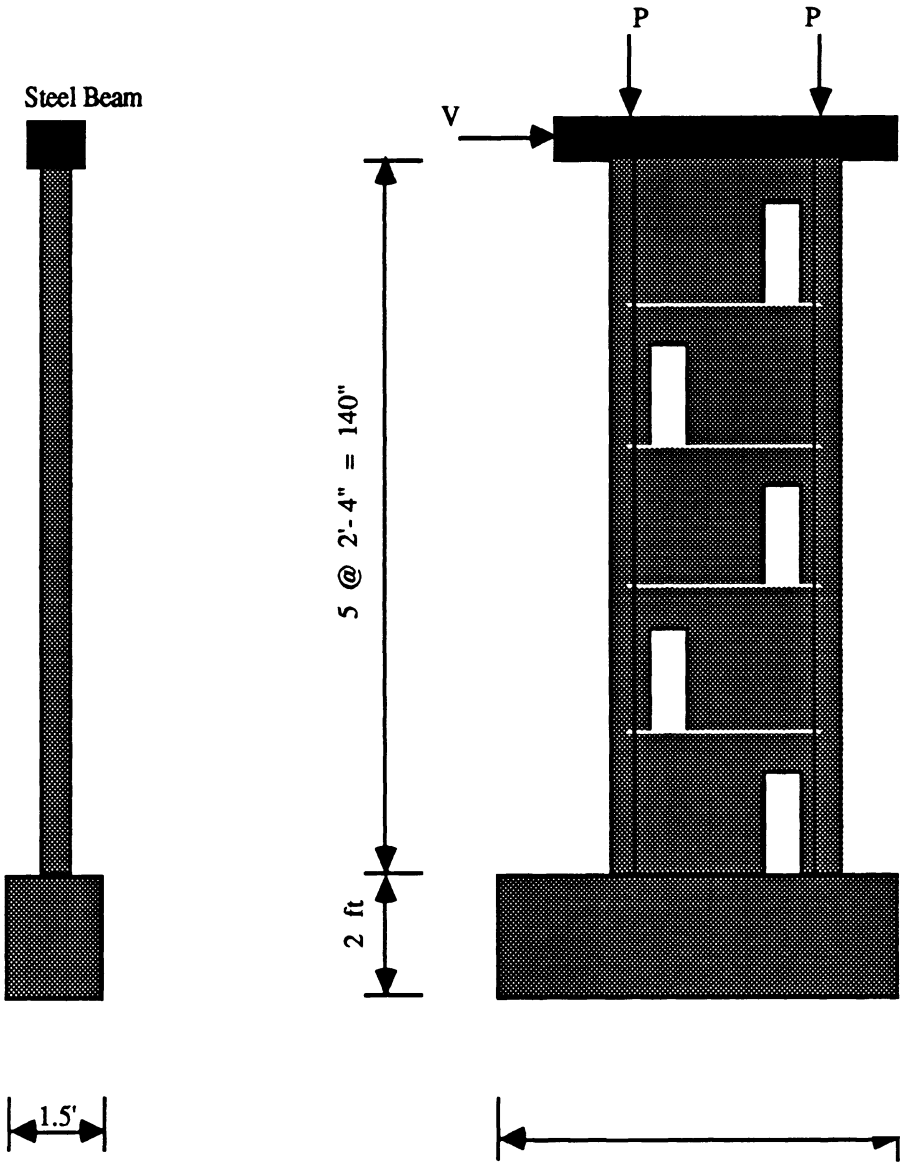

Fig. 3.1(b) : Specimen W-2.

SPECIMEN W-3

Total height = 12' + 2' base block
Total width = 4'
Story Height = 2' - 4"
No. of Stories = 5
Wall Panel Thickness = 3"
Overall Aspect Ratio = 2.92
Story Aspect Ratio = 0.583

Opening Size = 9" x 20"
Opening Area/Wall Area = 13.4 %
Lintel Beam Depth = 8"

Clear Vertical Distance between Openings = 8"
Clear Horizontal Distance between Openings = 8"
Angle between Corners = 45 deg.

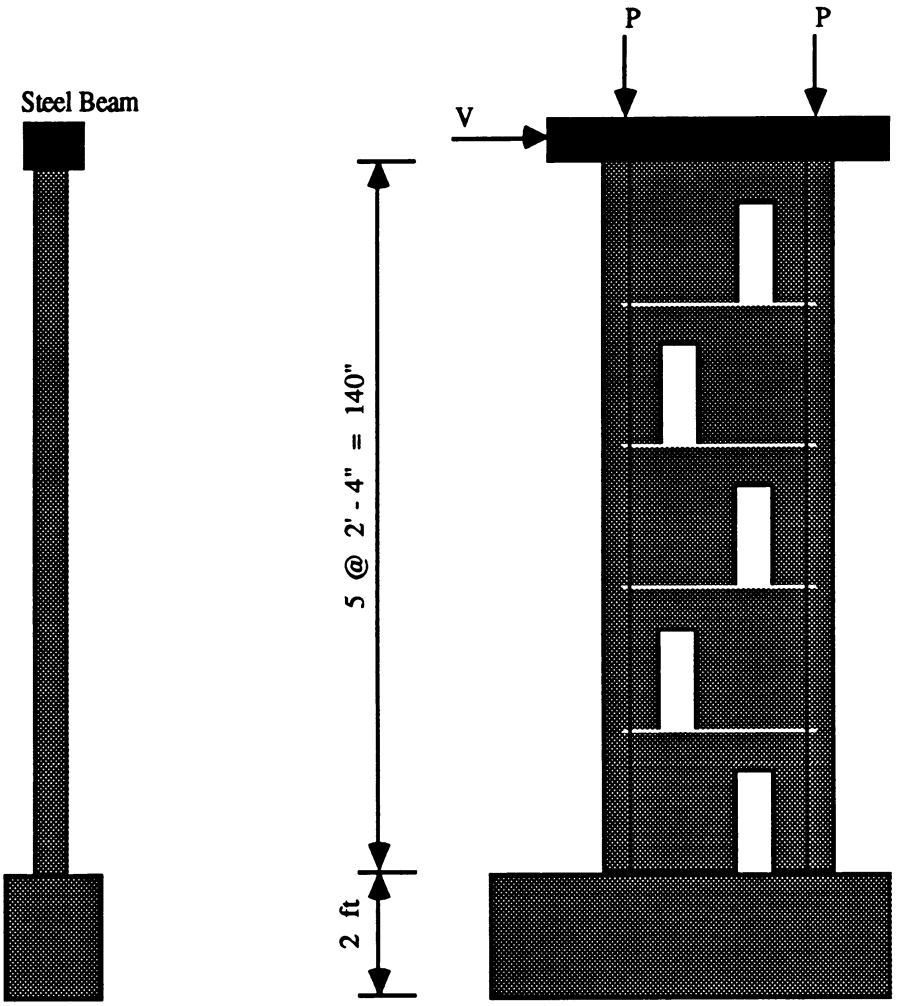

Fig. 3.1(c) : Specimen W-3.

SPECIMEN W-4

Total height = 12' + 2' base block
Total width = 4'
Story Height = 2' - 4"
No. of Stories = 5
Wall Panel Thickness = 3"
Overall Aspect Ratio = 2.92
Story Aspect Ratio = 0.583

Opening Size = 9" x 20"
Opening Area/Wall Area = 13.4 %
Lintel Beam Depth = 8"

Clear Vertical Distance between Openings = 8"
Clear Horizontal Distance between Openings = 5"
Angle between Corners = 58 deg.

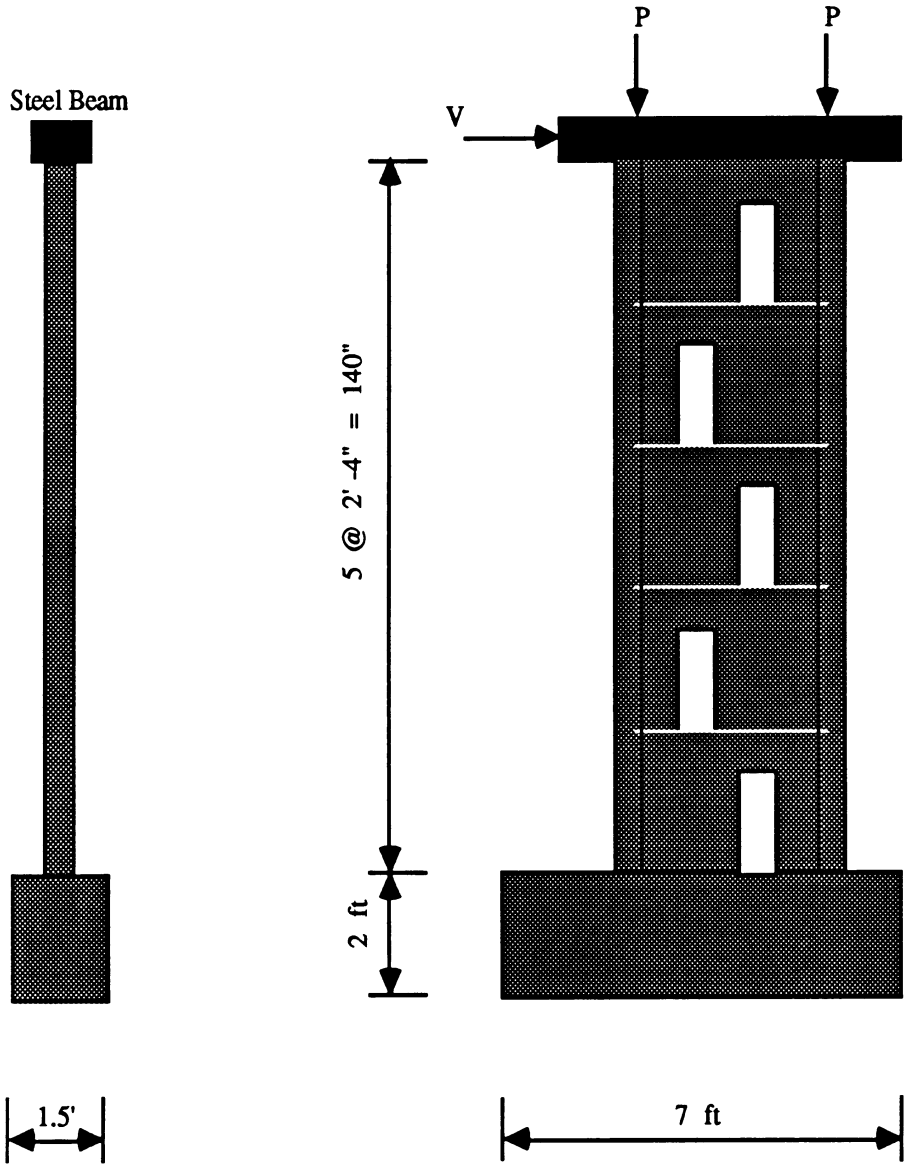

Fig. 3.1(d) : Specimen W-4.

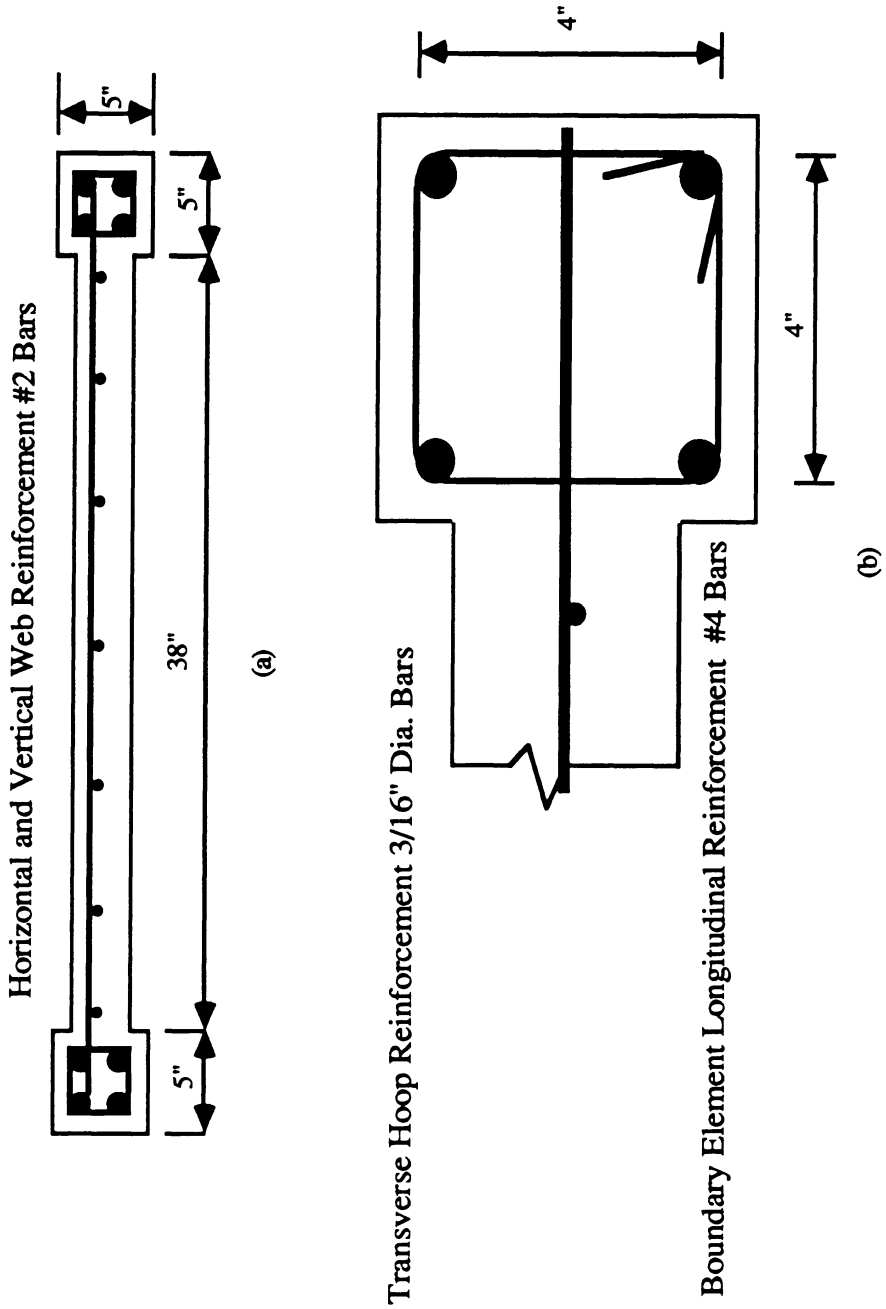

Fig. 3.2 : (a) Typical Cross-Section of Specimen.
(b) Boundary Element Details.

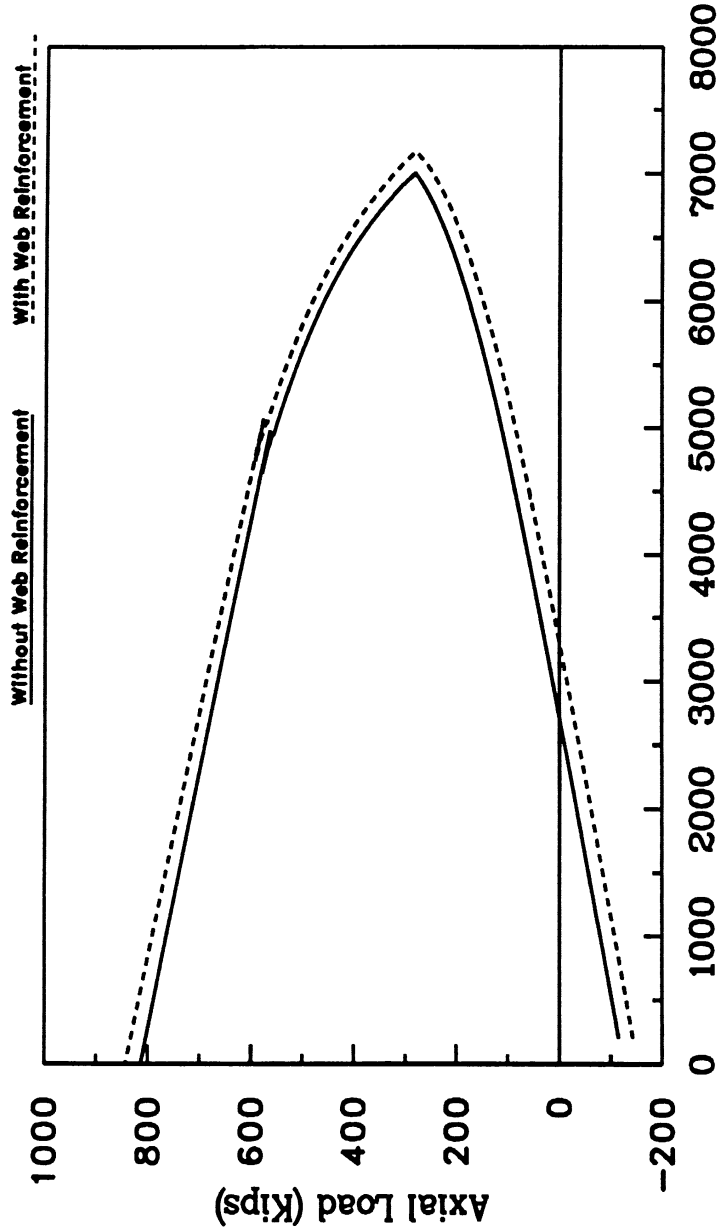

Fig. 3.3 : Axial Load-Moment Interaction Diagram.

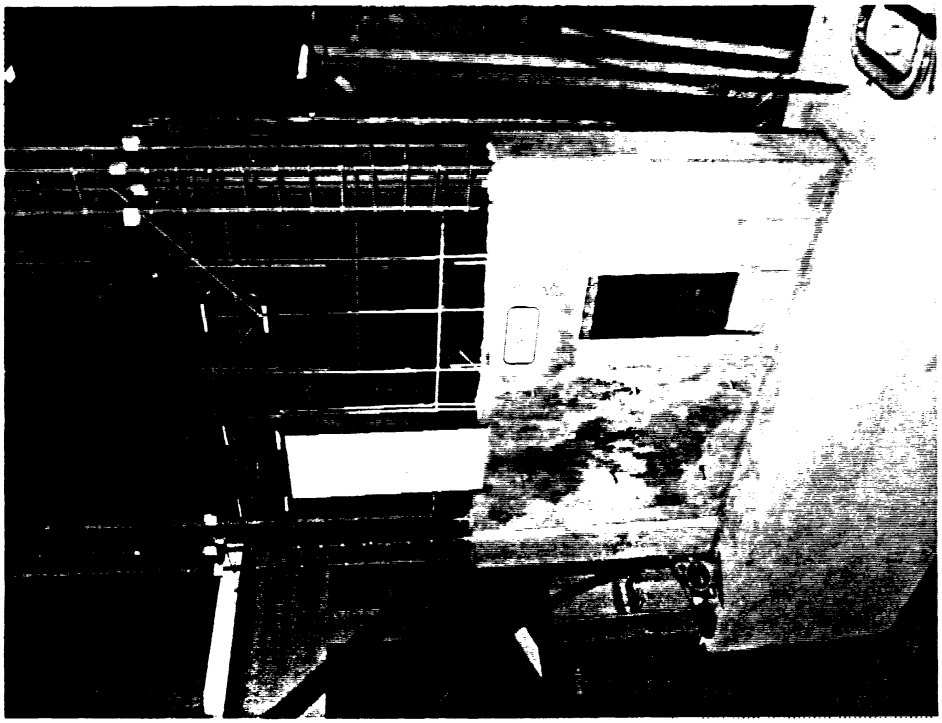

(b)

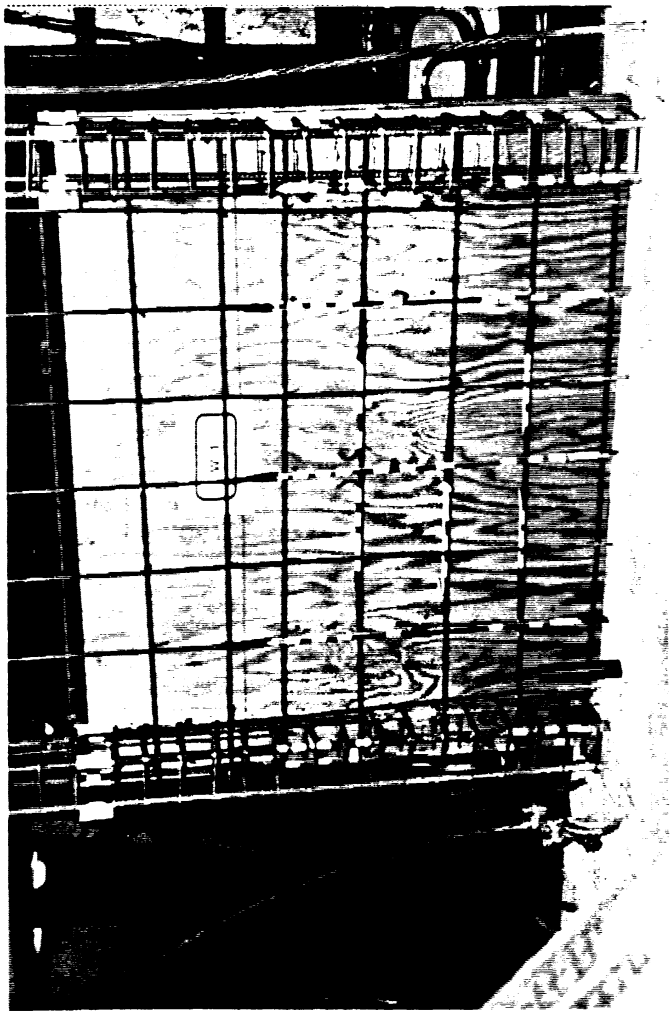

(a)

Fig. 3.4 : Typical Reinforcement for (a) Wall W-1, (b) Wall W-3.

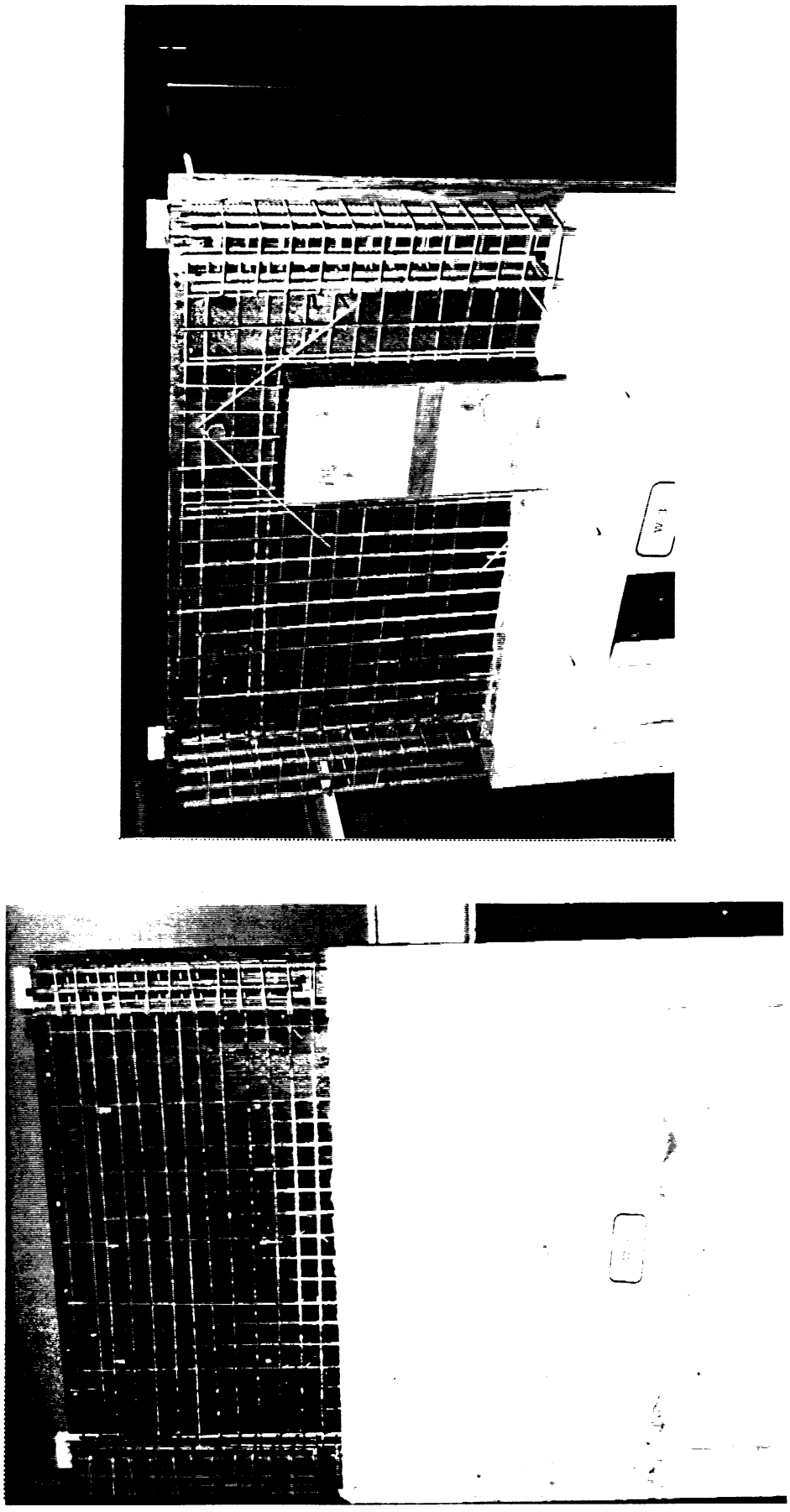

(b)

(a)

Fig. 3.5 : Closer Spaced Web Reinforcement for Top Story in (a) Wall W-1, (b) Wall W-3.

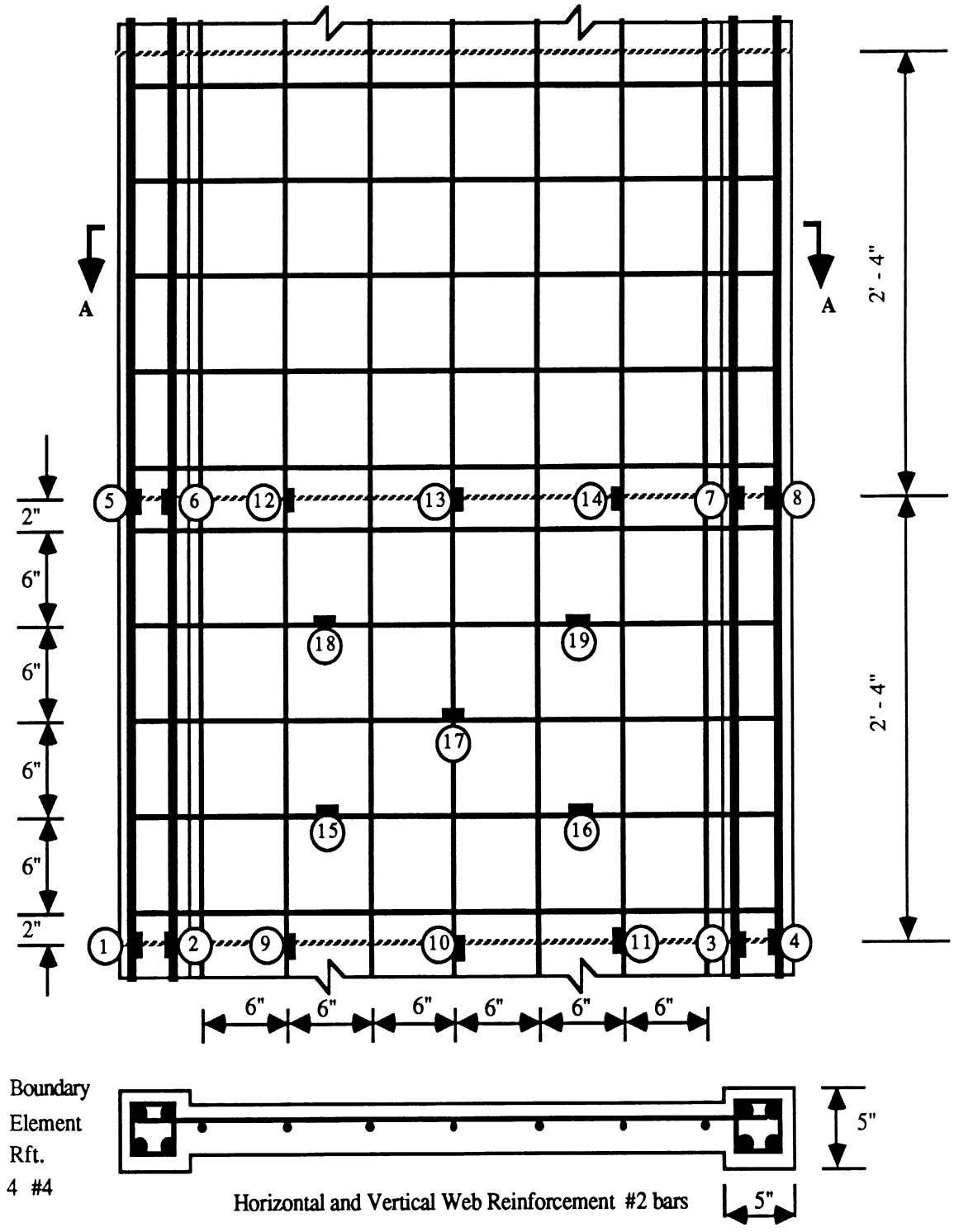

Section A - A

Fig. 3.6(a) : Wall Elevation with Gage Locations
and Cross Sections of Specimen W-1.

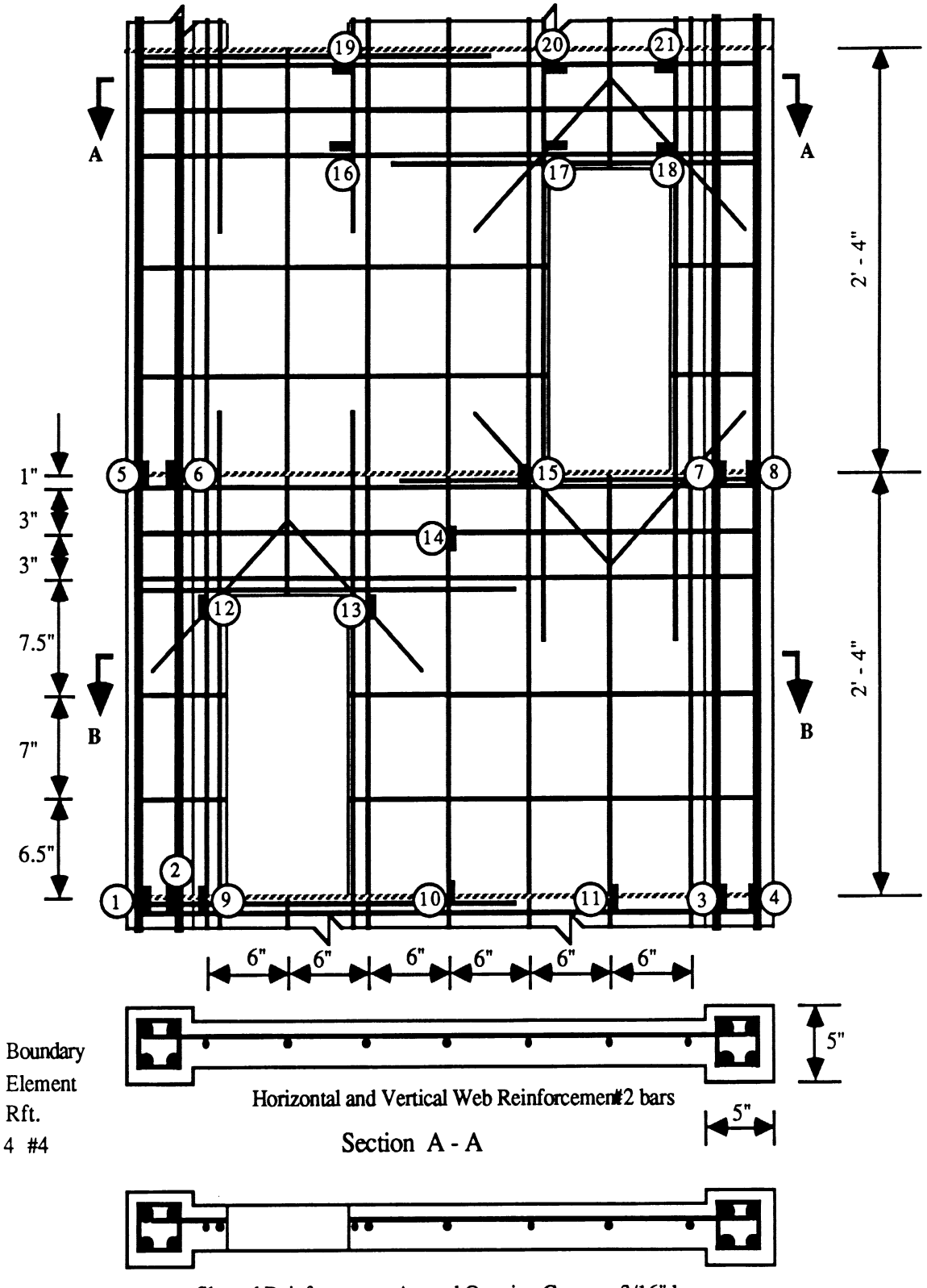

Fig. 3.6(b) : Wall Elevation with Gage Locations
and Cross Sections of Specimen W-2.

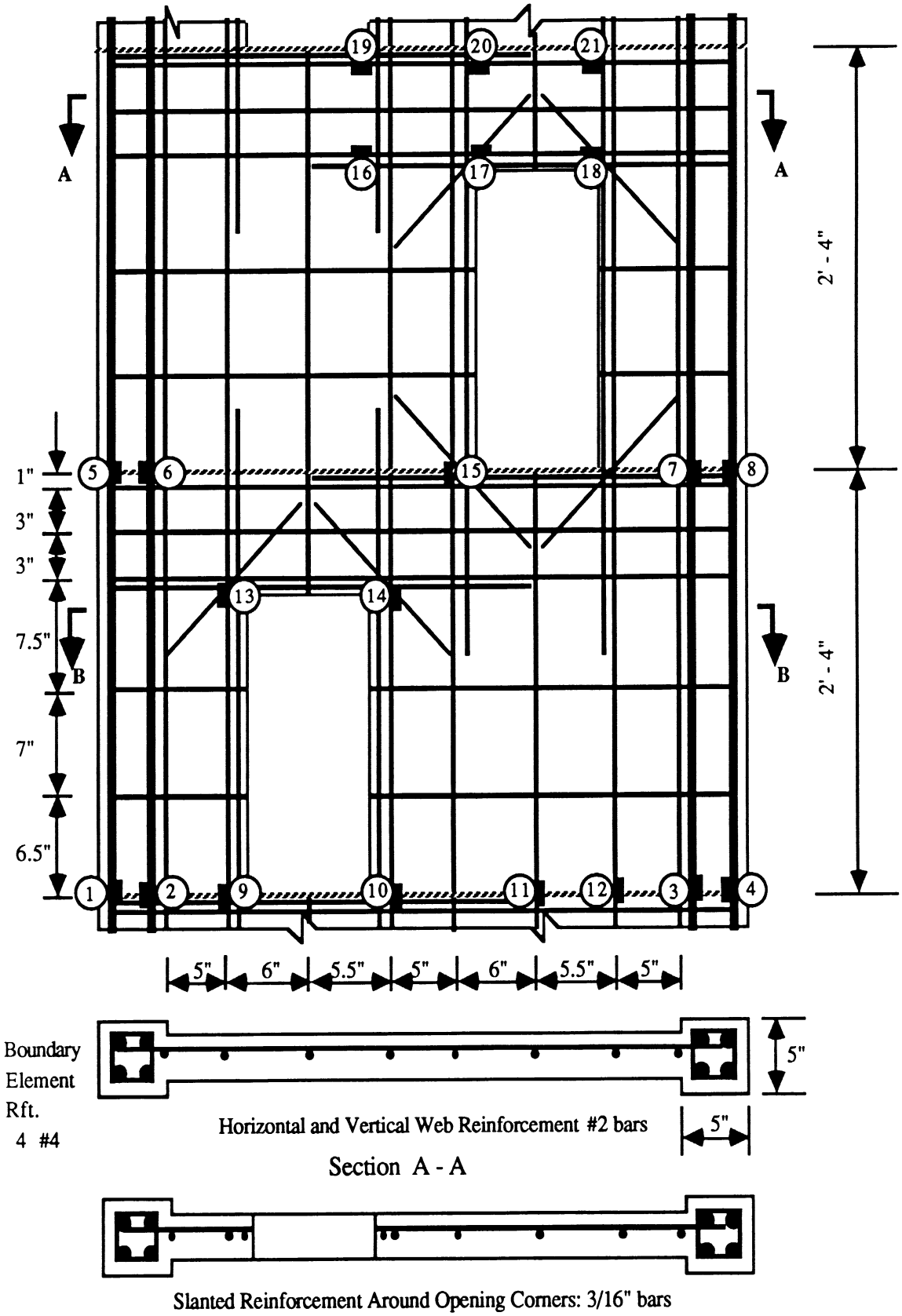

Fig. 3.6(c) : Wall Elevation with Gage Locations
and Cross Sections of Specimen W-3.

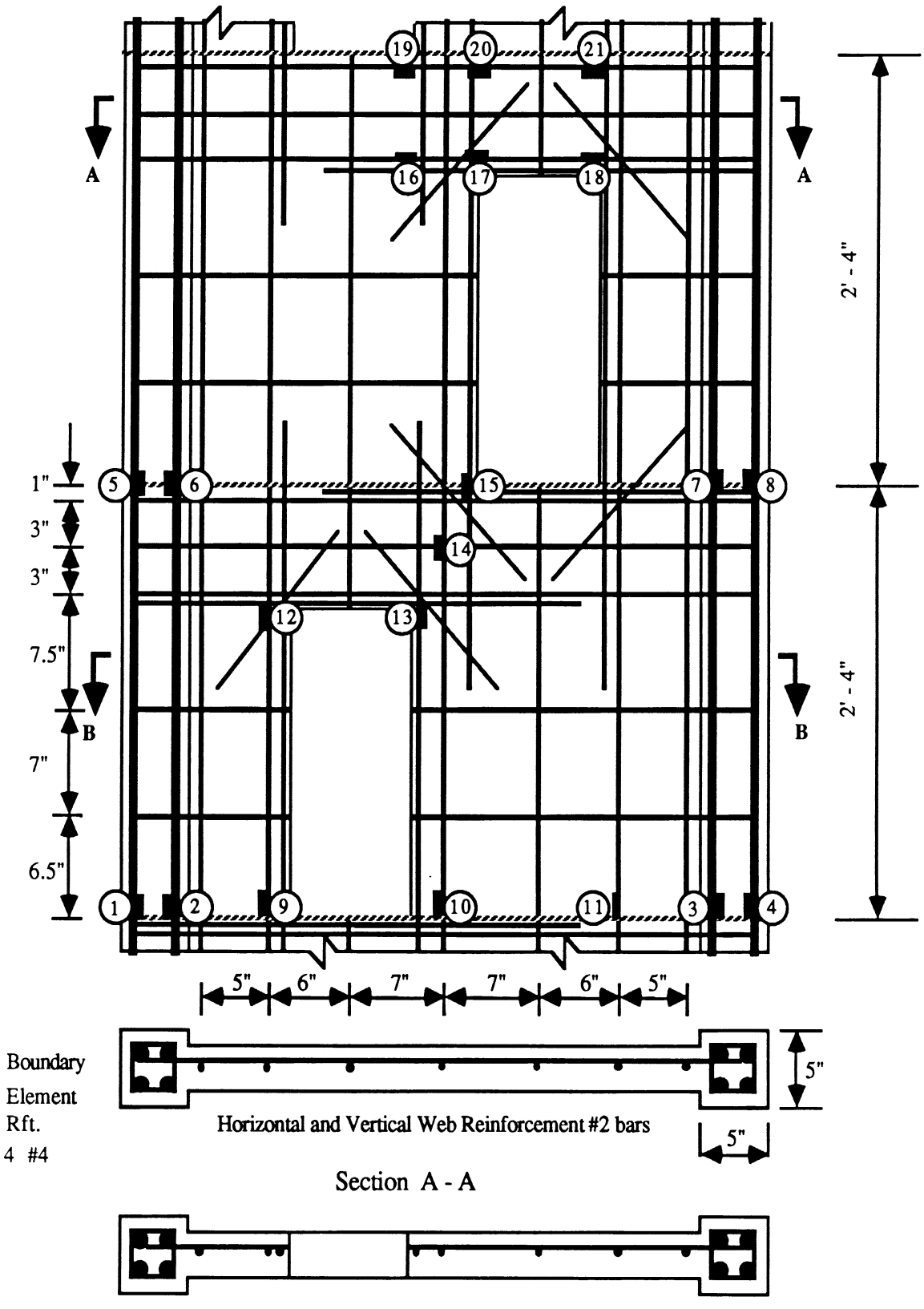

Section A - A

Slanted Reinforcement Around Opening Corners: 3/16" bars

Section B - B

Fig. 3.6(d) : Wall Elevation with Gage Locations and Cross Sections of Specimen W-4.

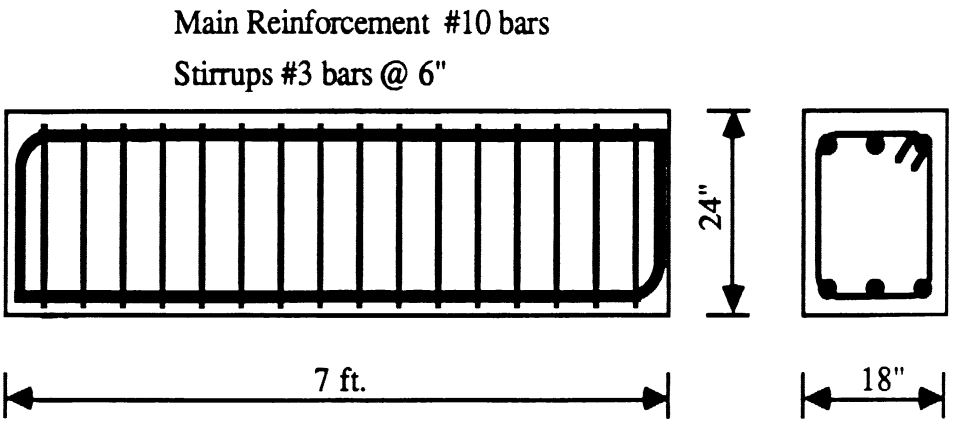

Fig. 3.7 : Base Blocks Reinforcement Details.

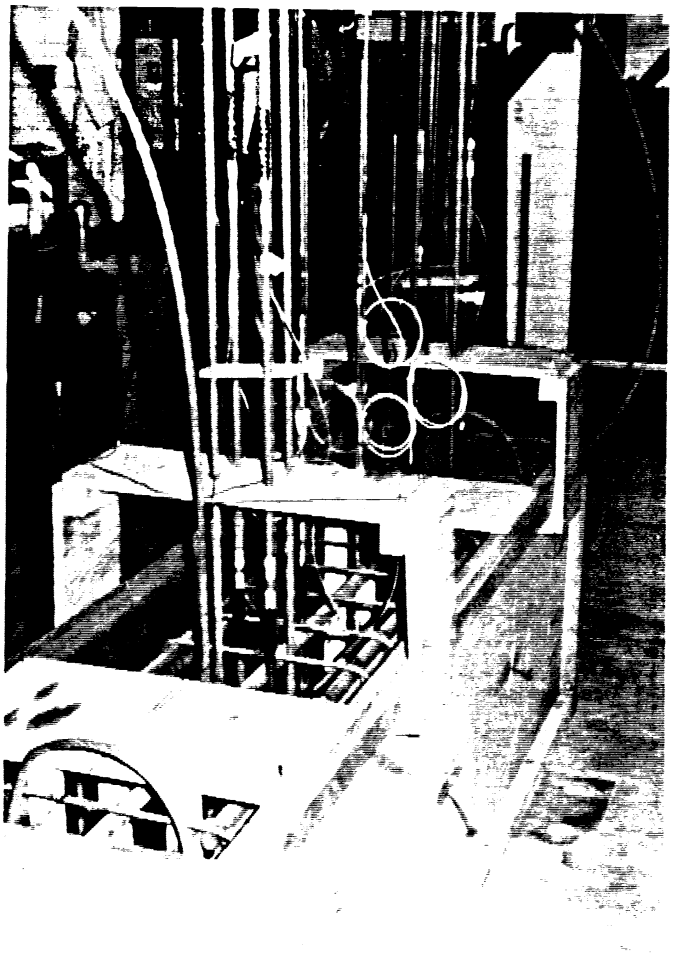

Fig. 3.8 : Base Block under Construction.

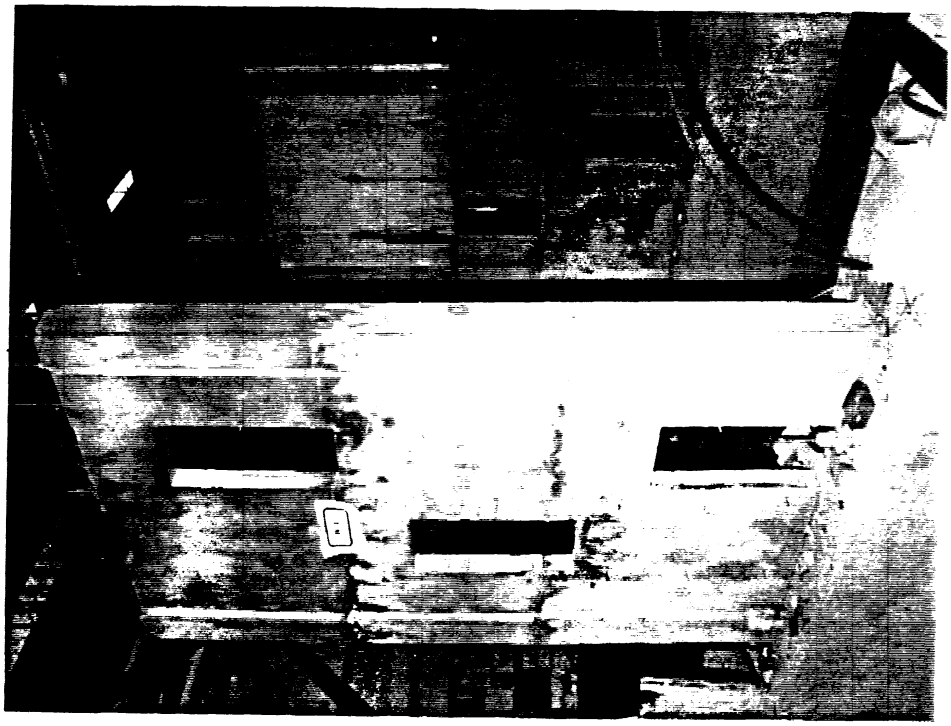

Fig. 3.10 : Wall W-2 under Construction.

Fig. 3.9 : Wall W-1 under Construction.

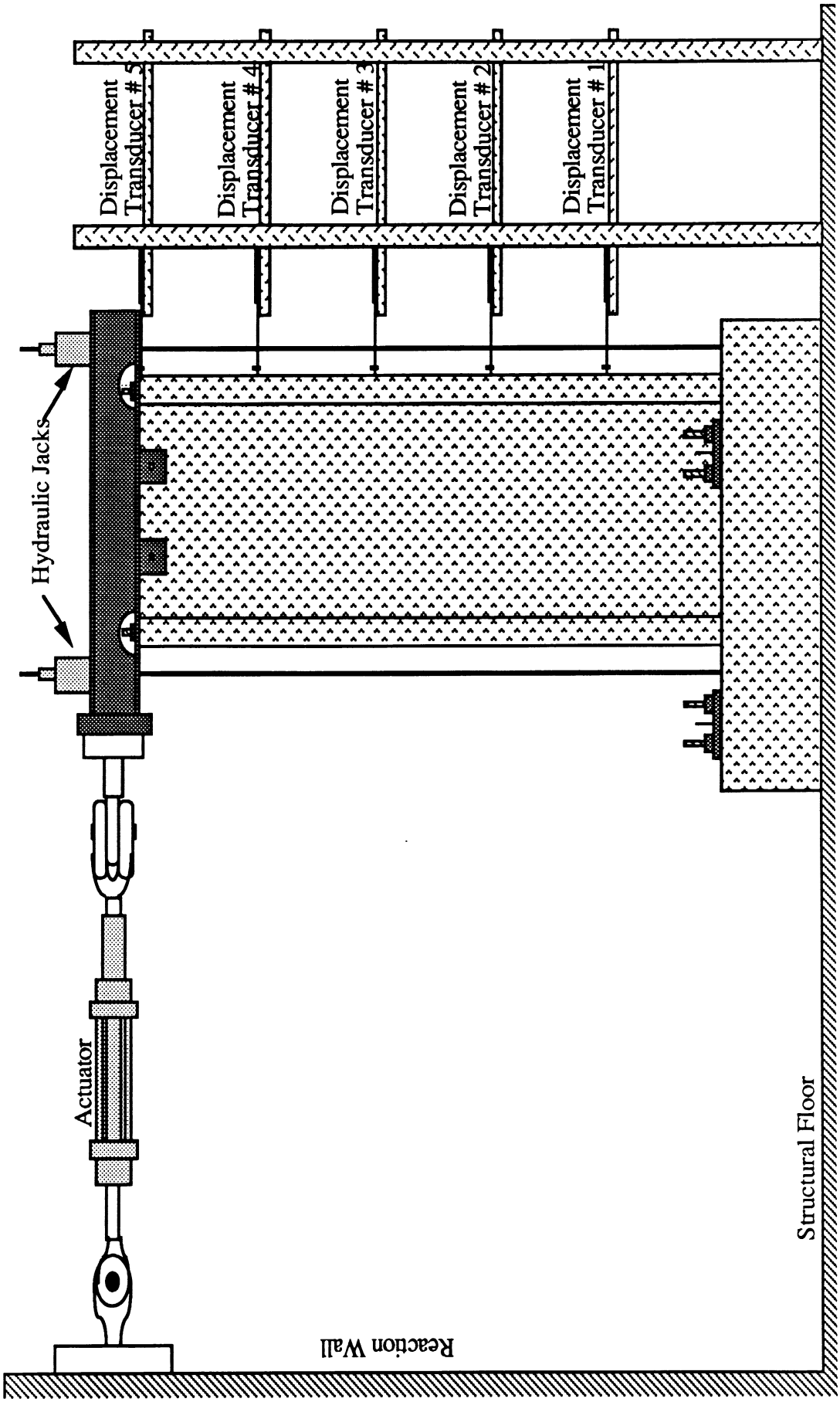

Fig. 3.11 : Test Setup.

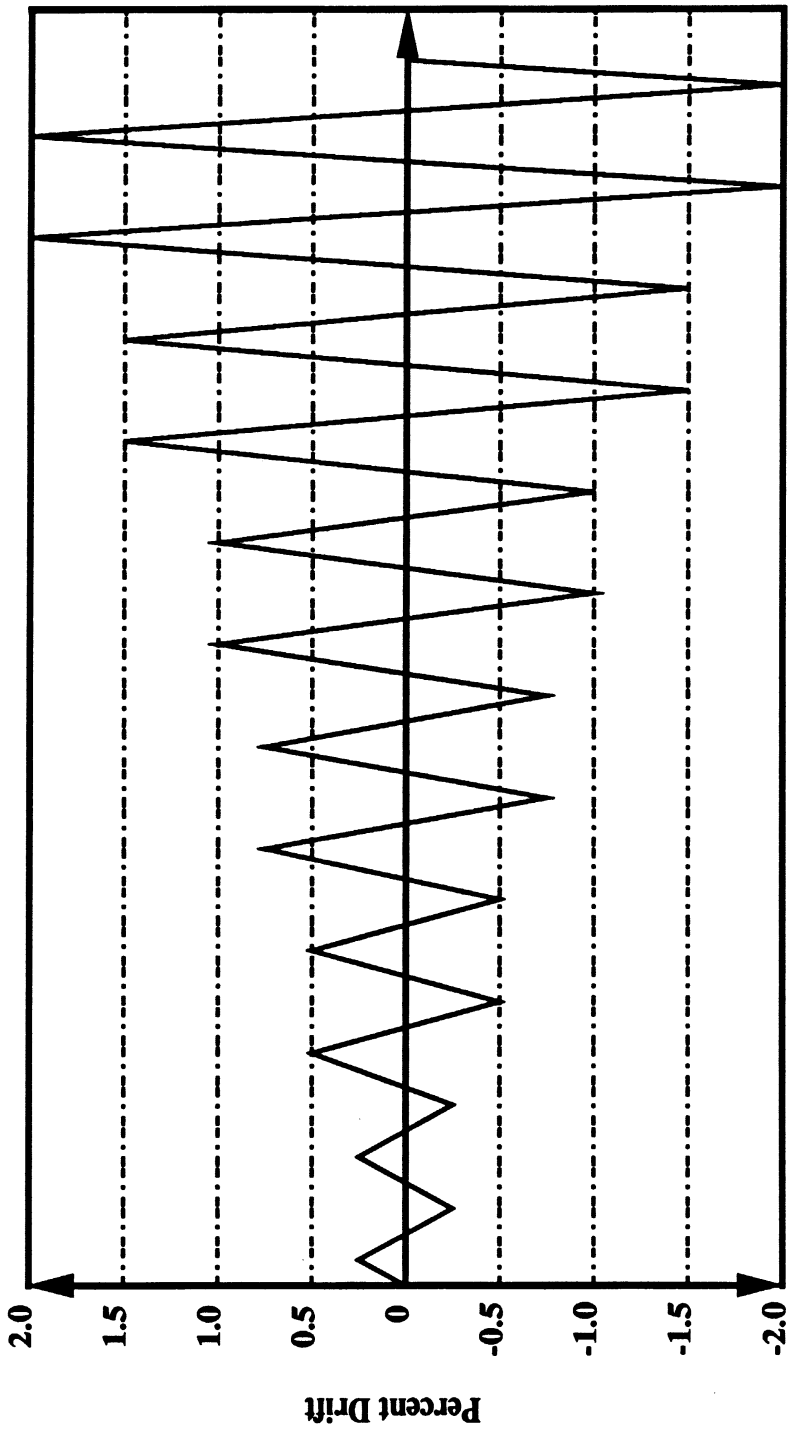

Fig. 3.12 : Loading History.

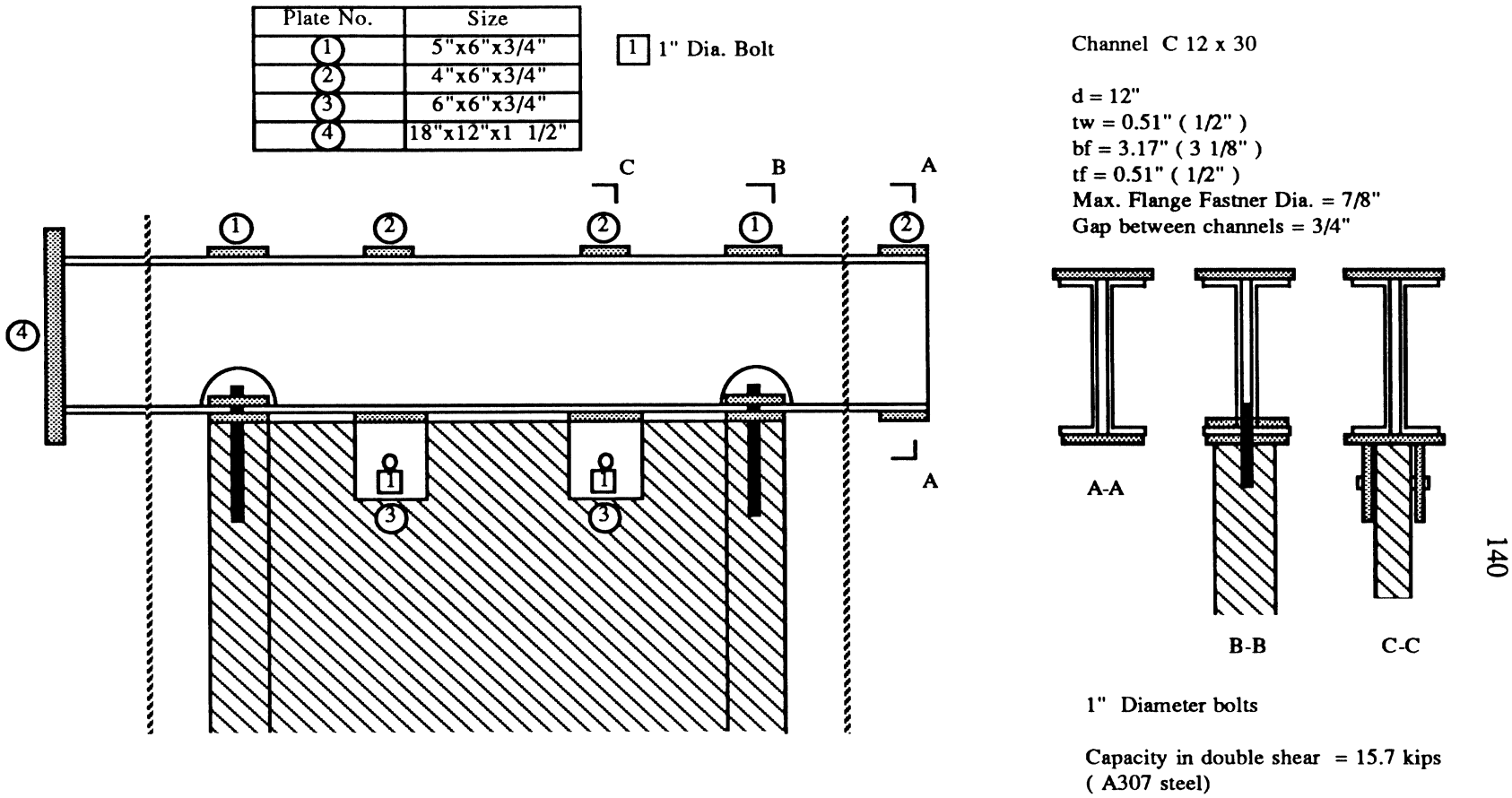

Fig. 3.13 : Top Beam Details.

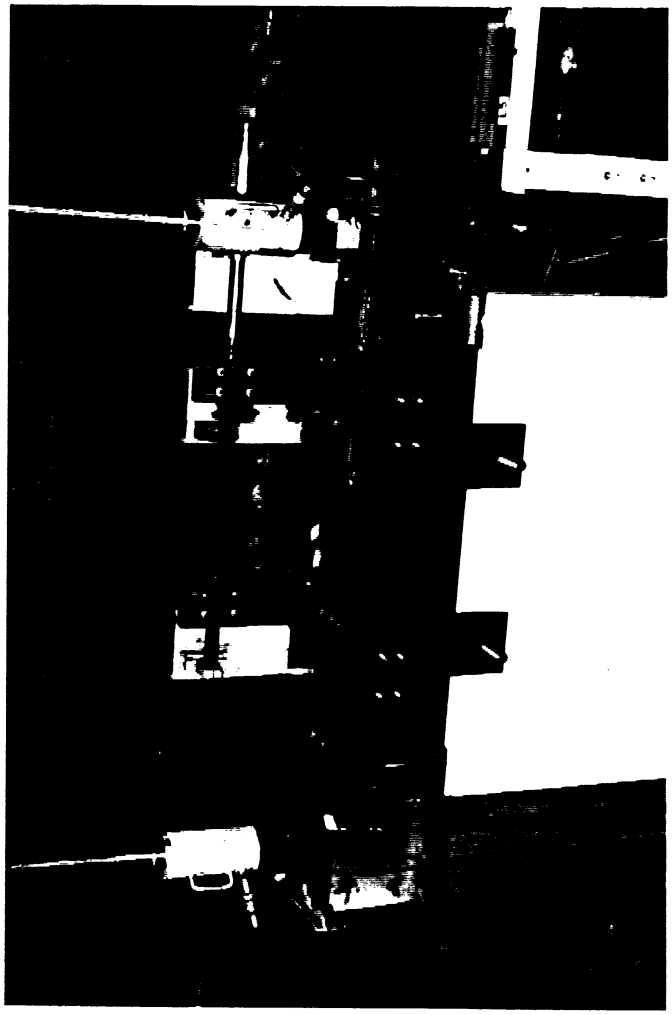

Fig. 3.14 : Top Beam Assembly.

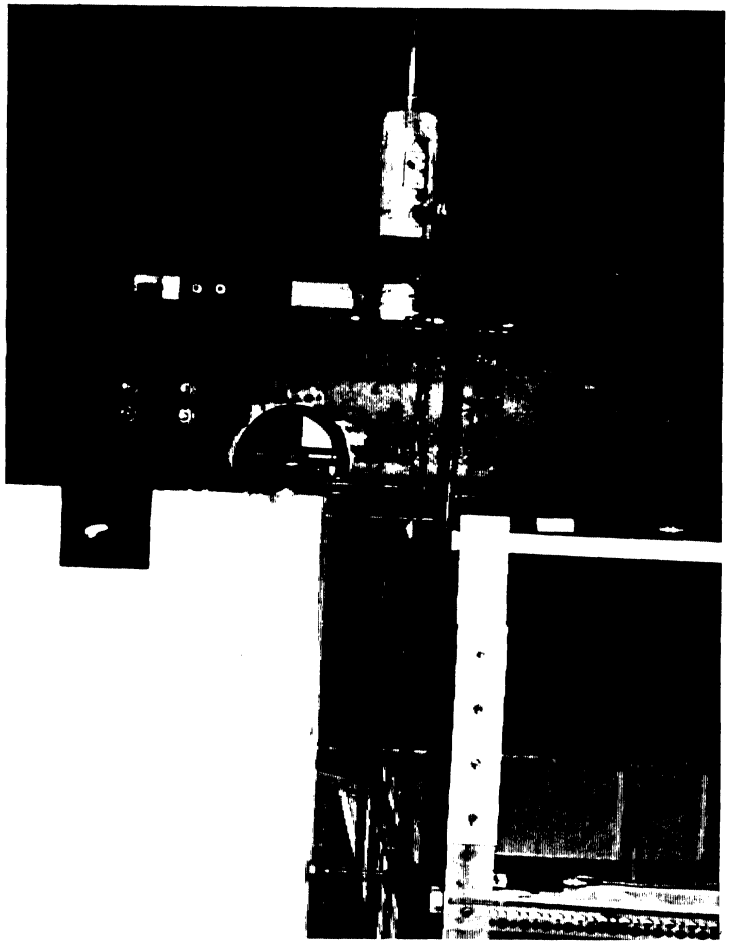

Fig. 3.15 : Hydraulic Jack-Strand Chuck Assembly used for the Application of Axial Load.

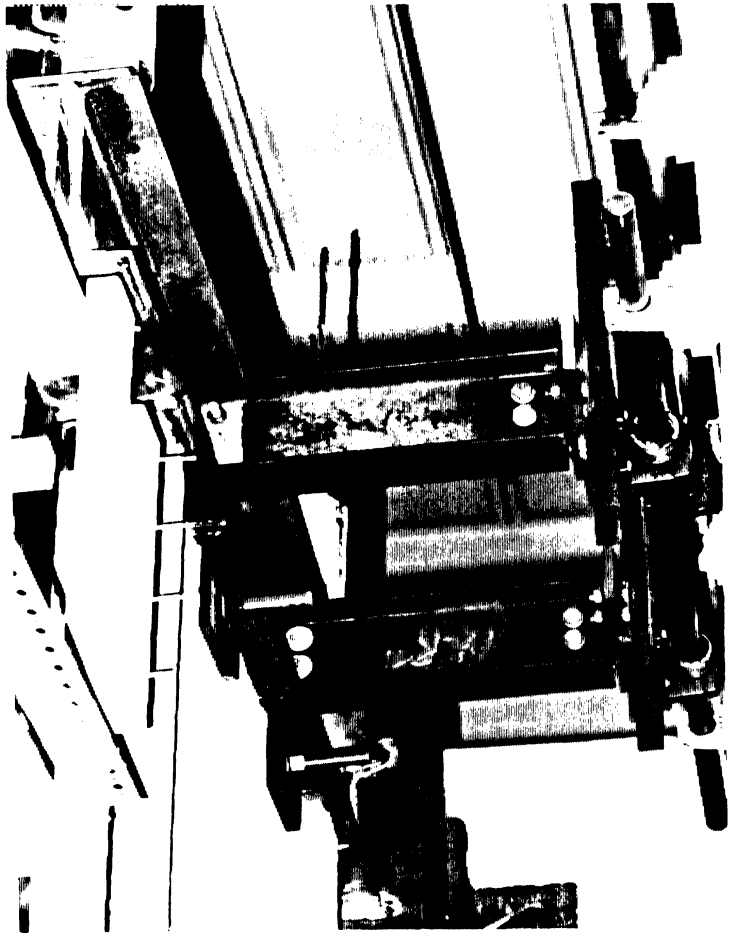

Fig. 3.16 : Attachment of Linear Bearing Assembly providing Lateral Support to the Test Specimen.

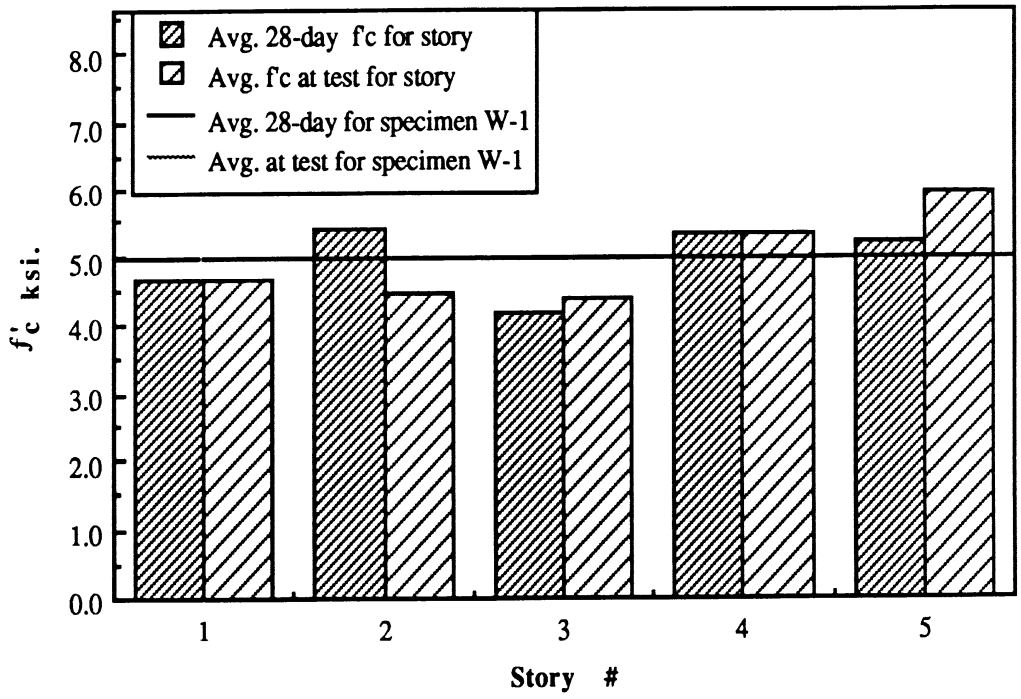

Fig. 3.17(a) : Variation of Concrete Compressive Strength for Wall W-1.

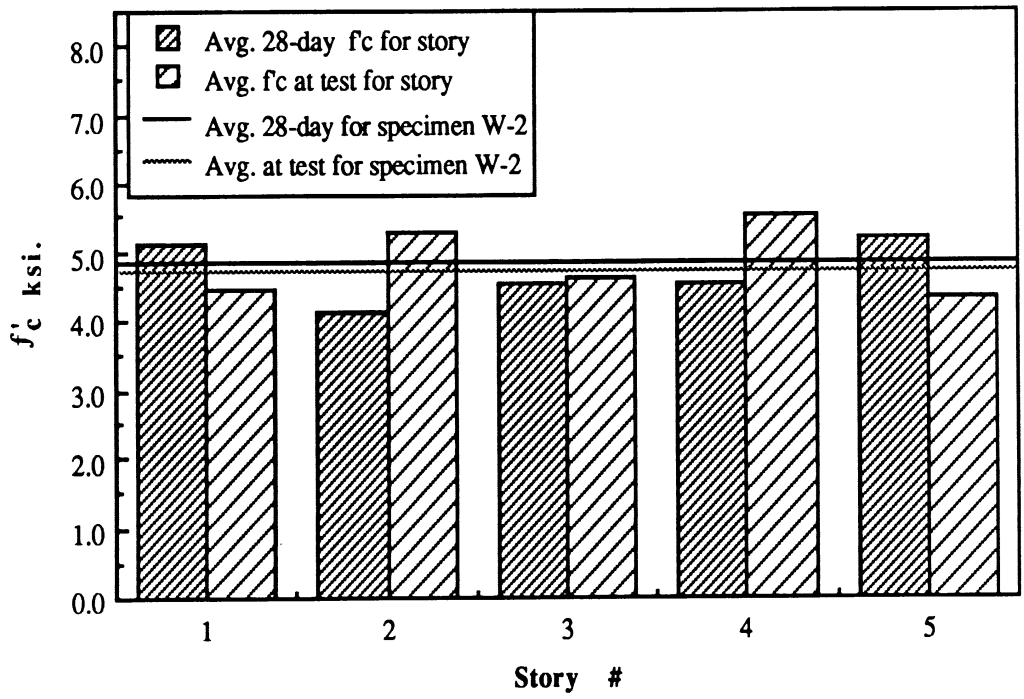

Fig. 3.17(b) : Variation of Concrete Compressive Strength for Wall W-2.

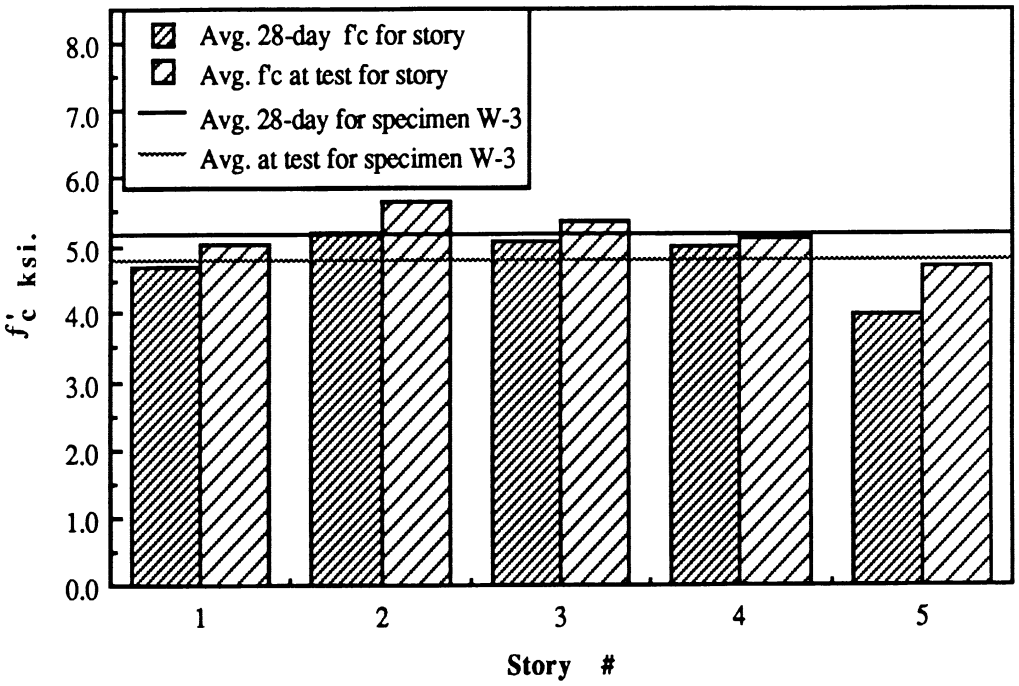

Fig. 3.17(c) : Variation of Concrete Compressive Strength for Wall W-3.

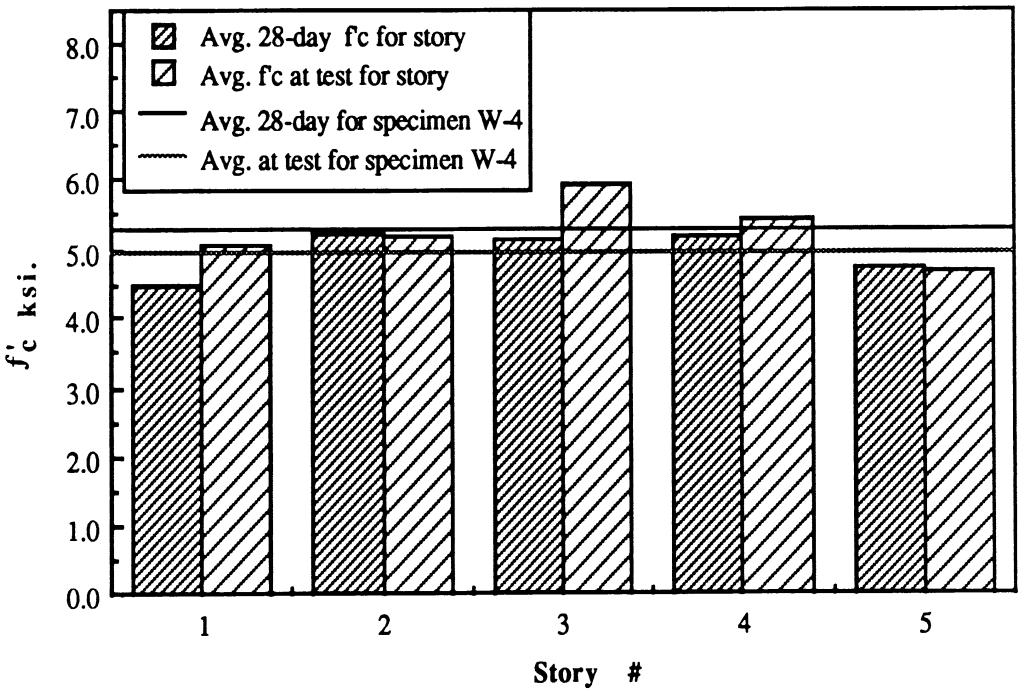

Fig. 3.17(d) : Variation of Concrete Compressive Strength for Wall W-4.

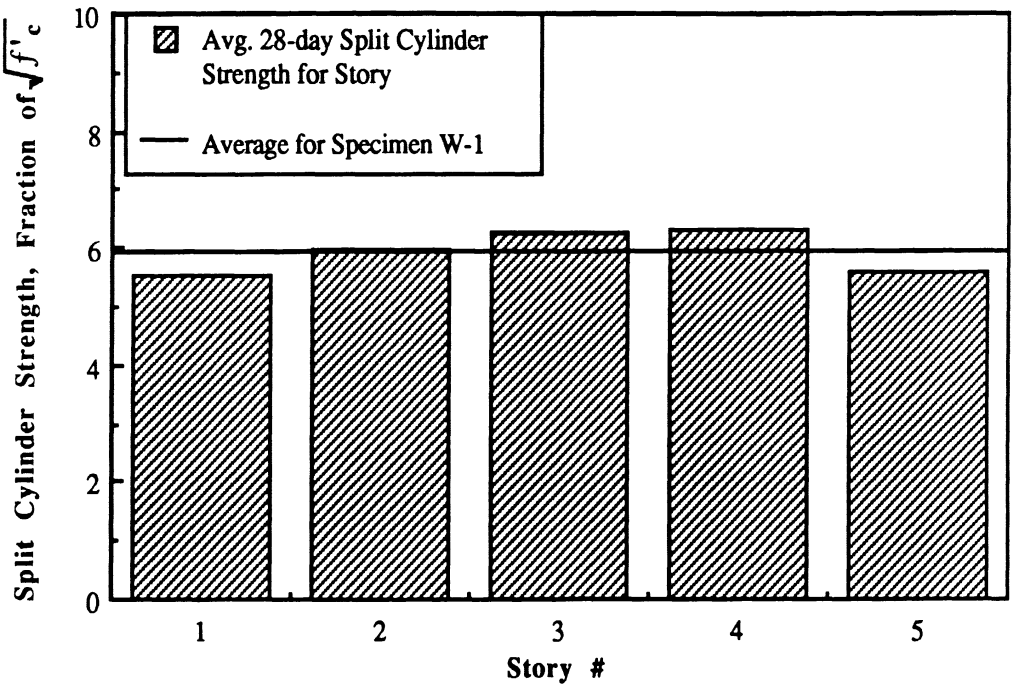

Fig. 3.18(a) : Variation of Concrete Split Cylinder Strength for Wall W-1.

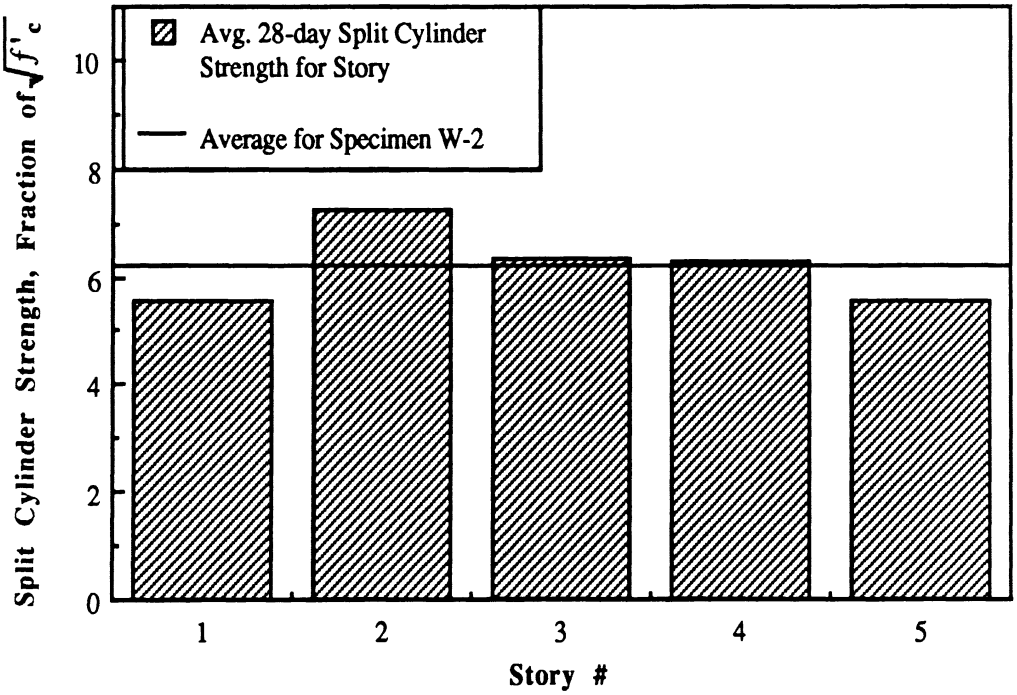

Fig. 3.18(b) : Variation of Concrete Split Cylinder Strength for Wall W-2.

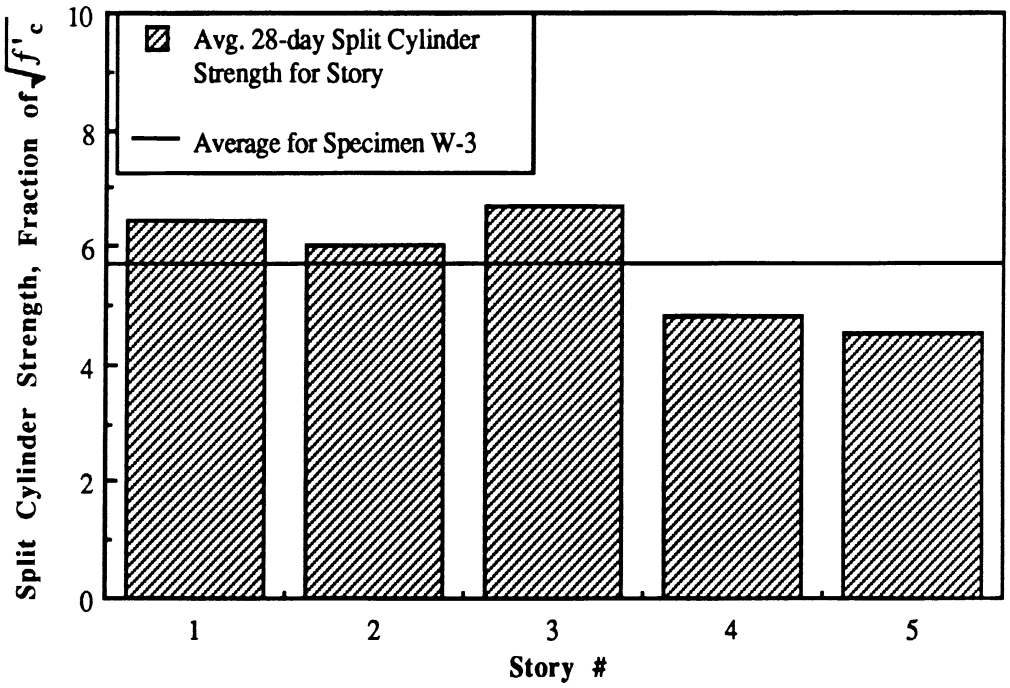

Fig. 3.18(c) : Variation of Concrete Split Cylinder Strength for Wall W-3.

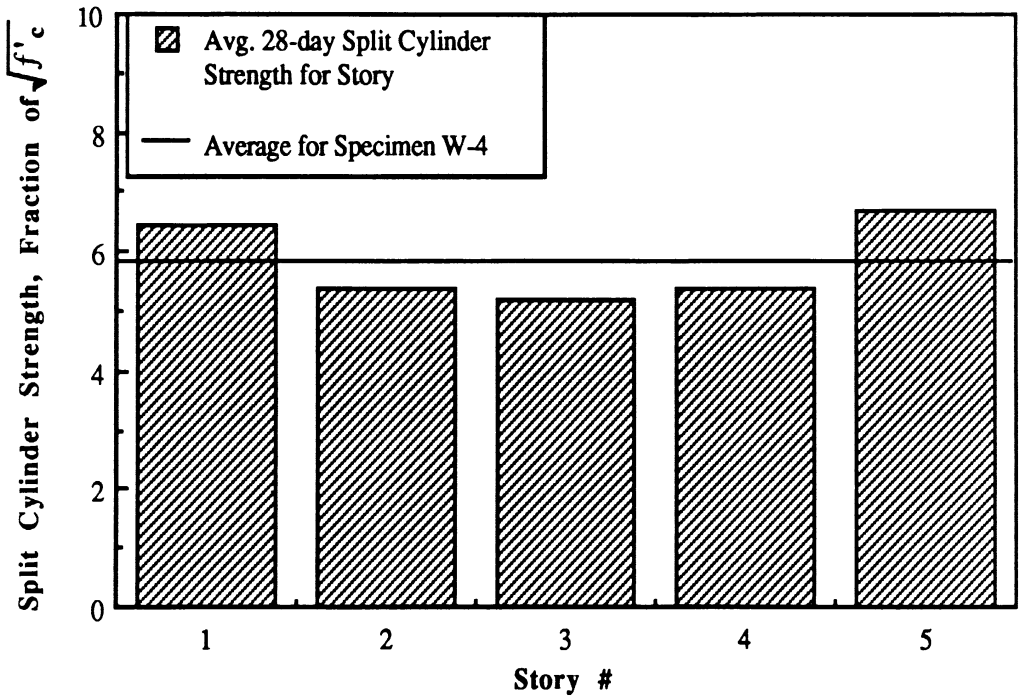

Fig. 3.18(d) : Variation of Concrete Split Cylinder Strength for Wall W-4.

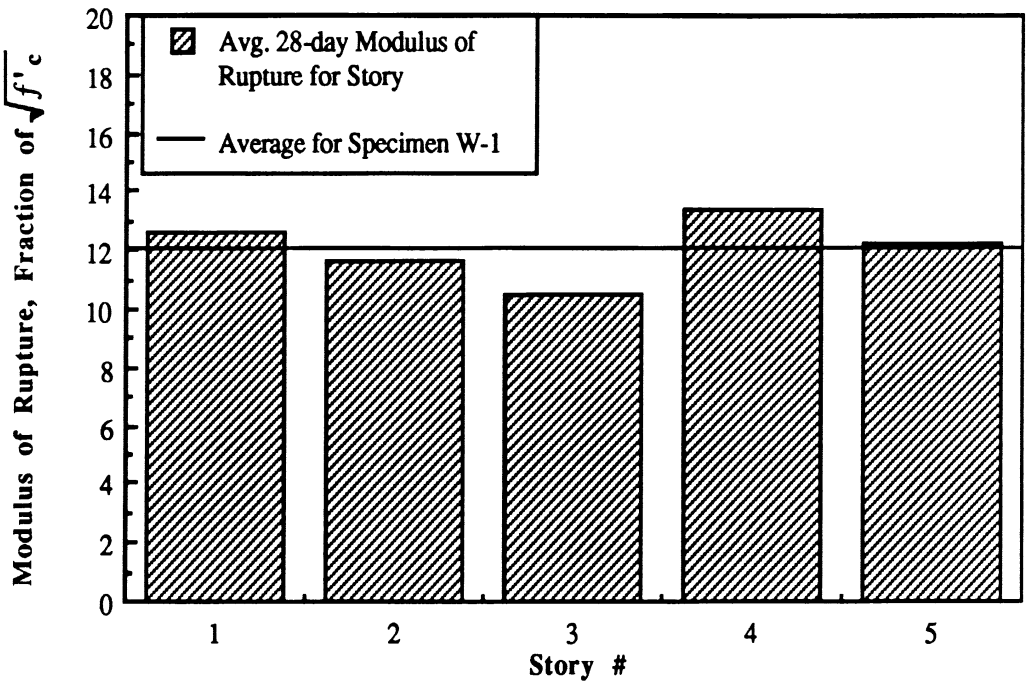

Fig. 3.19(a) : Variation of Concrete Modulus of Rupture for Wall W-1.

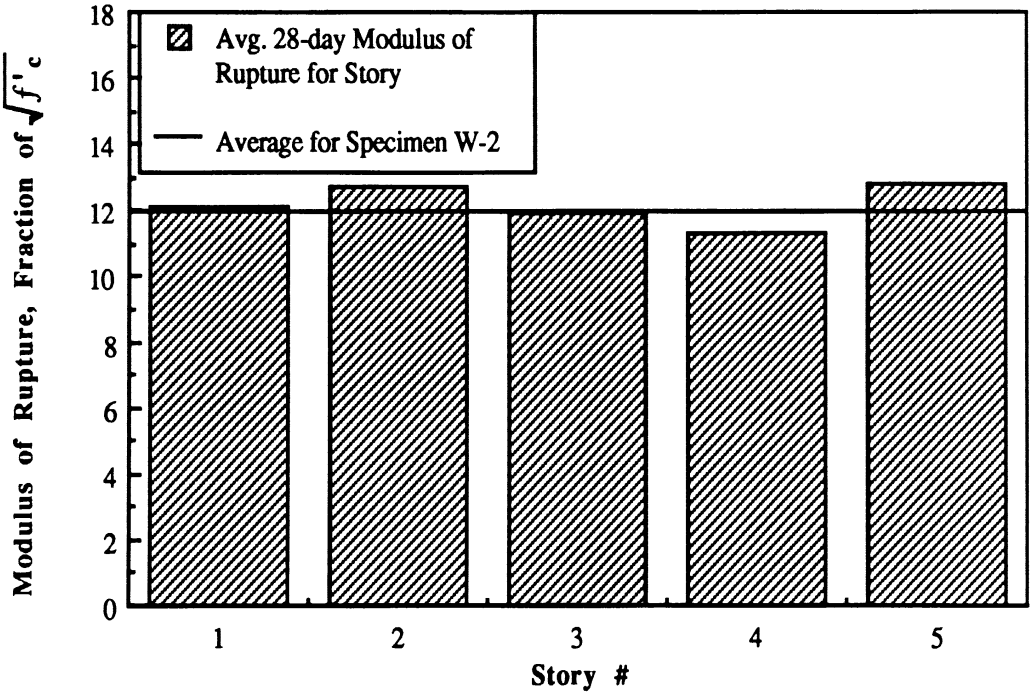

Fig. 3.19(b) : Variation of Concrete Modulus of Rupture for Wall W-2.

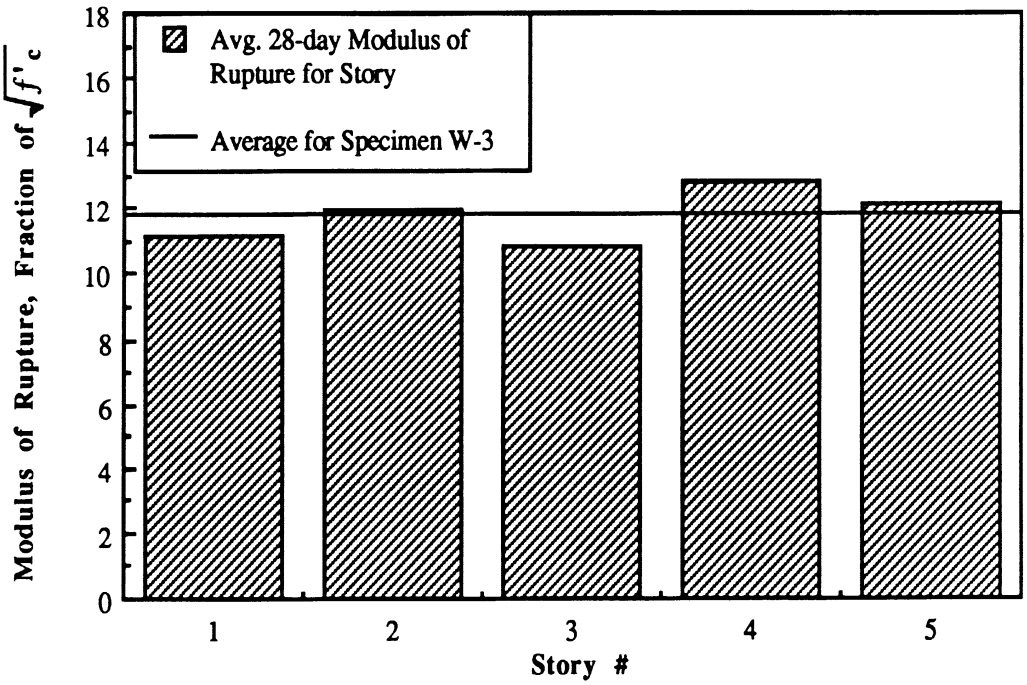

Fig. 3.19(c) : Variation of Concrete Modulus of Rupture for Wall W-3.

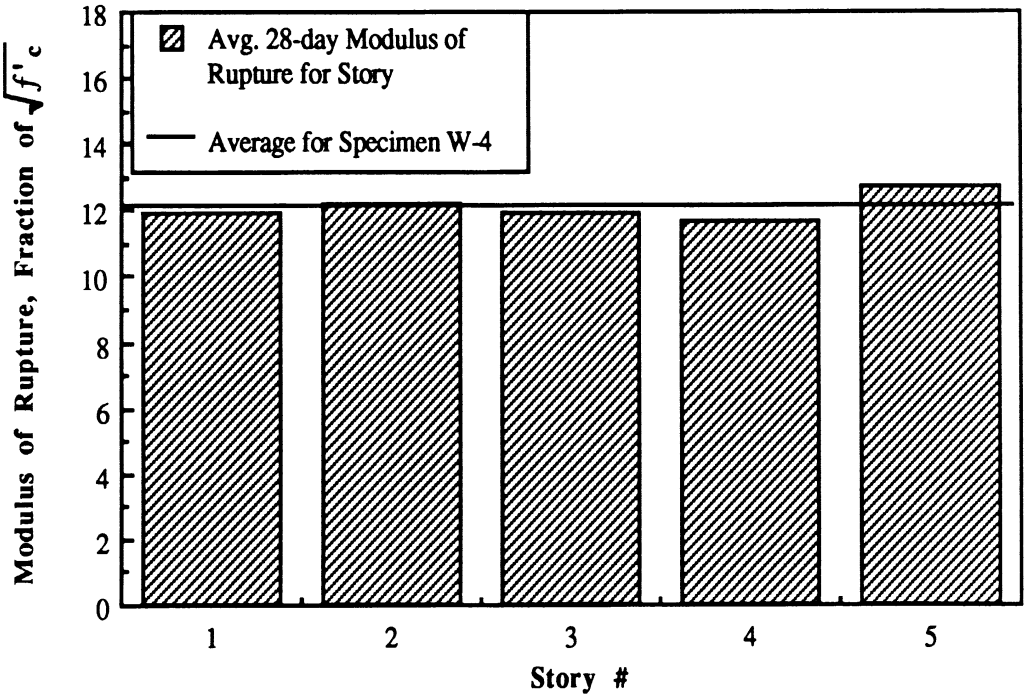

Fig. 3.19(d) : Variation of Concrete Modulus of Rupture for Wall W-4.

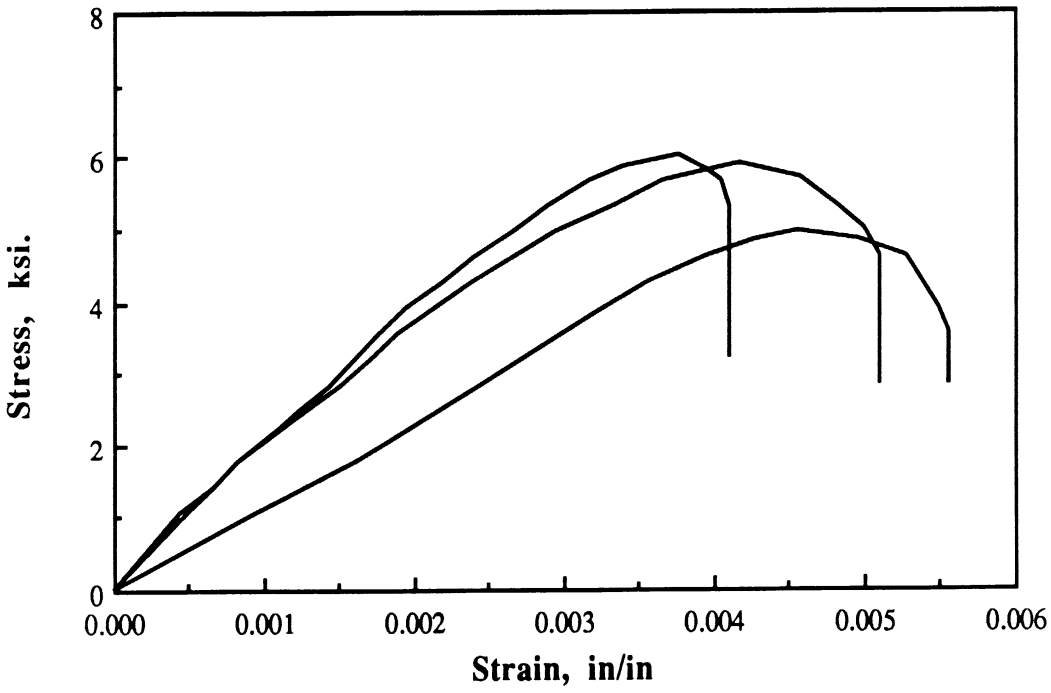

Fig. 3.20 : Stress-Strain Relationship for Concrete.

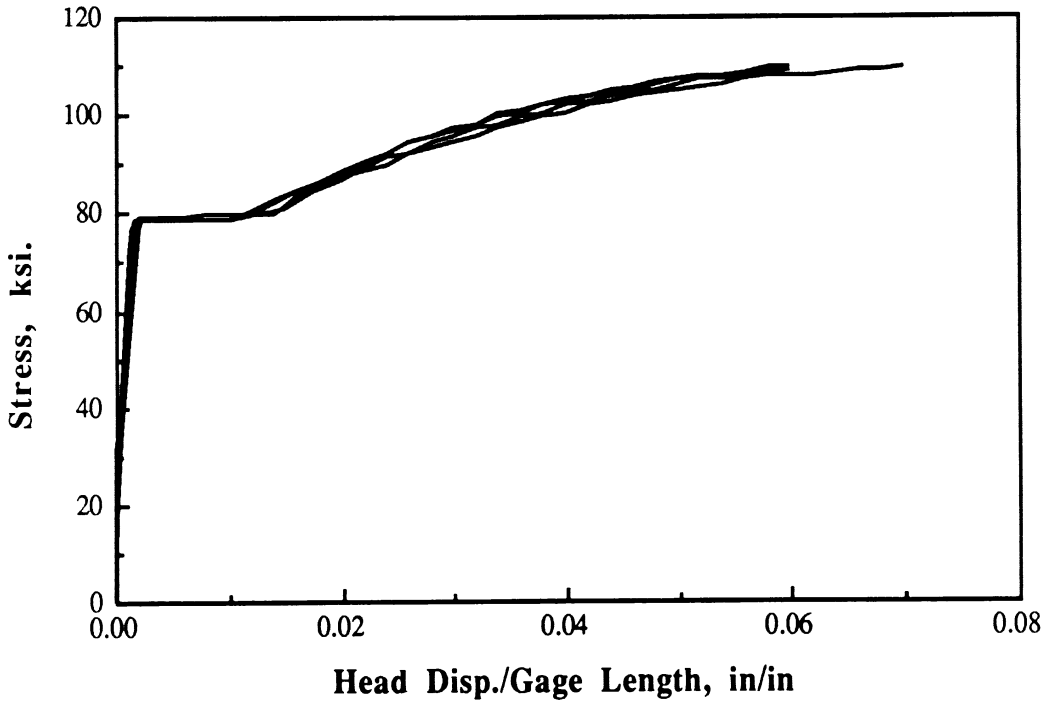

Fig. 3.21 : Stress vs. Normalized Head Displacement for No. 4 bar.

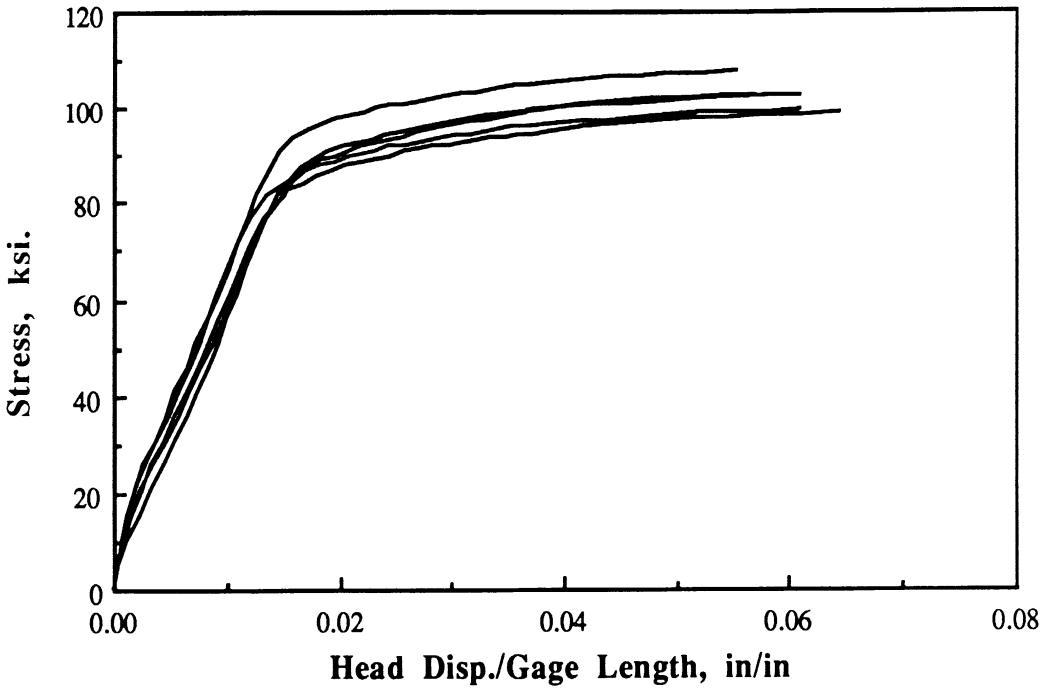

Fig. 3.22 : Stress vs. Normalized Head Displacement for No. 2 bar.

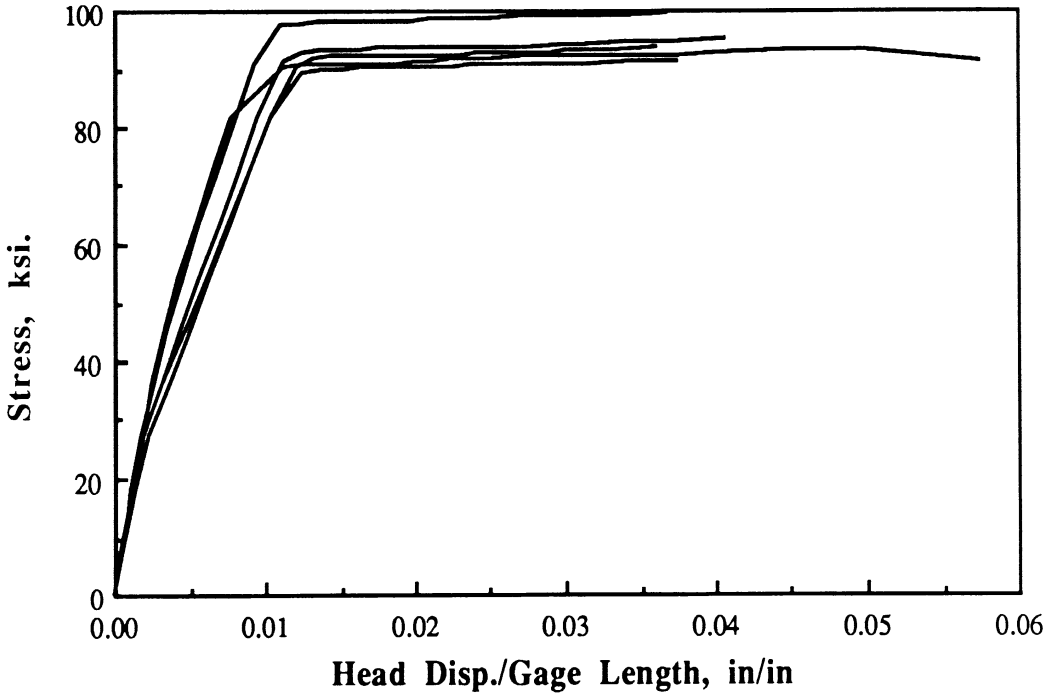

Fig. 3.23 : Stress vs. Normalized Head Displacement for 3/16" bar.

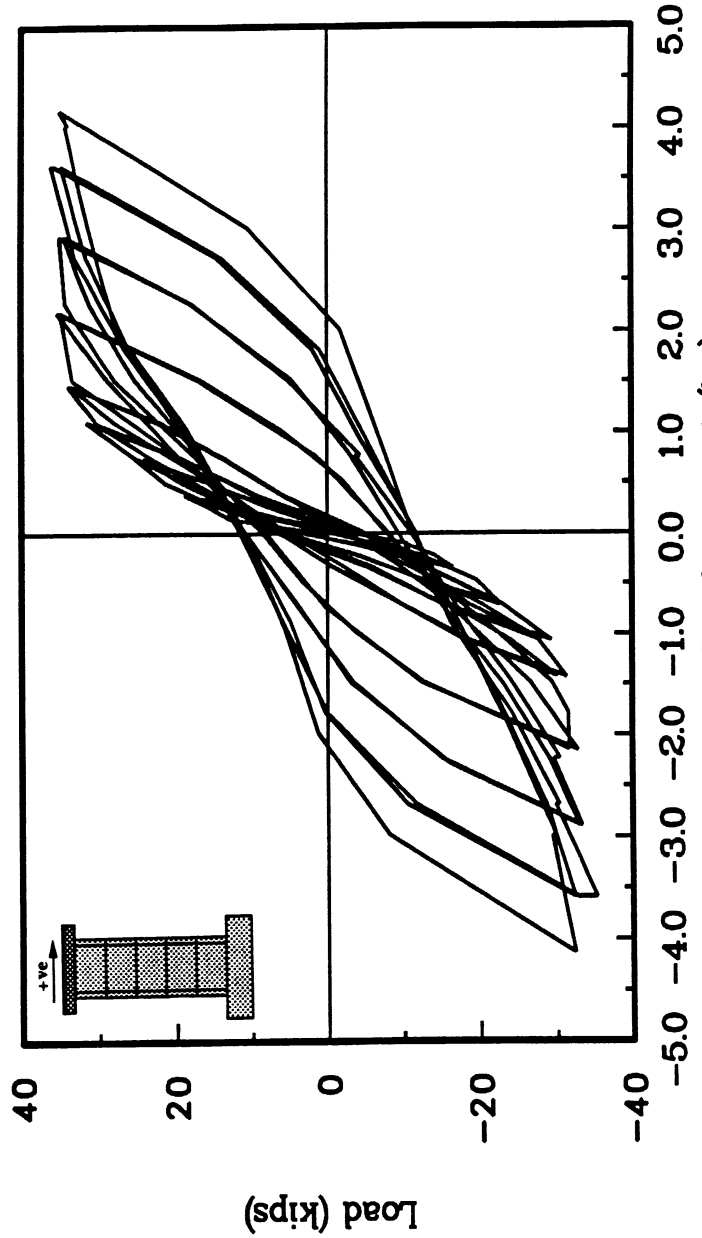

Fig. 4.1 : Force-Displacement Relationship for Wall W-1.

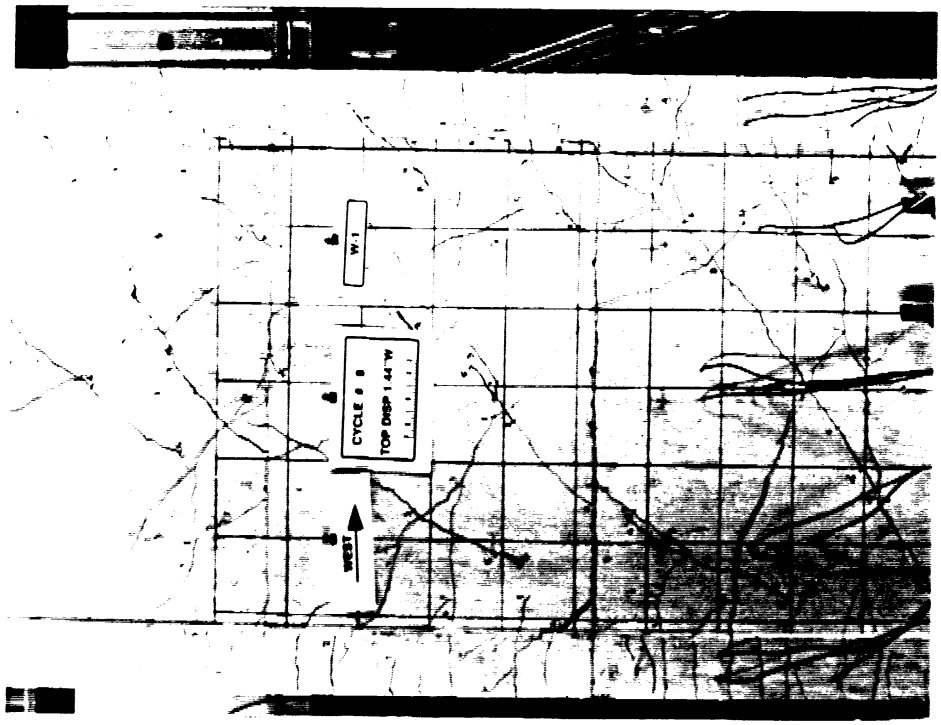

Fig. 4.3 : Specimen W-1 during Cycle 8 (Disp. 1.44 in. West).

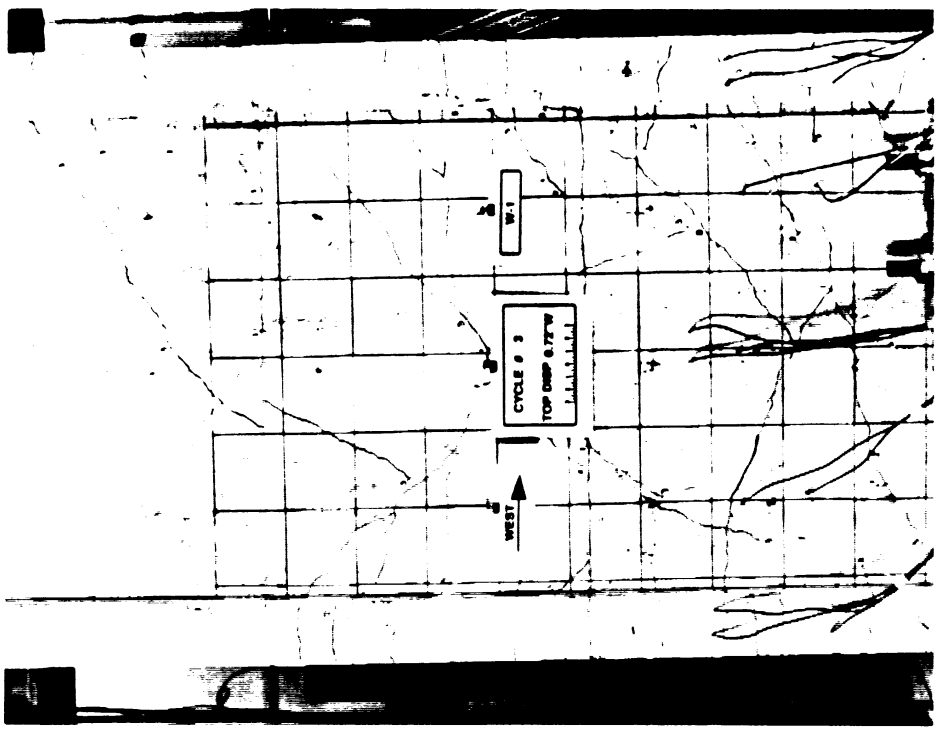

Fig. 4.2 : Specimen W-1 during Cycle 3 (Disp. 0.72 in. West).

Fig. 4.4 : Formation of Compression Struts in the Top Portion of W-1 during Cycle 9.

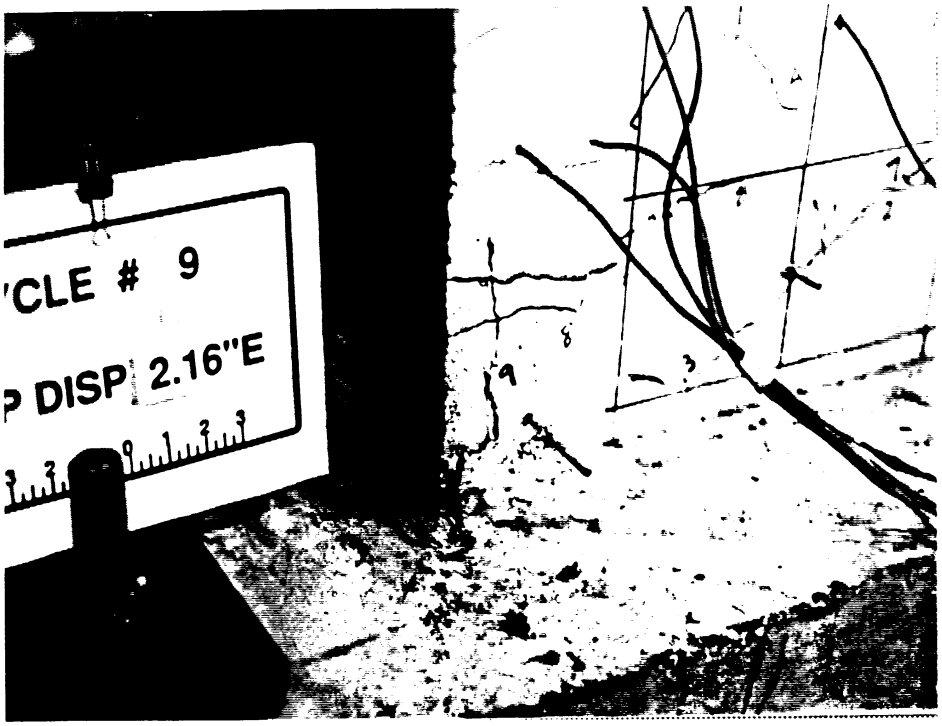

Fig. 4.5 : Initiation of Crushing in East Boundary Column of W-1 during Cycle 9.

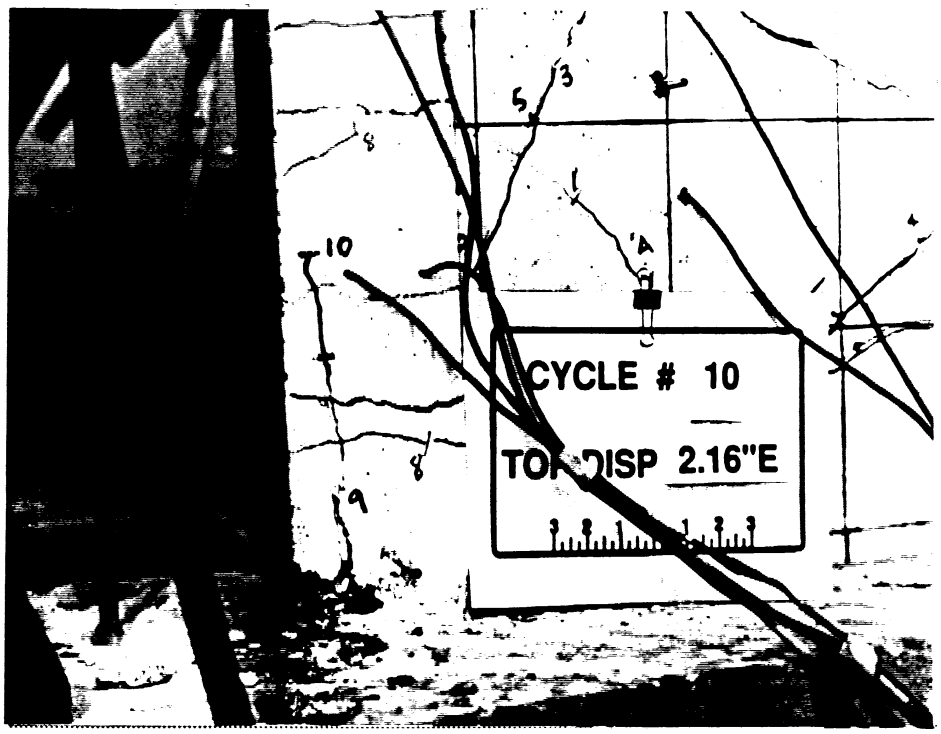

Fig. 4.6 : Spalling of Cover in the East Boundary Column of W-1 during Cycle 10.

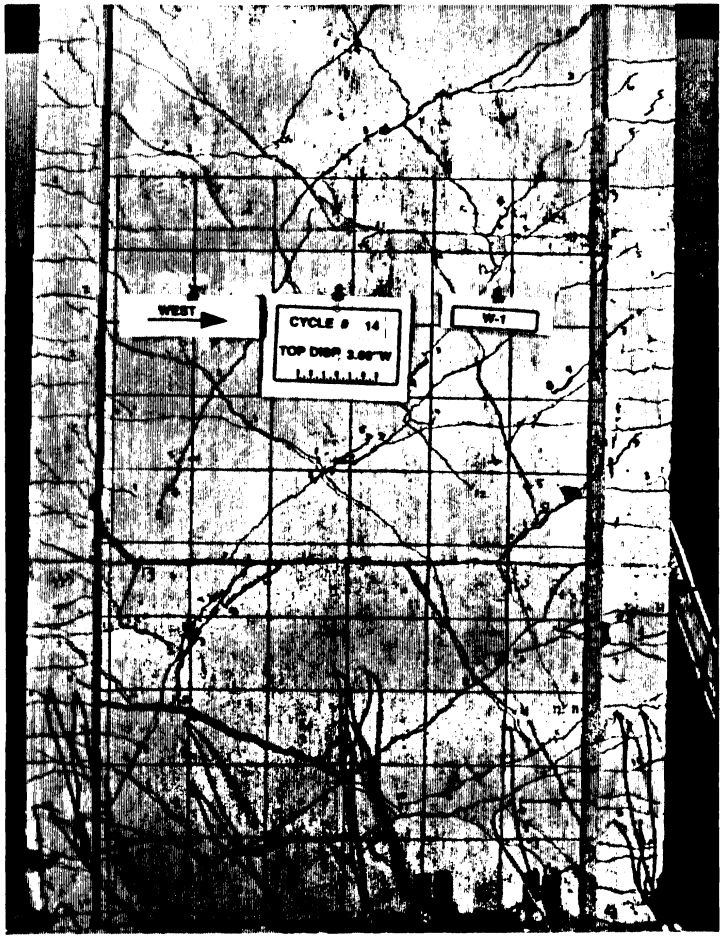

Fig. 4.7 : Major Cracks widen during Cycle 14 in the First Story Level of W-1.

Fig. 4.8 : A General View of Wall W-1 during the last Cycle of the Test.

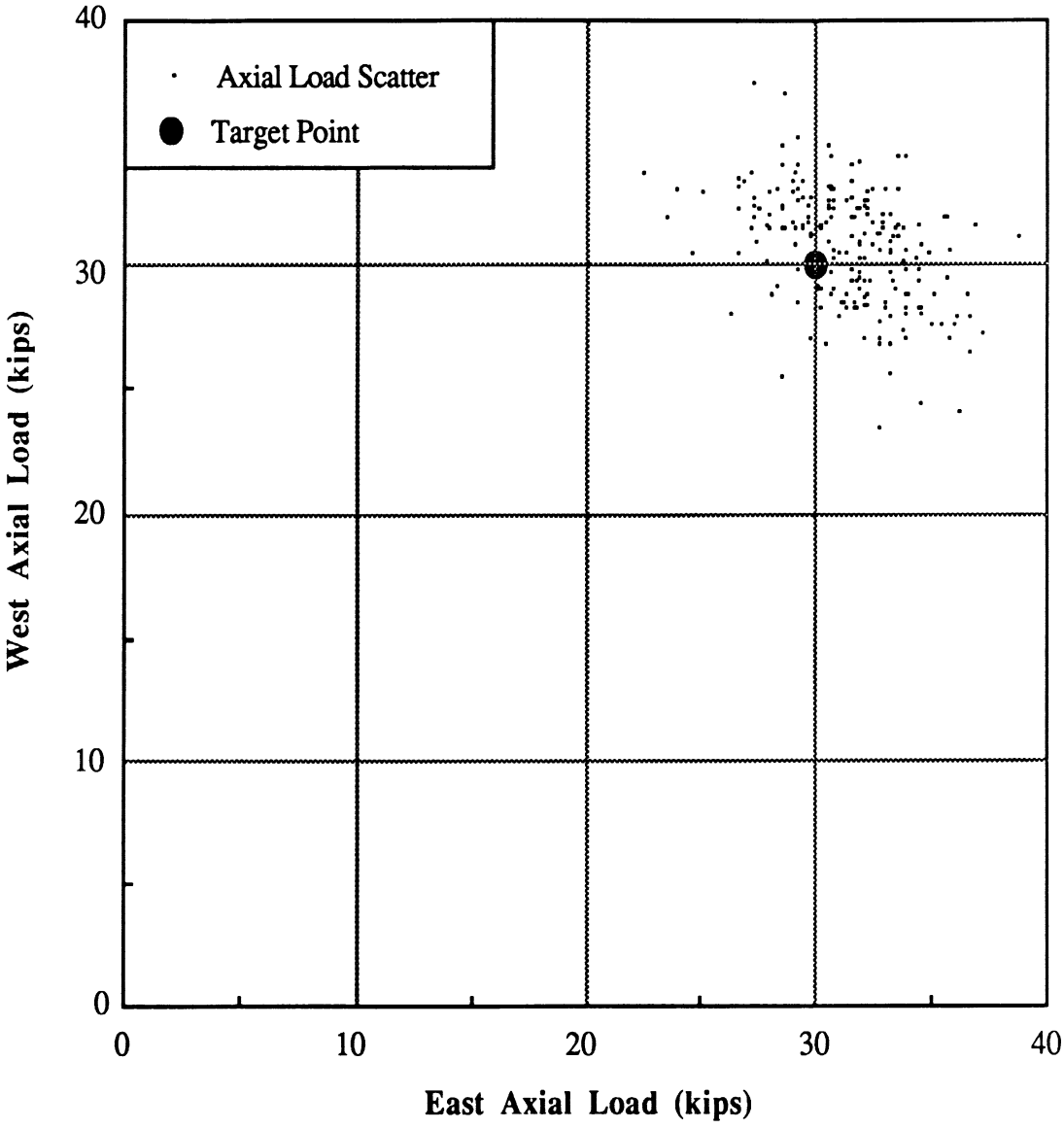

Fig. 4.9 : Scatter in the Applied Axial Load for Specimen W-1.

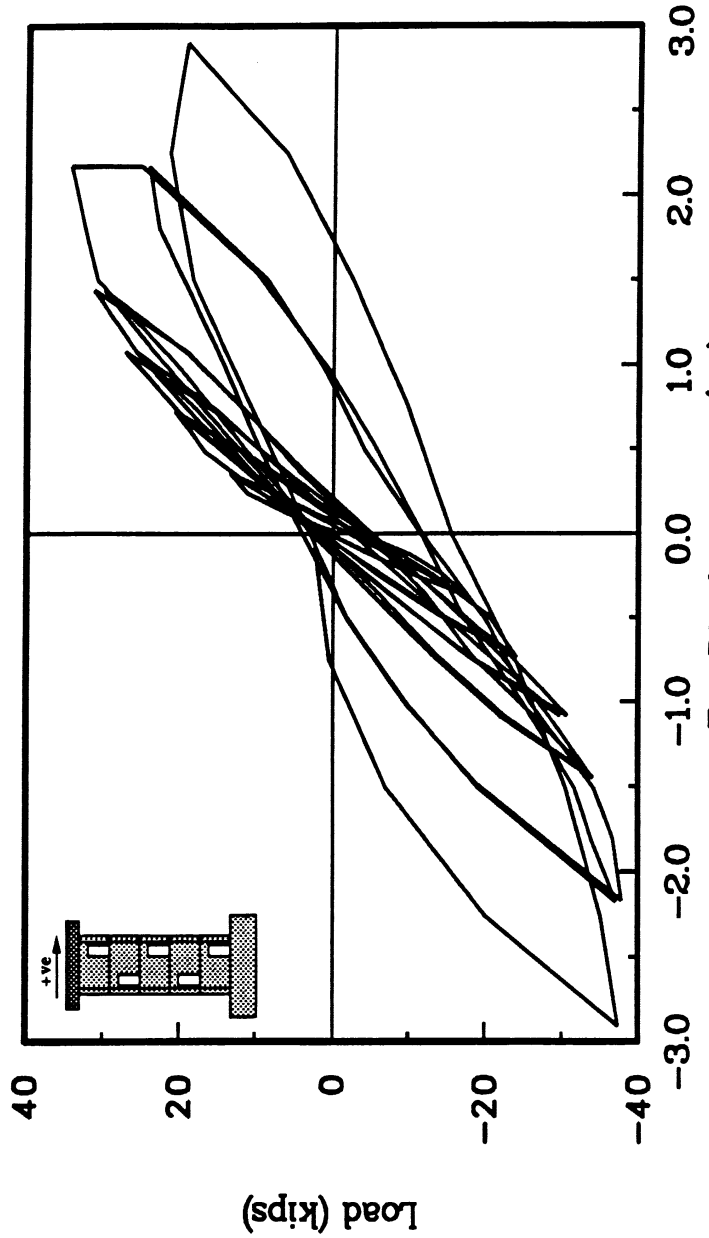

Fig. 4.10 : Force-Displacement Relationship for Wall W-2.

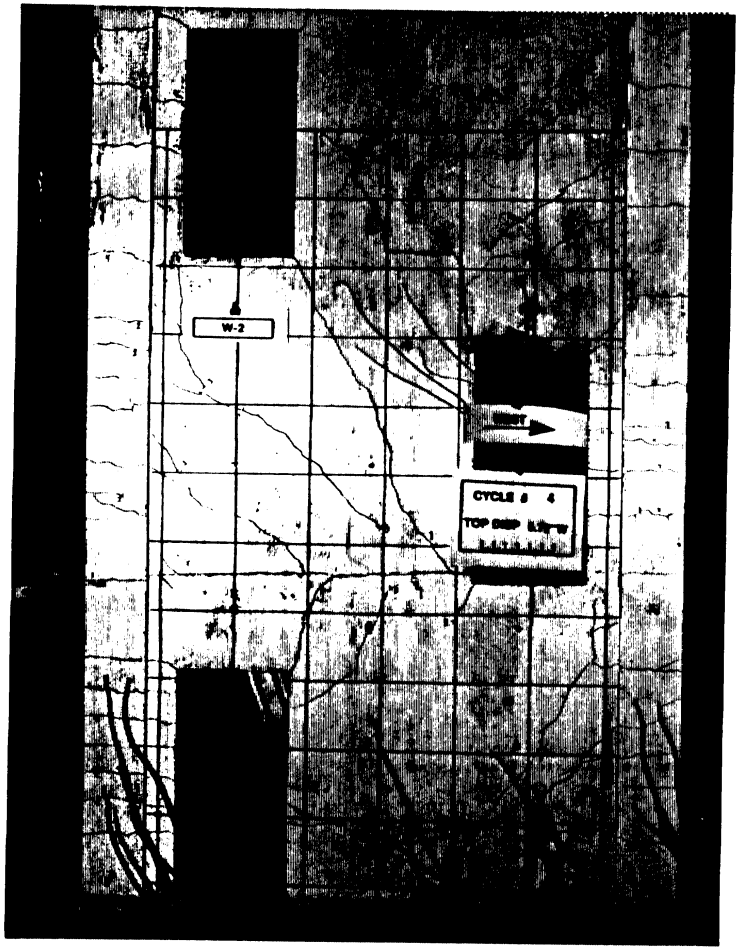

Fig. 4.11 : Specimen W-2 during Cycle 4.

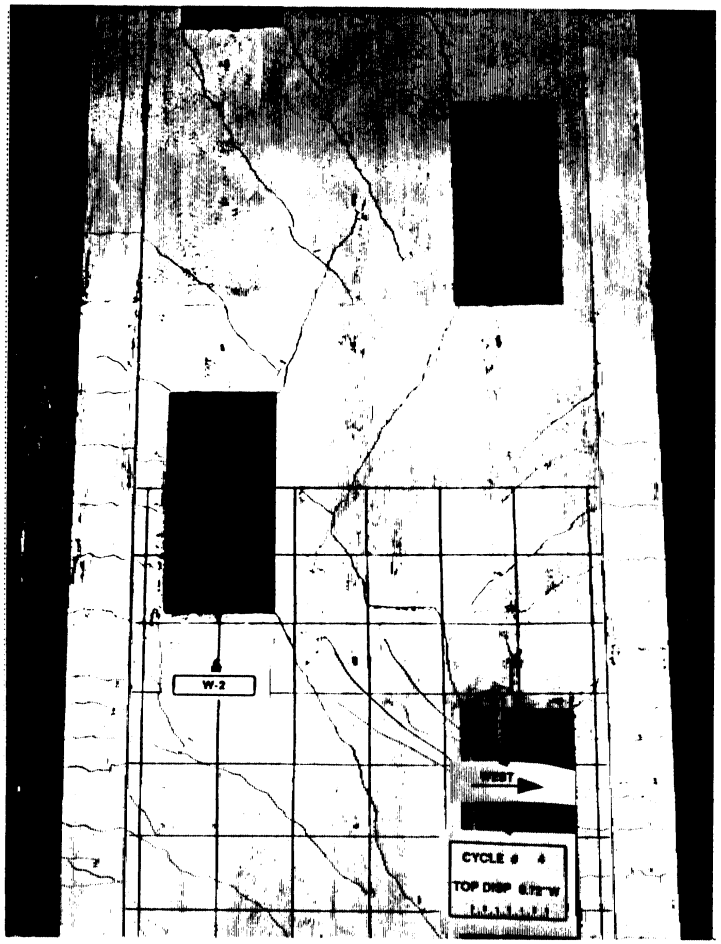

Fig. 4.12 : Diagonal Cracking extends into the Fourth Story of W-2 in Cycle 4.

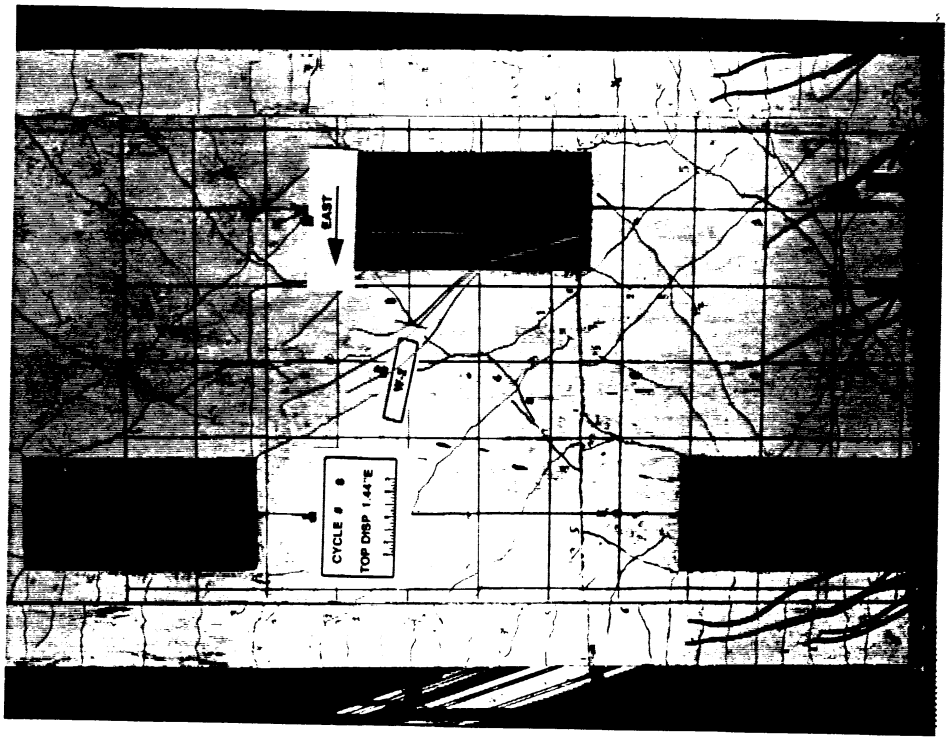

Fig. 4.13 : Compression Struts in the Lower Half of W-2 continue across the Joint during Cycle 8.

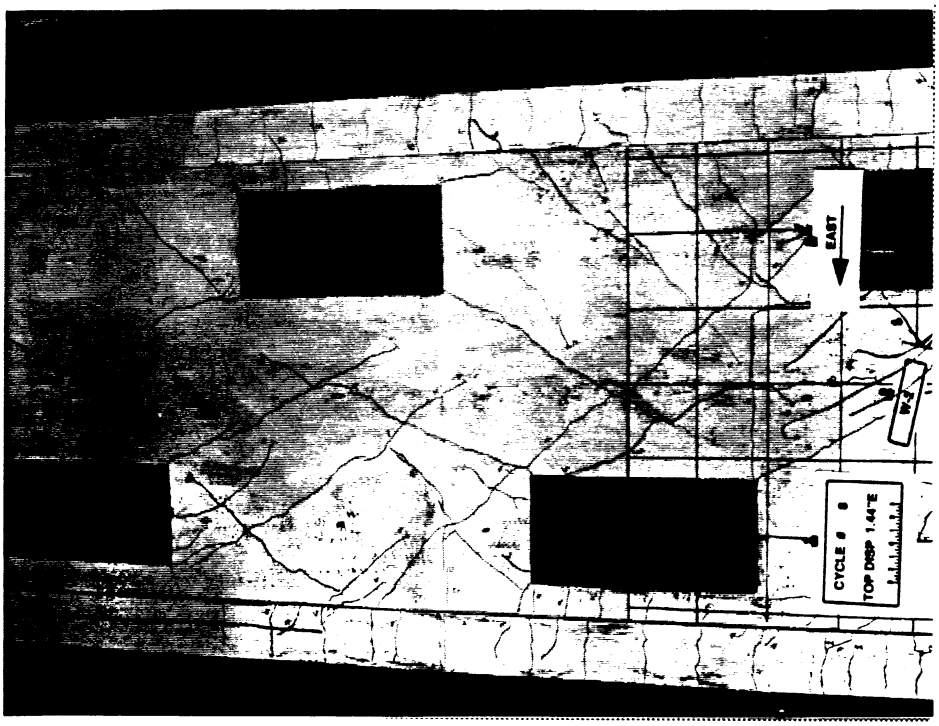

Fig. 4.14 : Upper Half of W-2 during Cycle 8.

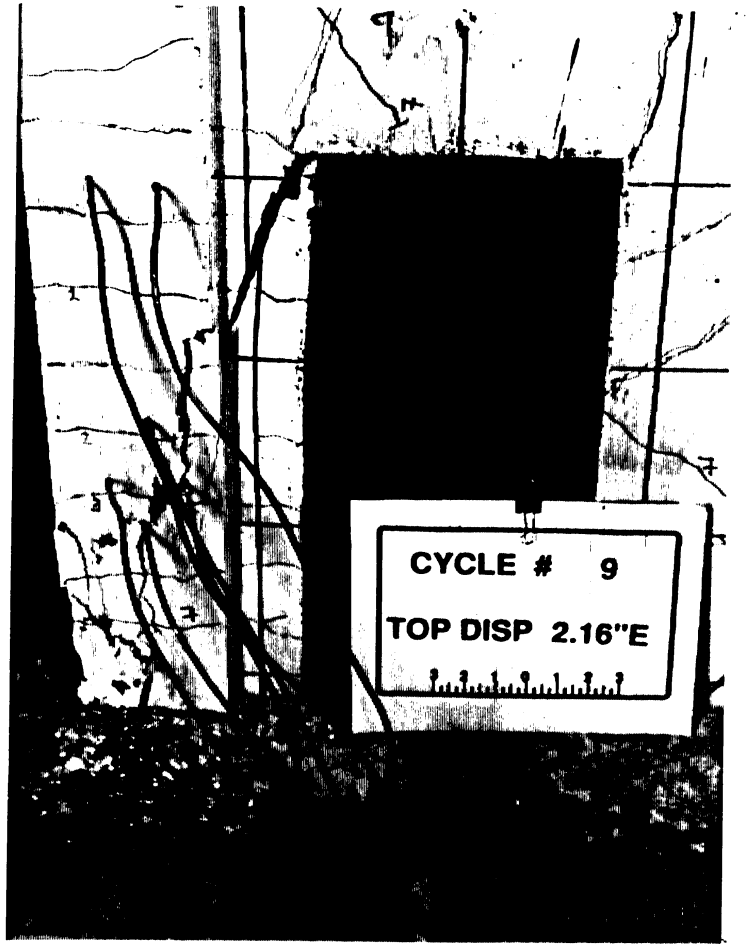

Fig. 4.15 : Shear Compression Failure in the East Boundary Column during Cycle 9.

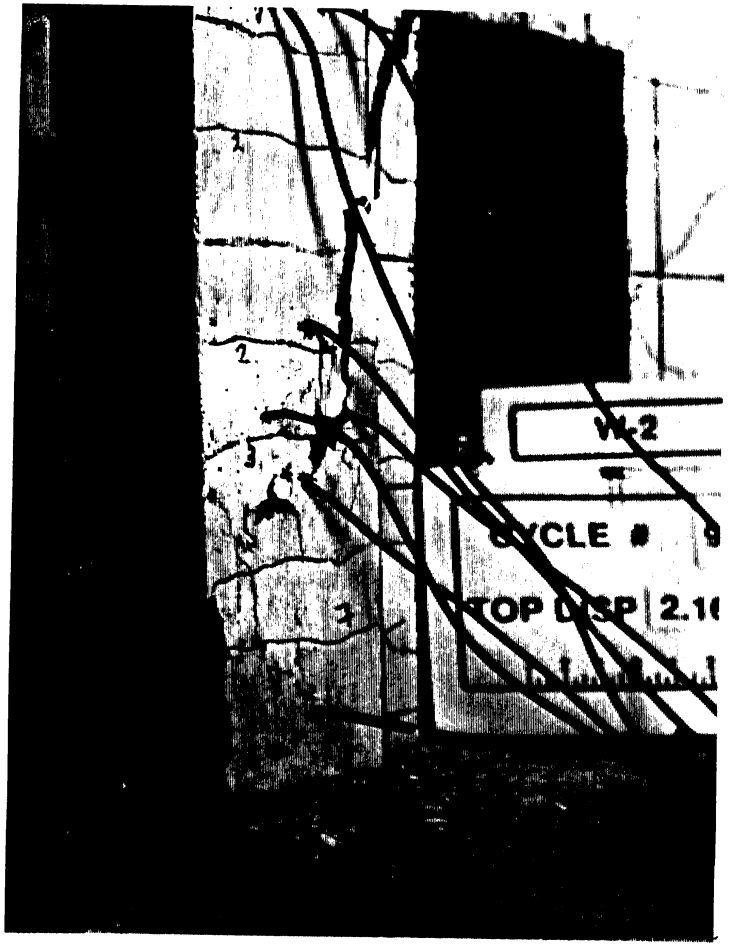

Fig. 4.16 : Concrete in the East Boundary Column crushes and spalls as a result of Shear Compression Failure in Cycle 9.

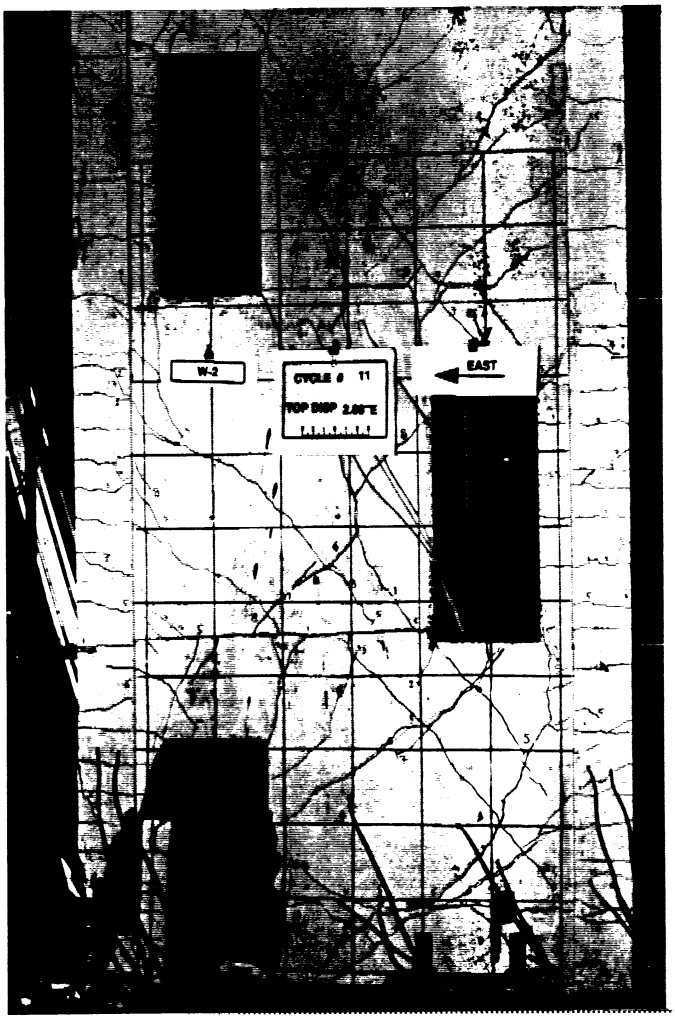

Fig. 4.17 : Crushing on the West Edge of Opening is Accompanied by Buckling of Reinforcement Bars during Cycle 11.

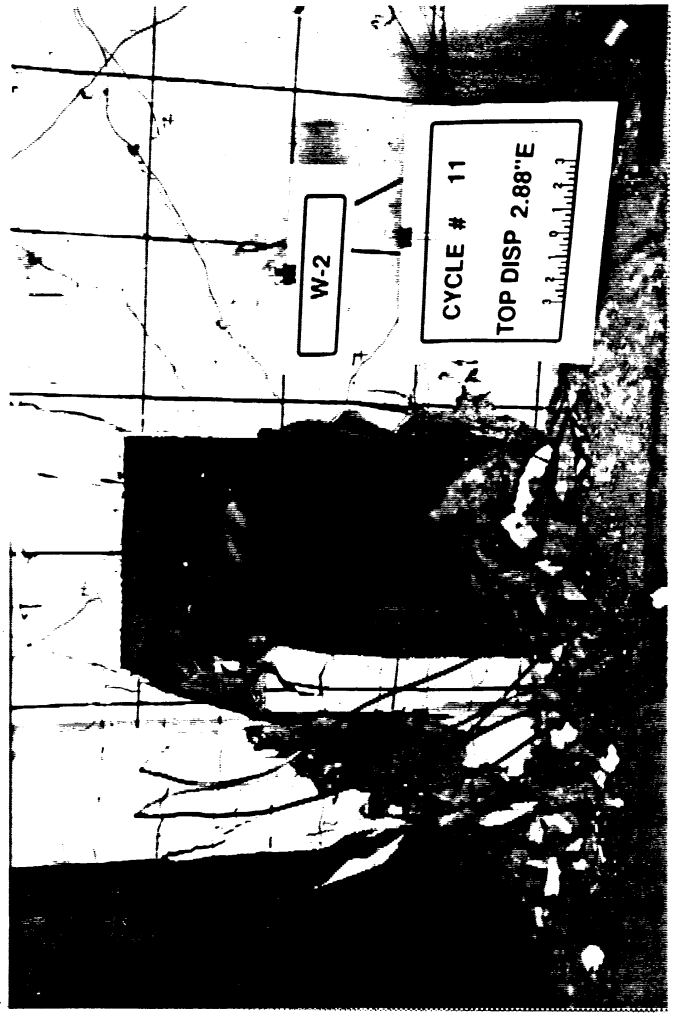

Fig. 4.18 : Reinforcing Bars Buckle as a Drift Ratio of 2 Percent is Approached.

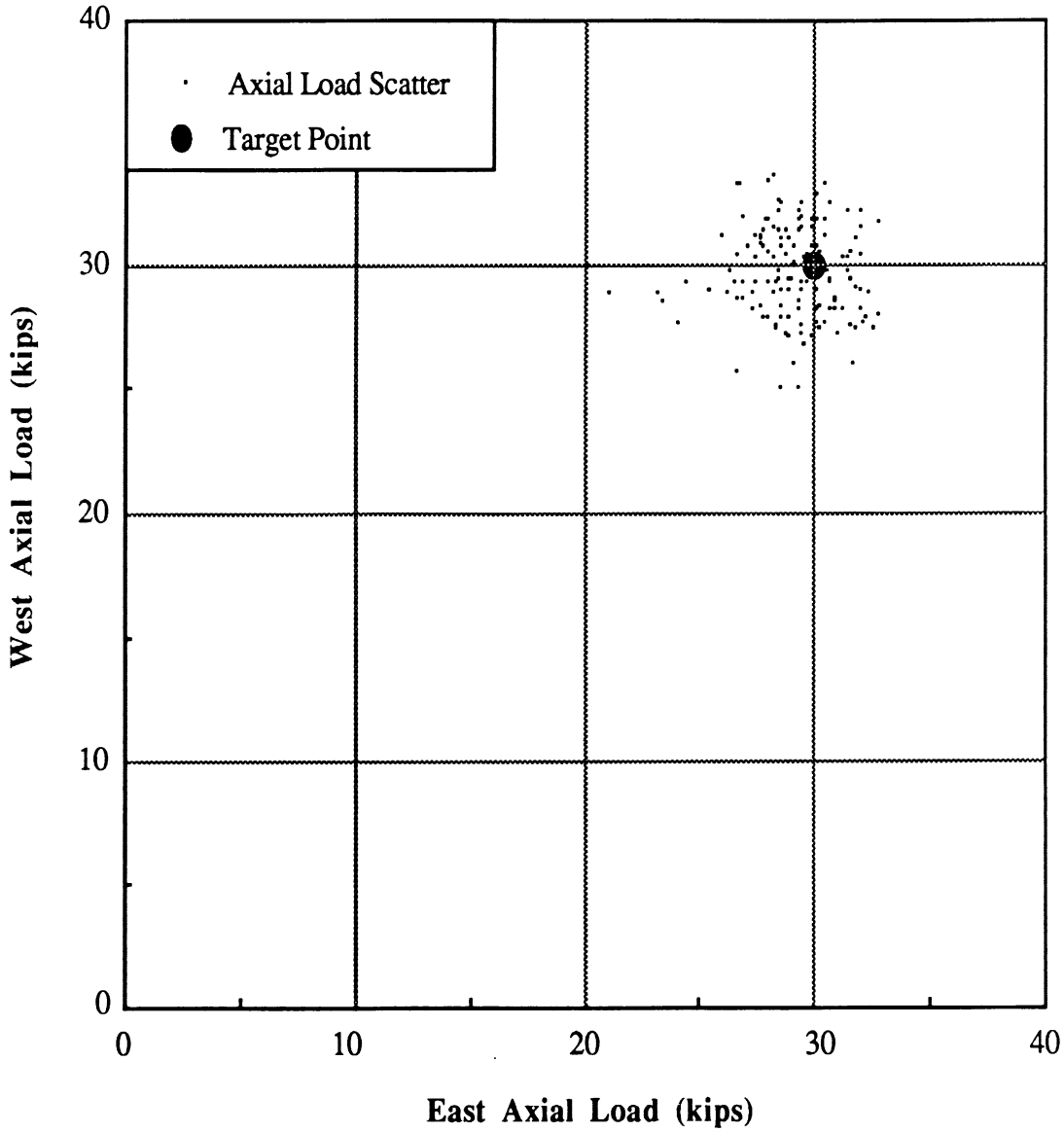

Fig. 4.19 : Scatter in the Applied Axial Load for Specimen W-2.

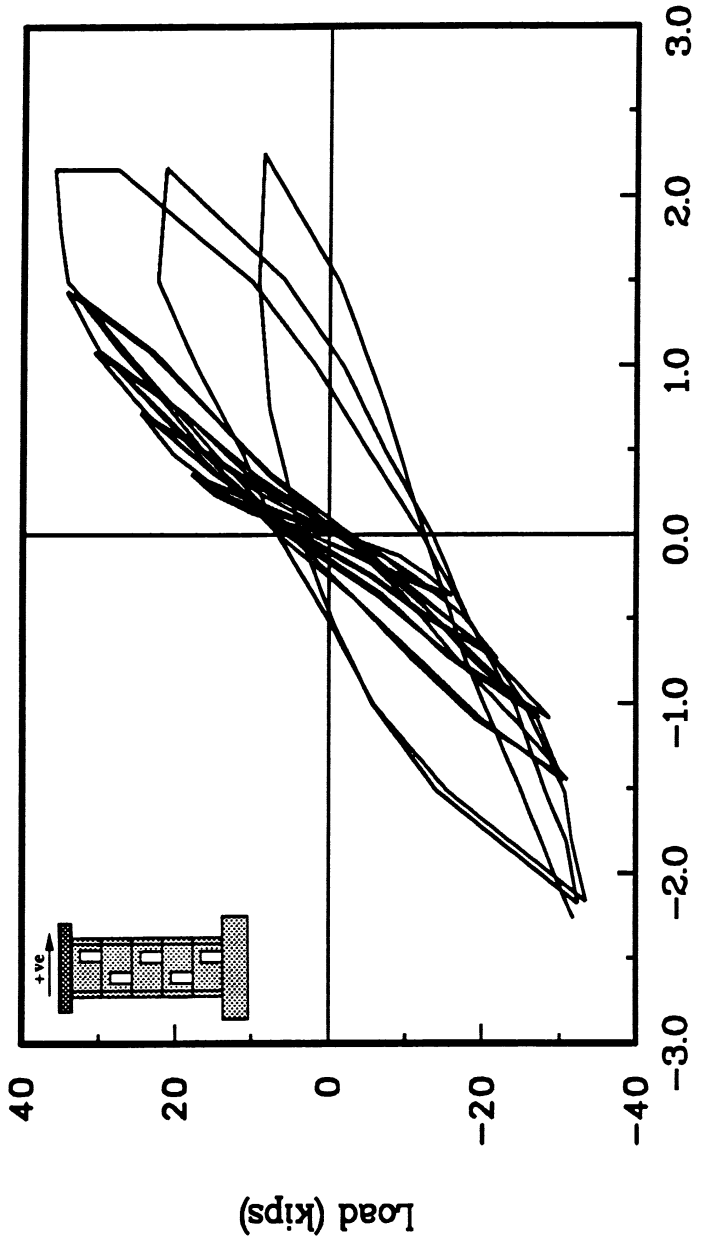

Fig. 4.20 : Force-Displacement Relationship for Wall W-3.

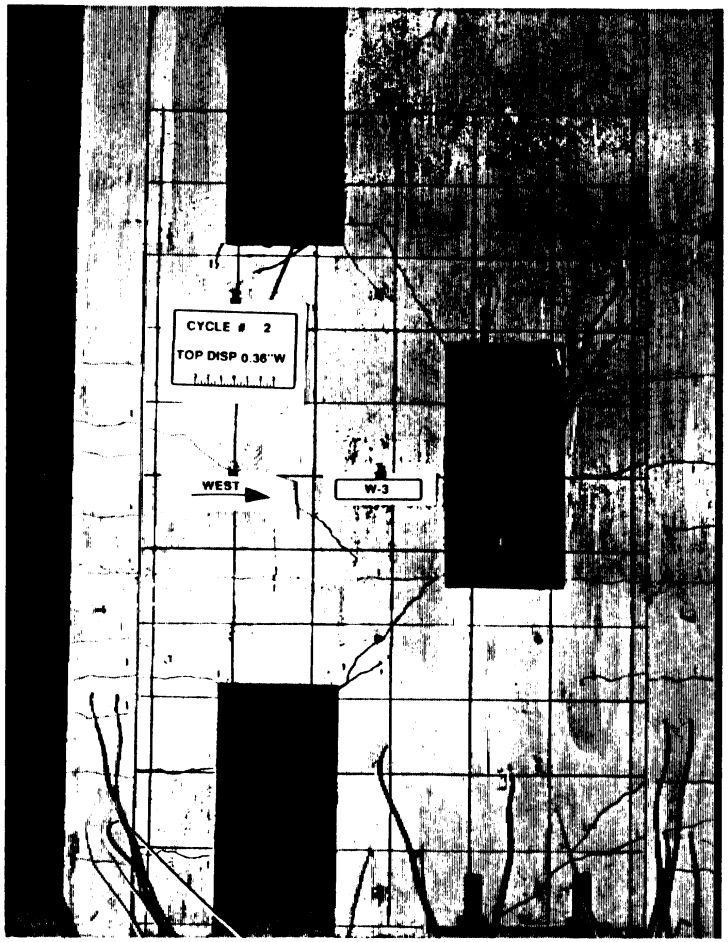

Fig. 4.21 : Diagonal Cracks extend between the Openings' Corners in Specimen W-3 during Cycle 2.

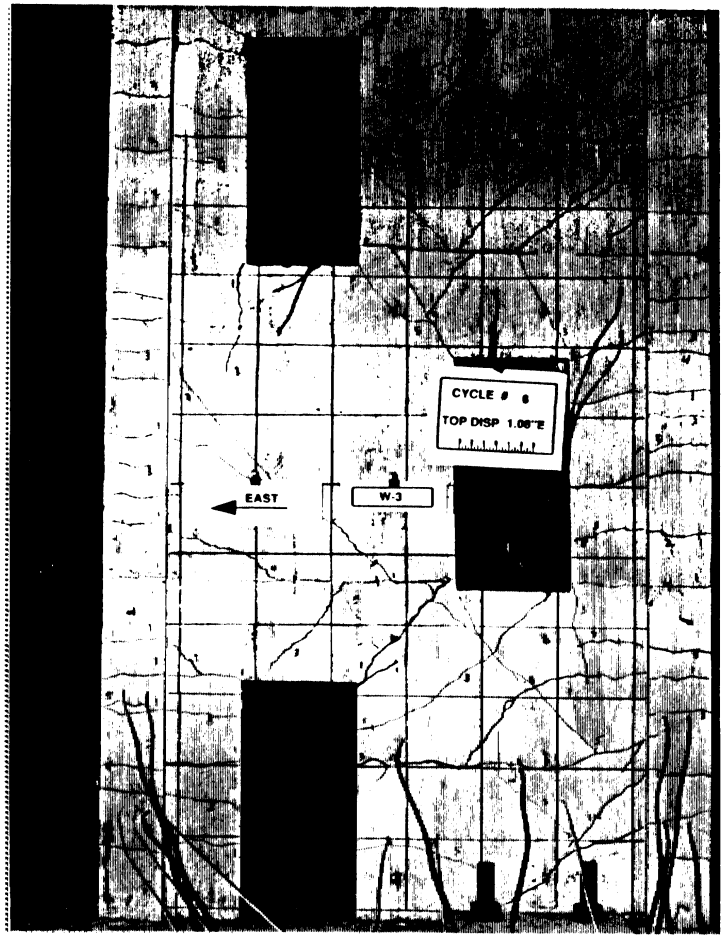

Fig. 4.22 : General Crack Pattern in Specimen W-3 during Cycle 6.

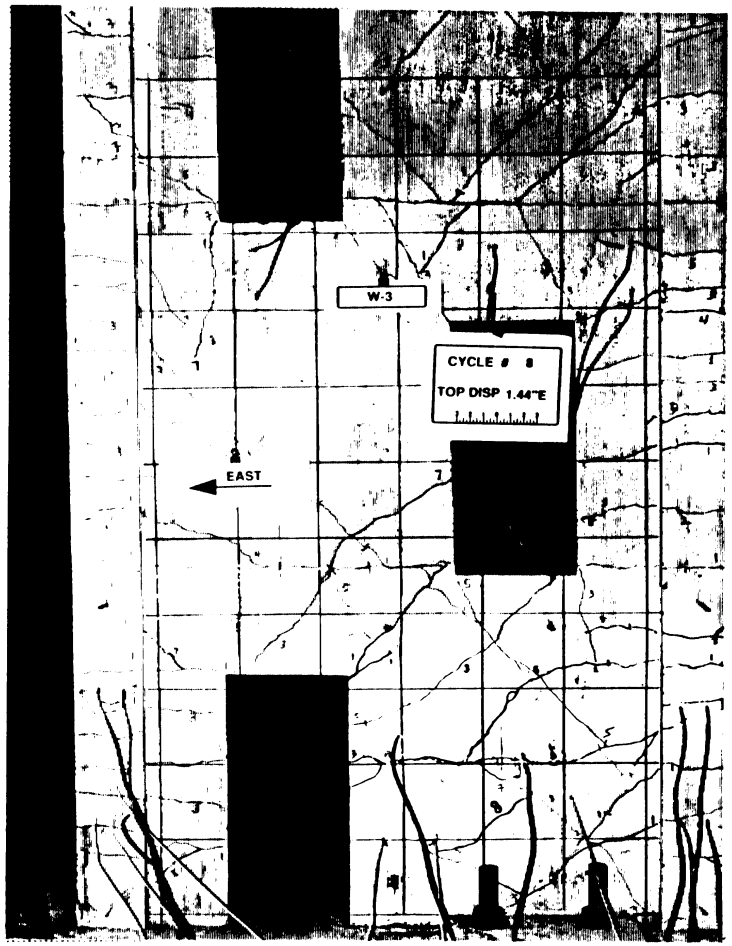

Fig. 4.23 : Crushing initiates at the Base of East Boundary Column during Cycle 8 in Specimen W-3.

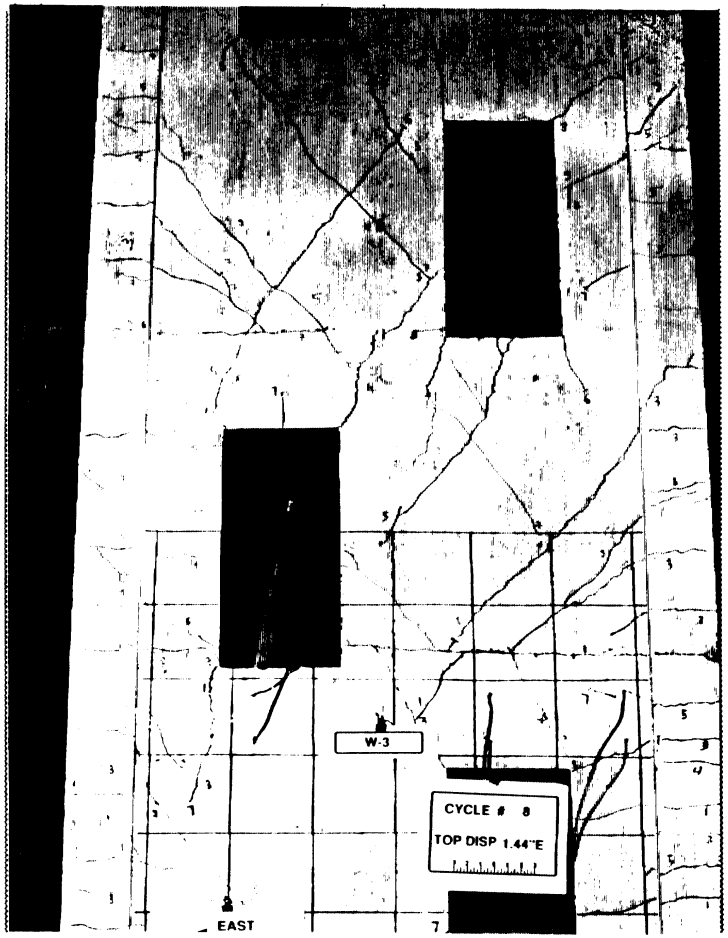

Fig. 4.24 : Crack Pattern in the Upper Half of W-3 during Cycle 8.

Fig. 4.25 : Shear Compression Failure in Wall W-3 during Cycle 9.

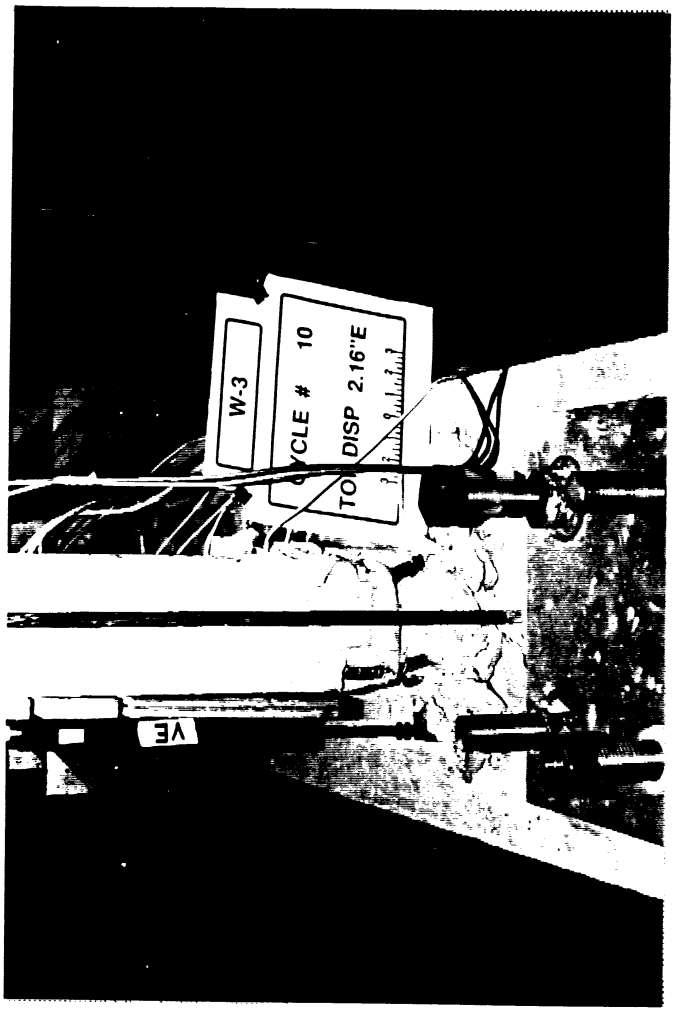

Fig. 4.26 : Out of Plane Buckling in Specimen W-3 during Cycle 10.

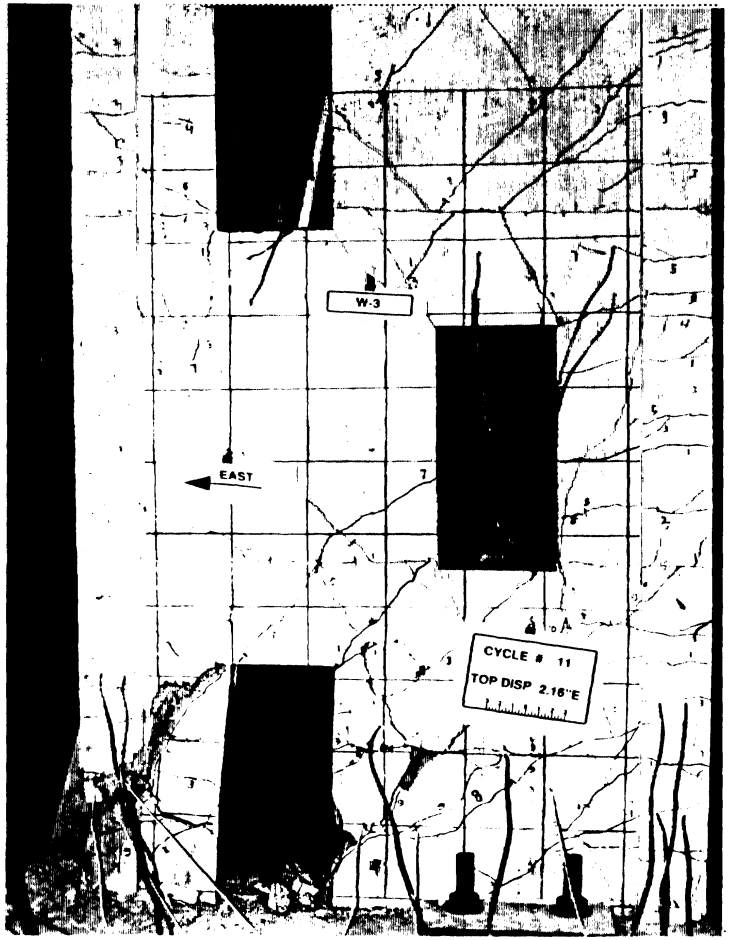

Fig. 4.27 : Crushing and Spalling of Concrete on Either Sides of Opening weakens the Specimen W-3 during Cycle 11.

Fig. 4.28 : Specimen W-3 after Shear Failure.

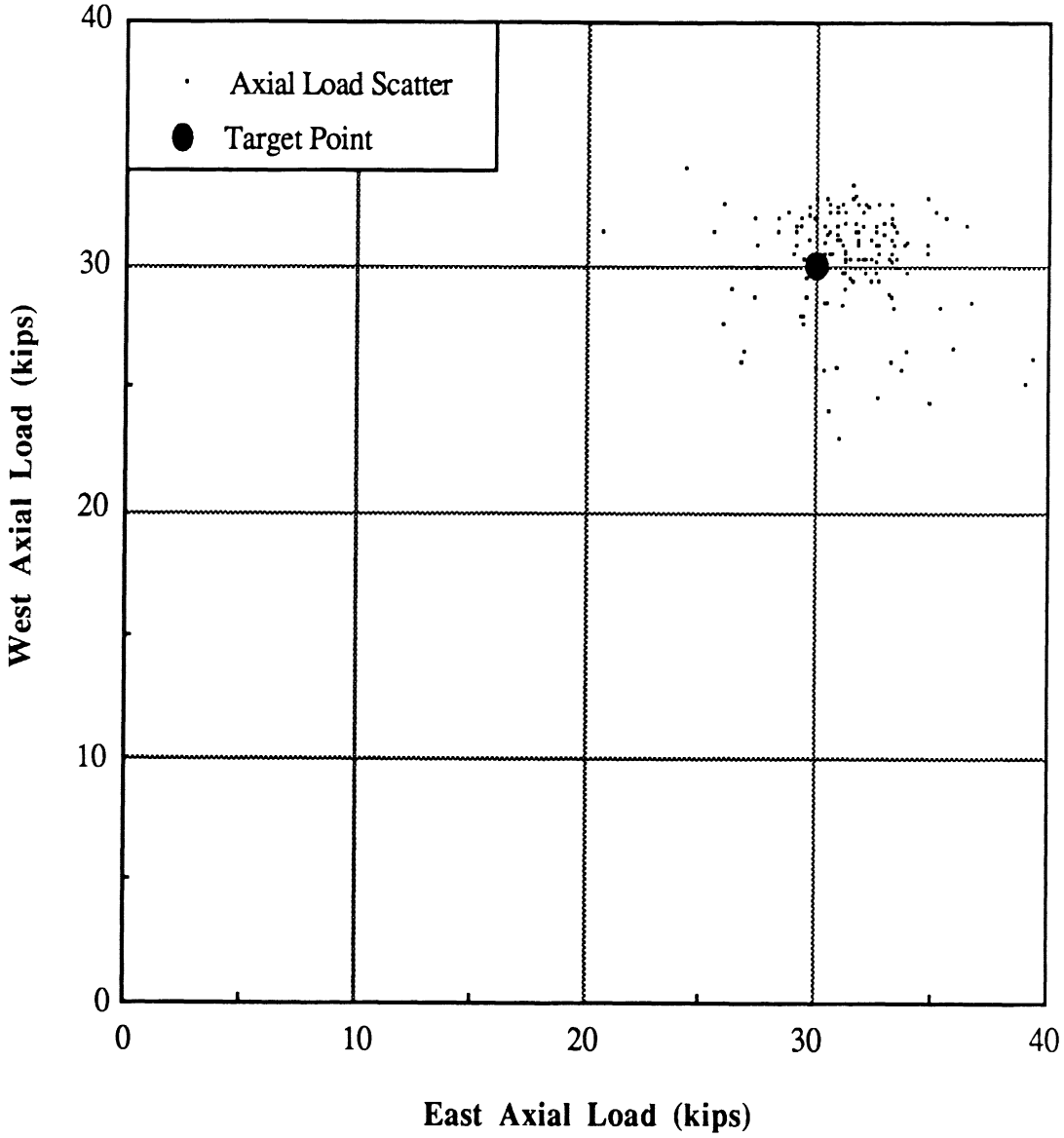

Fig. 4.29 : Scatter in the Applied Axial Load for Specimen W-3.

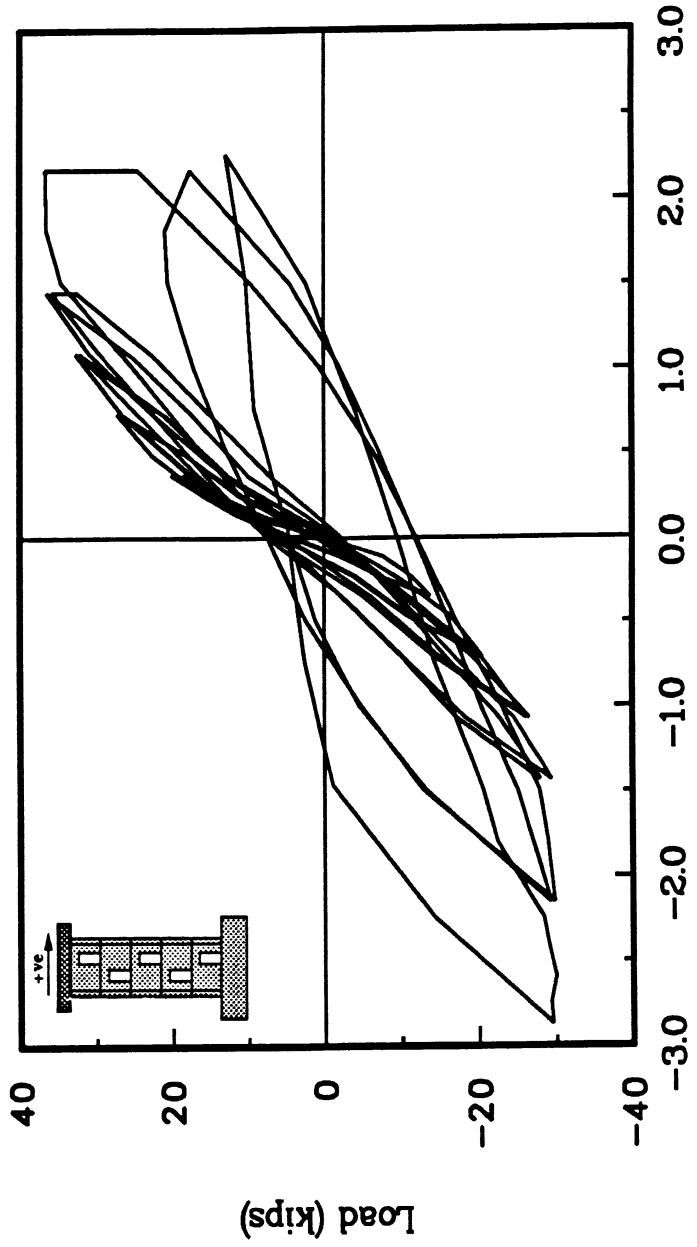

Fig. 4.30 : Force-Displacement Relationship for Wall W-4.

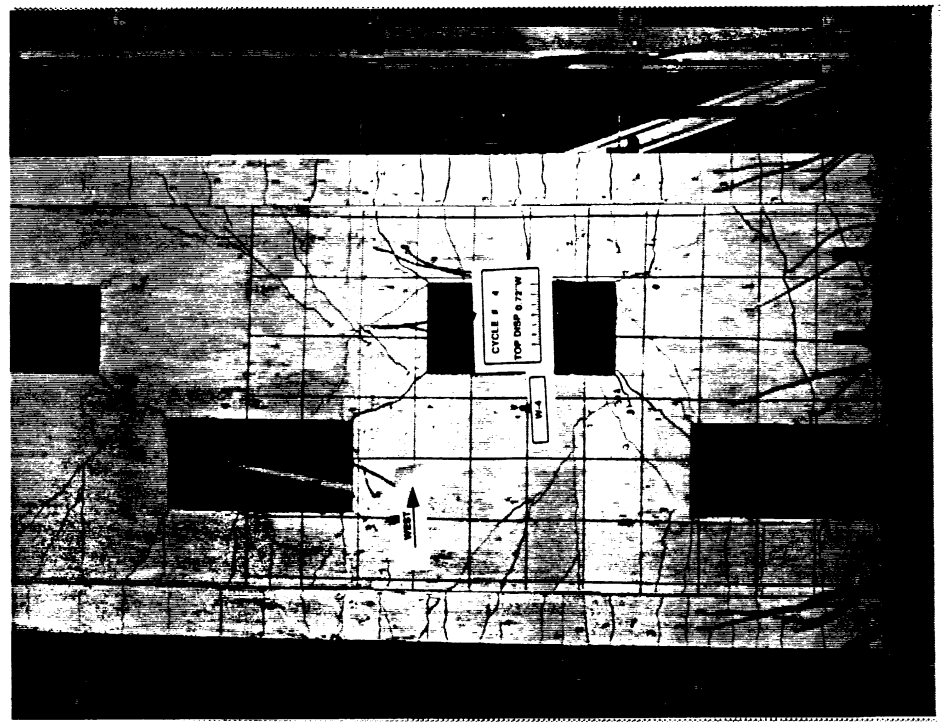

Fig. 4.32 : Flexural Shear Cracks in Specimen W-4 during Cycle 4.

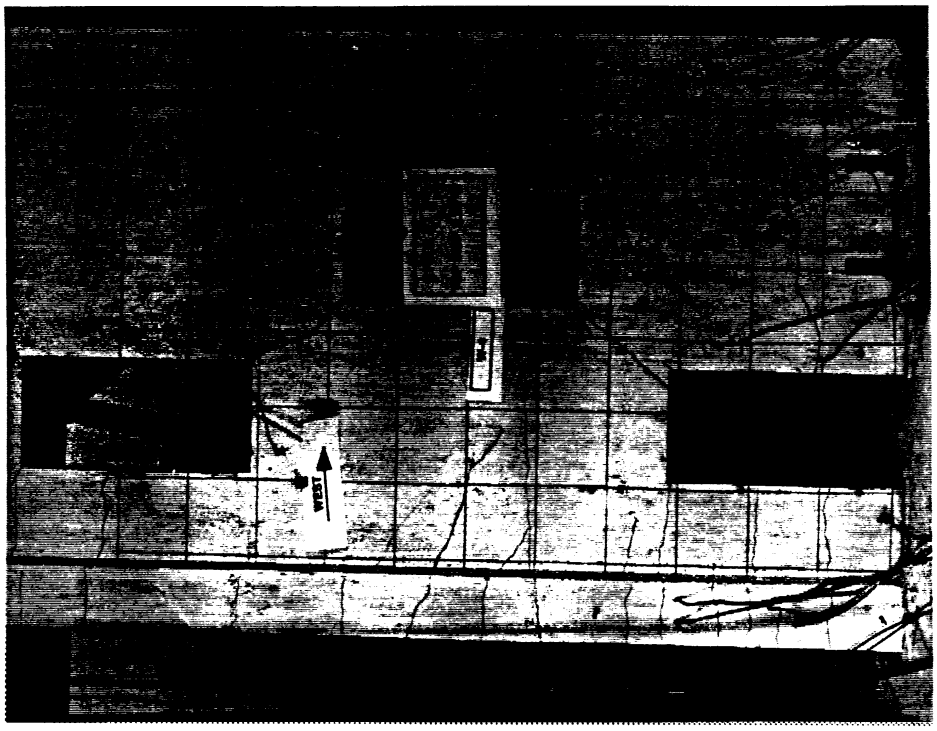

Fig. 4.31 : Cracks form during the Second Cycle in Wall W-4.

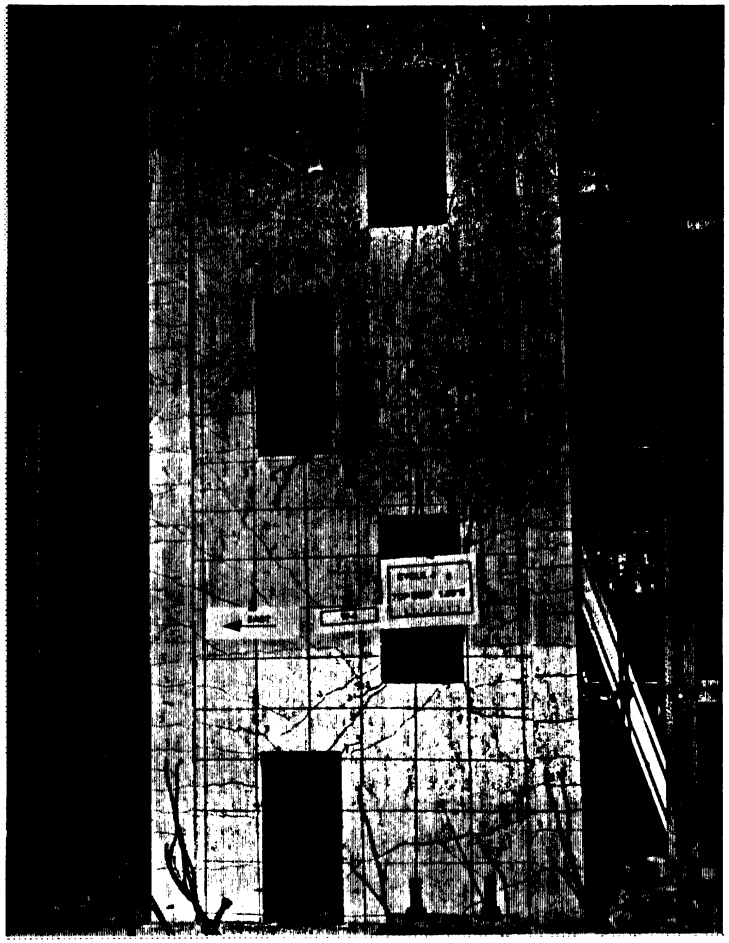

Fig. 4.33 : Flexural Shear Cracks progress during Cycle 6 in W-4.

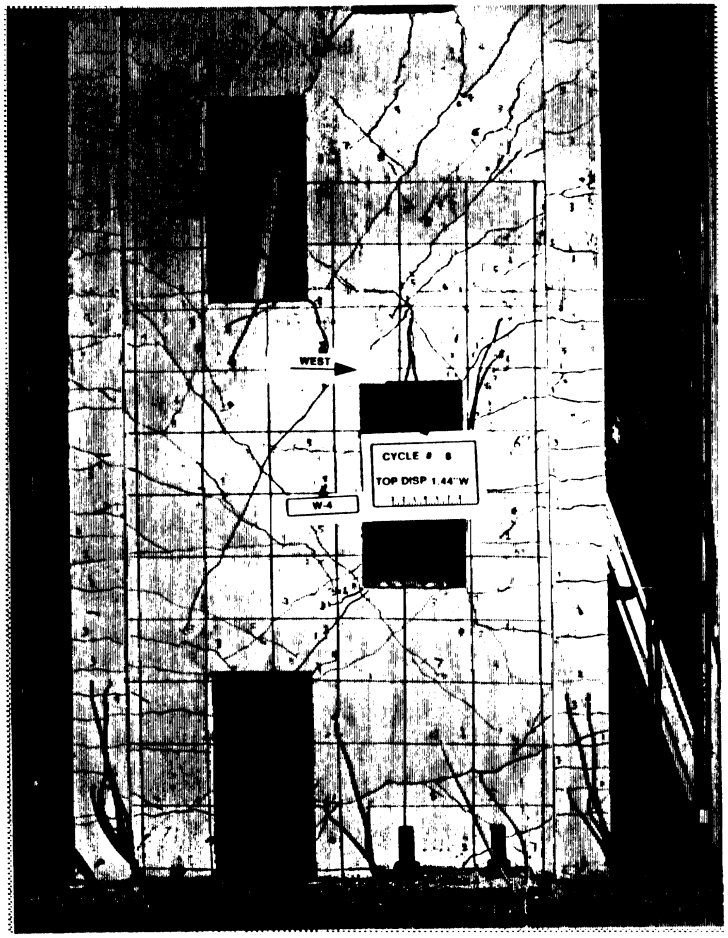

Fig. 4.34 : Diagonal Compression Struts run across the Web in W-4 after 8 Cycles.

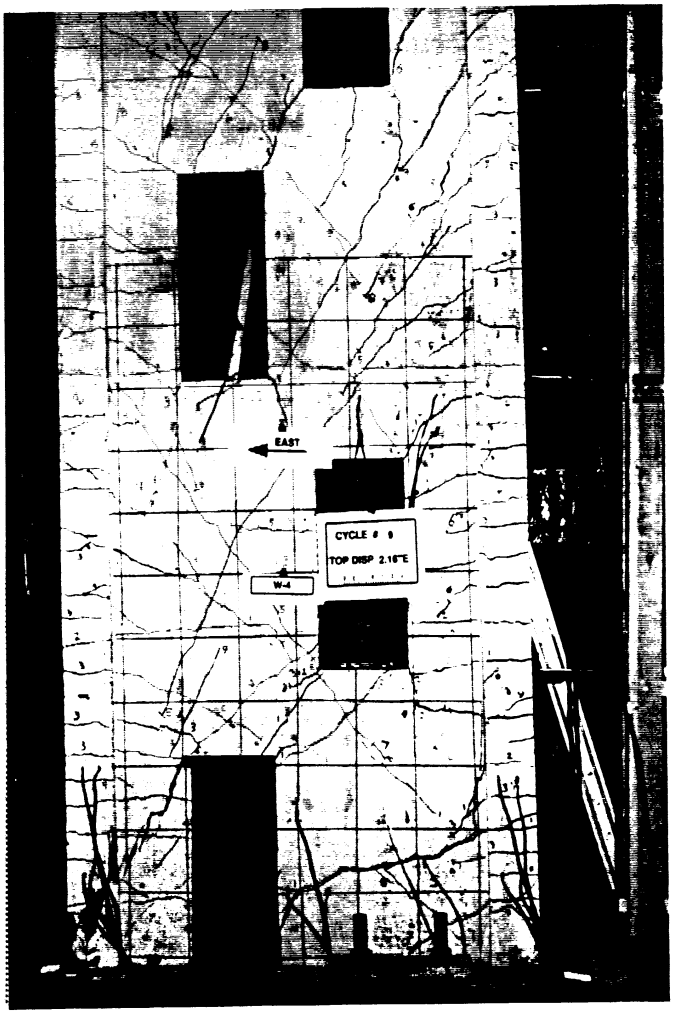

Fig. 4.35 : Shear Compression Failure of East Boundary Column in W-4 during Cycle 9.

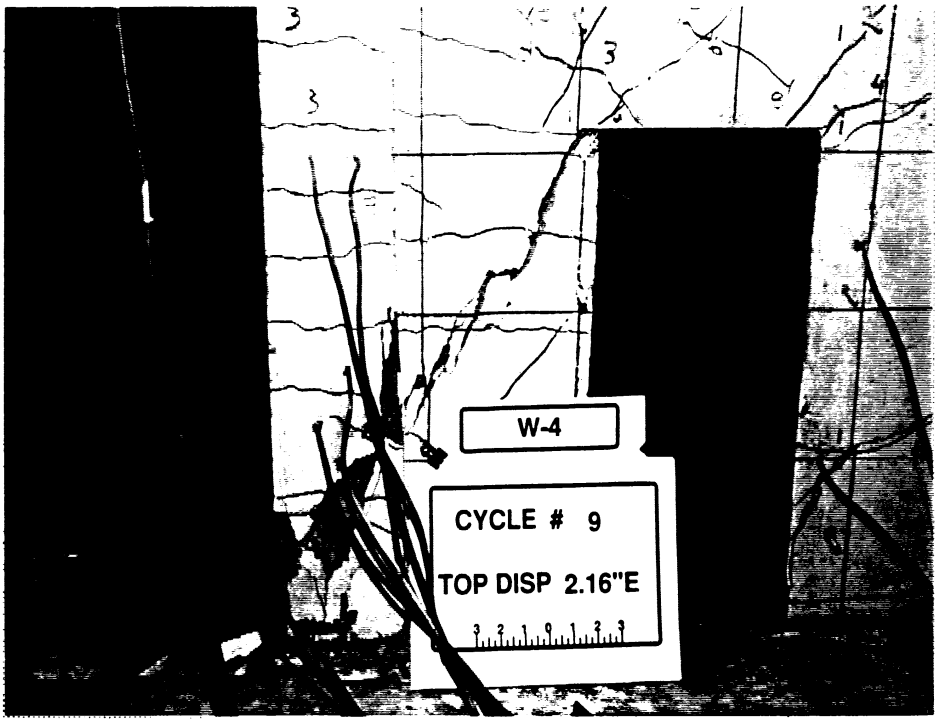

Fig. 4.36 : Close up of the East Boundary Column after Shear Compression Failure.

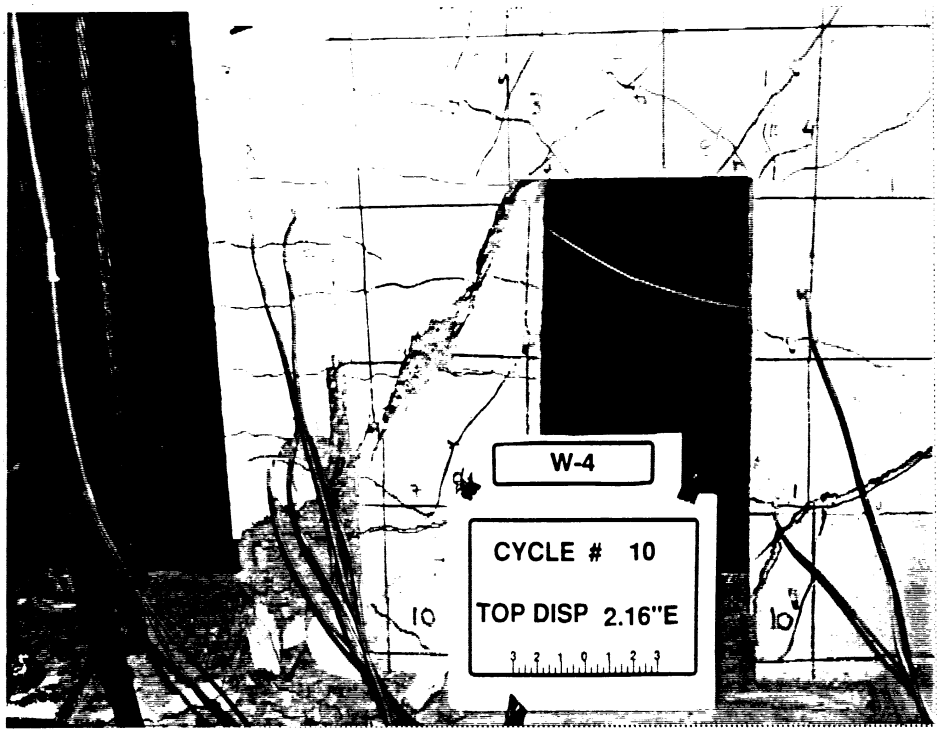

Fig. 4.37 : East Boundary Column deteriorates in Repeat Cycle 10.

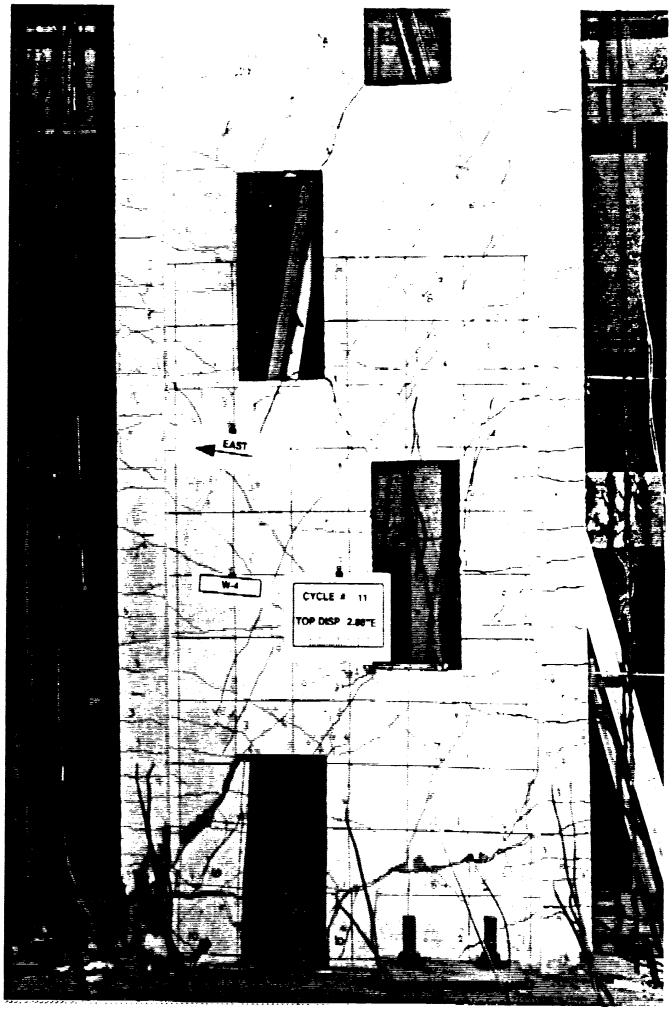

Fig. 4.38 : General Condition of Specimen W-4 during the Last Cycle.

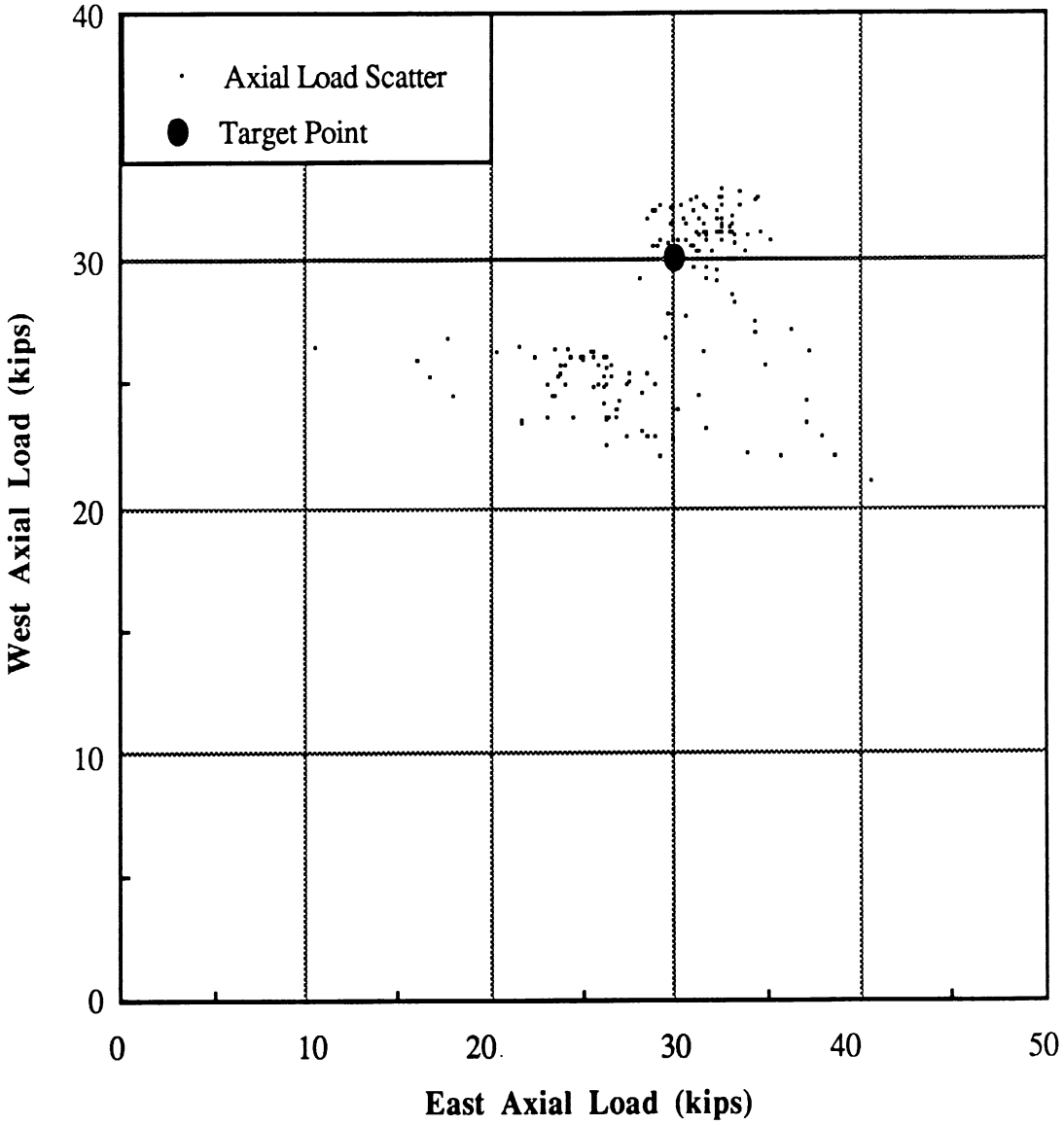

Fig. 4.39 : Scatter in the Applied Axial Load for Specimen W-4.

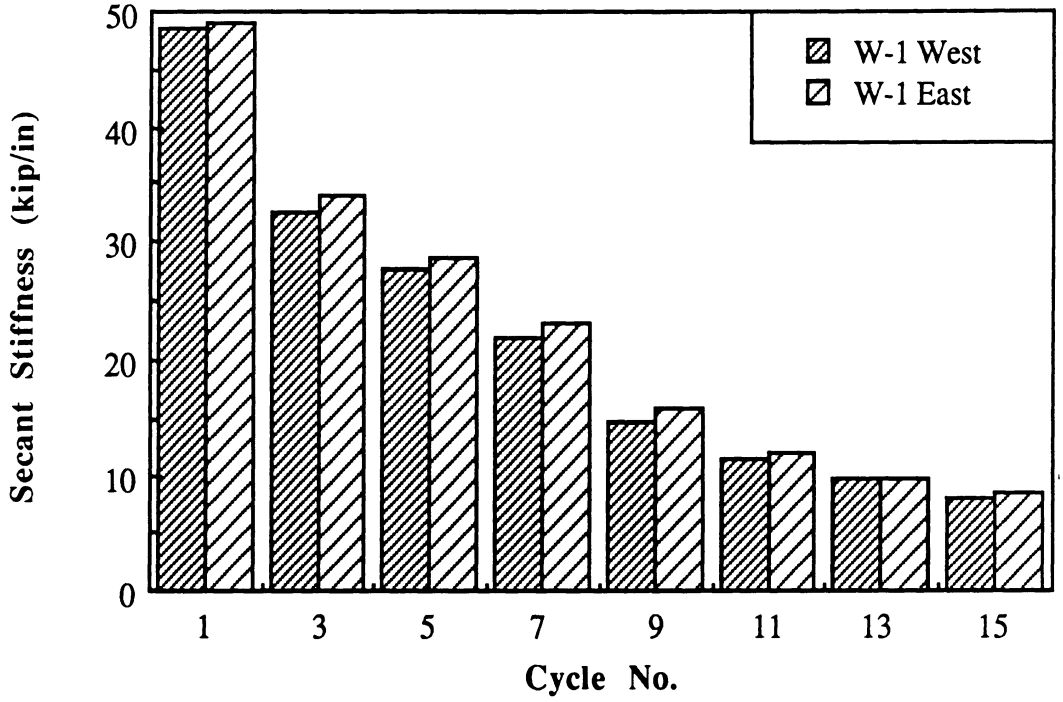

Fig. 4.40 : Comparison of Secant Stiffnesses for Wall W-1.

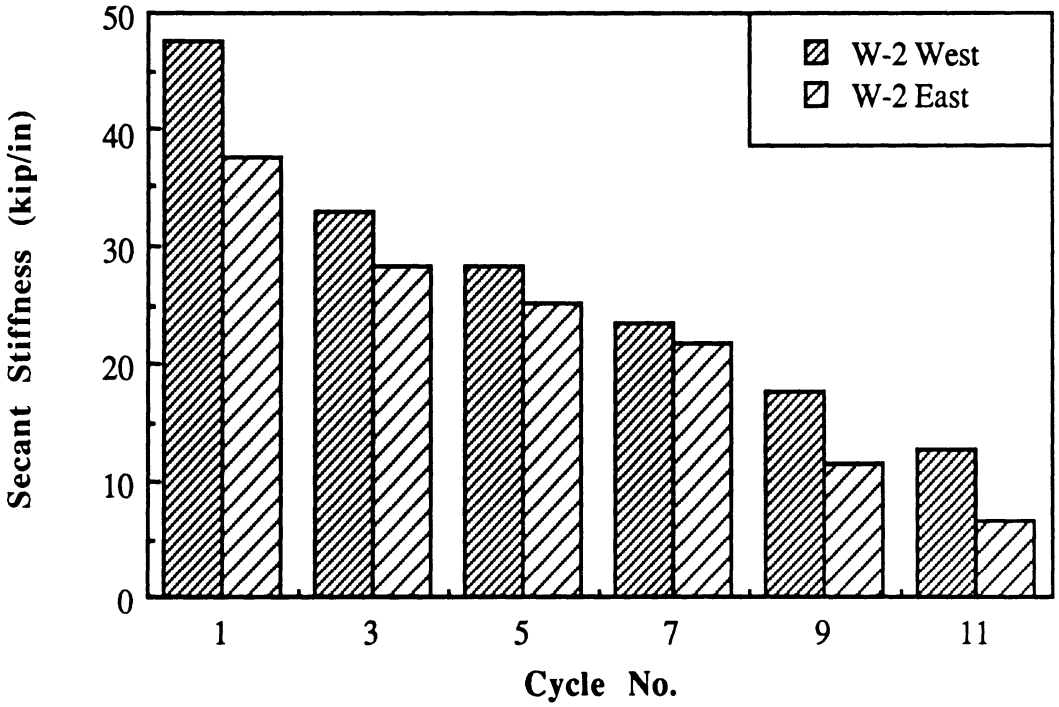

Fig. 4.41 : Comparison of Secant Stiffnesses for Wall W-2.

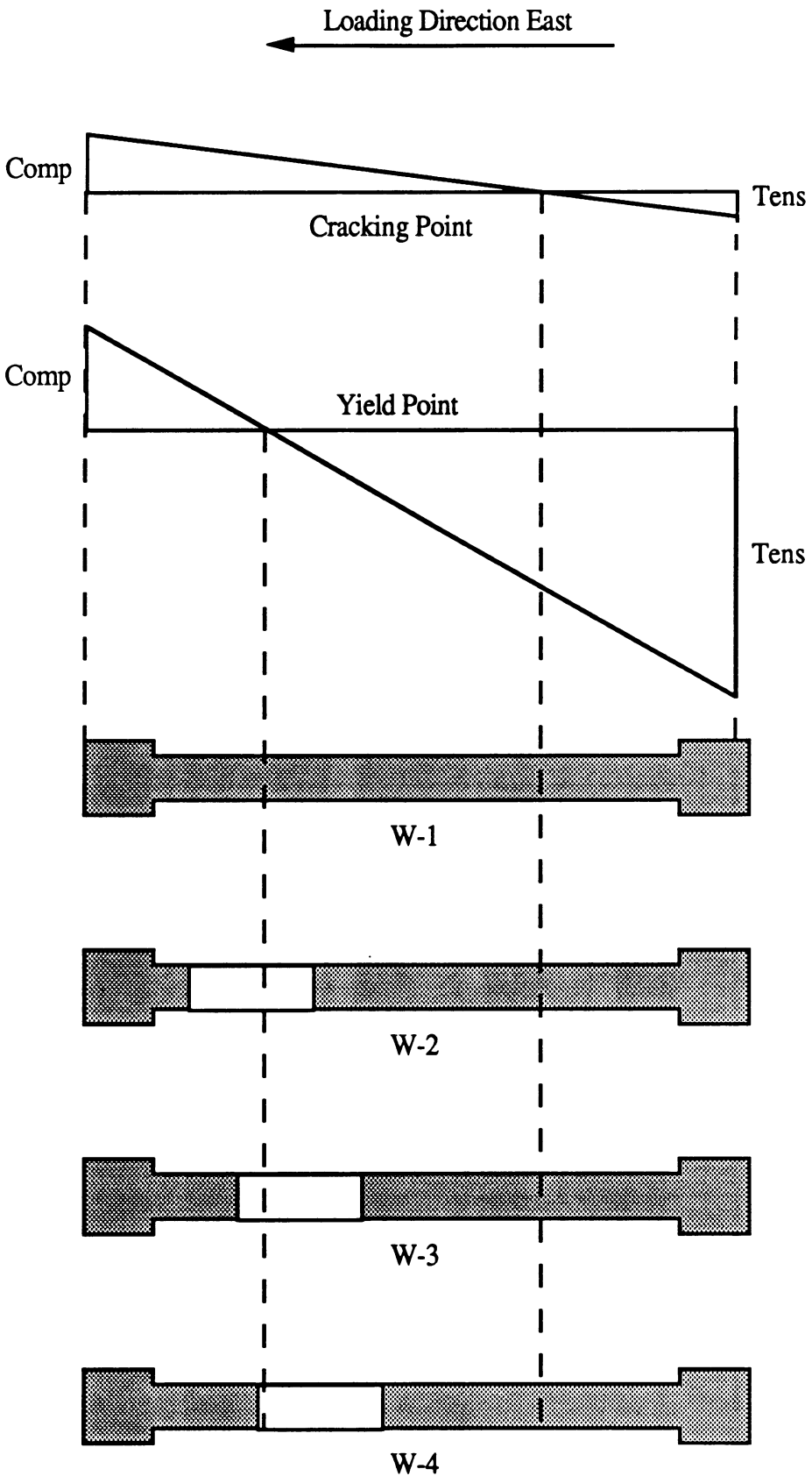

Fig. 4.42(a) : Strain Distributions at Cracking and Yield Points for Wall W-1 through W-4 for Loading in East Direction.

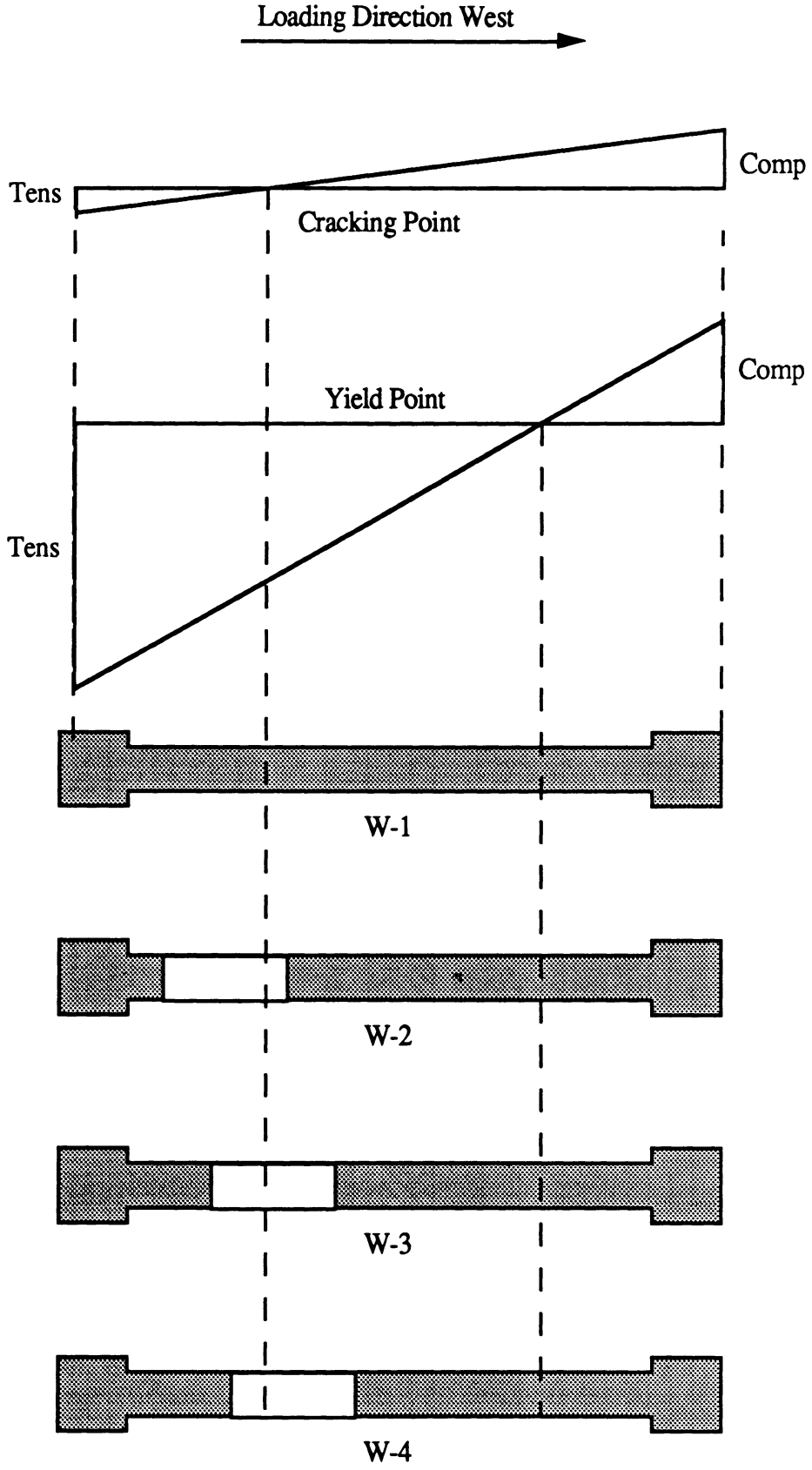

Fig. 4.42(b) : Strain Distributions at Cracking and Yield Points for Wall W-1 through W-4 for Loading in West Direction.

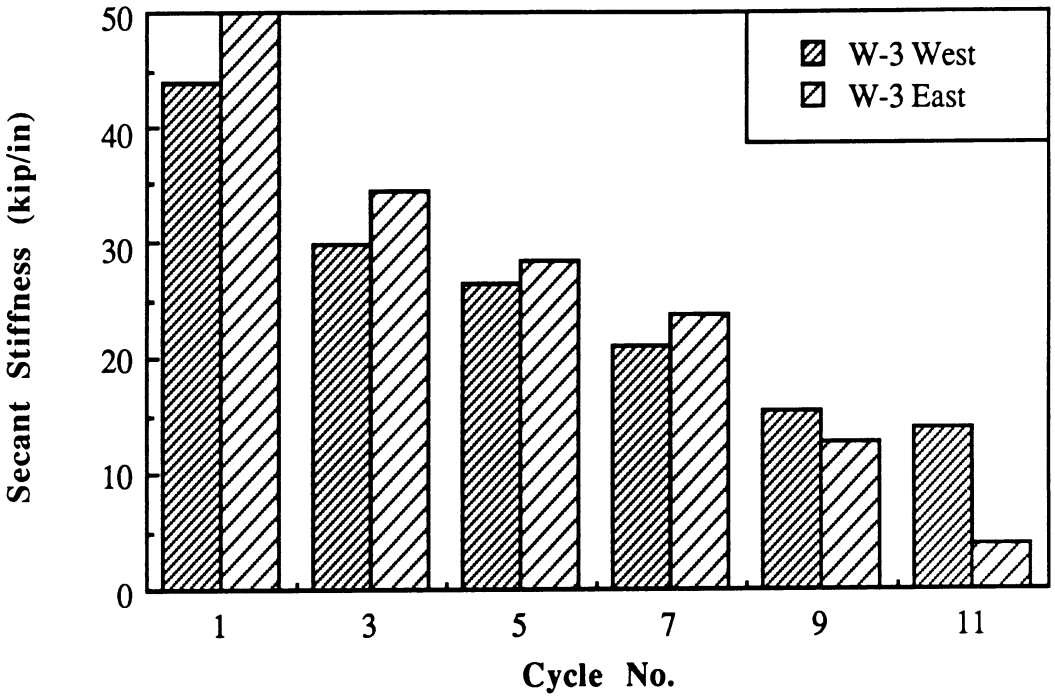

Fig. 4.43 : Comparison of Secant Stiffnesses for Wall W-3.

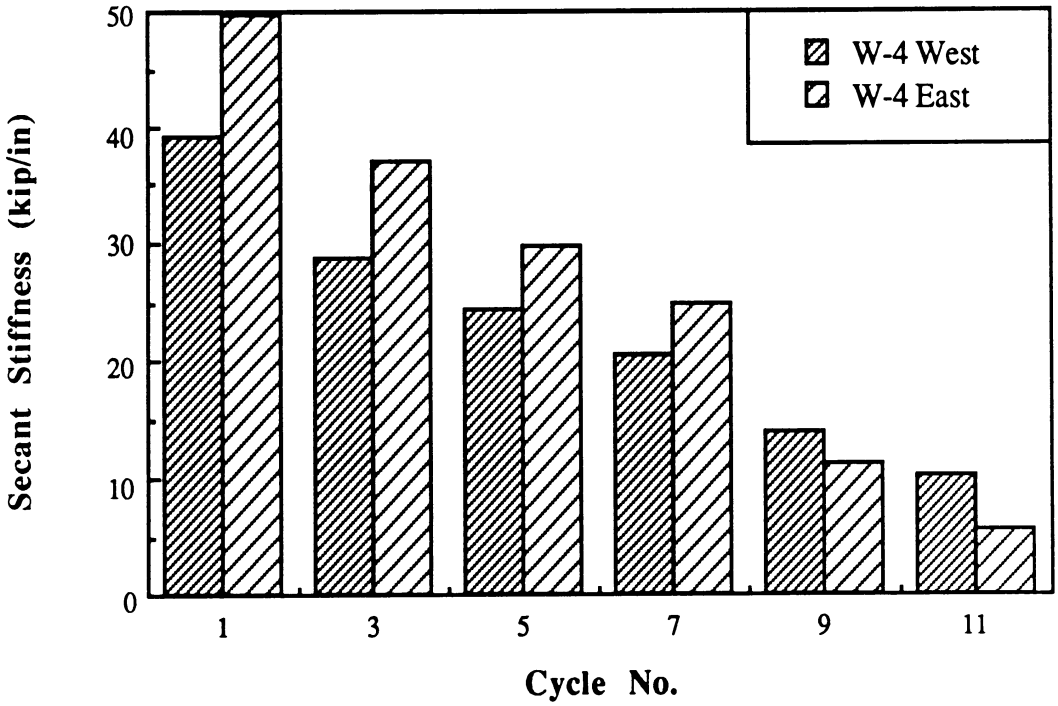

Fig. 4.44 : Comparison of Secant Stiffnesses for Wall W-4.

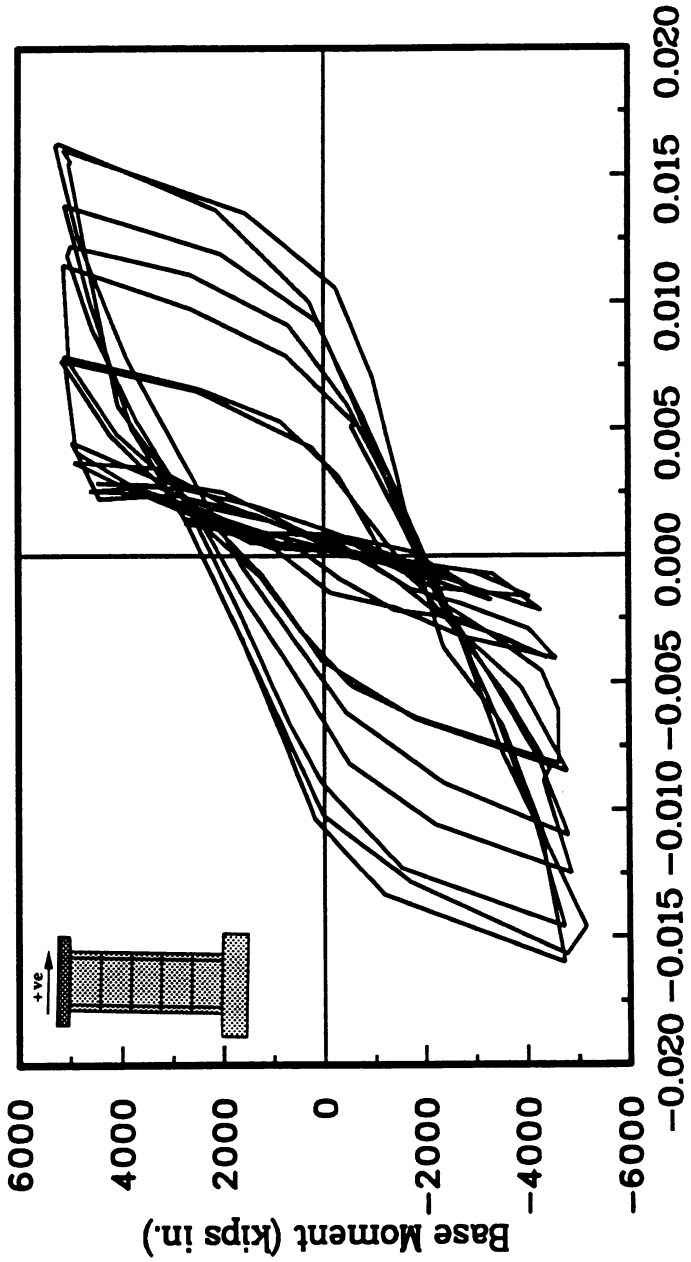

Fig. 4.45 : Base Moment-First Story Rotation Relationship for Wall W-1.

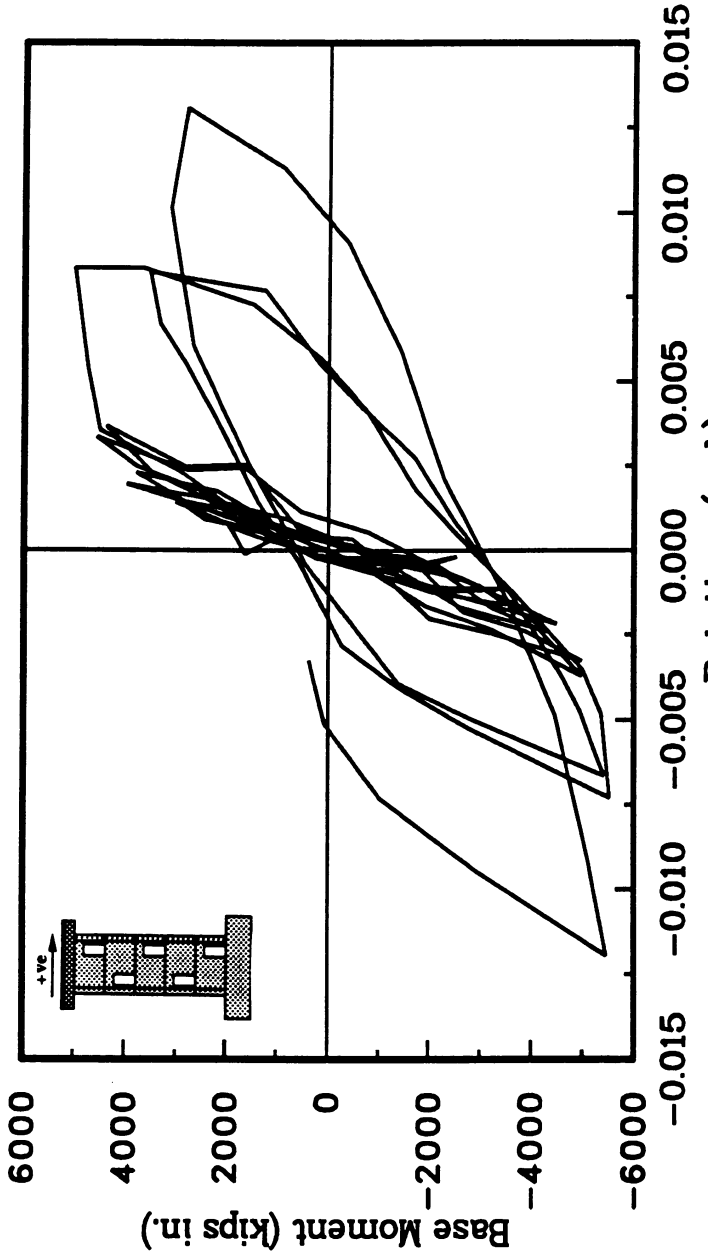

Fig. 4.46 : Base Moment-First Story Rotation Relationship for Wall W-2.

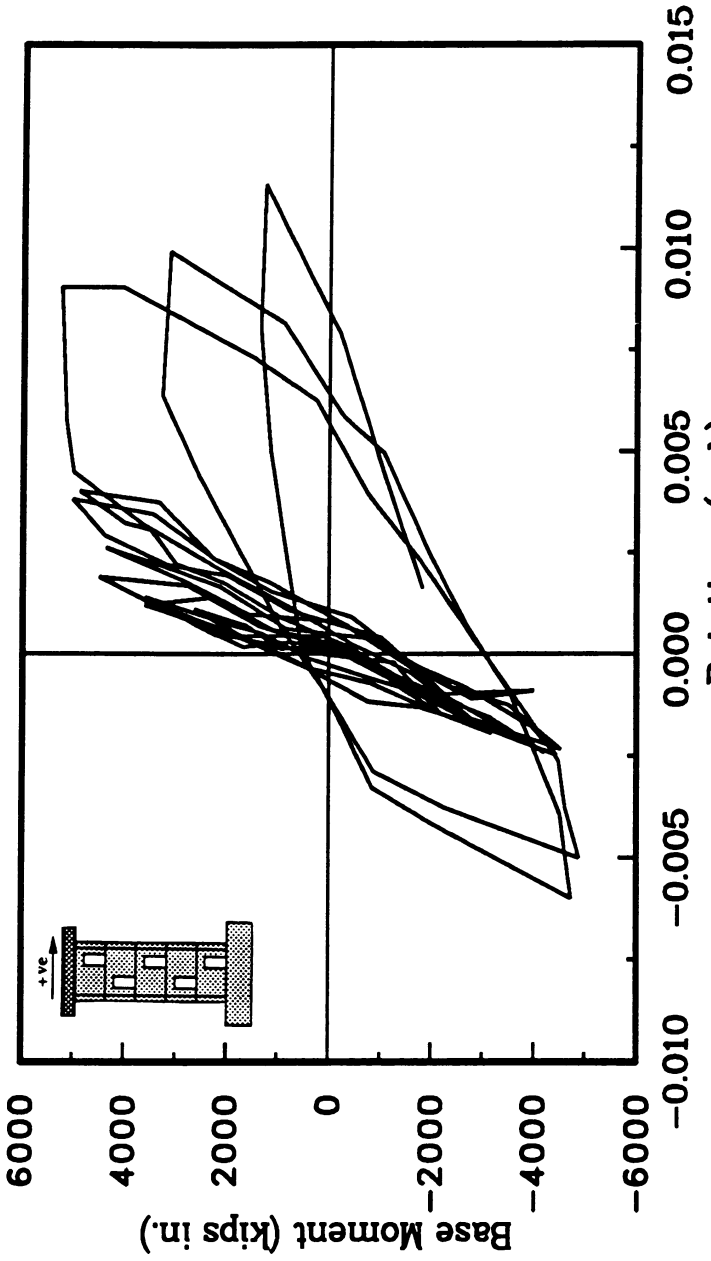

Fig. 4.47 : Base Moment-First Story Rotation Relationship for Wall W-3.

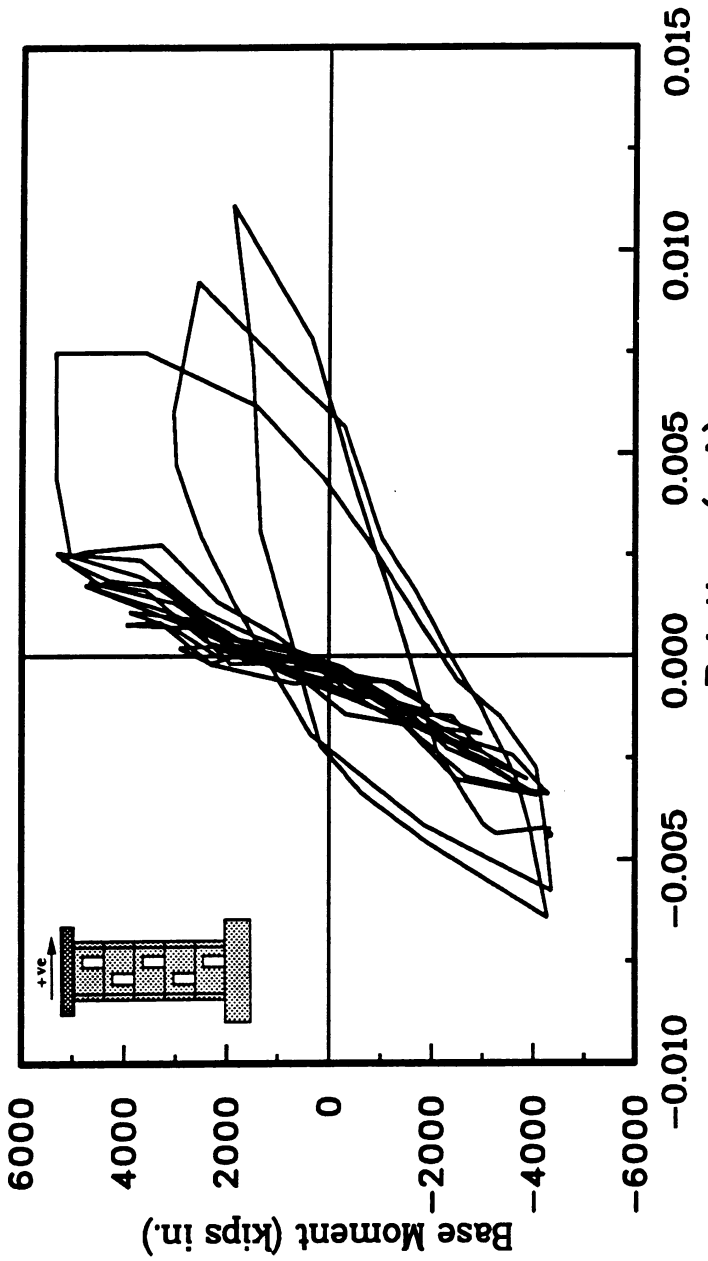

Fig. 4.48 : Base Moment-First Story Rotation Relationship for Wall W-4.

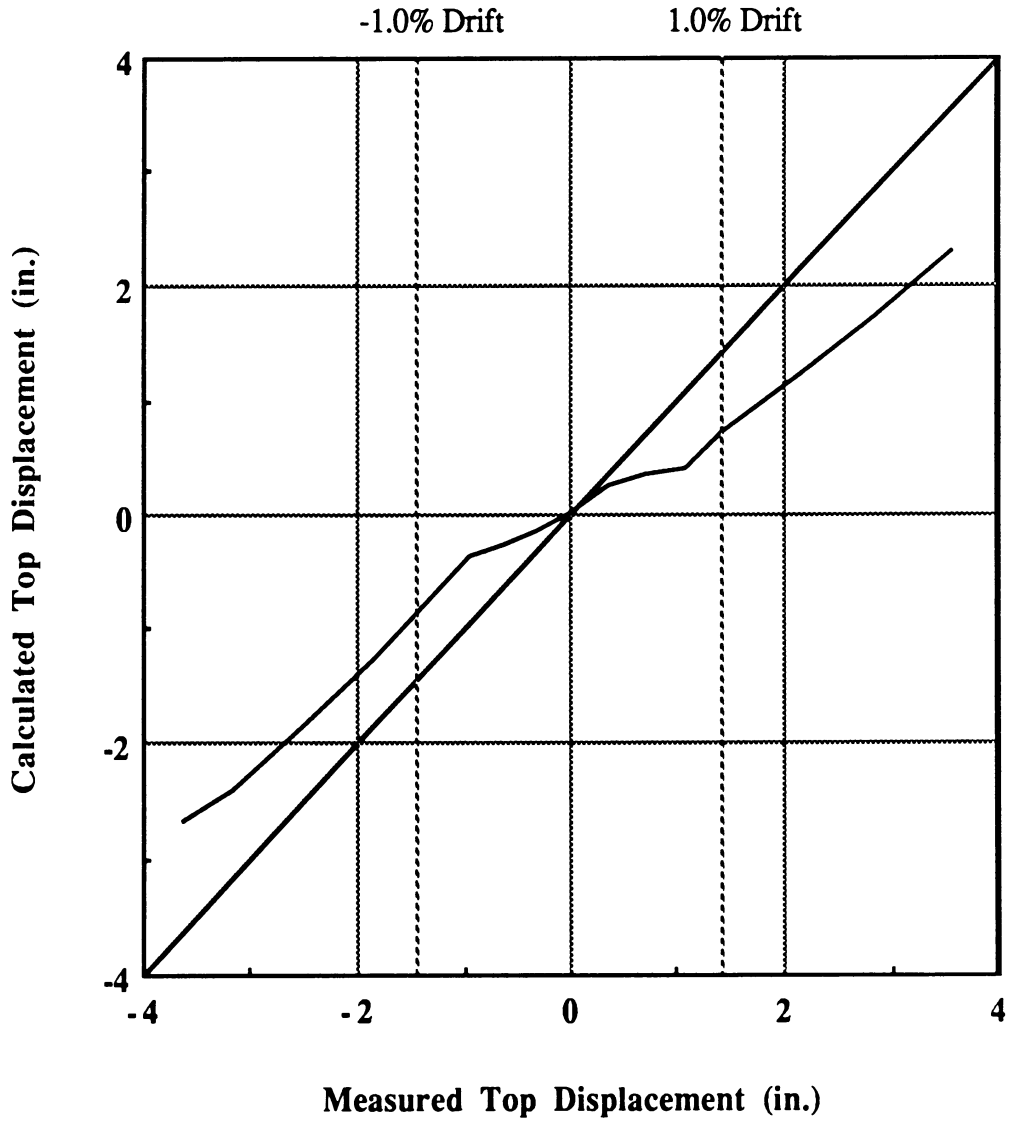

Fig. 4.49 : Effect of First Story Rotation of Wall W-1 on Top Displacement.

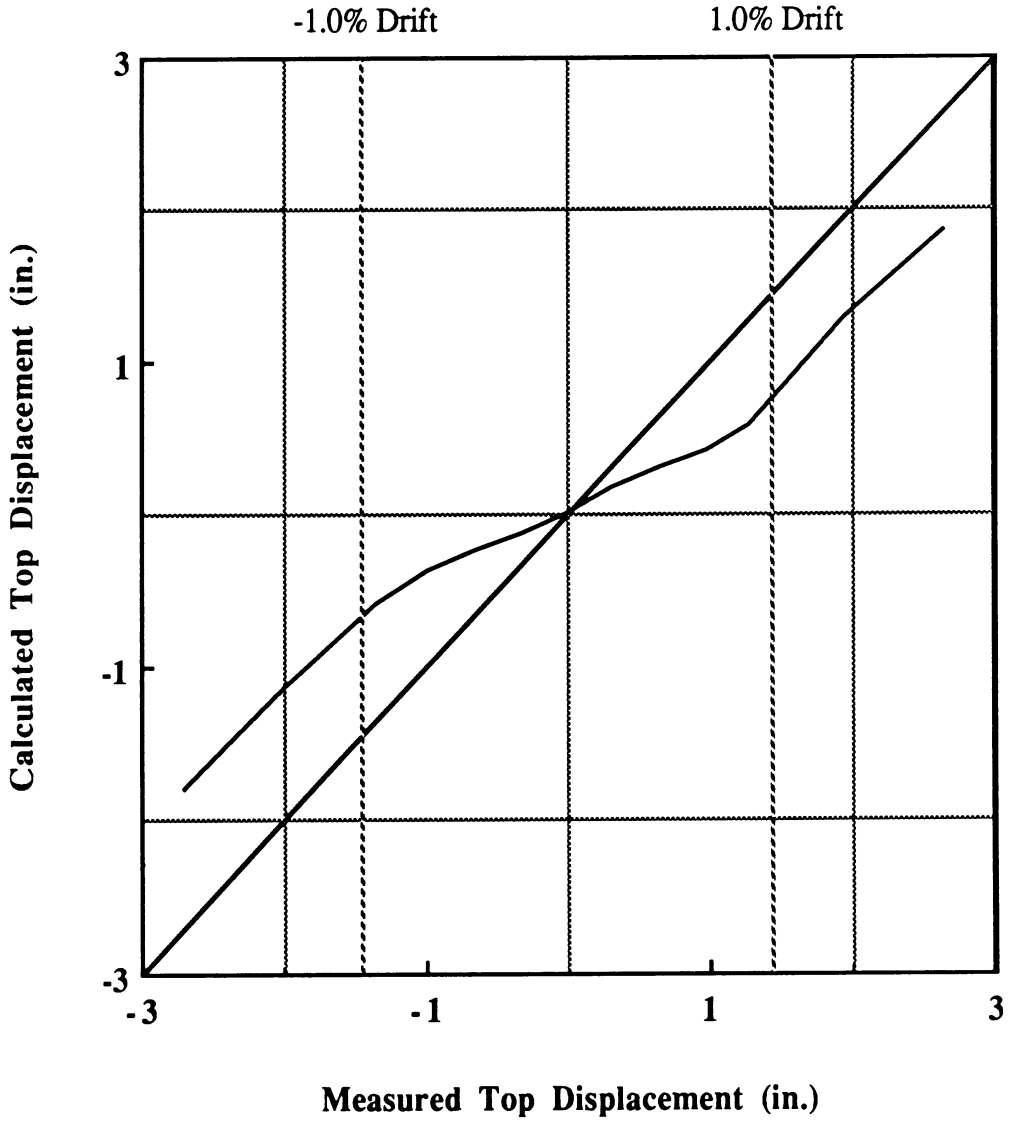

Fig. 4.50 : Effect of First Story Rotation of Wall W-2 on Top Displacement.

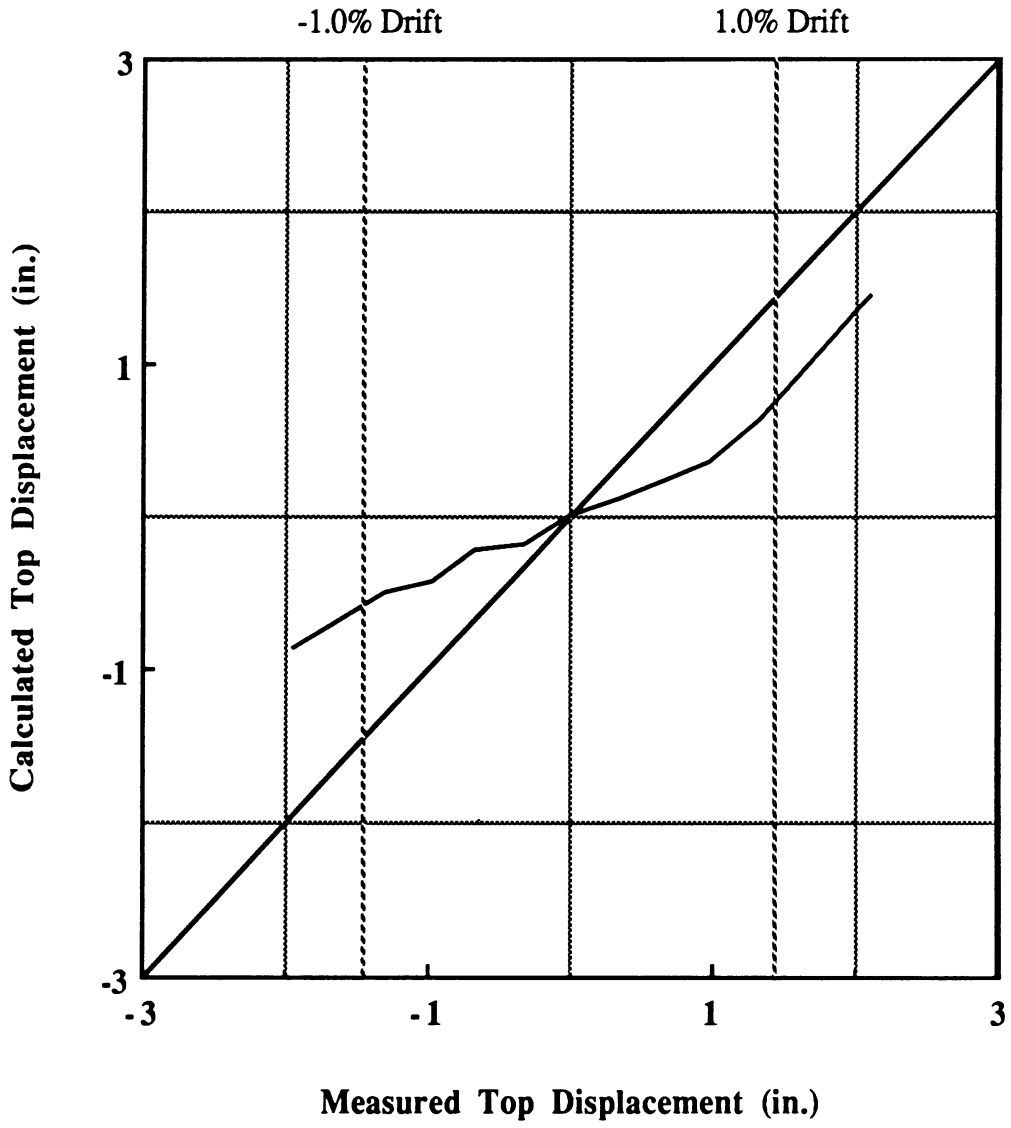

Fig. 4.51 : Effect of First Story Rotation of Wall W-3 on Top Displacement.

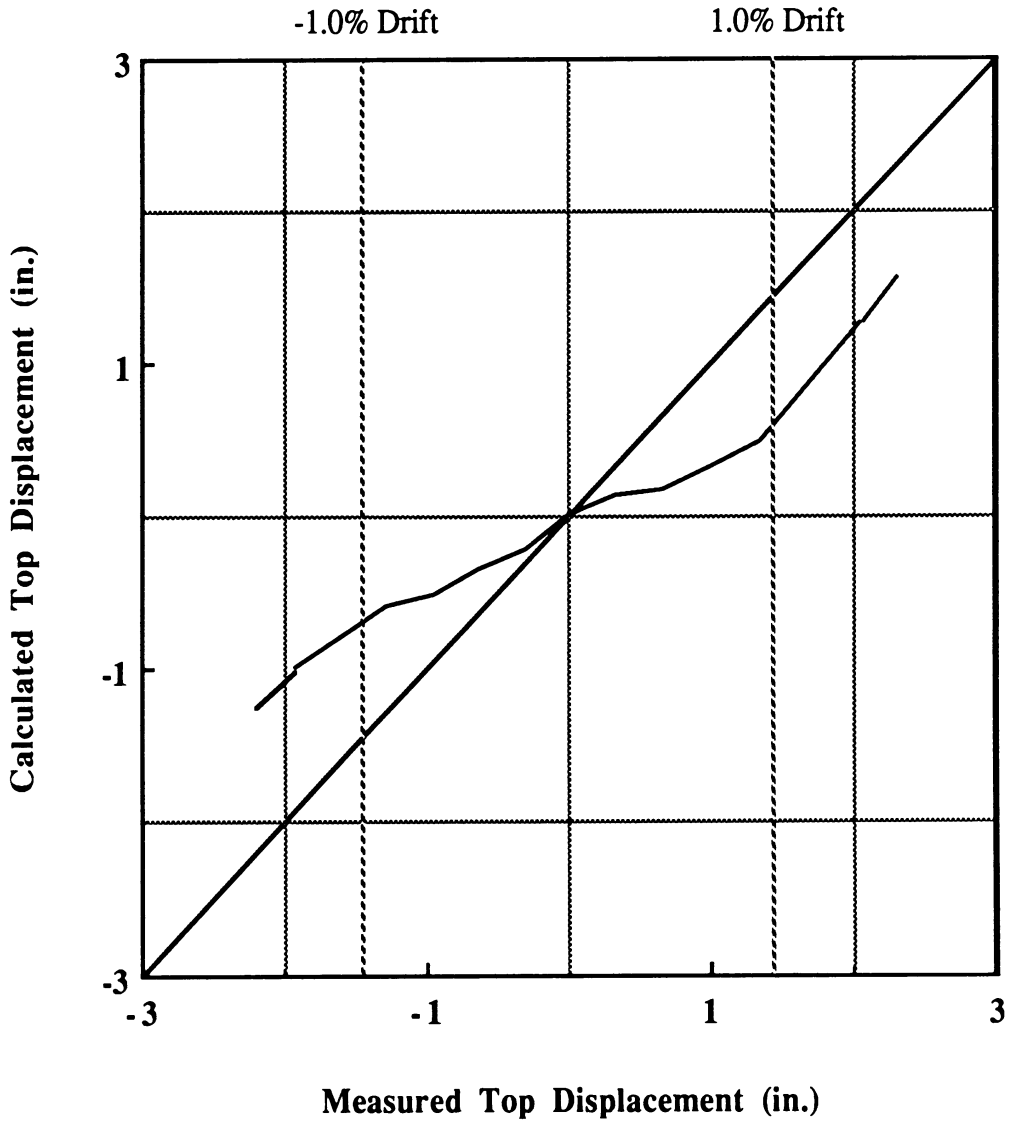

Fig. 4.52 : Effect of First Story Rotation of Wall W-4 on Top Displacement.

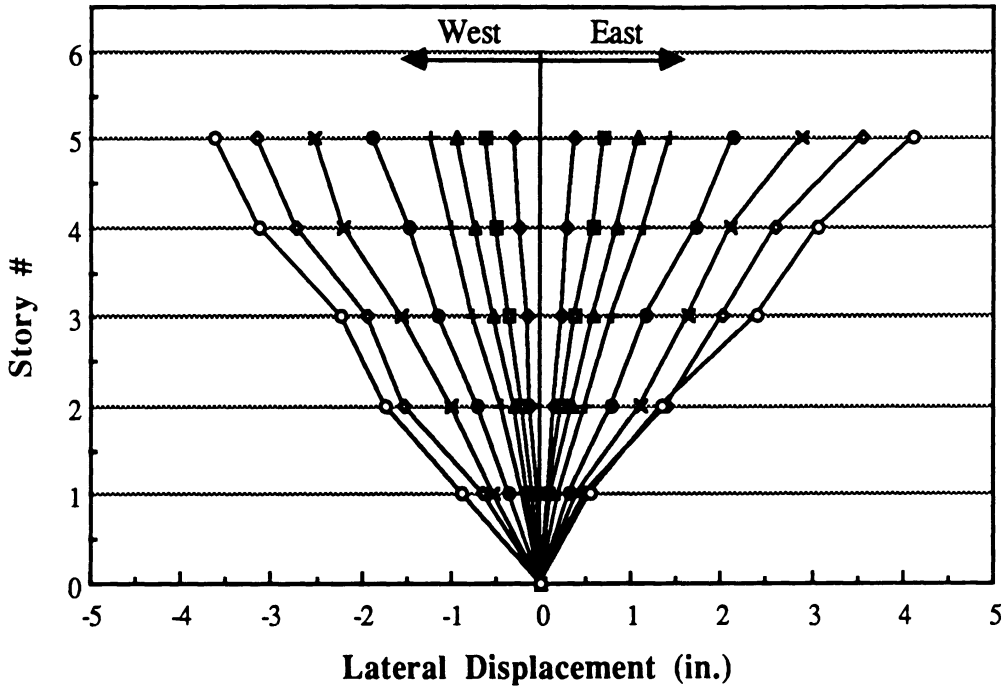

Fig. 4.53 : Displacement Profile along the Wall Height for W-1.

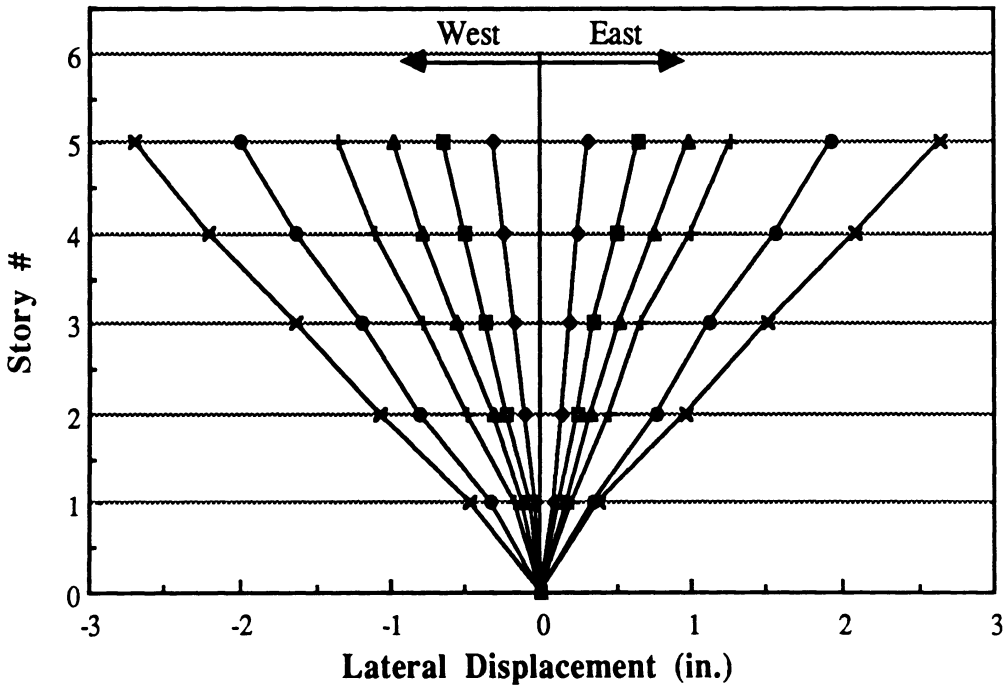

Fig. 4.54 : Displacement Profile along the Wall Height for W-2.

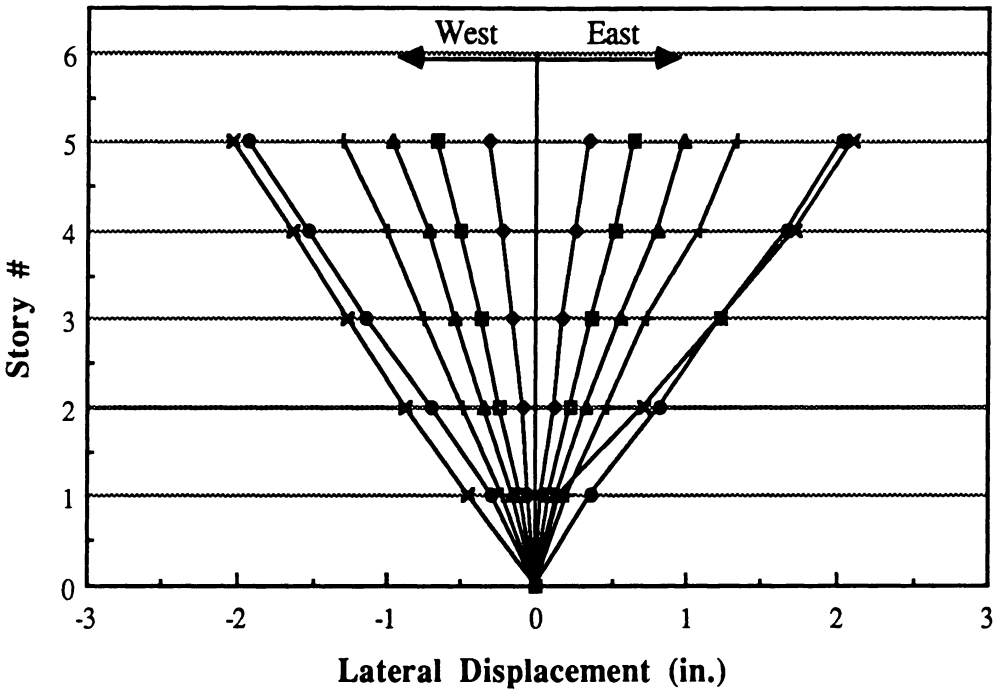

Fig. 4.55 : Displacement Profile along the Wall Height for W-3.

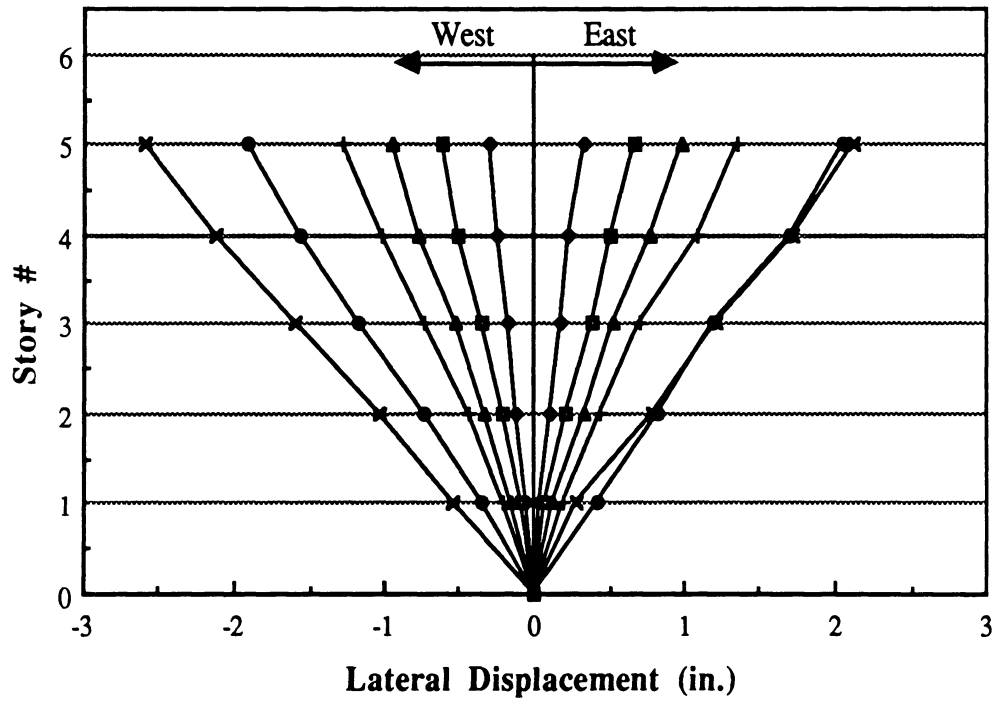

Fig. 4.56 : Displacement Profile along the Wall Height for W-4.

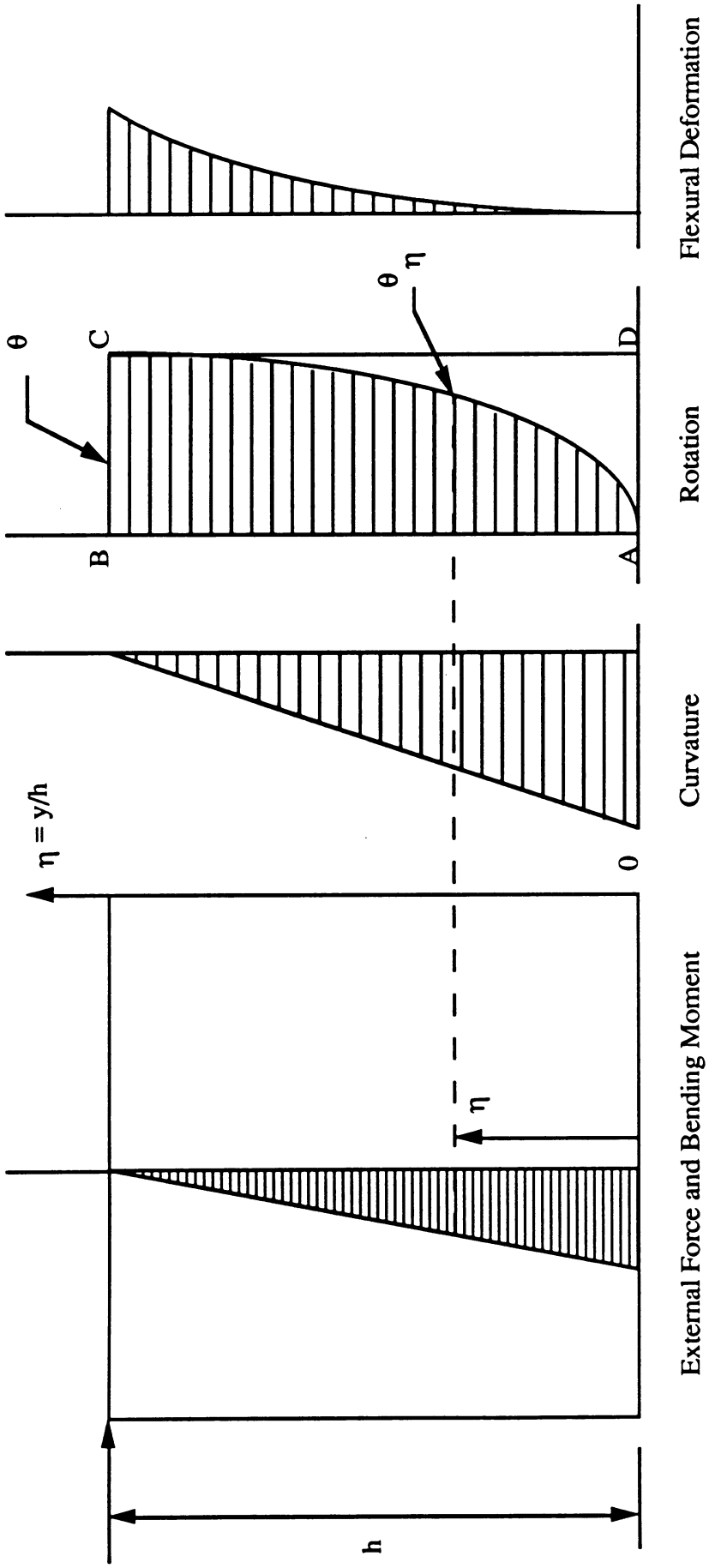

Fig. 4.57(a) : Distribution of Rotation of a Cantilever Type Shear Wall.

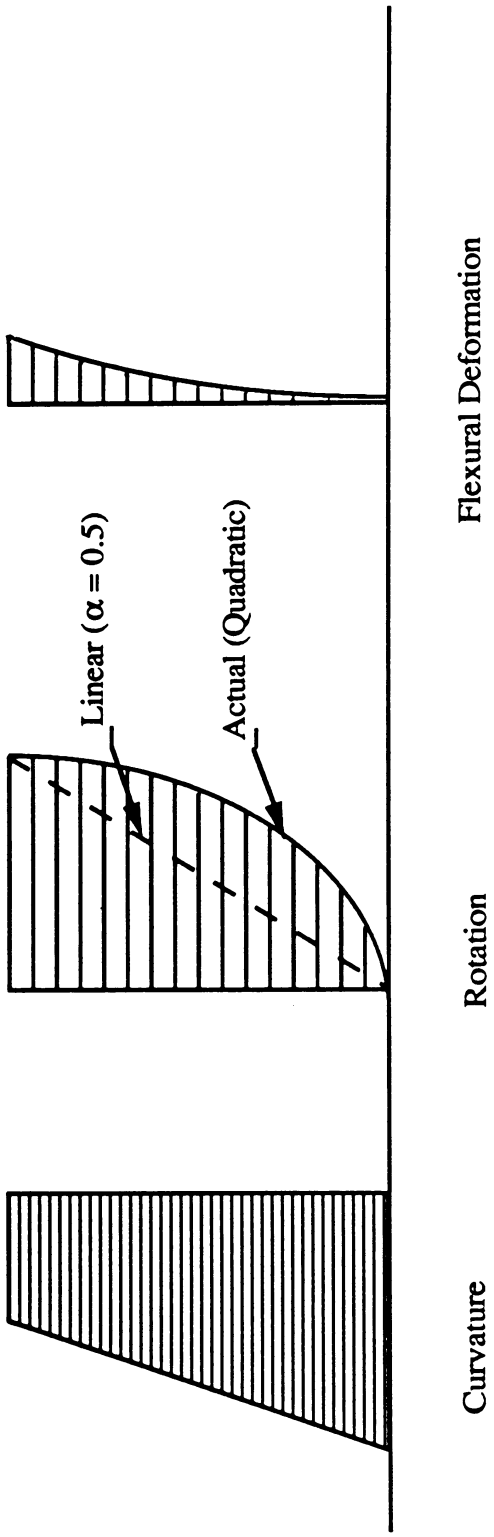

Fig. 4.57(b) : First Story Rotation in a Cantilever Shear Wall.

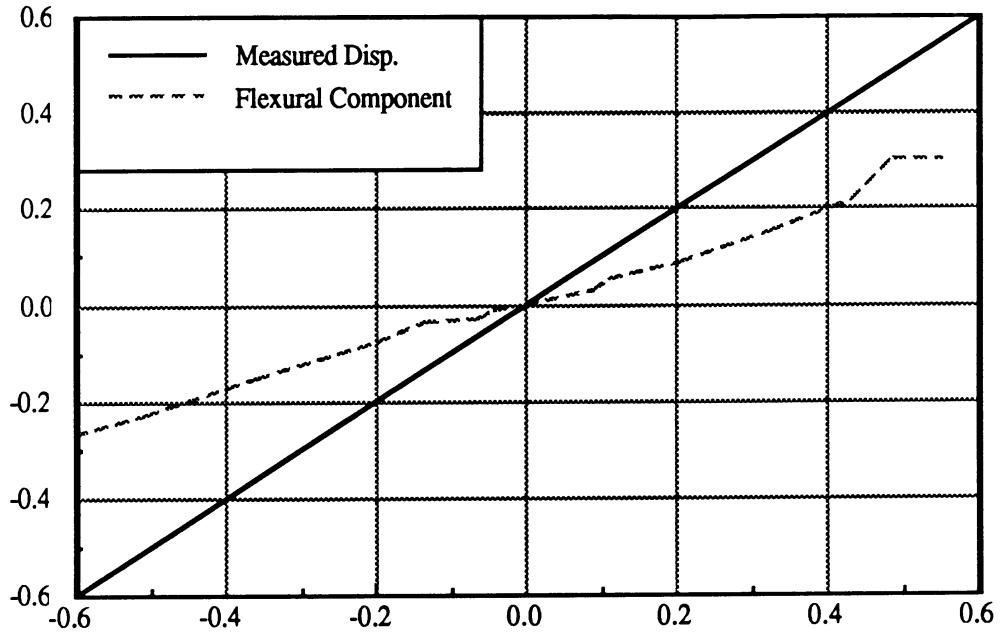

Fig. 4.58 : Flexural and Shear Components of First Story Displacement in W-1.

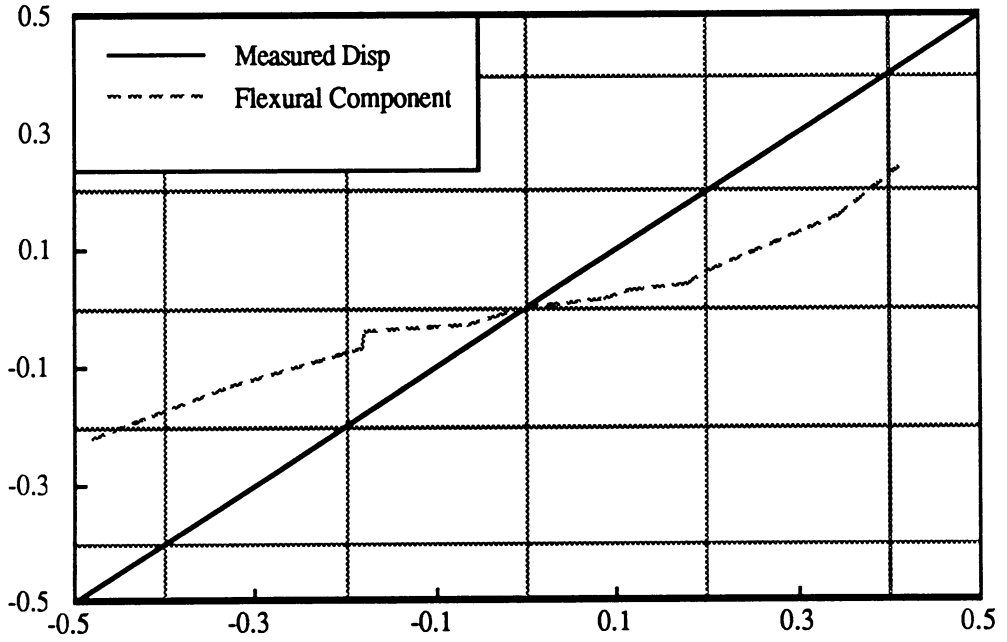

Fig. 4.59 : Flexural and Shear Components of First Story Displacement in W-2.

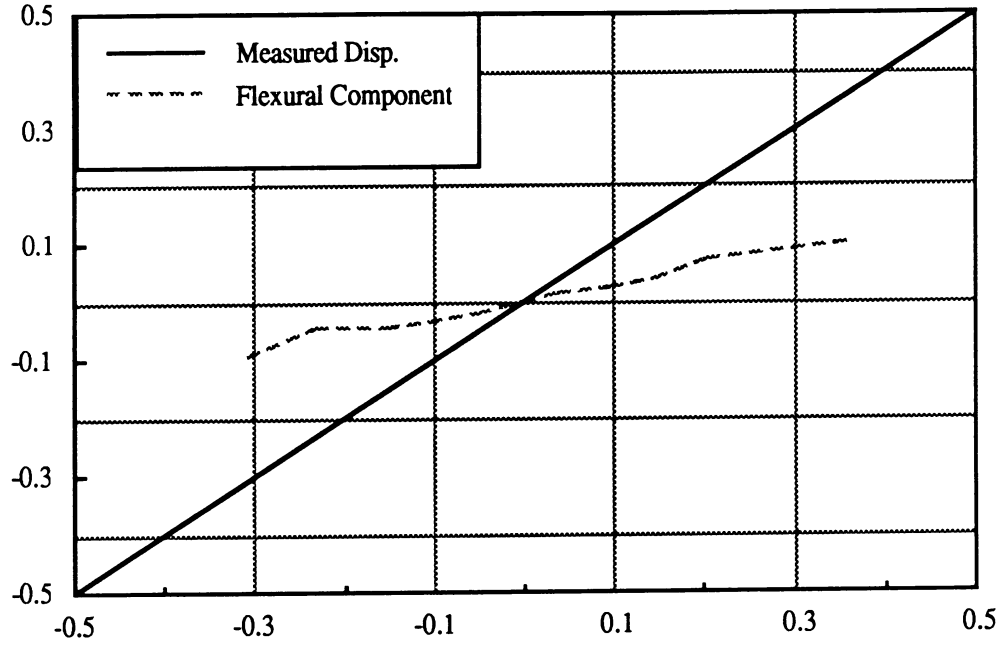

Fig. 4.60 : Flexural and Shear Components of First Story Displacement in W-3.

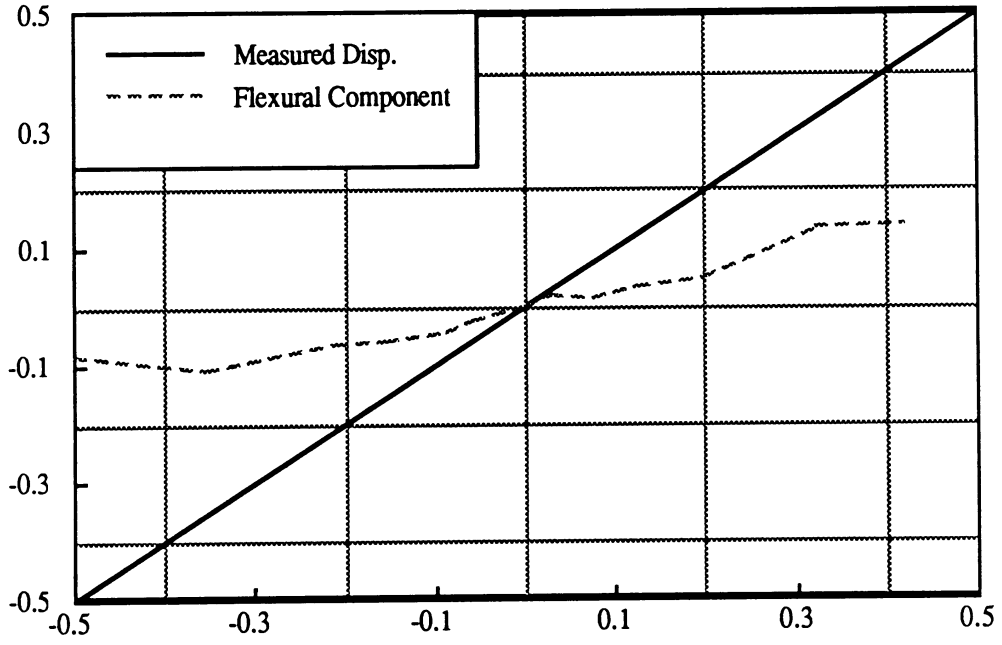

Fig. 4.61 : Flexural and Shear Components of First Story Displacement in W-4.

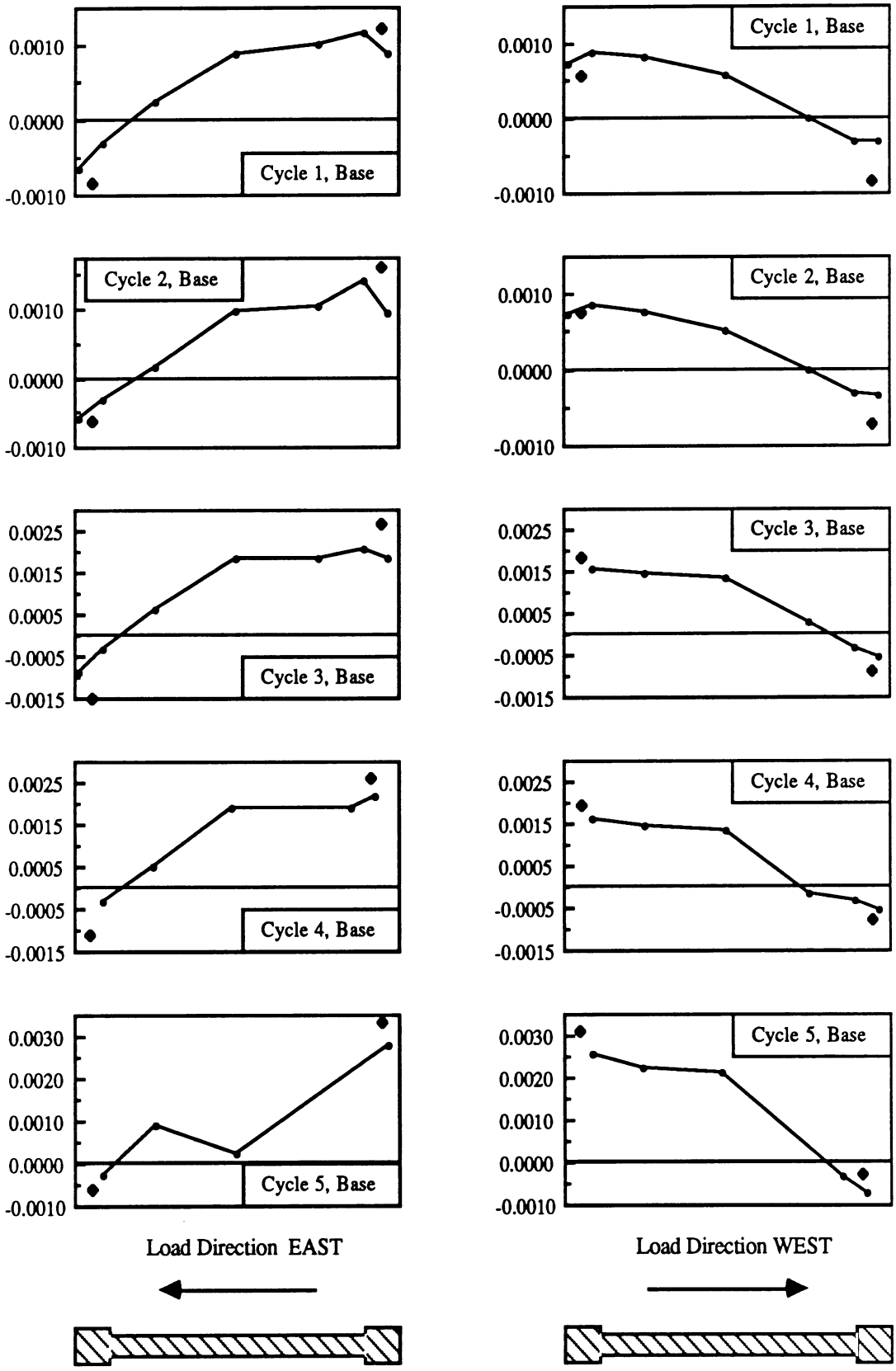

Fig. 4.62 : Strain Profiles for Wall W-1 at Base.

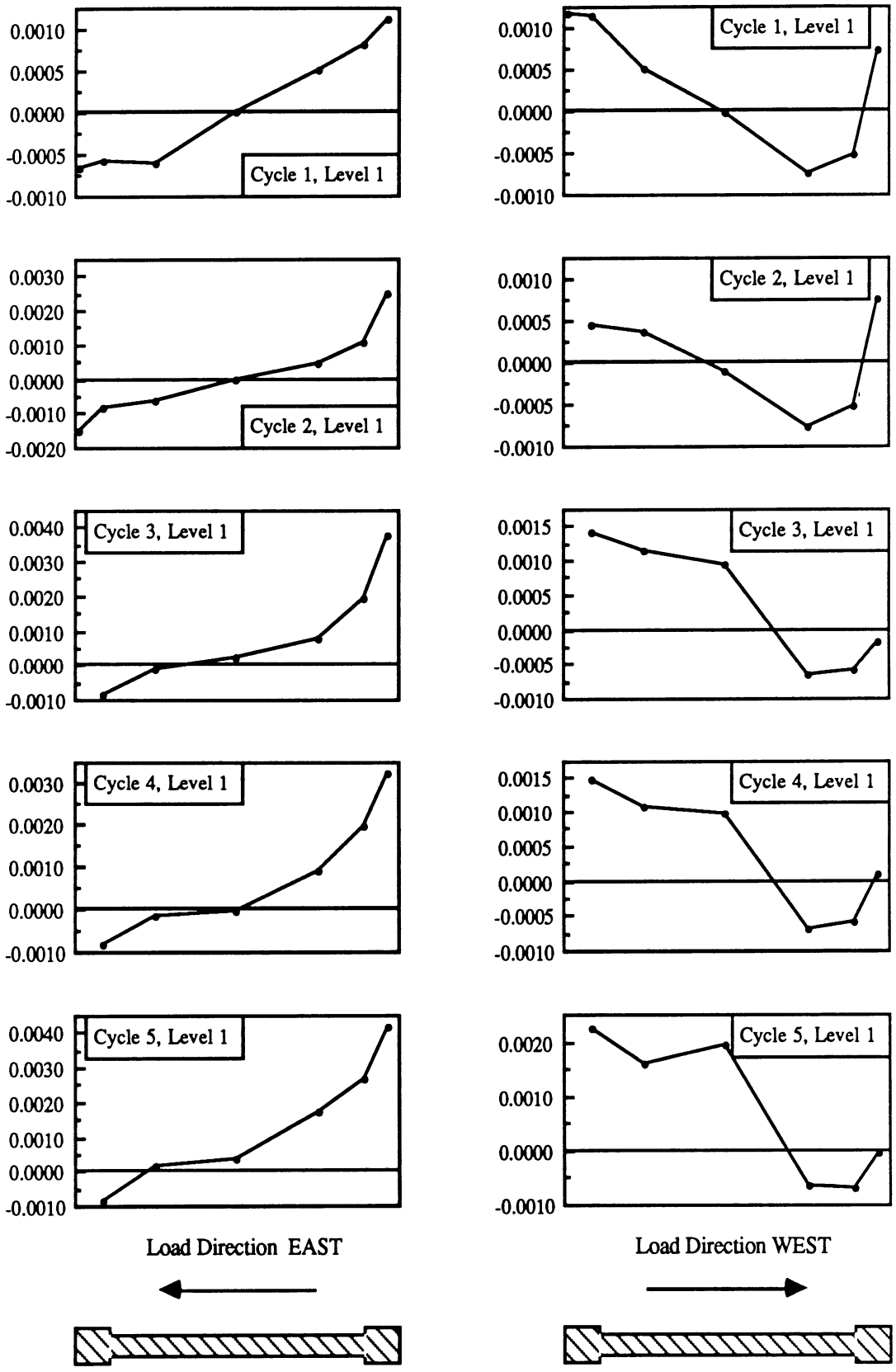

Fig. 4.63 : Strain Profiles for Wall W-1 at Story Level 1.

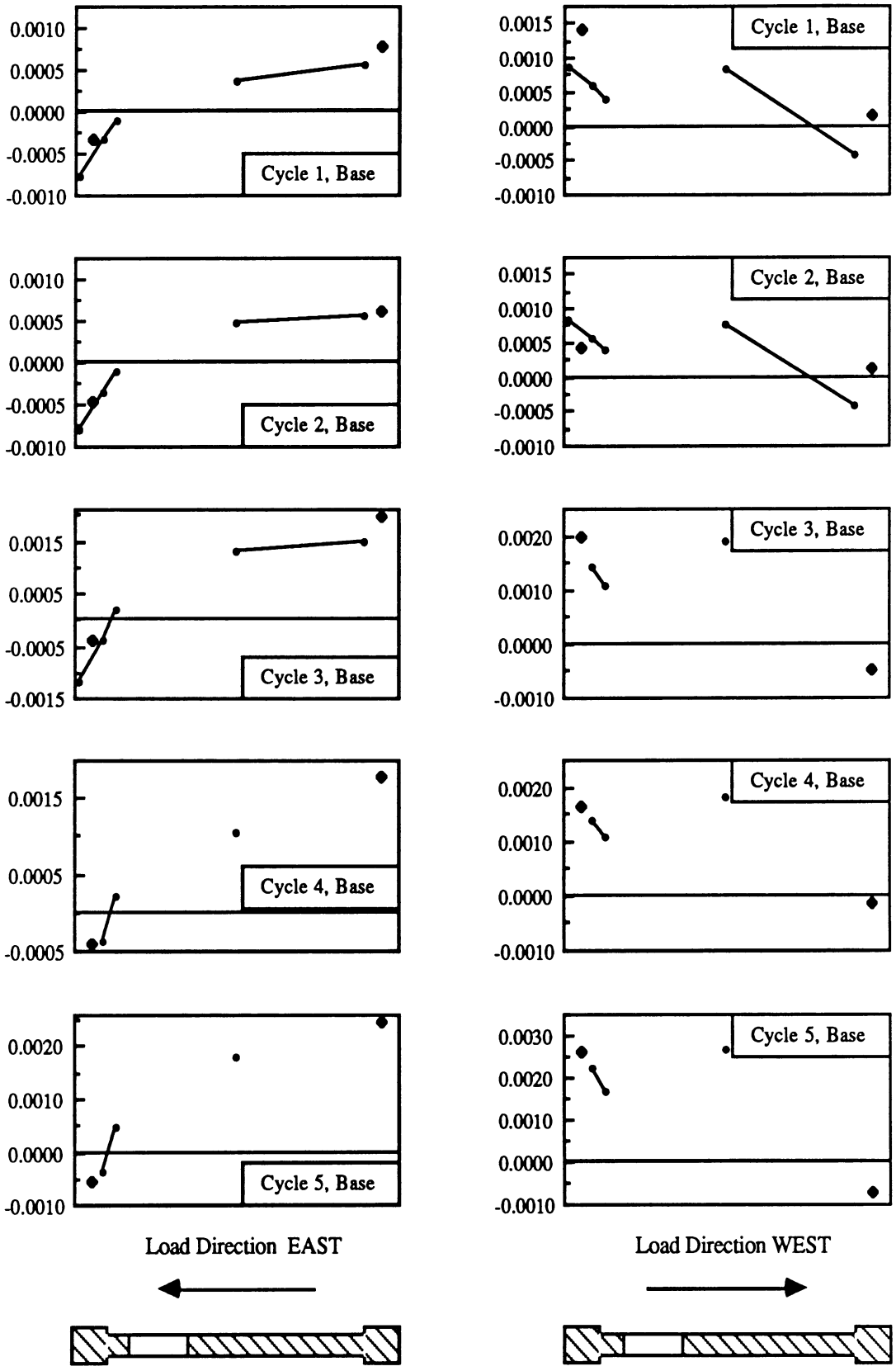

Fig. 4.64 : Strain Profiles for Wall W-2 at Base.

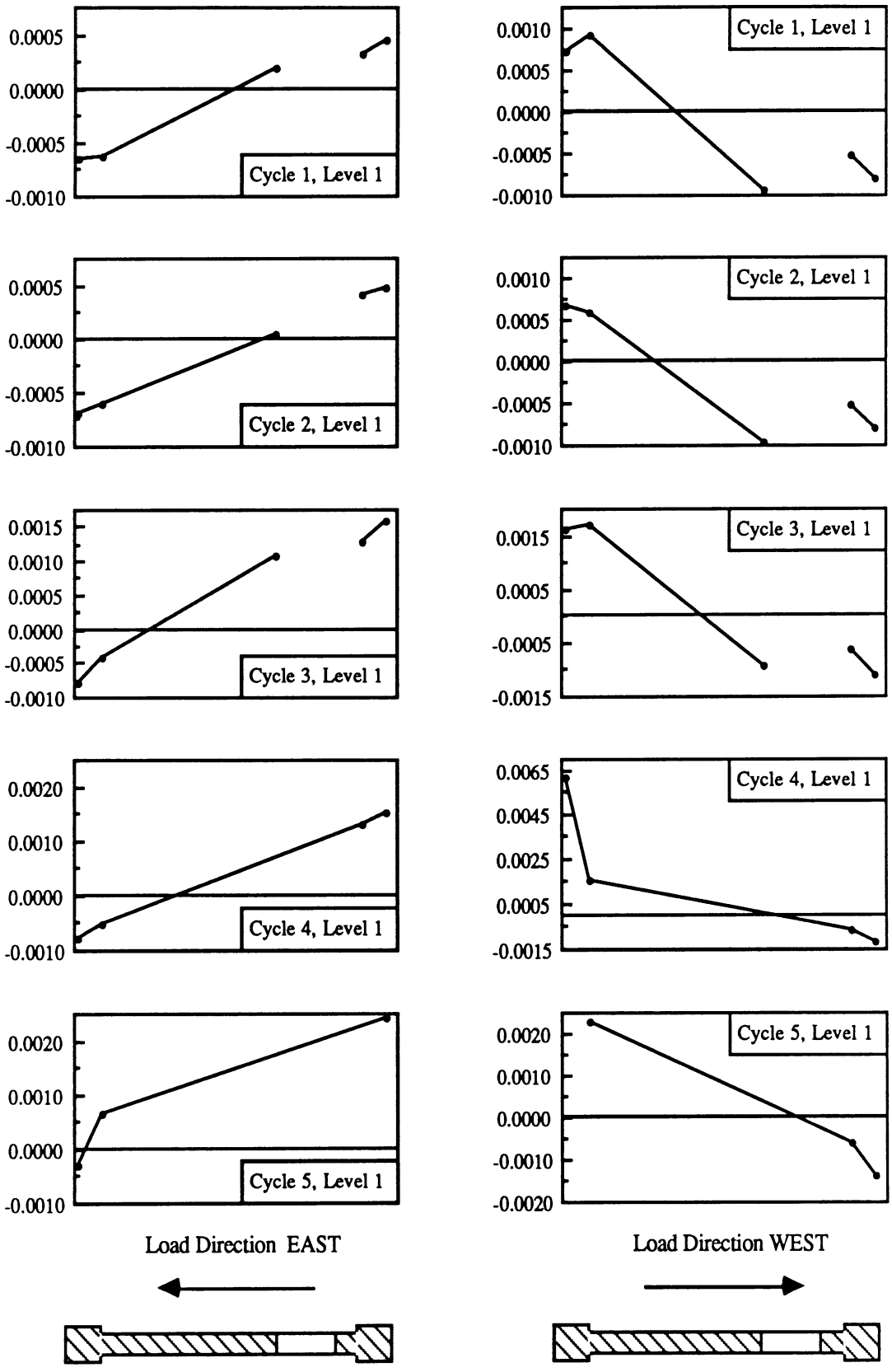

Fig. 4.65 : Strain Profiles for Wall W-2 at Story Level 1.

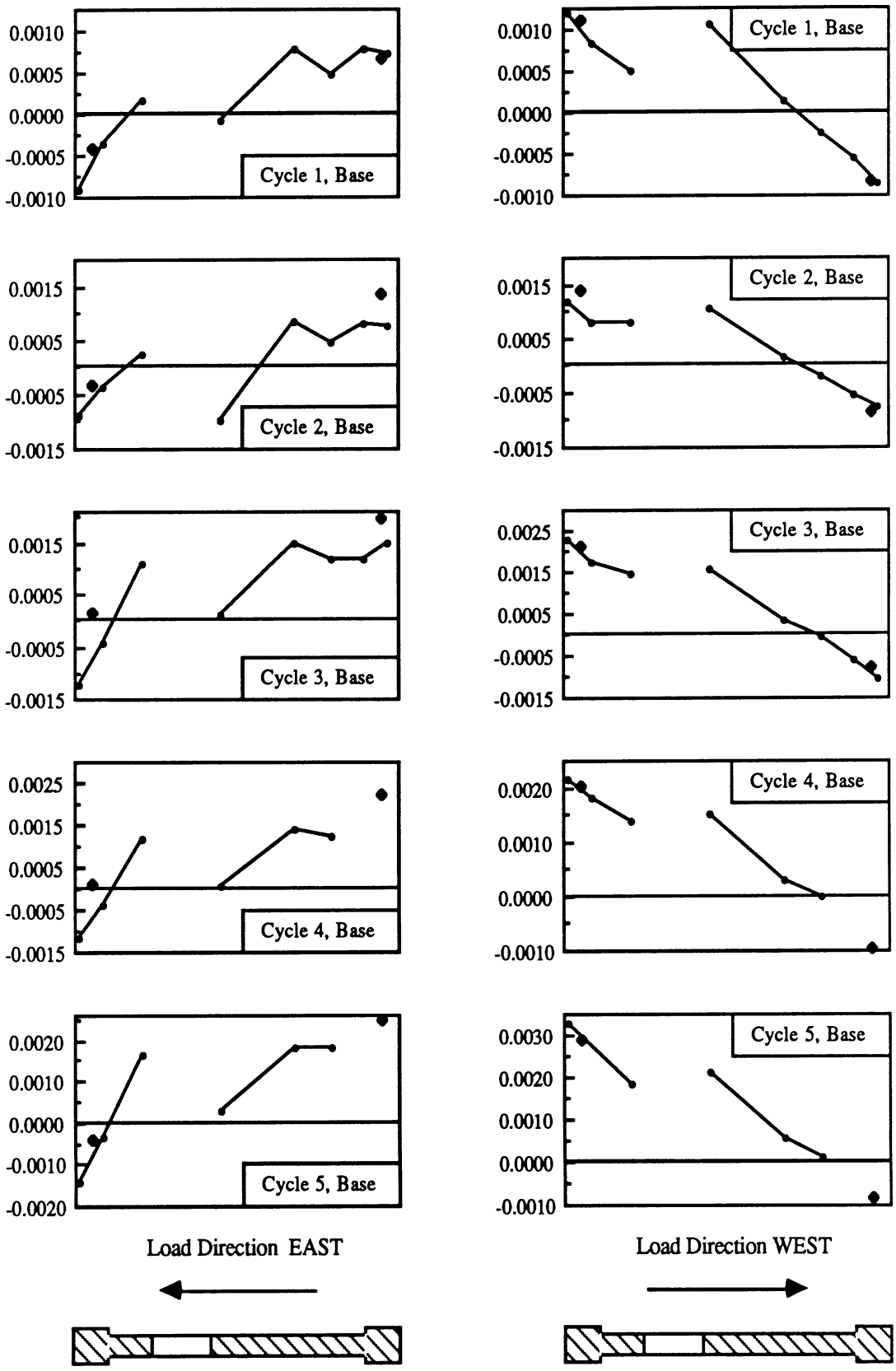

Fig. 4.66 : Strain Profiles for Wall W-3 at Base.

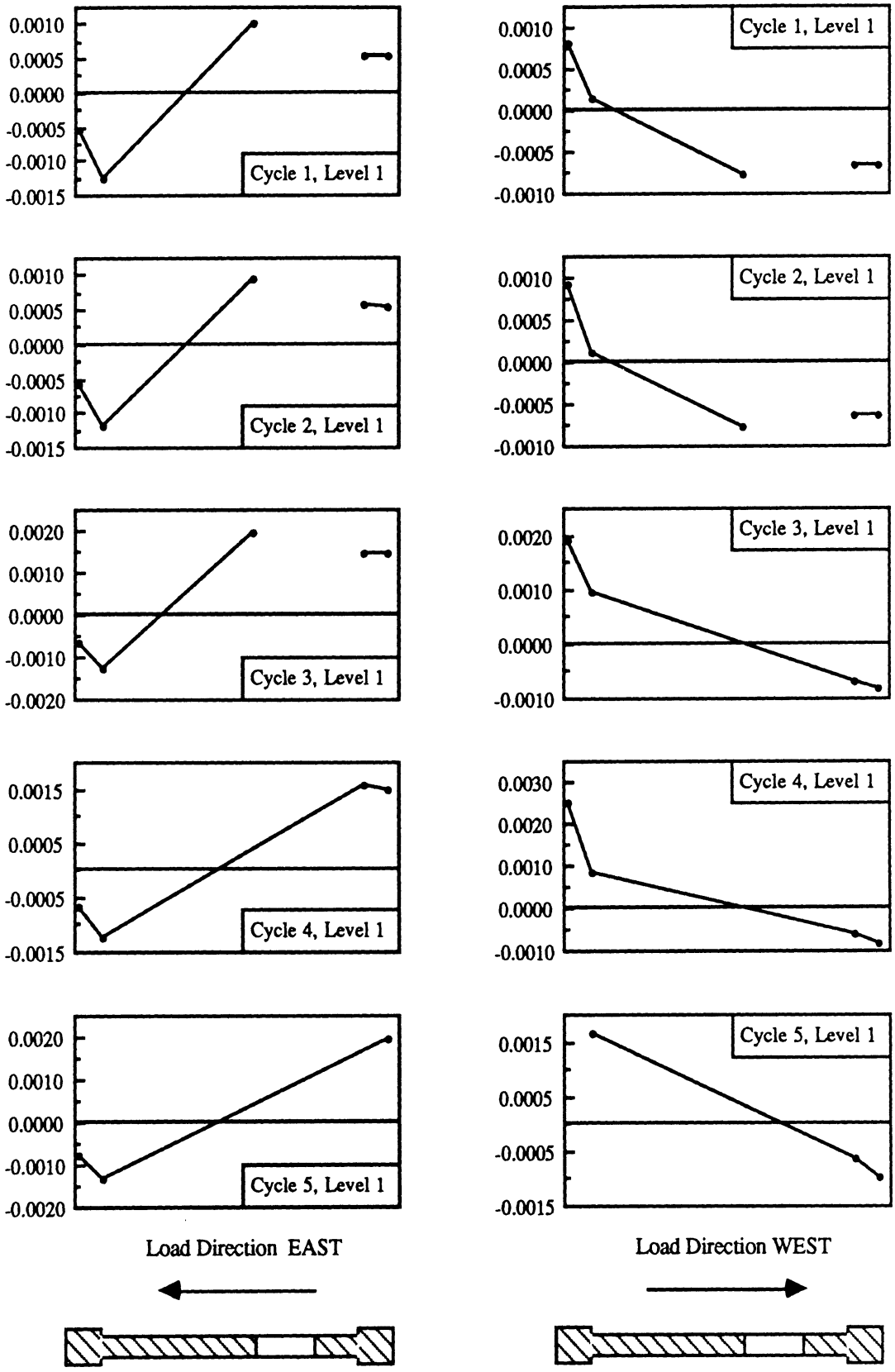

Fig. 4.67 : Strain Profiles for Wall W-3 at Story Level 1.

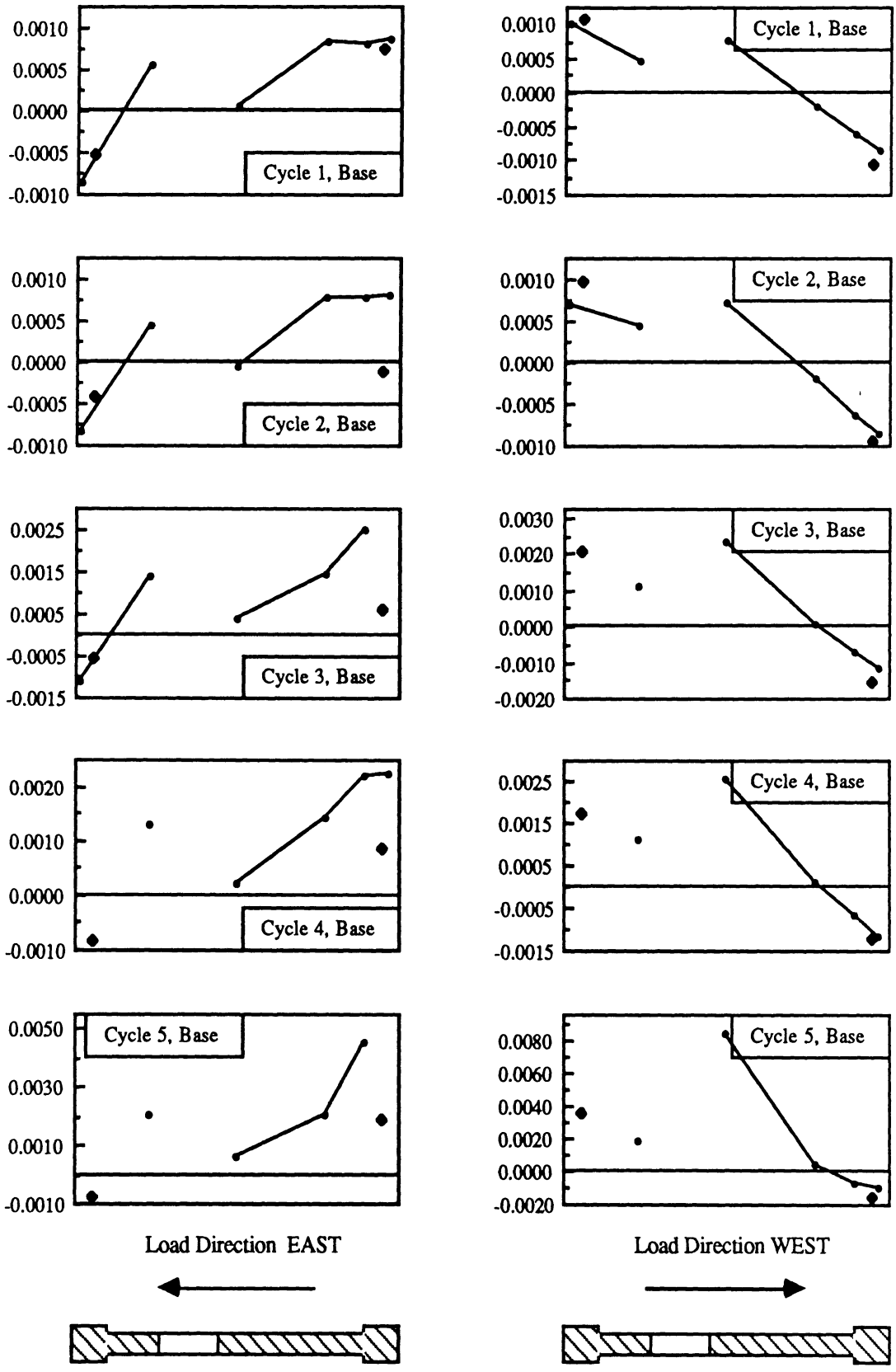

Fig. 4.68 : Strain Profiles for Wall W-4 at Base.

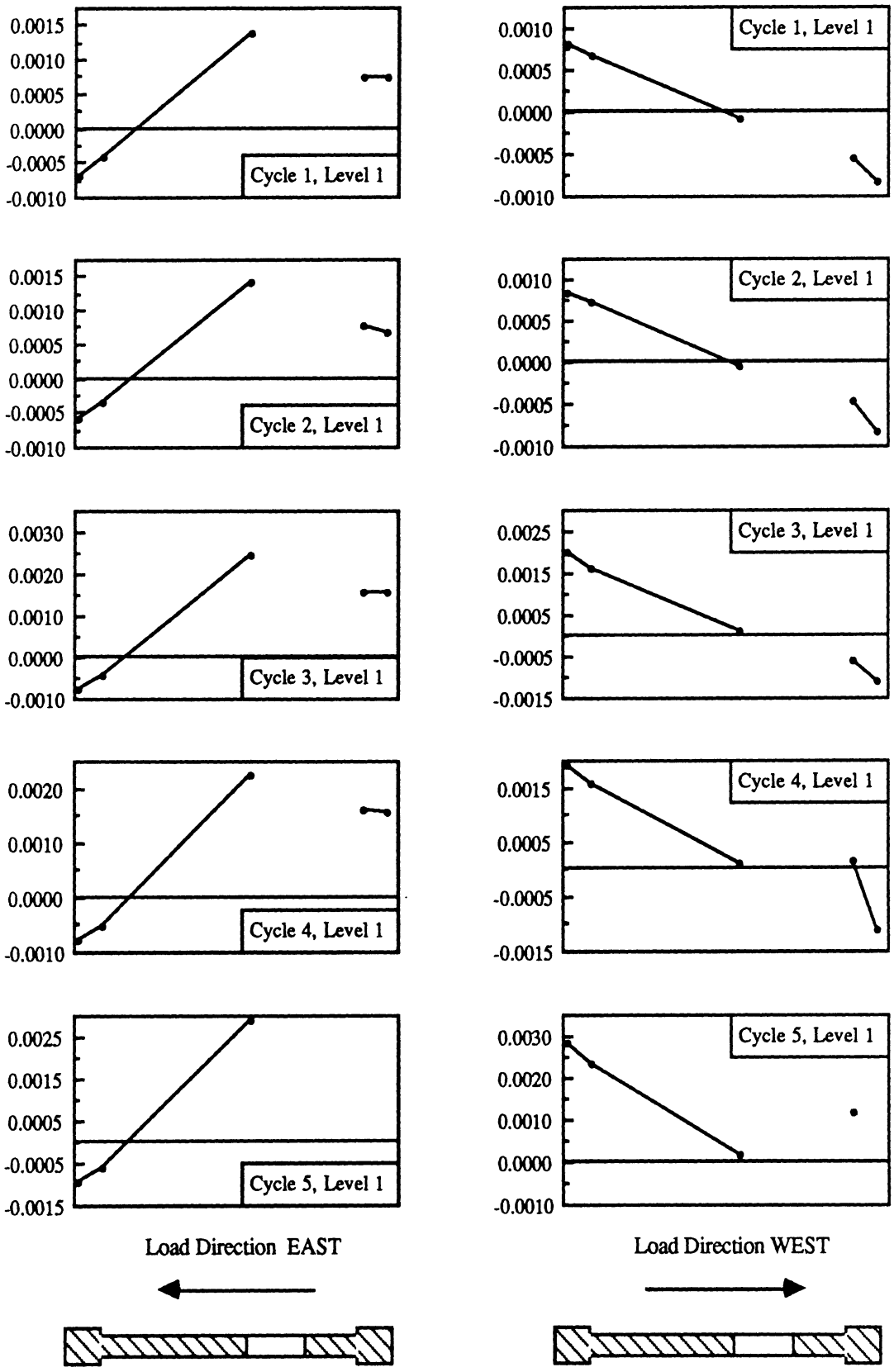

Fig. 4.69 : Strain Profiles for Wall W-4 at Story Level 1.

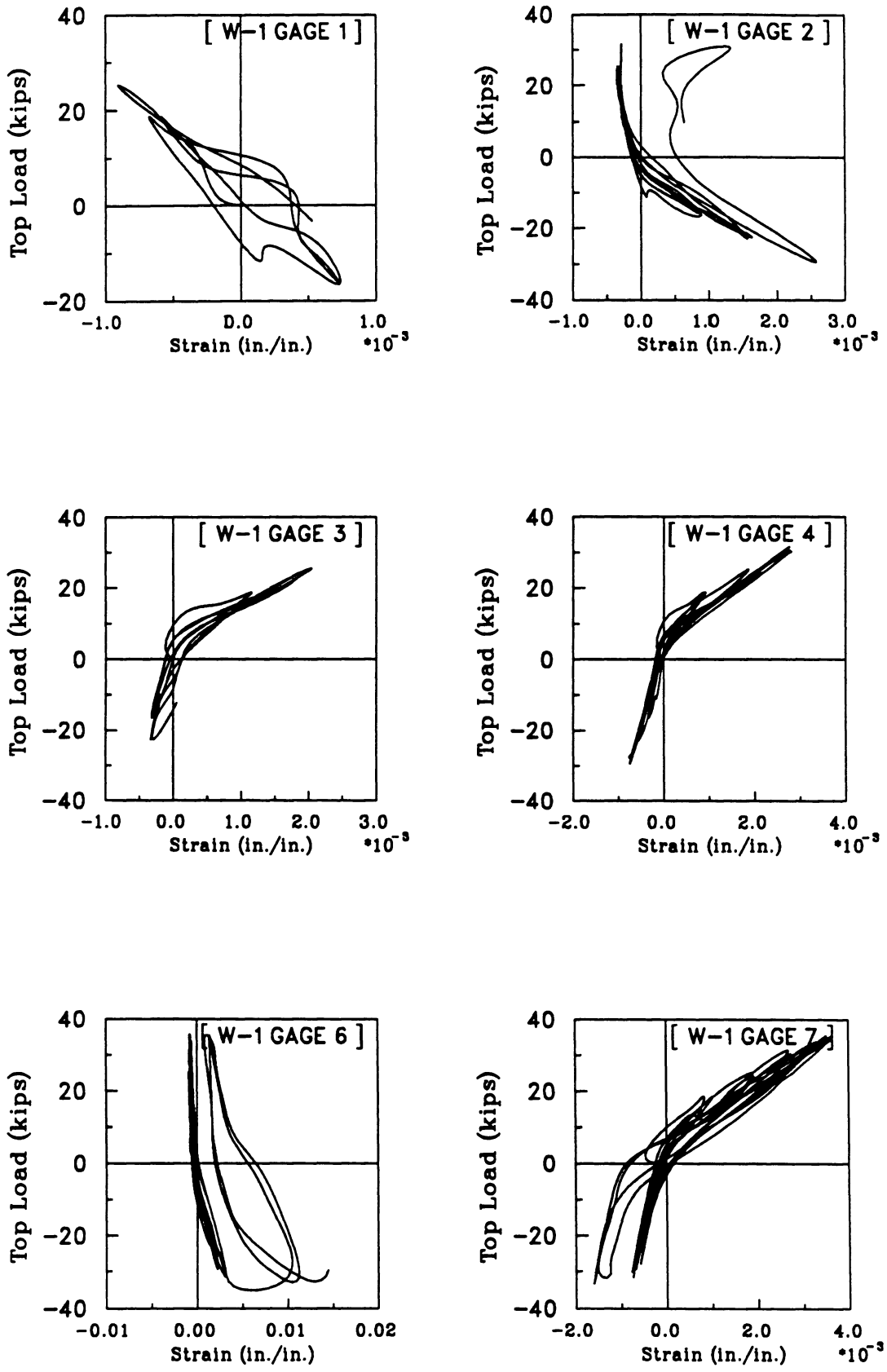

Fig. 4.70(a) : Strain Histories for Gages 1, 2, 3, 4, 6 and 7 in Wall W-1.

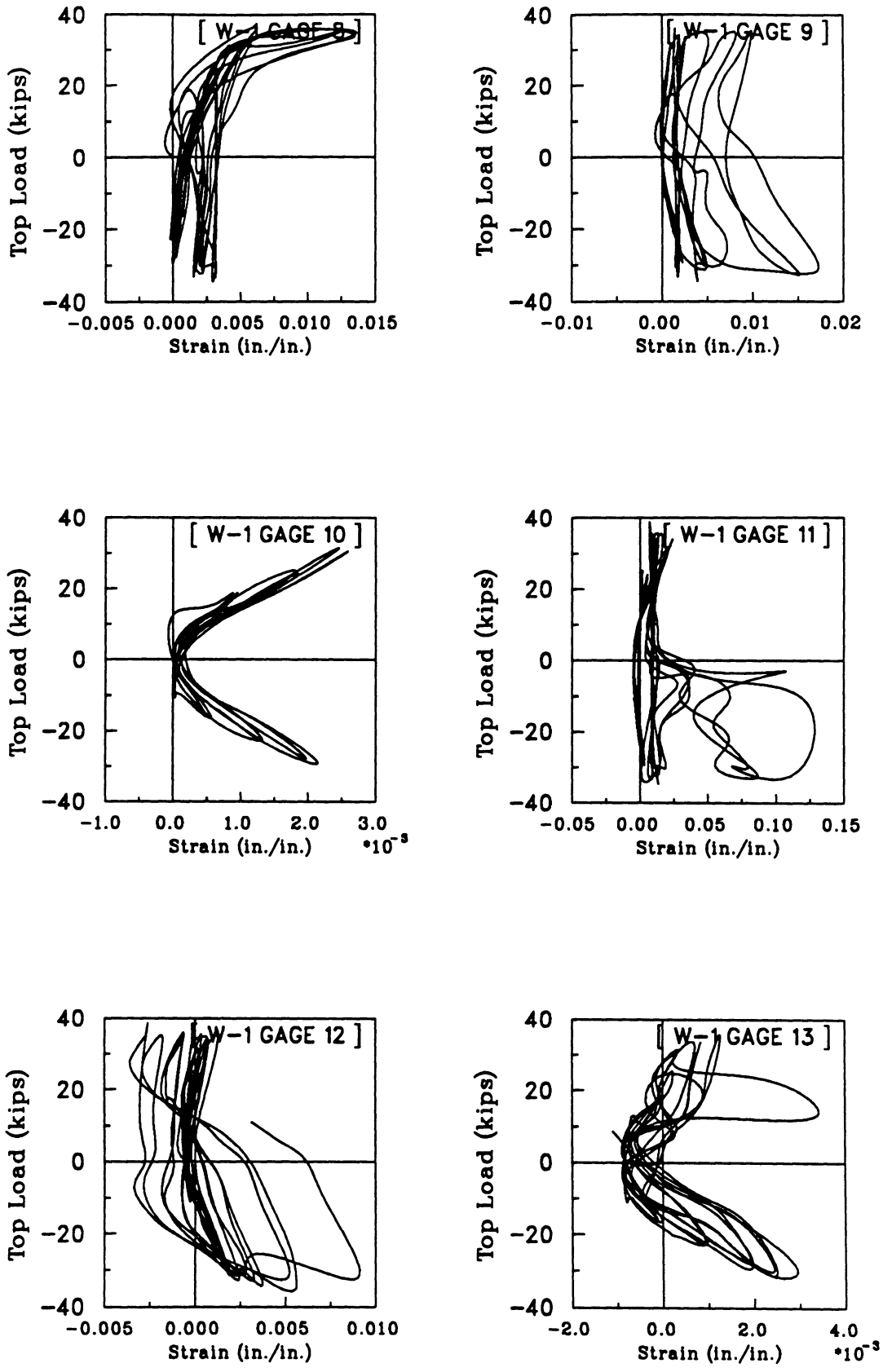

Fig. 4.70(b) : Strain Histories for Gages 8, 9, 10, 11, 12 and 13 in Wall W-1.

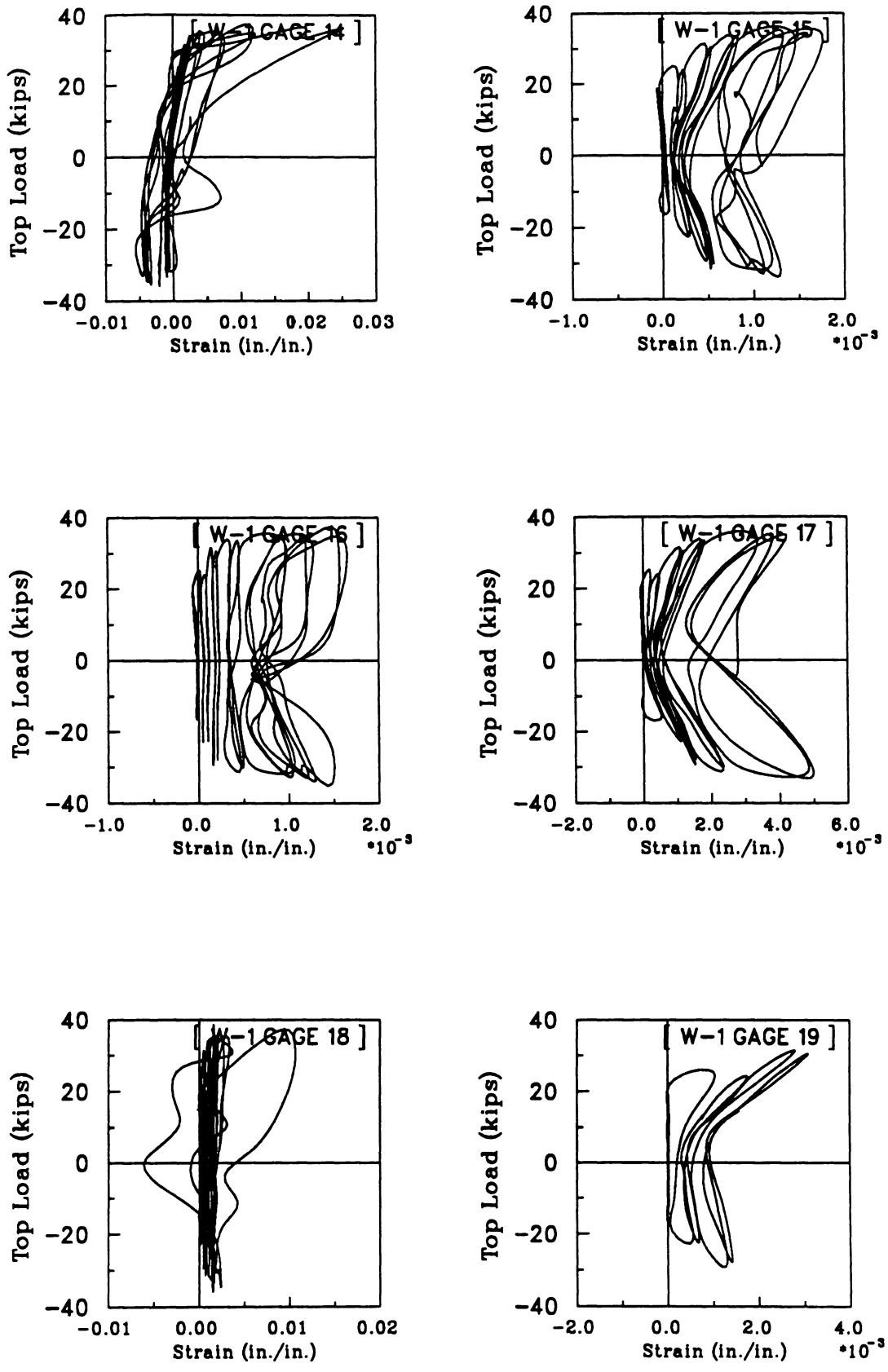

Fig. 4.70(c) : Strain Histories for Gages 14, 15, 16, 17, 18 and 19 in Wall W-1.

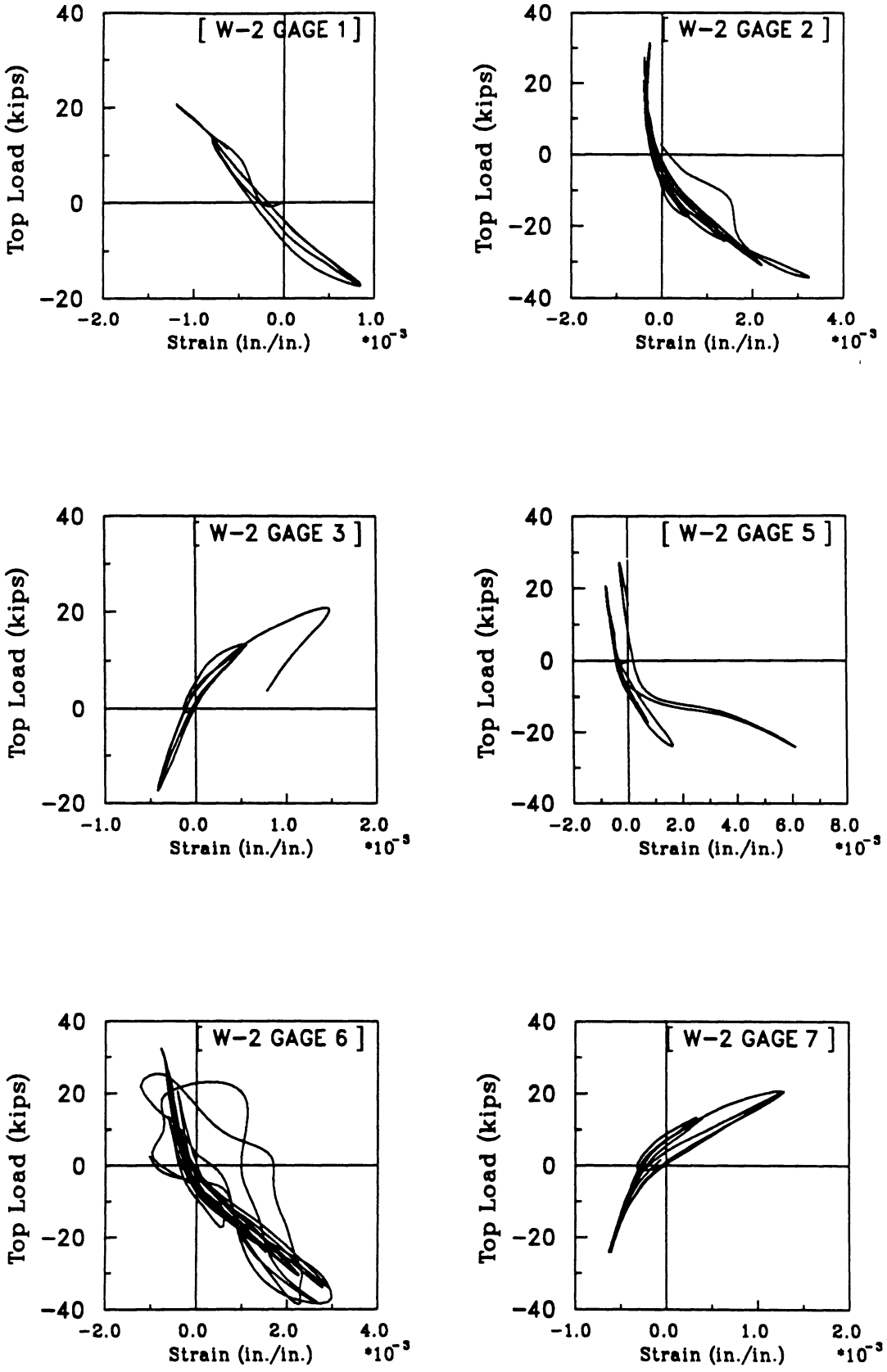

Fig. 4.71(a) : Strain Histories for Gages 1, 2, 3, 5, 6 and 7 in Wall W-2.

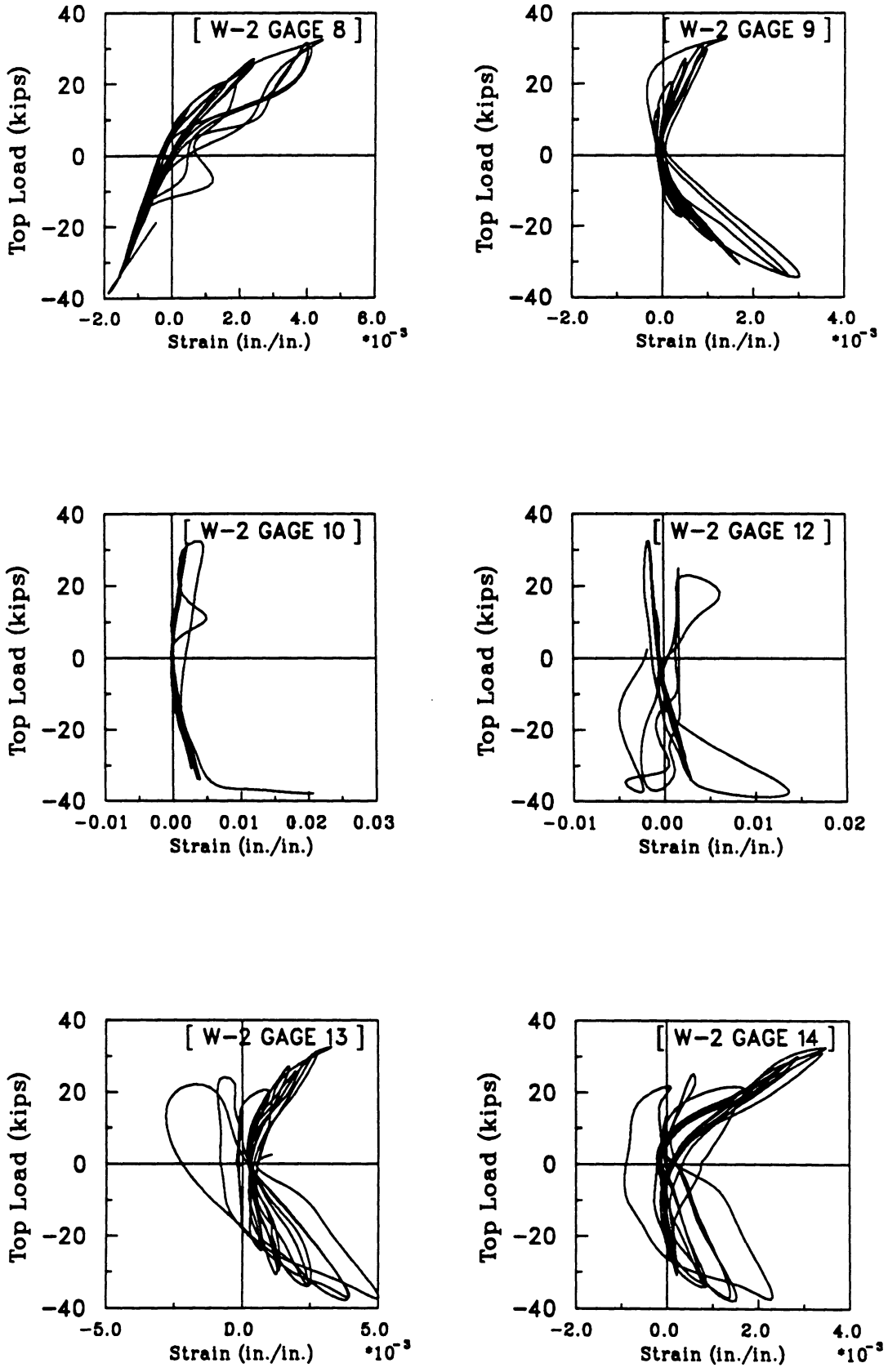

Fig. 4.70(b) : Strain Histories for Gages 8, 9, 10, 12, 13 and 14 in Wall W-2.

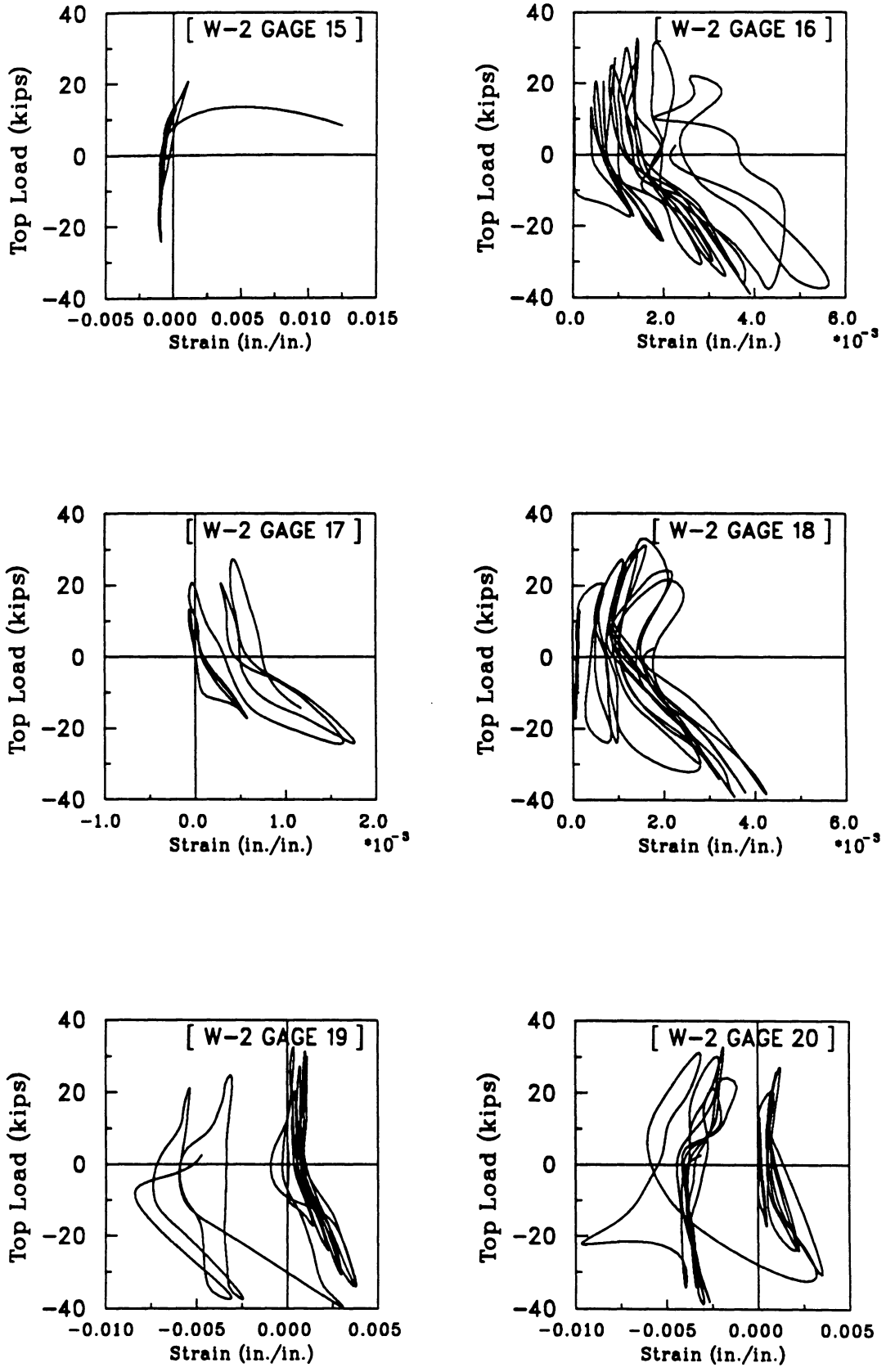

Fig. 4.71(c) : Strain Histories for Gages 15, 16, 17, 18, 19 and 20 in Wall W-2.

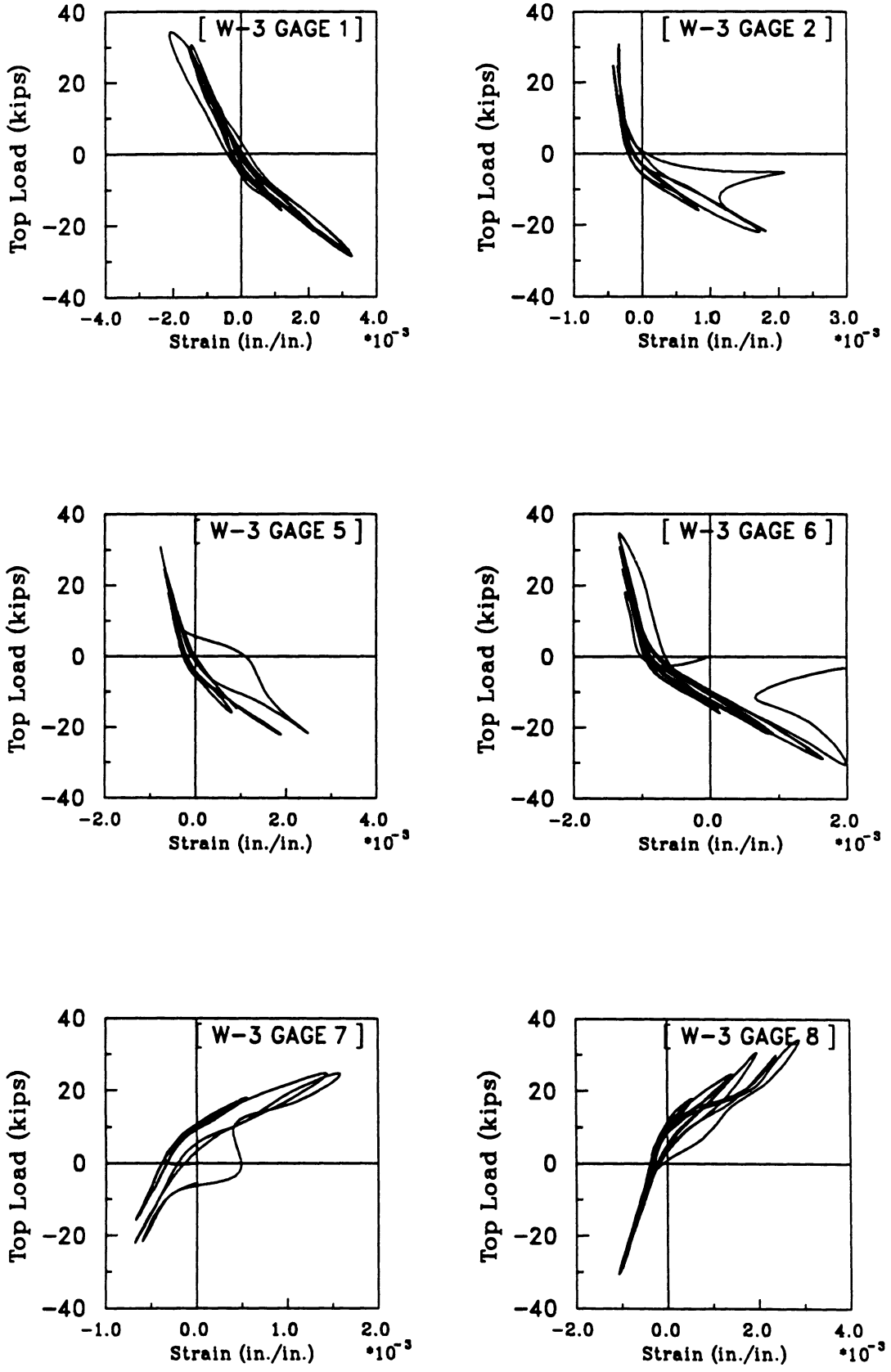

Fig. 4.72(a) : Strain Histories for Gages 1, 2, 5, 6, 7 and 8 in Wall W-3.

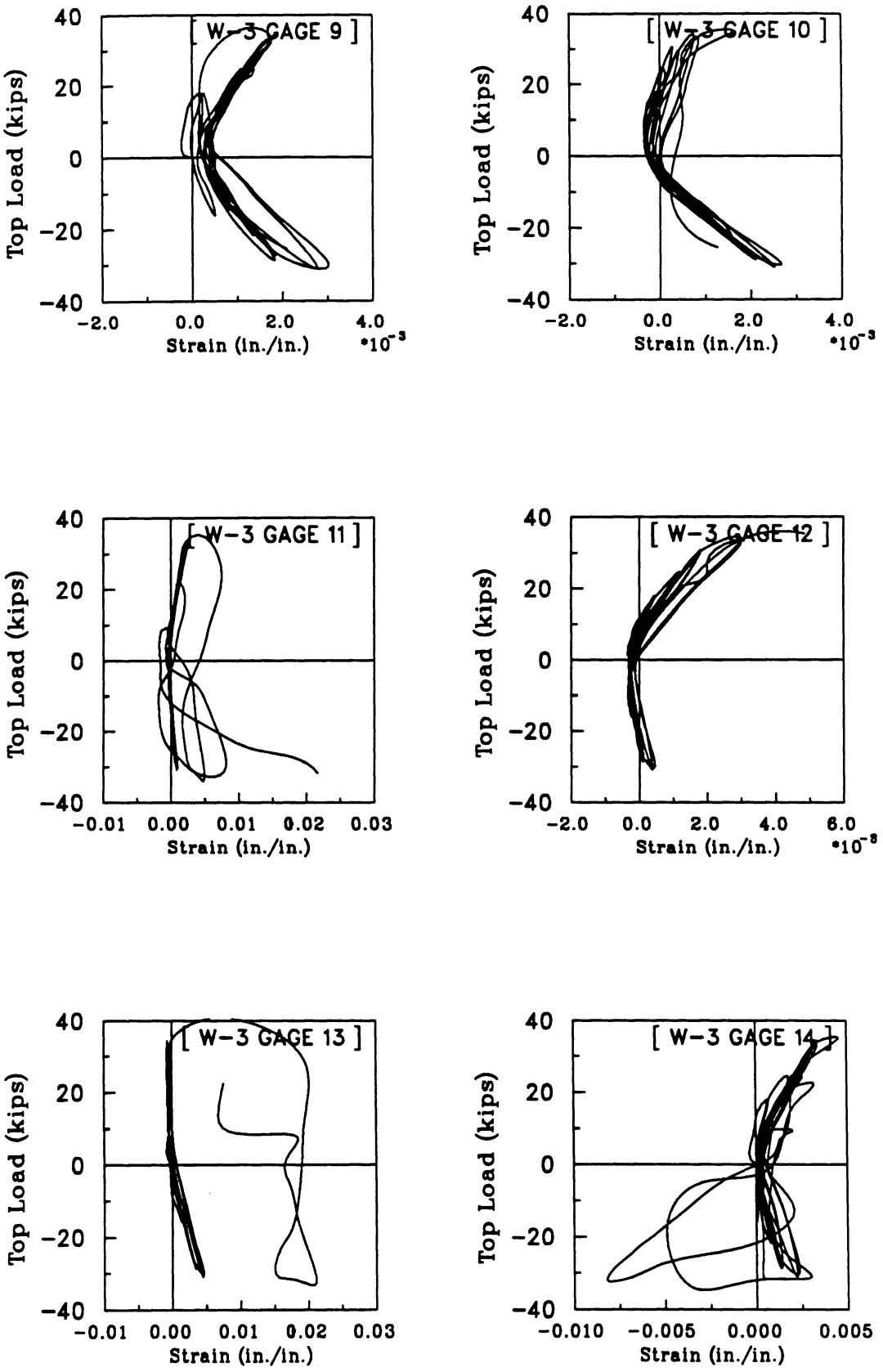

Fig. 4.72(b) : Strain Histories for Gages 9, 10, 11, 12, 13 and 14 in Wall W-3.

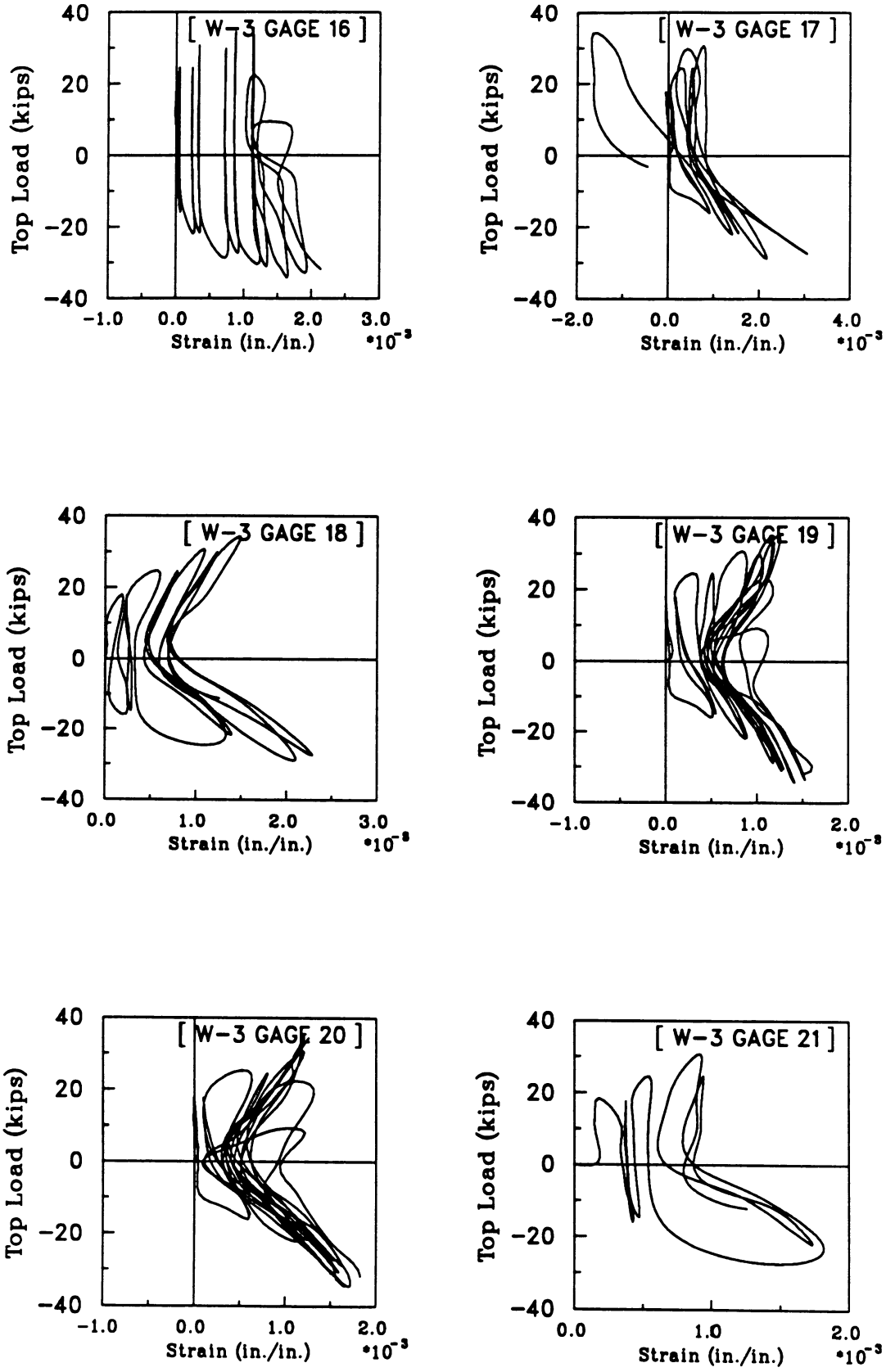

Fig. 4.72(c) : Strain Histories for Gages 16, 17, 18, 19, 20 and 21 in Wall W-3.

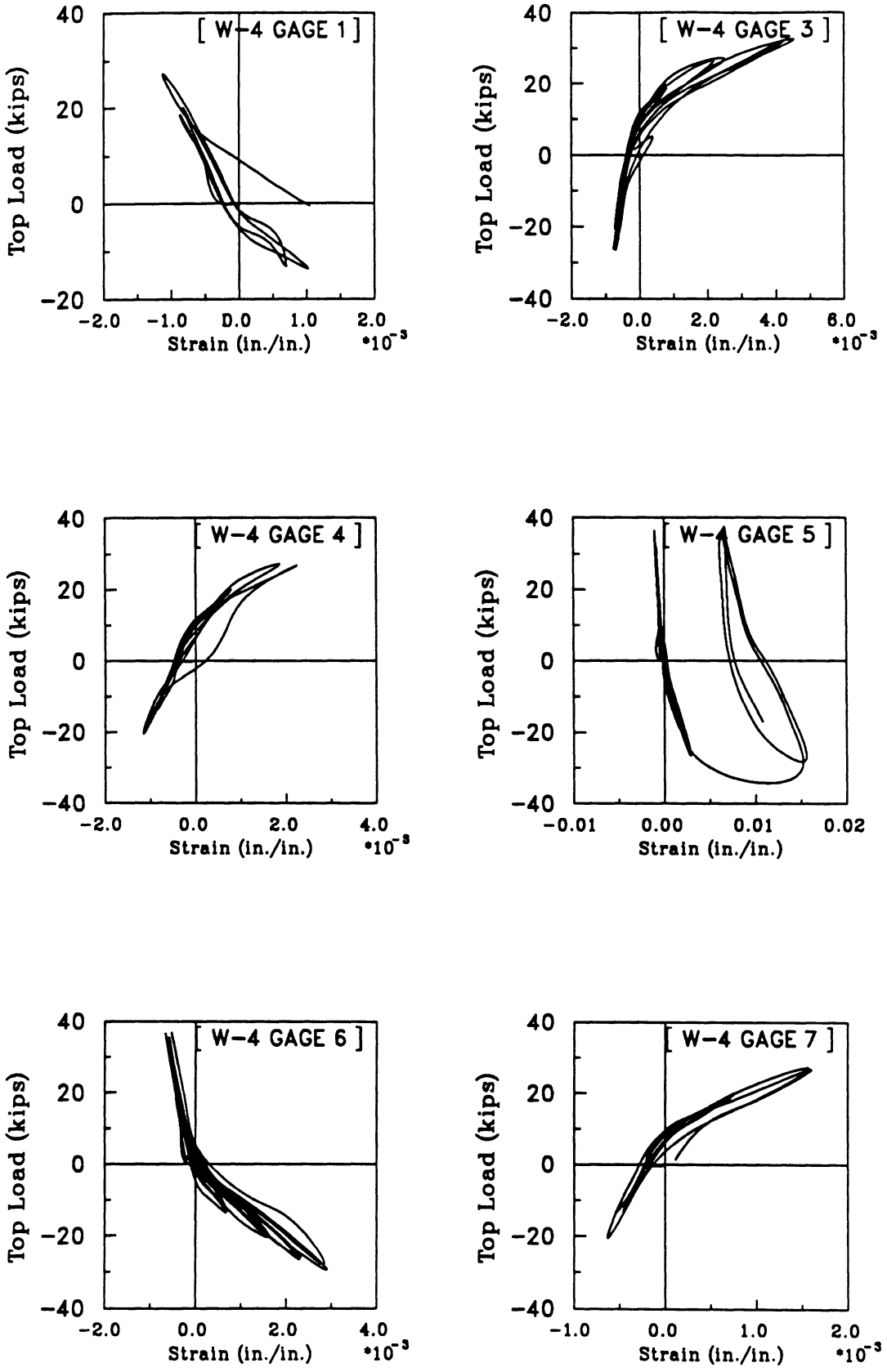

Fig. 4.73(a) : Strain Histories for Gages 1, 3, 4, 5, 6 and 7 in Wall W-4.

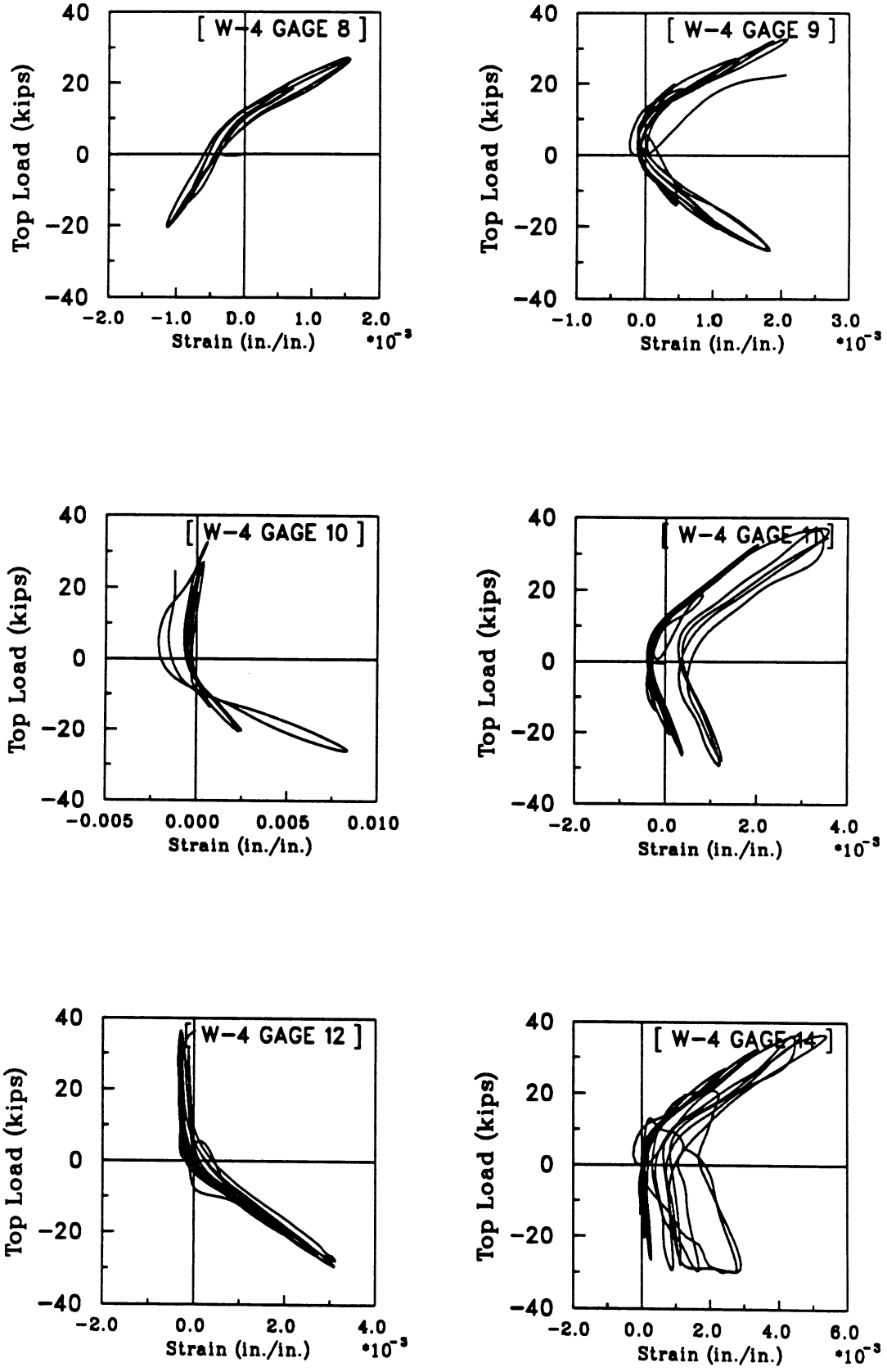

Fig. 4.73(b) : Strain Histories for Gages 8, 9, 10, 11, 12 and 14 in Wall W-4.

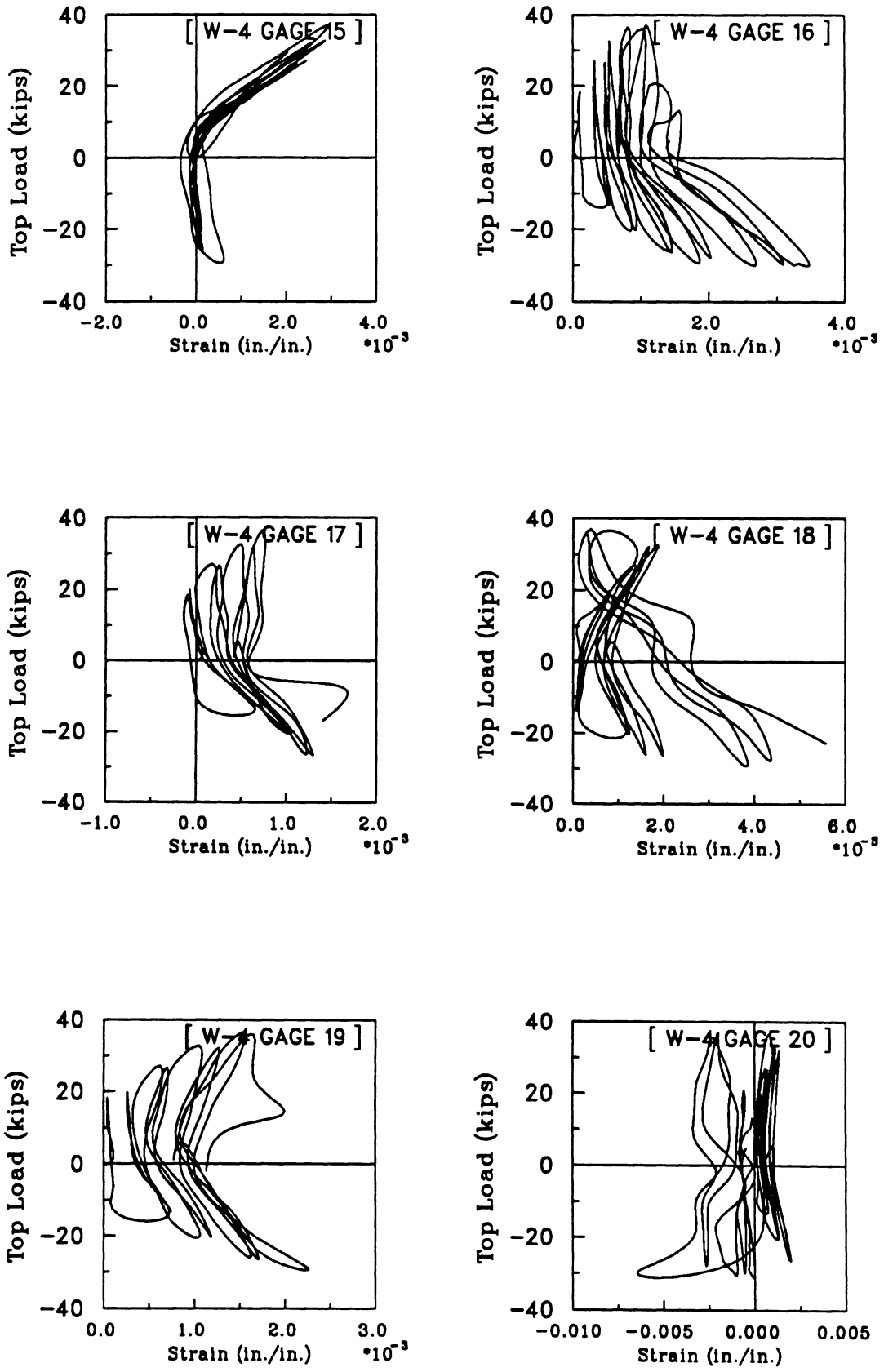

Fig. 4.73(c) : Strain Histories for Gages 15, 16, 17, 18, 19 and 20 in Wall W-4.

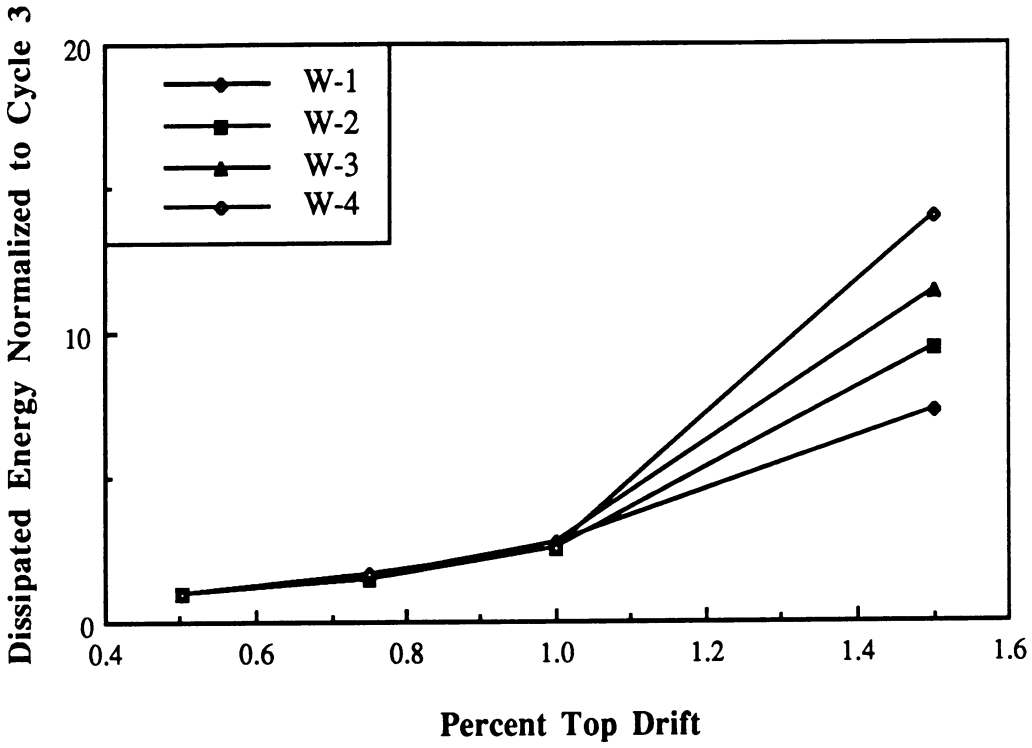

Fig. 4.74 : Comparison Energy Normalized Dissipation Capacities for Initial Cycles.

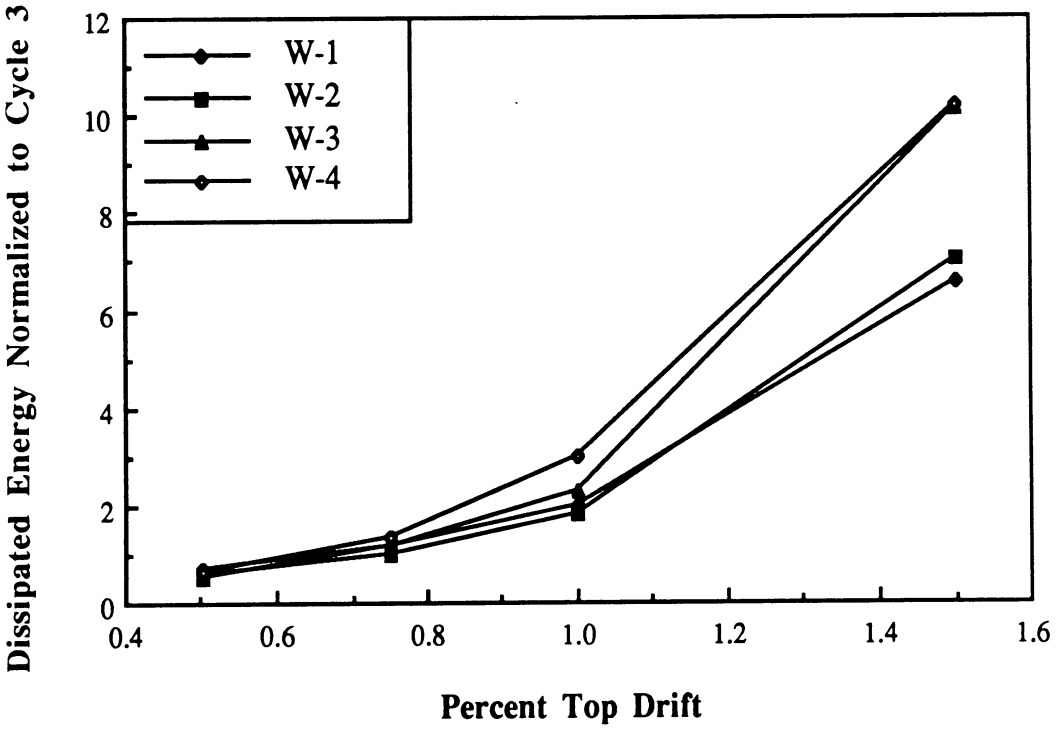

Fig. 4.75 : Comparison Energy Normalized Dissipation Capacities for Repeat Cycles.

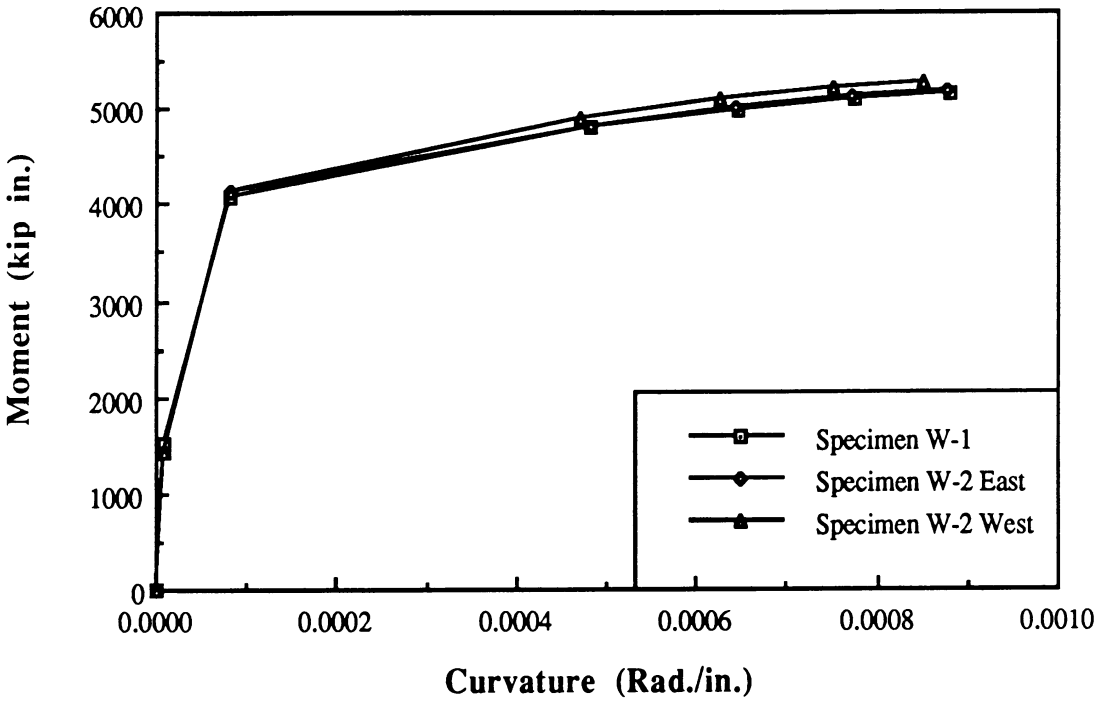

Fig. 5.1 : Comparison of Moment-Curvature Relationships for Walls W-1 and W-2.

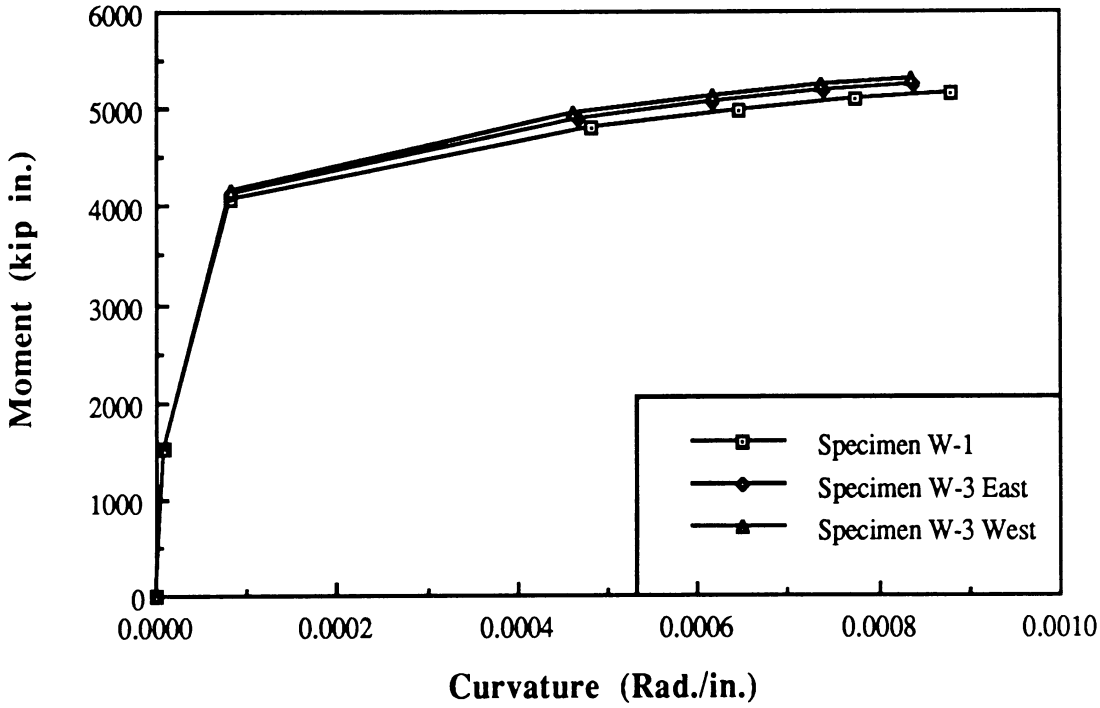

Fig. 5.2 : Comparison of Moment-Curvature Relationships for Walls W-1 and W-3.

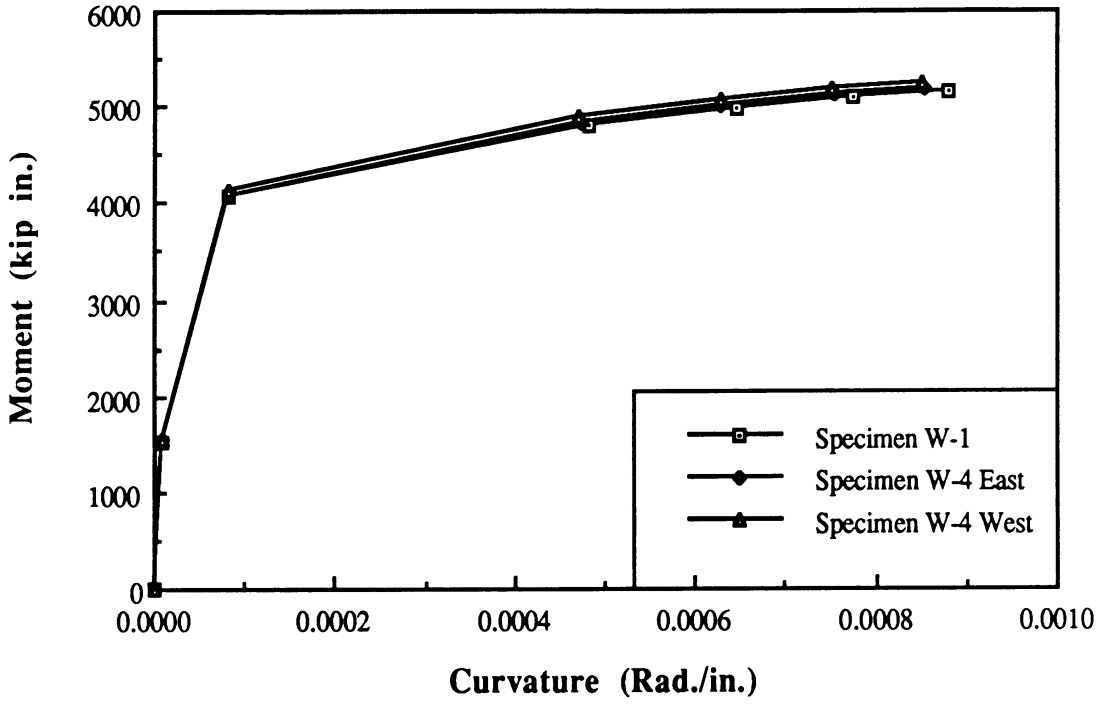

Fig. 5.3 : Comparison of Moment-Curvature Relationships for Walls W-1 and W-4.

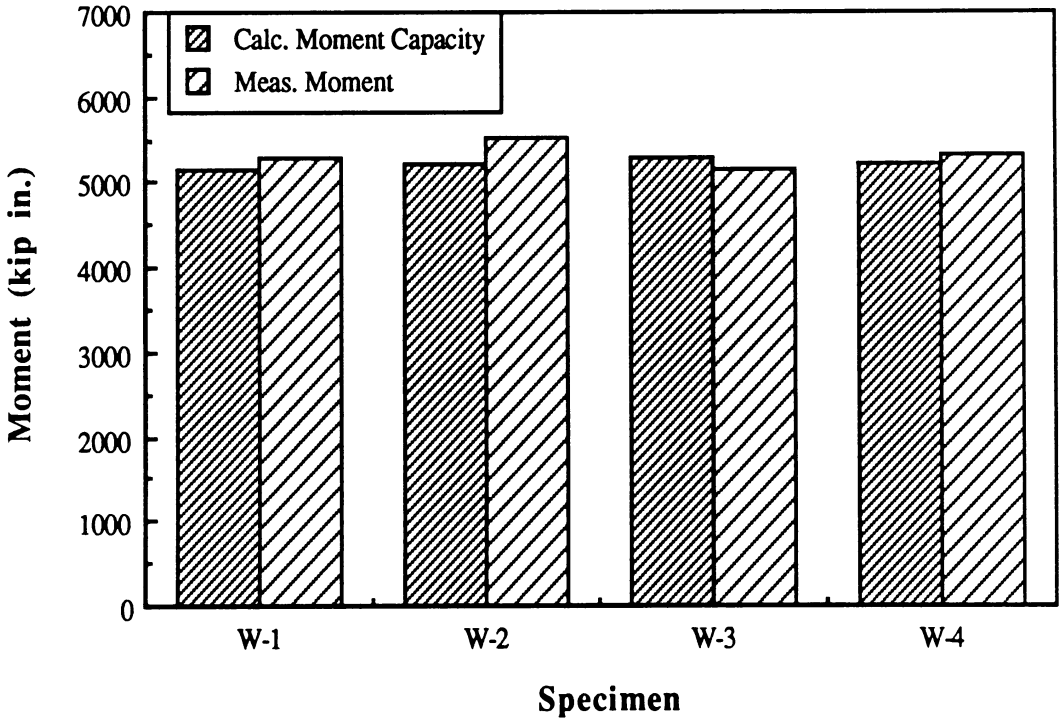

Fig. 5.4 : Comparison of Measured and Calculated Flexural Capacities of Wall Specimens.

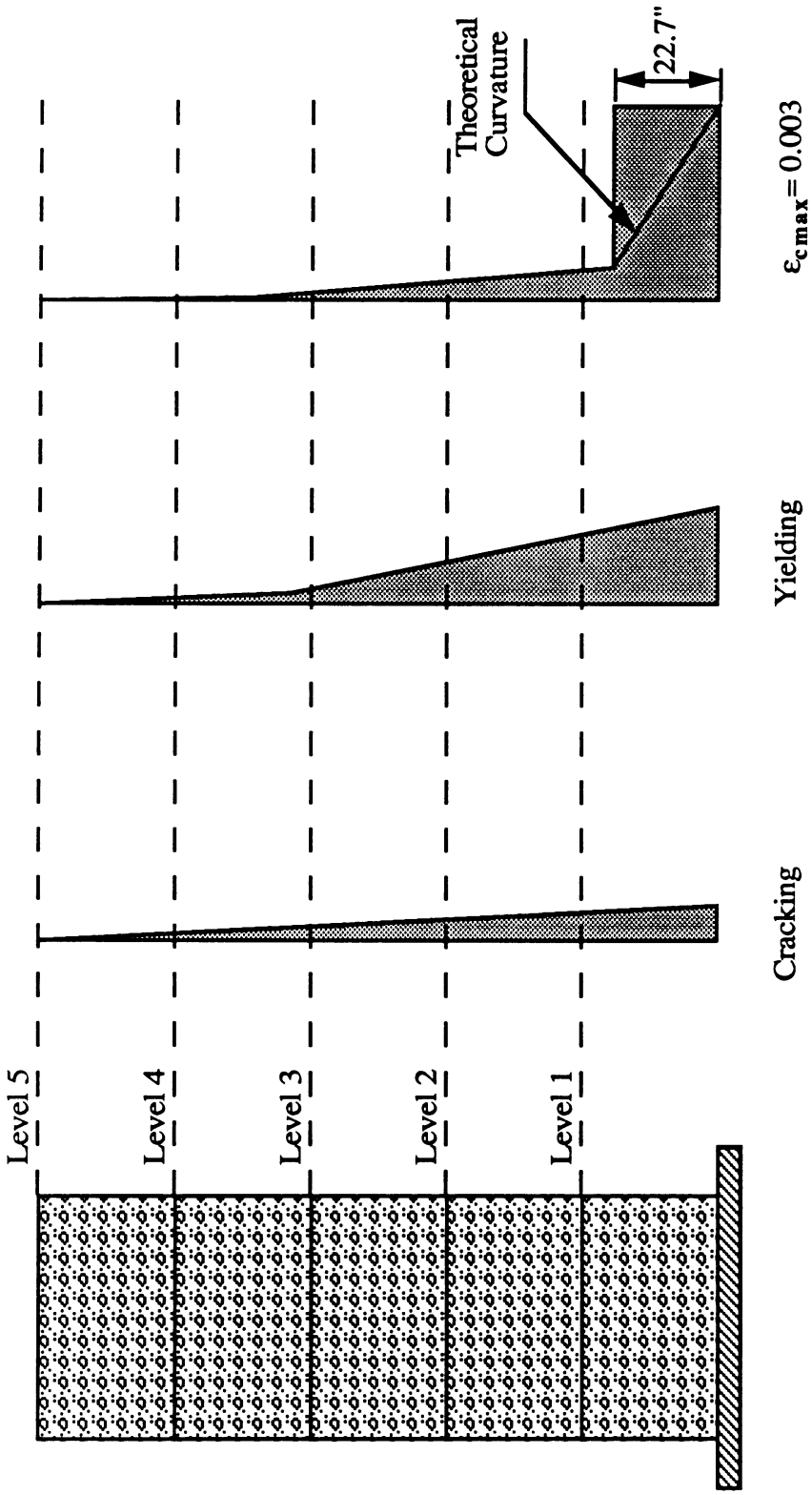

Fig. 5.5(a) : Actual and Effective Curvature Distributions for Wall Specimens at Cracking, Yielding and Nominal Strains.

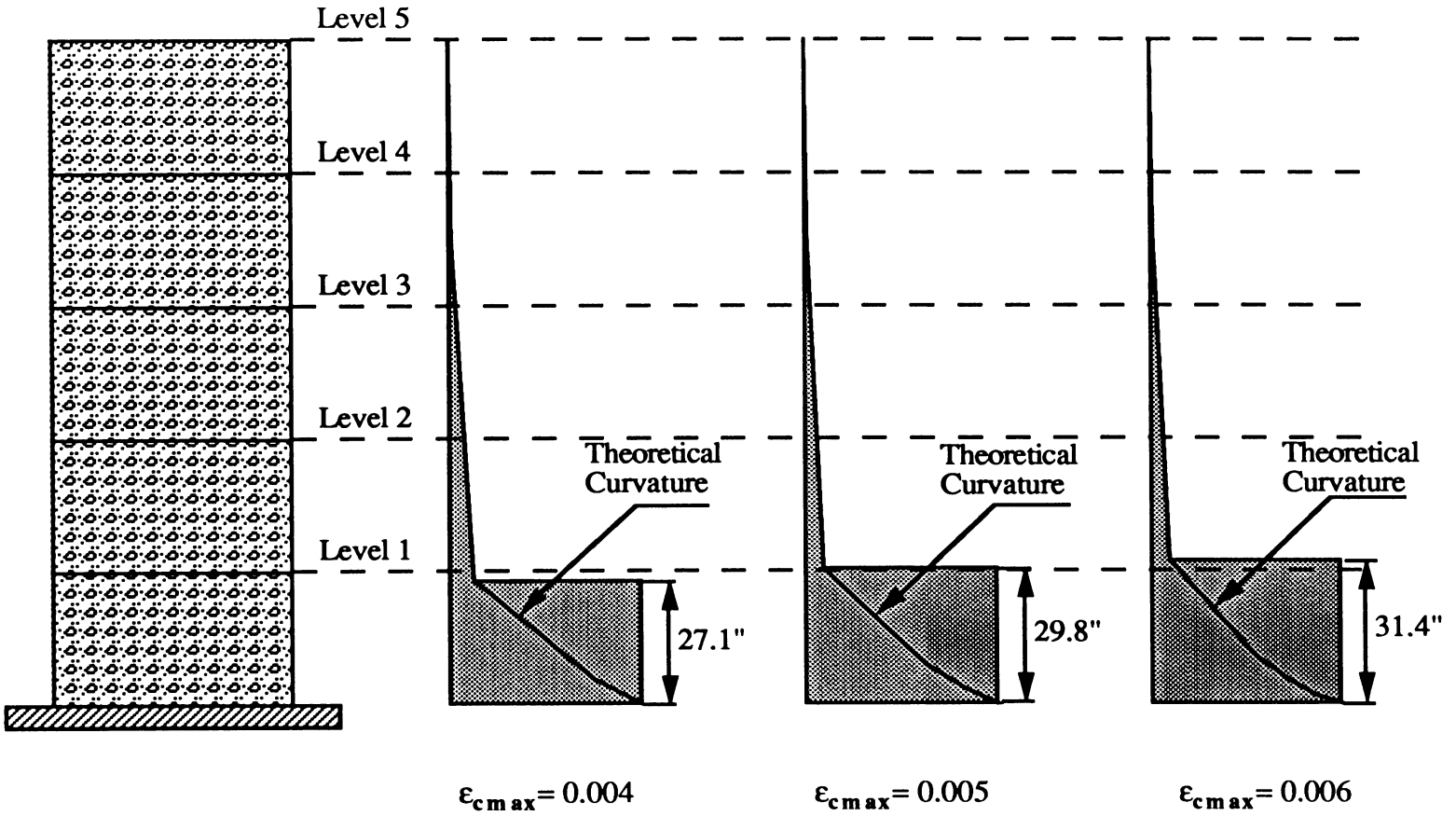

Fig. 5.5(b) : Actual and Effective Curvature Distributions for Wall Specimens at Maximum Concrete Compressive Fiber Strains of 0.004, 0.005, and 0.006.

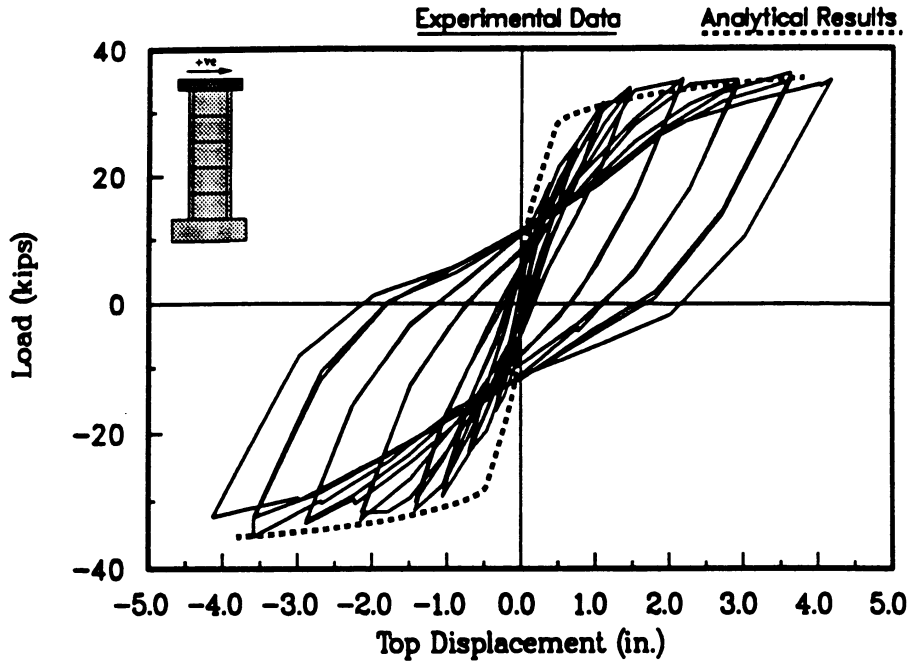

Fig. 5.6 : Analytical and Experimental Force-Displacement Relationships for Wall W-1.

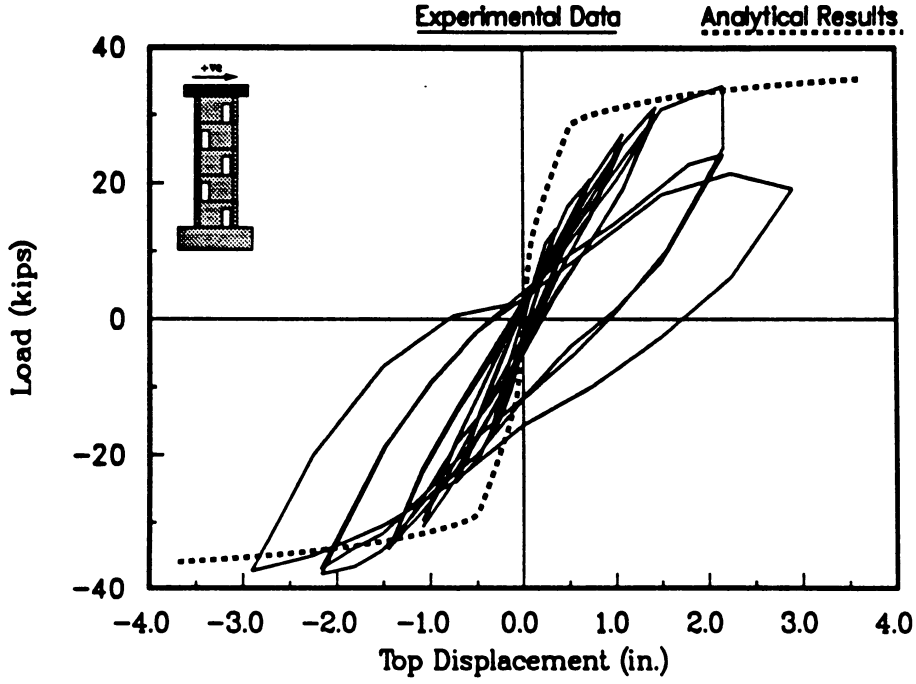

Fig. 5.7 : Analytical and Experimental Force-Displacement Relationships for Wall W-2.

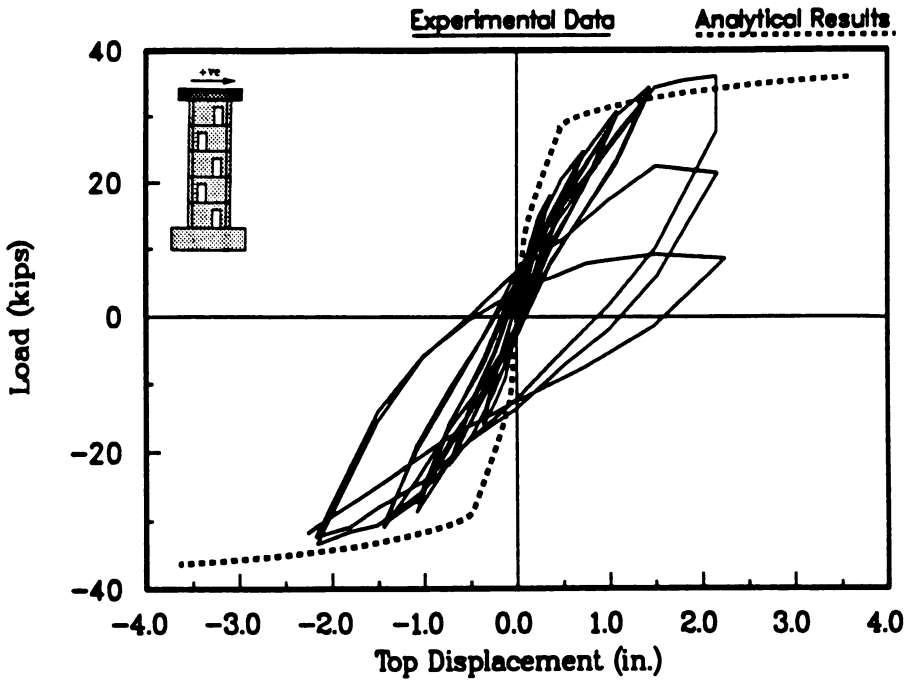

Fig. 5.8 : Analytical and Experimental Force-Displacement Relationships for Wall W-3.

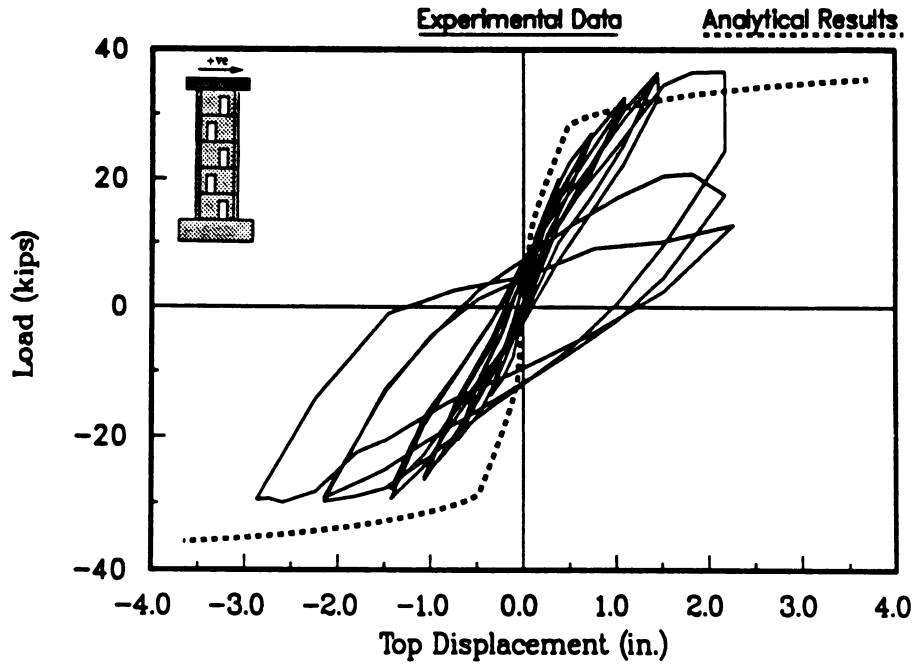

Fig. 5.9 : Analytical and Experimental Force-Displacement Relationships for Wall W-4.

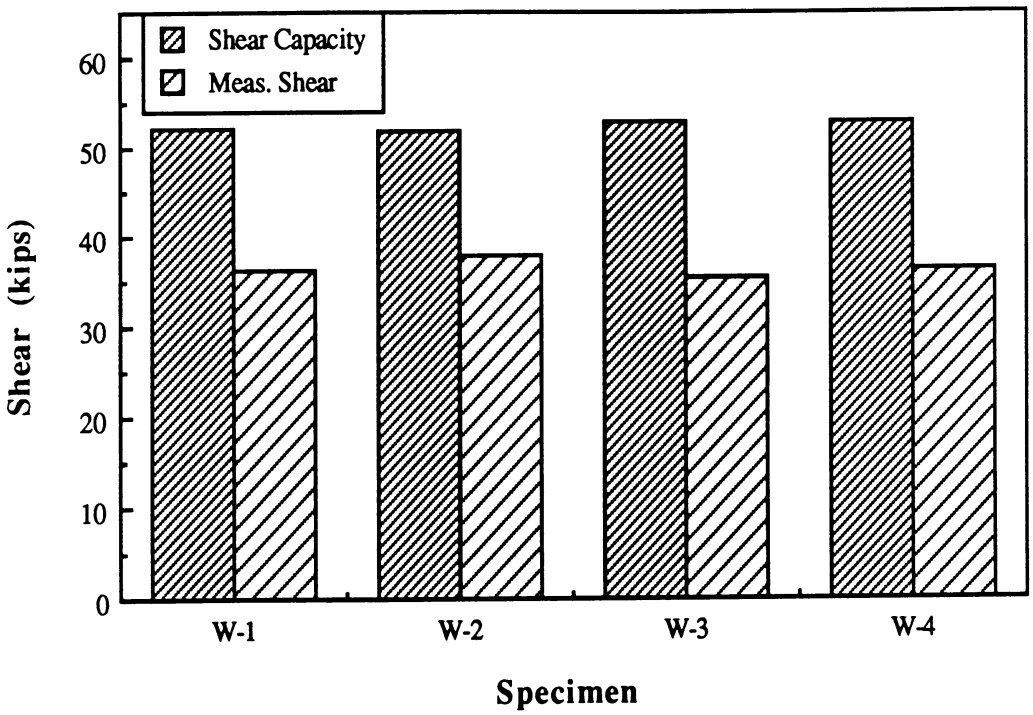

Fig. 5.10 : Comparison of Measured and Calculated Shear Capacities of Wall Specimens.

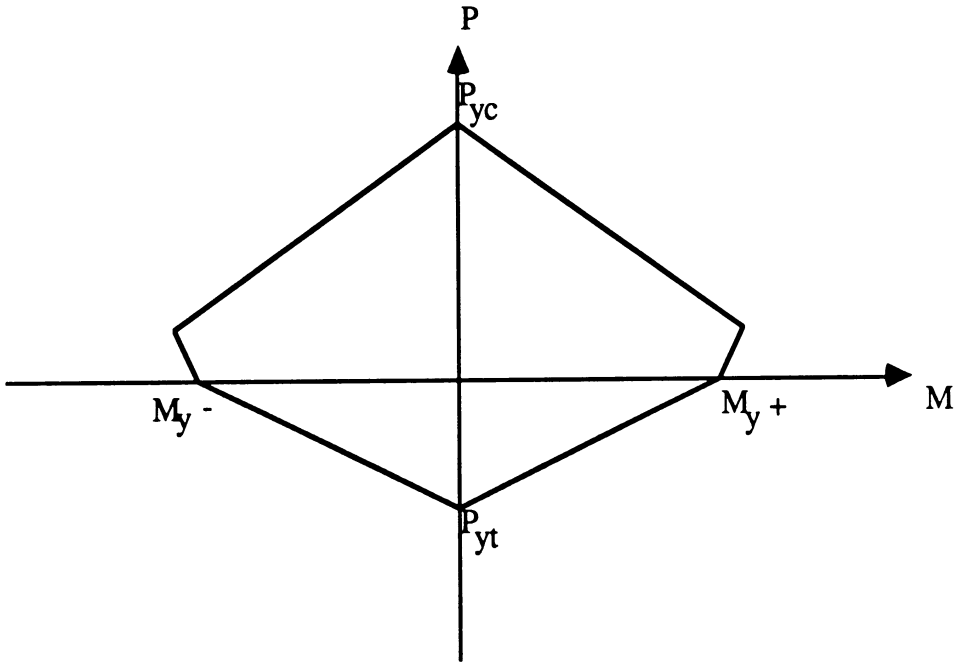

Fig. 5.11 : Yield Interaction Surface for Reinforced Concrete [27].

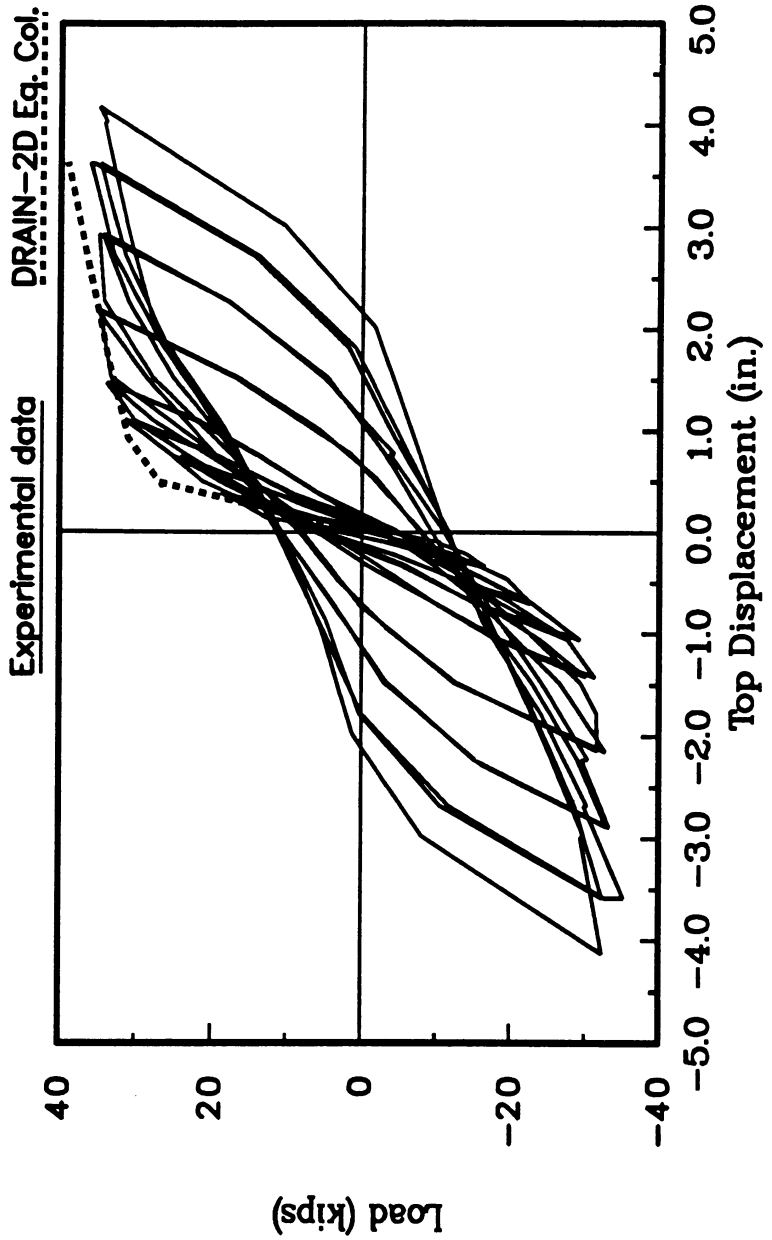

Fig. 5.12 : Comparison of DRAIN-2DM Eq. Col. and Experimental Force-Displacement Relationships for Wall W-1.

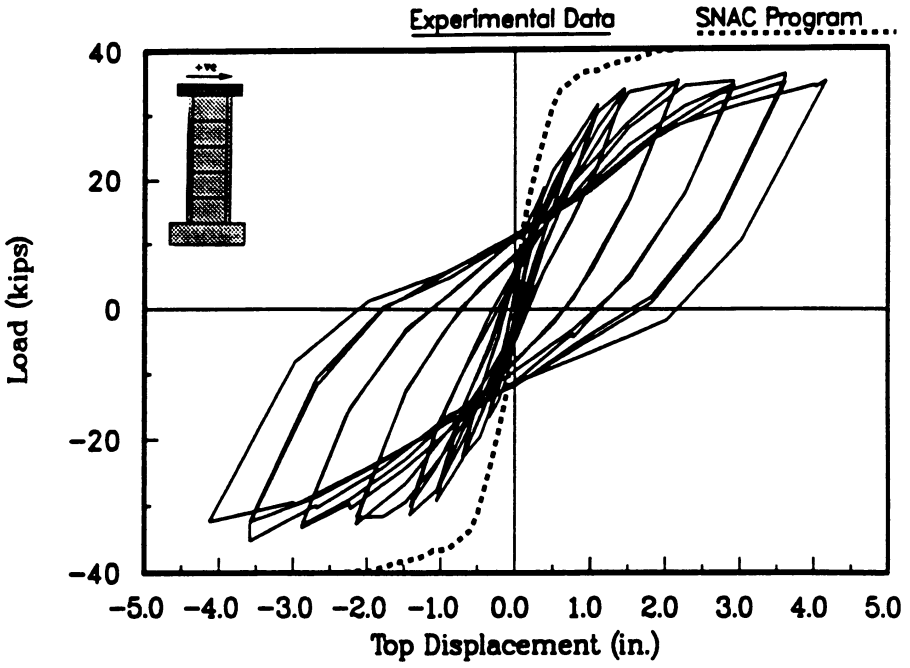

Fig. 5.13 : Comparison of Experimental and Finite Element Response of Wall W-1.

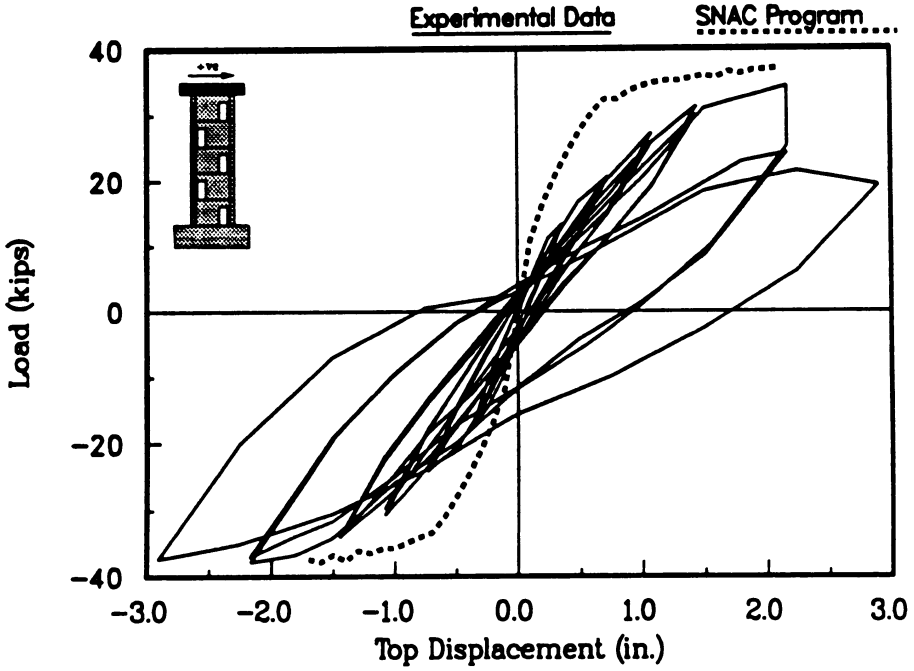

Fig. 5.14 : Comparison of Experimental and Finite Element Response of Wall W-2.

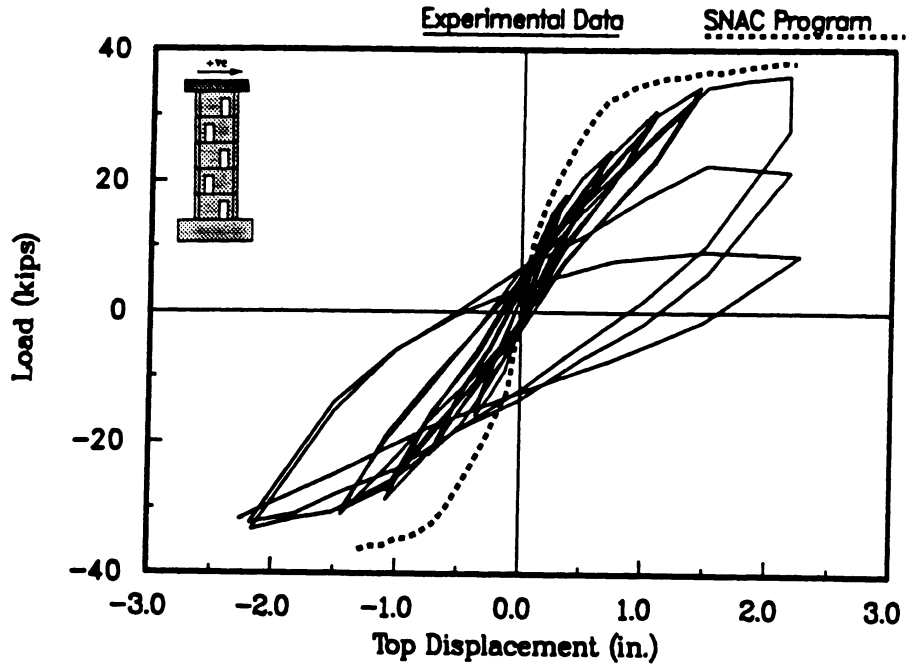

Fig. 5.15 : Comparison of Experimental and Finite Element Response of Wall W-3.

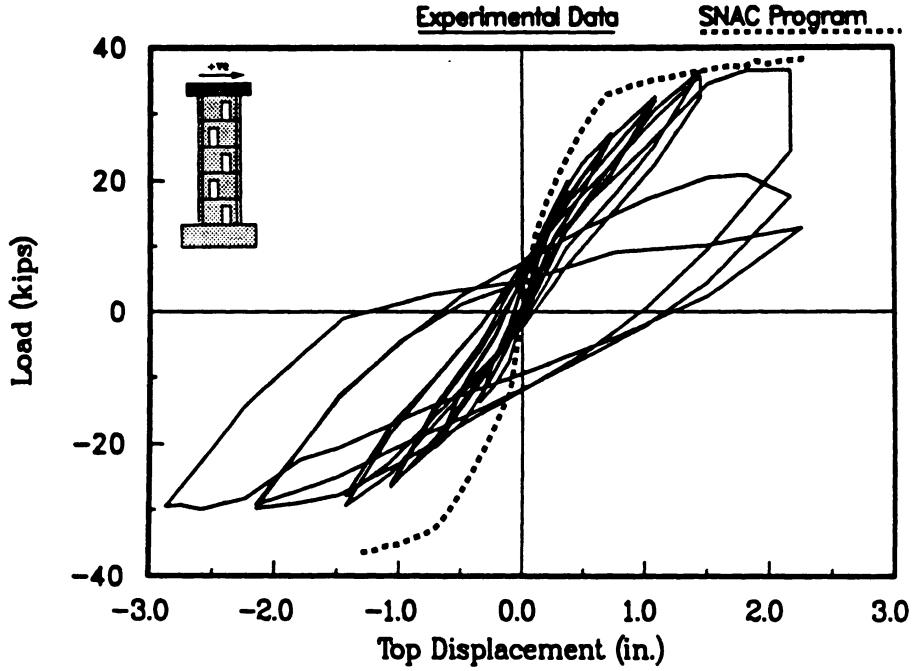

Fig. 5.16 : Comparison of Experimental and Finite Element Response of Wall W-4.

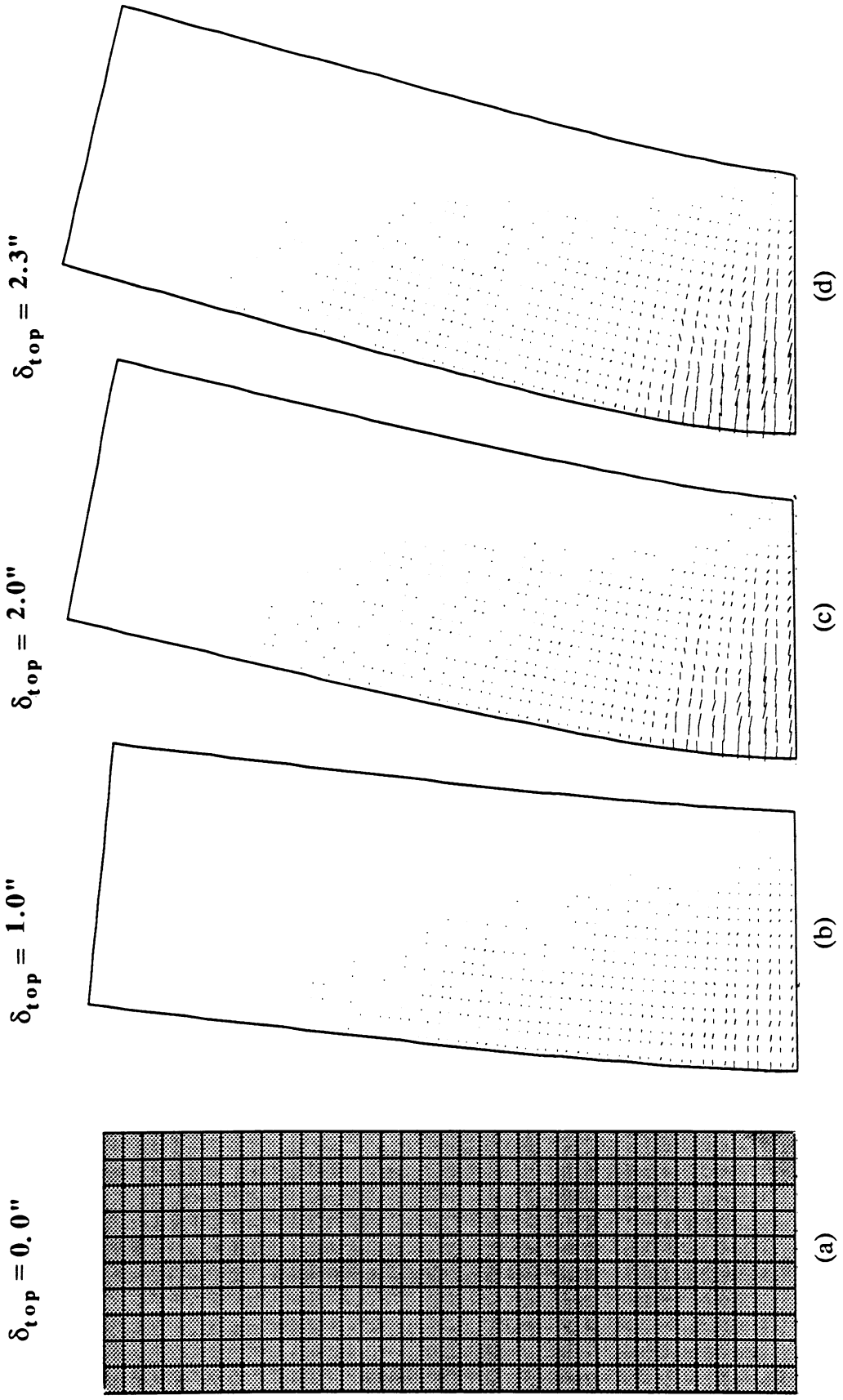

Fig. 5.17 : Undeformed Geometry and Nonlinear Trends in Wall W-1 at Selected Top Displacements.

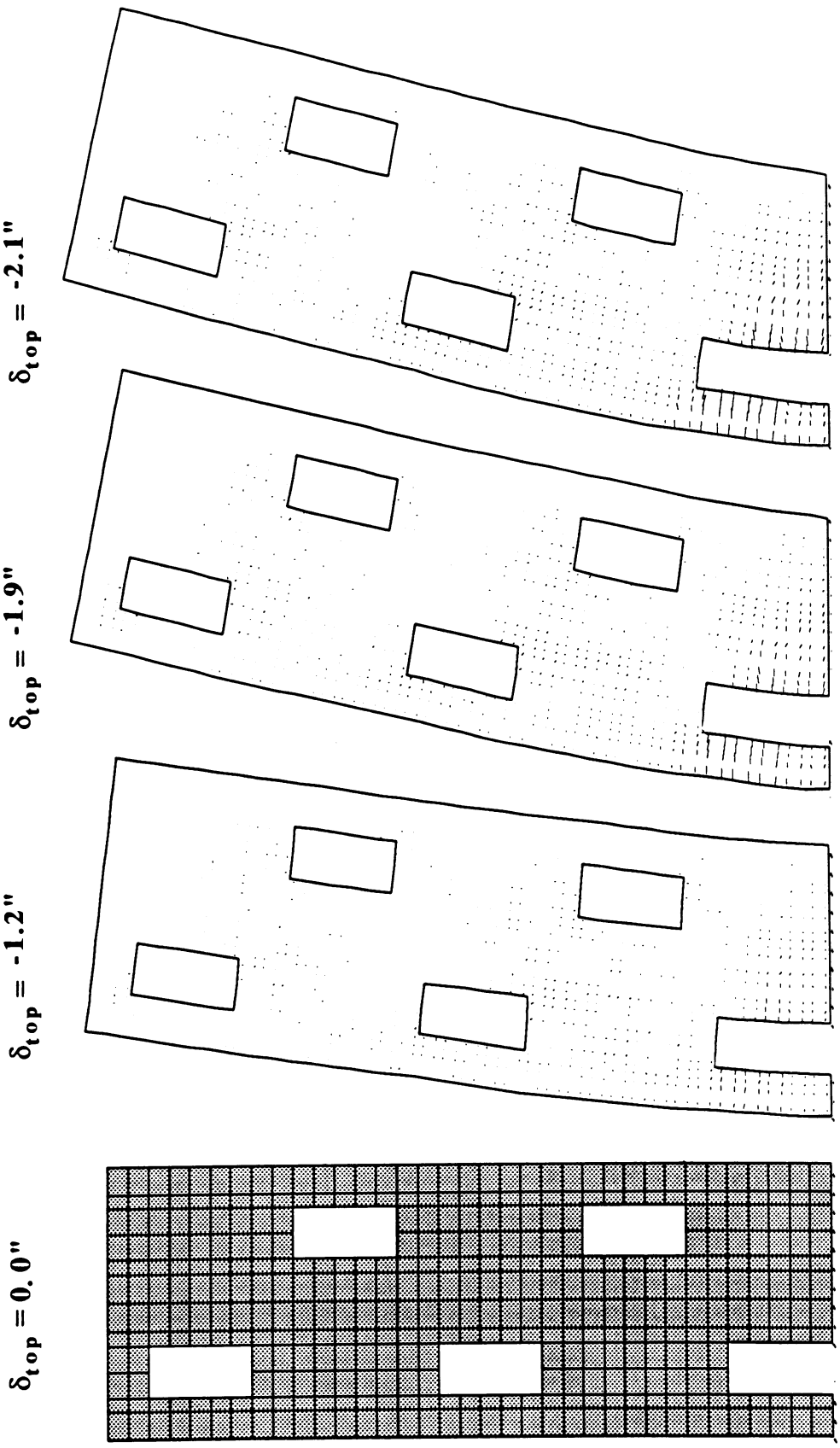

Fig. 5.18 : Undeformed Geometry and Nonlinear Trends in Wall W-2 at Selected Top Displacements.

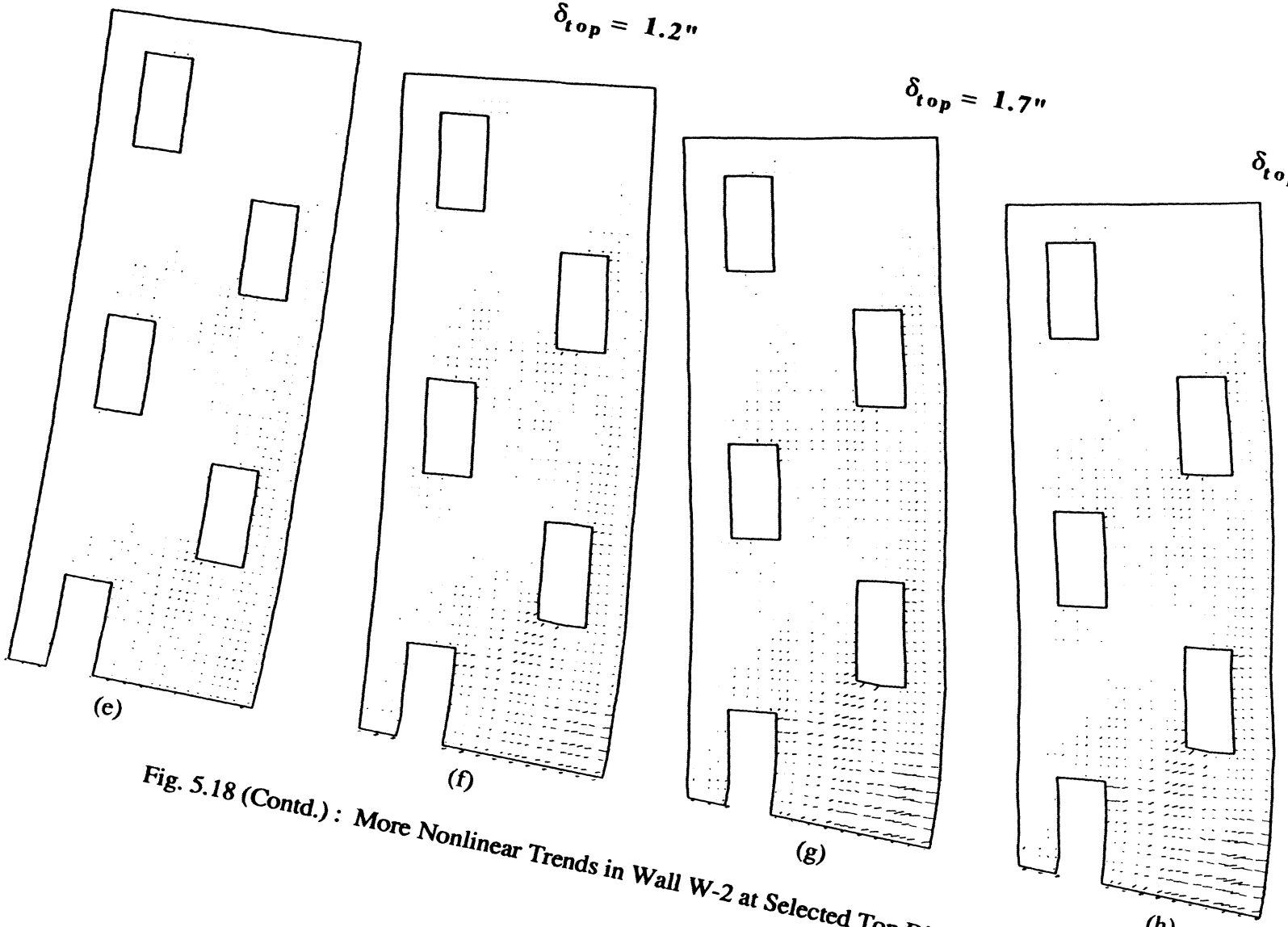

Fig. 5.18 (Contd.) : More Nonlinear Trends in Wall W-2 at Selected Top Displacements.

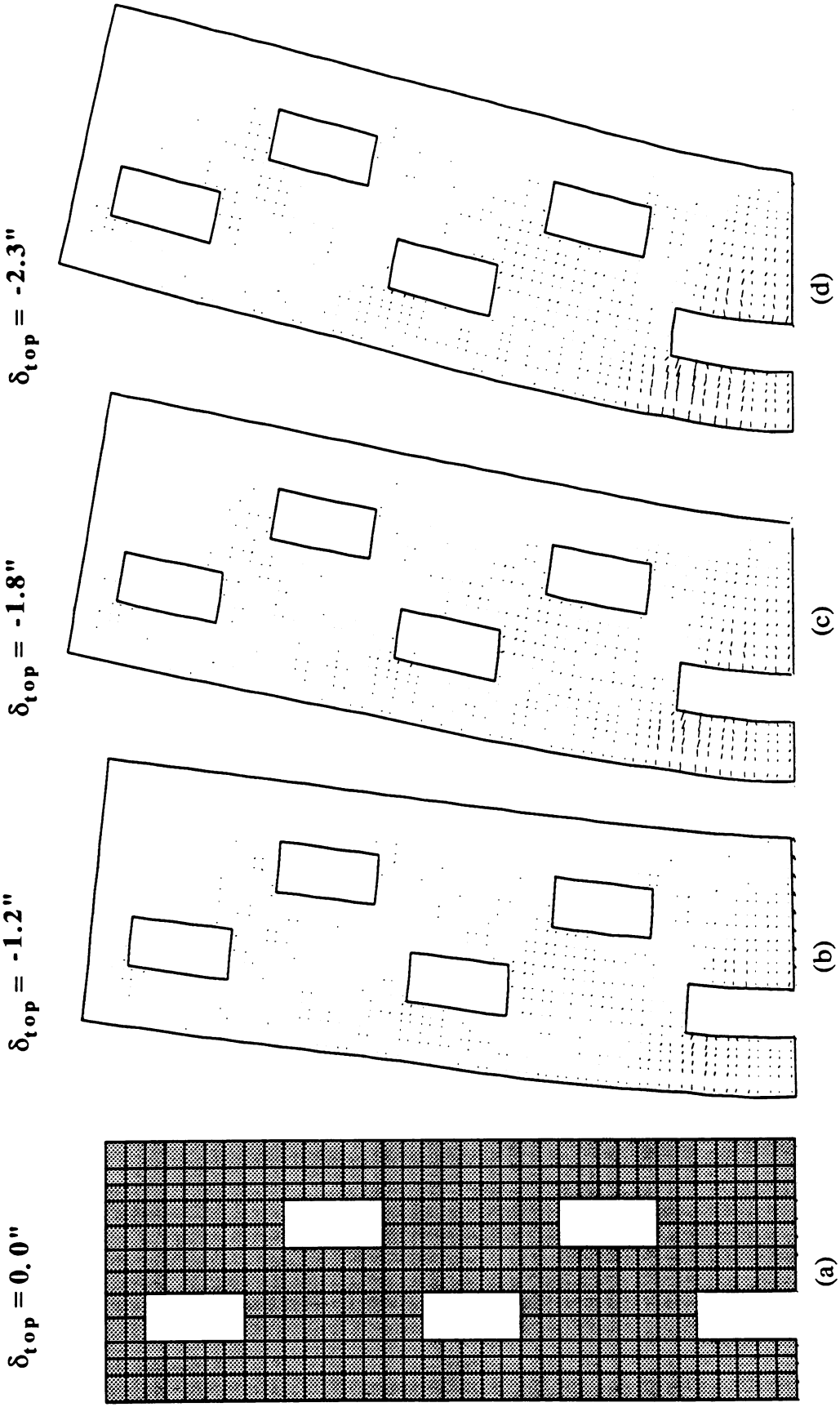

Fig. 5.19 : Undeformed Geometry and Nonlinear Trends in Wall W-3 at Selected Top Displacements.

Fig. 5.19 (Contd.) : More Nonlinear Trends in Wall W-3 at Selected Top Displacements.

Fig. 5.20 : Undeformed Geometry and Nonlinear Trends in Wall W-4 at Selected Top Displacements.

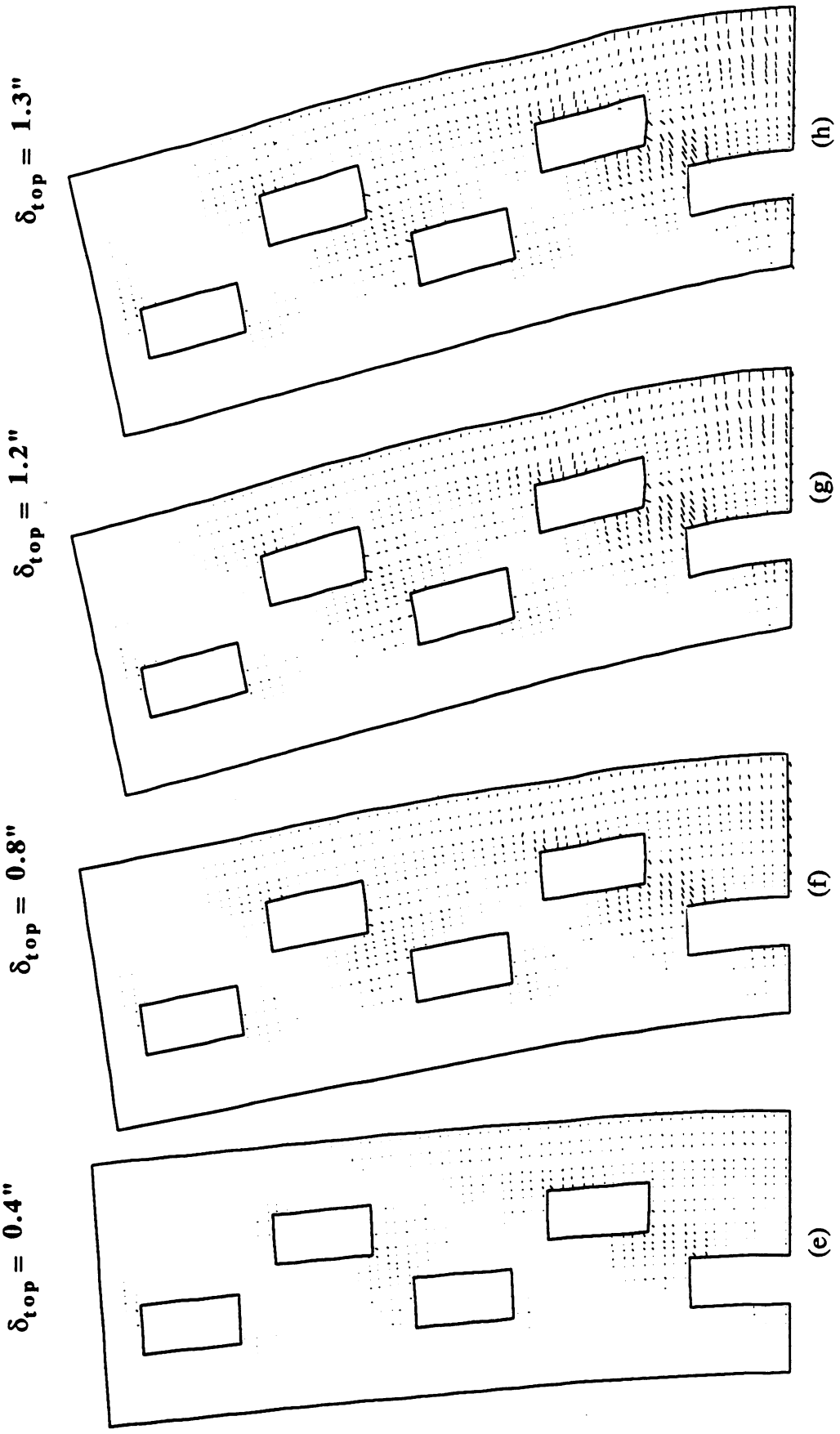

Fig. 5.20 (Contd.) : More Nonlinear Trends in Wall W-4 at Selected Top Displacements.

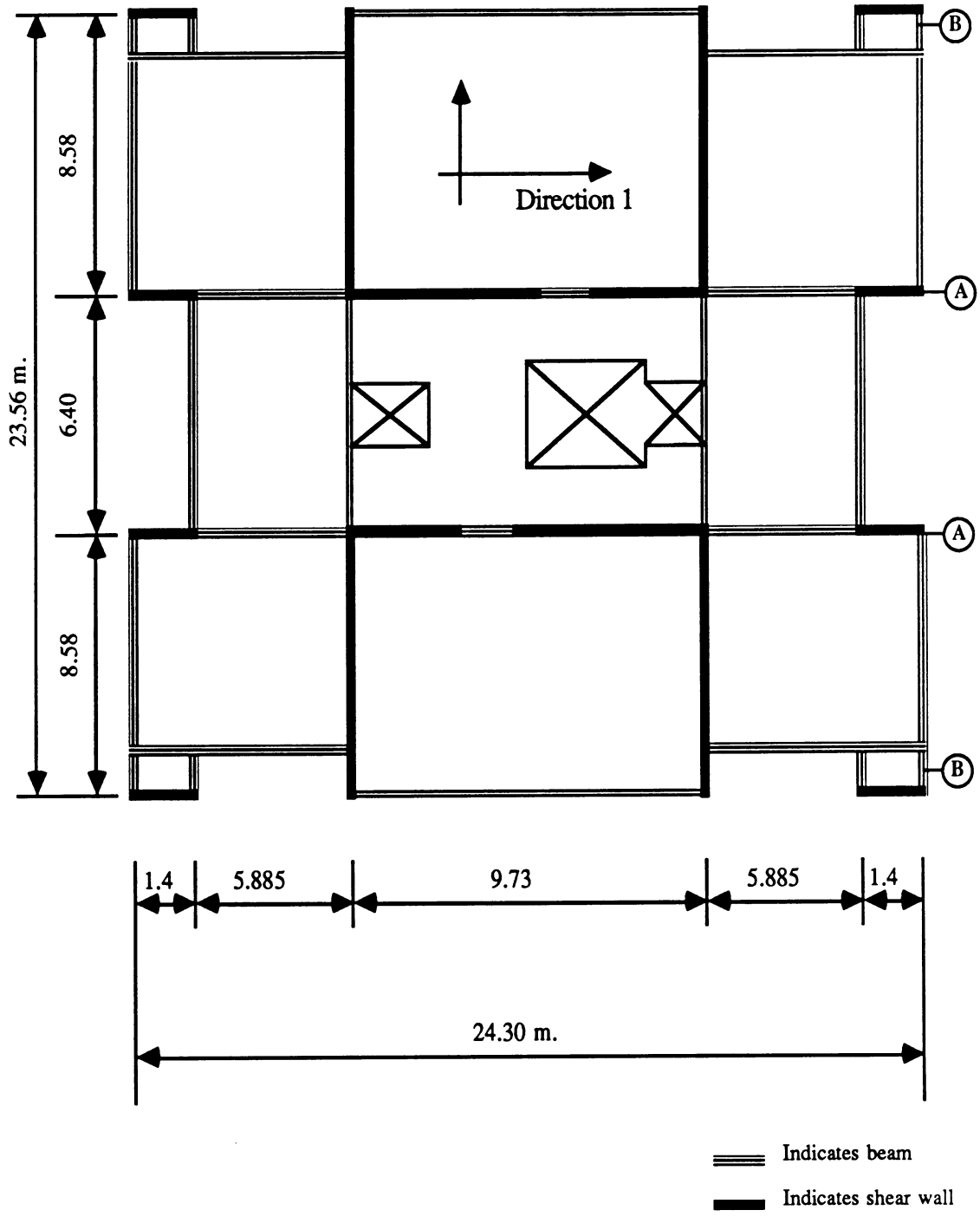

Fig 6.1(a) : Plan View of a Typical Story of Almendral Building.

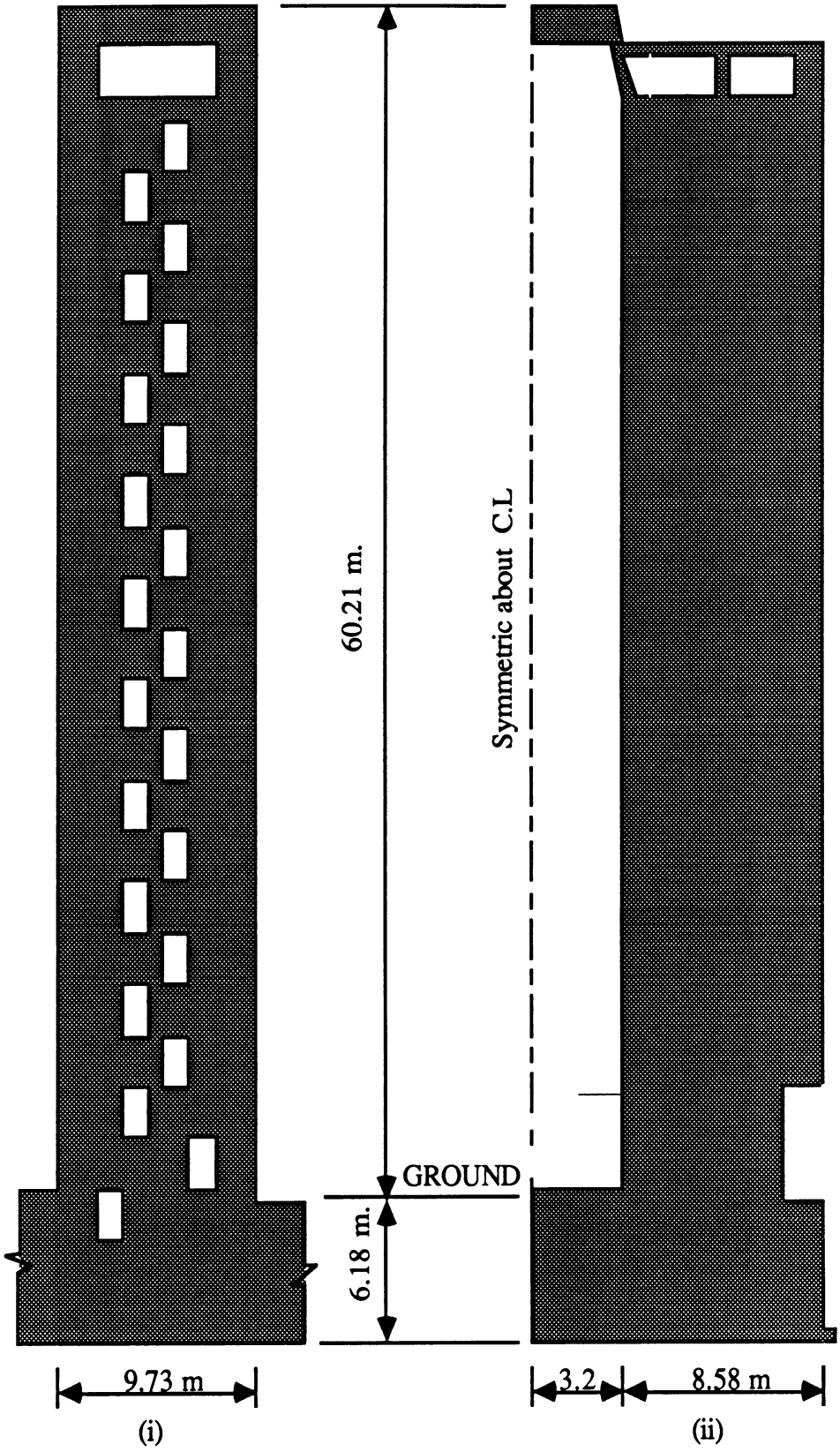

Fig. 6.1(b) : Elevations of Walls in Almendral Building along
(i) Web Portion (ii) Flange Portion.

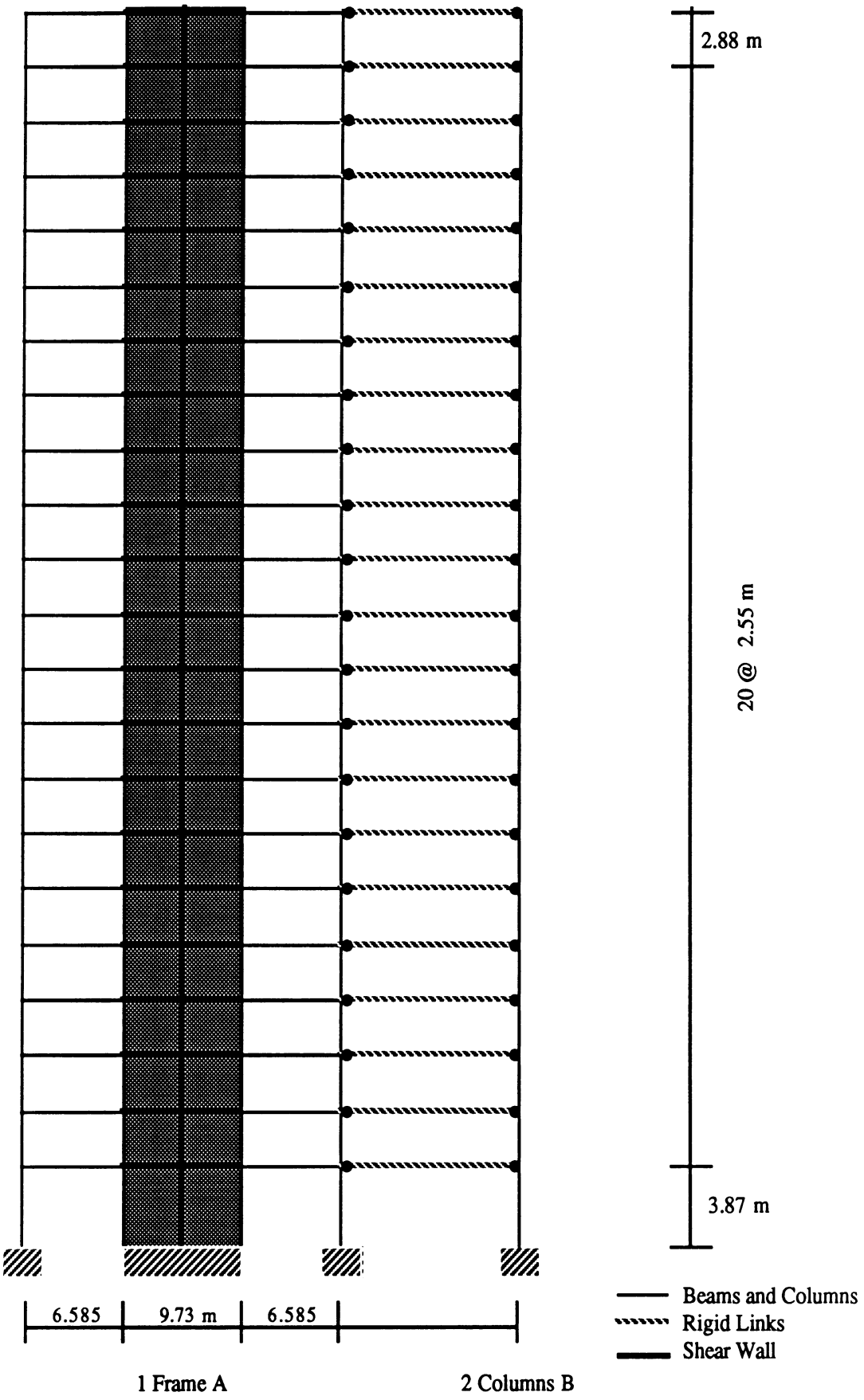

Fig. 6.2 : Structural Model for Almendral Building.

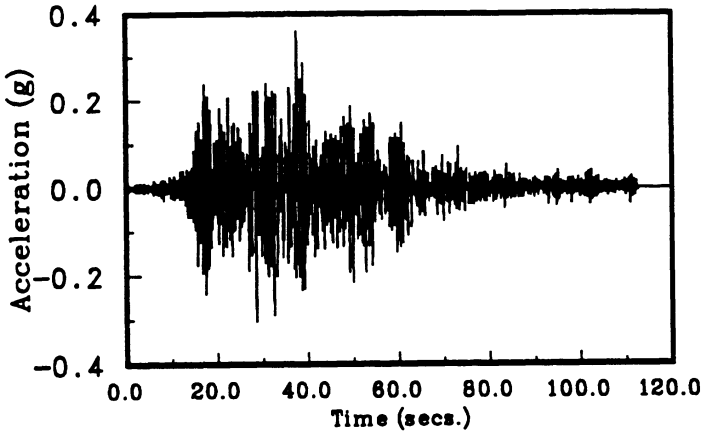

(a) Ground Acceleration Record

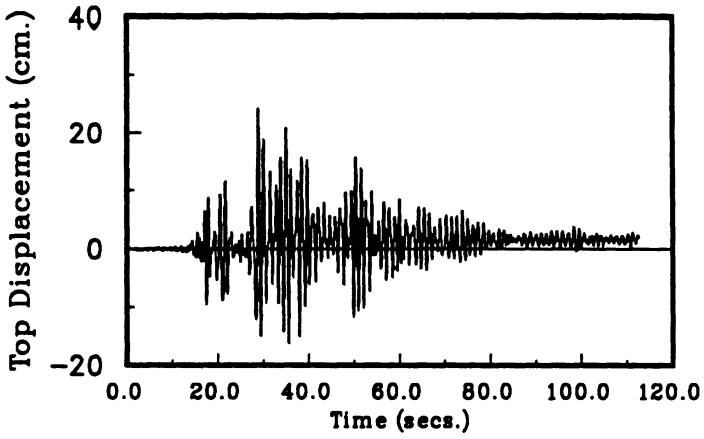

(b) Top Displacement Time History

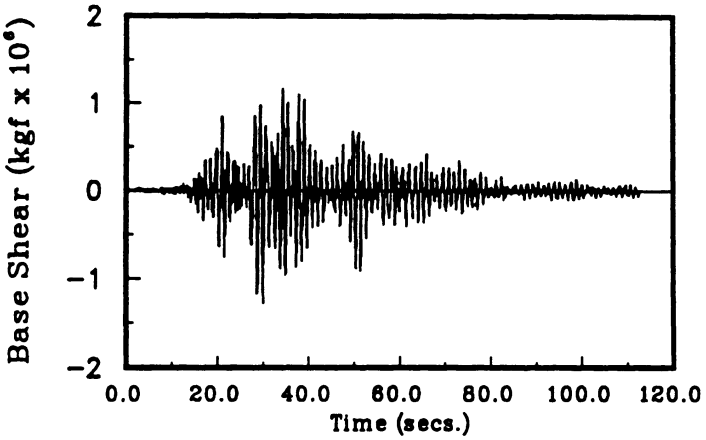

(c) Base Shear Time History

Fig. 6.3 : Response of Analytical Model of Almendral Building to Vina del Mar (S20W) Acceleration History (Cracked Stiffness).

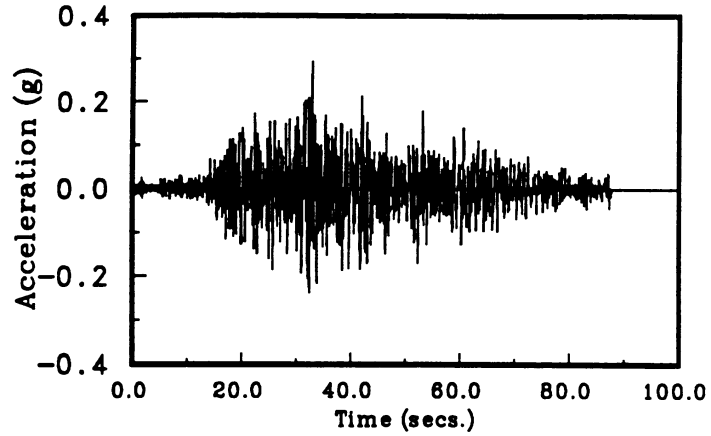

(a) Ground Acceleration Record

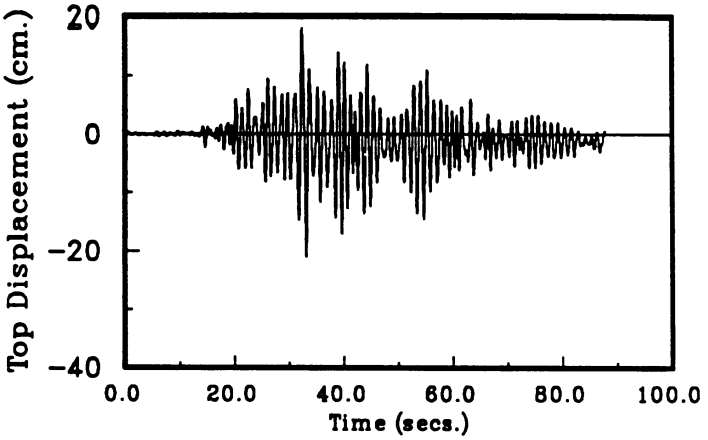

(b) Top Displacement Time History

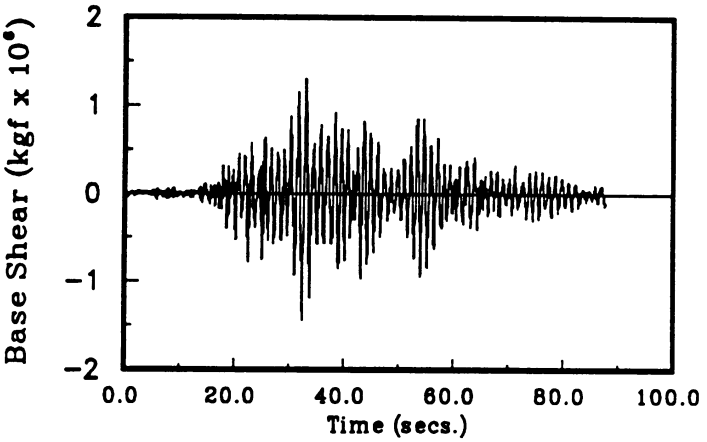

(c) Base Shear Time History

Fig. 6.4 : Response of Analytical Model of Almendral Building to Almendral (N50E) Acceleration History (Cracked Stiffness).

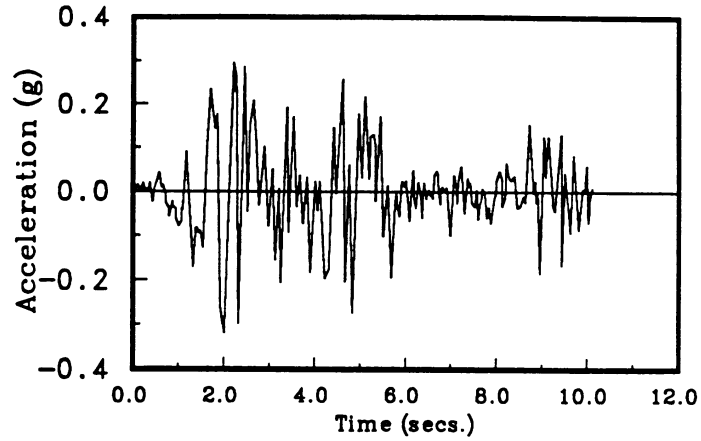

(a) Ground Acceleration Record

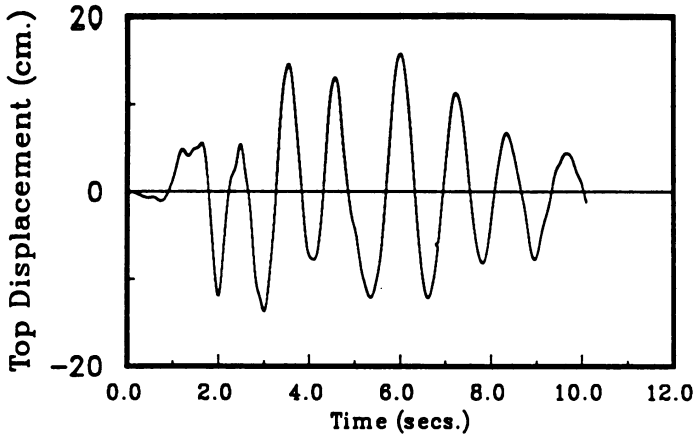

(b) Top Displacement Time History

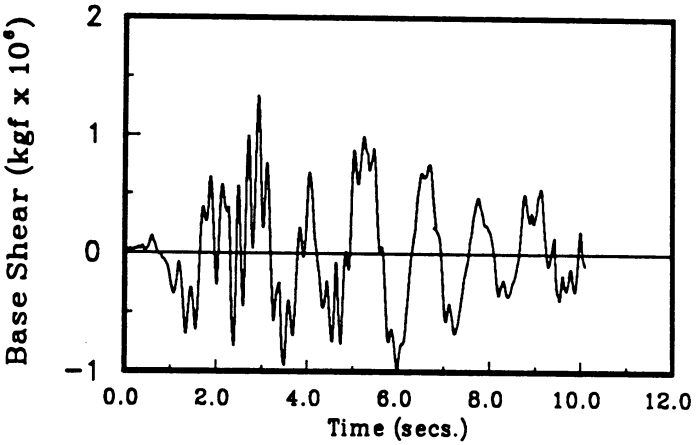

(c) Base Shear Time History

Fig. 6.5 : Response of Analytical Model of Almendral Building to El Centro (NS) Acceleration History (Cracked Stiffness).

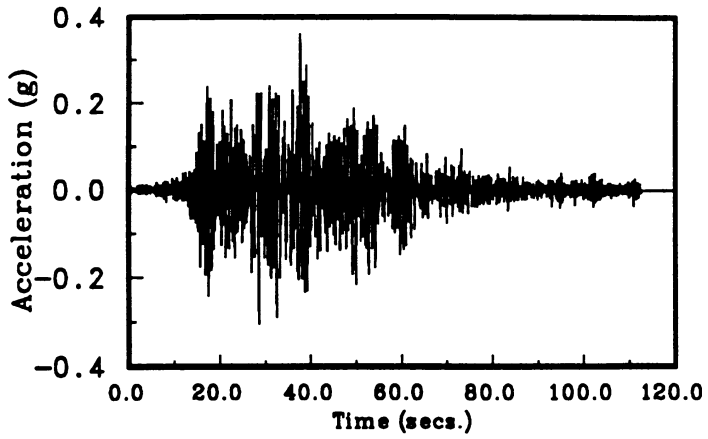

(a) Ground Acceleration Record

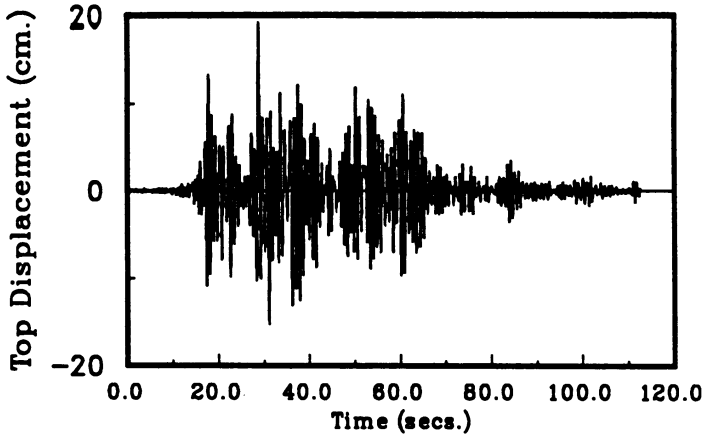

(b) Top Displacement Time History

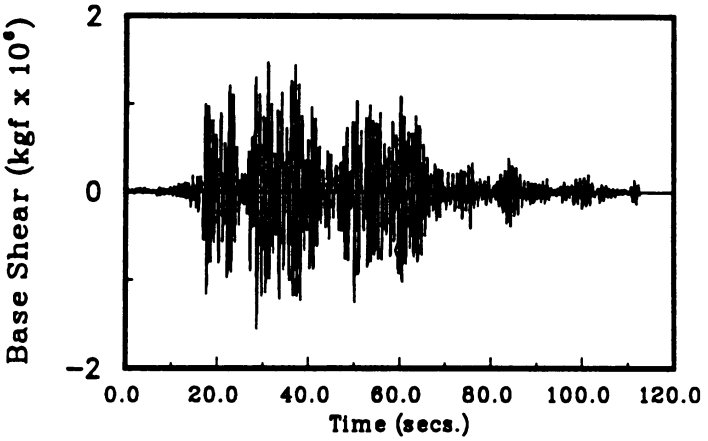

(c) Base Shear Time History

Fig. 6.6 : Response of Analytical Model of Almendral Building to Vina del Mar (S20W) Acceleration History (Uncracked Stiffness).

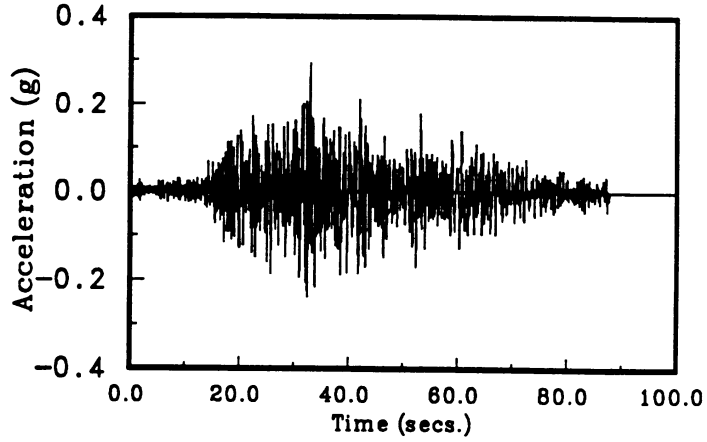

(a) Ground Acceleration Record

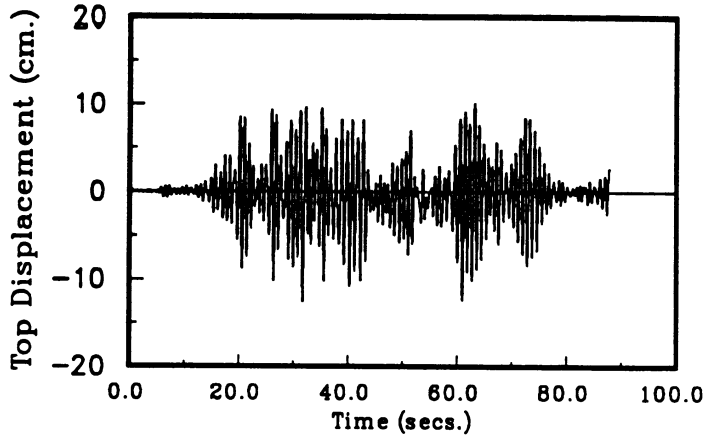

(b) Top Displacement Time History

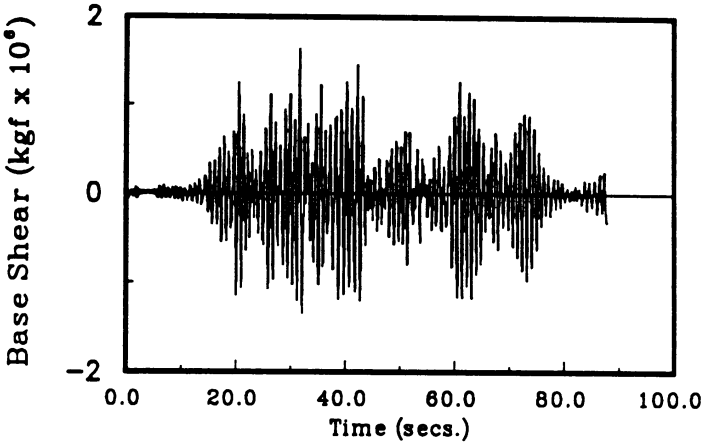

(c) Base Shear Time History

Fig. 6.7 : Response of Analytical Model of Almendral Building to Almendral (N50E) Acceleration History (Uncracked Stiffness).

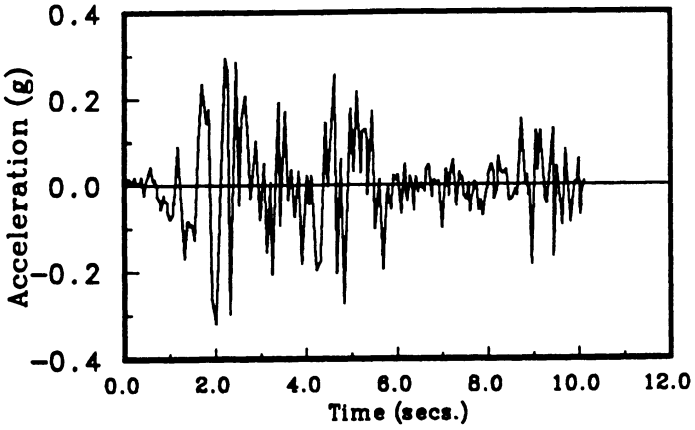

(a) Ground Acceleration Record

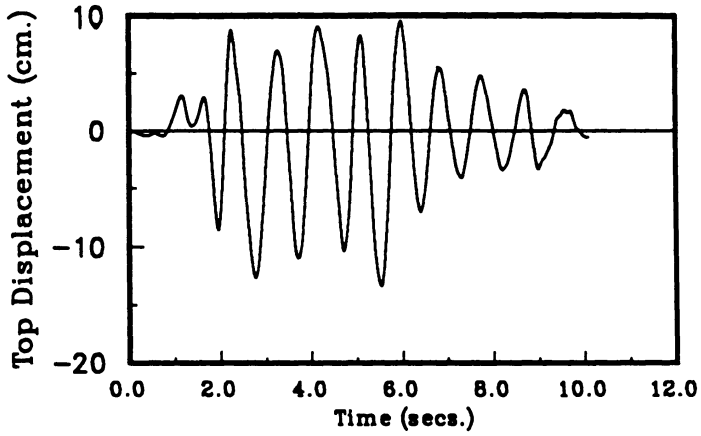

(b) Top Displacement Time History

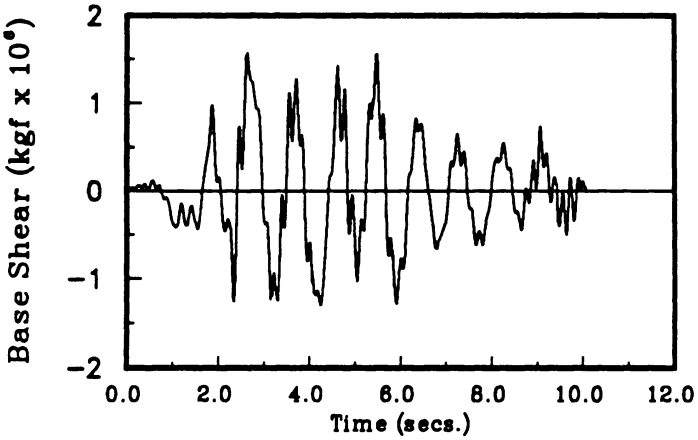

(c) Base Shear Time History

Fig. 6.8 : Response of Analytical Model of Almendral Building to El Centro (NS) Acceleration History (Uncracked Stiffness).